DOCTOR OF PHILOSOPHY

Intensity modulation of optical OFDM signals using low-cost semiconductor laser devices for next-generation PONs

Wei, Jinlong

Award date:
2010

Awarding institution:
Bangor University

Intensity Modulation of Optical OFDM Signals Using Low-Cost Semiconductor Laser Devices for Next-Generation PONs

Jinlong Wei

PRIFYSGOL
BANGOR
UNIVERSITY

A thesis submitted for the degree of
Doctor of Philosophy

School of Electronic Engineering
Bangor University

October 2010

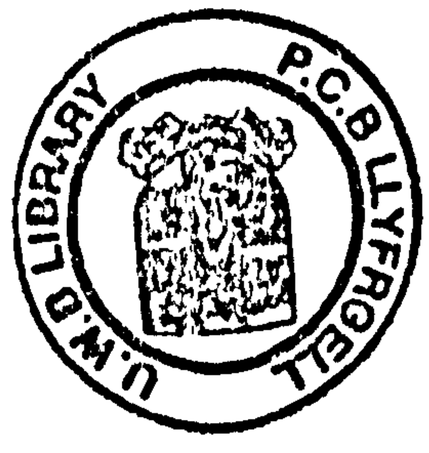

Abstract

Optical Orthogonal Frequency Division Multiplexing (OOFDM) has been widely considered as one of the strongest contenders for high-speed Next-Generation PONs (NG-PONs) to satisfy the continuously increasing bandwidth requirements from individual and business users. From telecommunication equipment vendor's and network operator's point of view, cost-effectiveness is a key factor for practical mass deployment of OOFDM-based NG-PONs in future. As the electro-optic convertors involved in OOFDM transceivers take the majority of the OOFDM transceiver cost, the convertors, therefore, play critical roles in determining the system performance and cost. The thesis aims to theoretically investigate the feasibility of using low-cost semiconductor laser devices including Directly Modulated DFB Lasers (DMLs), Semiconductor Optical Amplifiers (SOAs) and Reflective SOAs (RSOAs) for converting real-valued electrical OFDM signals into the optical domain for transmission over simple Intensity Modulation and Direct Detection (IMDD) NG-PON systems. The validity of various theoretical models employed in the thesis is also rigorously verified by comparing with real-time experimental measurements.

For DML-based OOFDM IMDD PON systems, special attention is first dedicated to extensive investigations of the impact of various physical mechanisms on the system performance to maximize the achievable optical power budget, transmission capacity and reach. The physical mechanisms include OOFDM signal Extinction Ratio (ER), DML-induced frequency chirp and subcarrier intermixing upon direct detection in the receiver. Results show that the low ER of a DML-modulated OOFDM signal is the predominate factor limiting the achievable optical power budget, and the subcarrier intermixing effect upon square-law photon detection in the receiver reduces the optical power budget by at least 1dB. The use of a 0.02nm bandwidth optical Gaussian bandpass filter in the transmitter with a 0.01nm wavelength offset with respect to the optical carrier wavelength is proposed to enhance the 11.25Gb/s OOFDM signal ER by approximately 1.24dB. This results in a 7dB optical power budget improvement at a total channel BER of 1×10^{-3}. Moreover, by adopting a DML-modulated carrier suppressed Single Sideband (SSB) OOFDM technique in NG-PONs, 30Gb/s carrier suppressed SSB OOFDM signal transmission over 80km SMF without in-line optical amplification is achievable, which doubles the performance corresponding to conventional Double Sideband (DSB) OOFDM

signals without carrier suppression. It is also shown that 10Gb/s carrier suppressed SSB OOFDM signal transmission over 1200km SMF incorporating in-line Erbium Doped Fibre Amplifiers (EDFAs) is feasible.

Given the fact that Wavelength-Division Multiplexing (WDM) has been widely deployed in practice, and that RSOAs/SOAs have advantages of compactness, capability of monolithic integration with electrical components and wide wavelength coverage of typically >100nm, in this thesis, RSOAs/SOAs are proposed to facilitate colourless transmitters for OOFDM IMDD WDM-PONs. Explorations show that, under optimized SOA operating conditions, 30Gb/s OOFDM signal transmission over 80km SMF without in-line optical amplification and dispersion compensation is feasible at 1550nm; and colourless transmissions of SOA-intensity modulated OOFDM signals of 30Gb/s over 60km SMF are also achievable for a wide wavelength range from 1510nm to 1590nm. Moreover, numerical investigations are also undertaken of the performance comparisons between RSOA and SOA intensity modulators, and detailed discussions are also made of the influence of RSOA rear-facet reflectivity on the achievable RSOA-modulated OOFDM signal performance. Results indicate that the maximum transmission performance of 30Gb/s over 60km SMF under optimum RSOA operating conditions is independent of rear-facet reflectivity, and the performance is very similar to that corresponding to SOAs; whilst under un-optimised operating conditions, the RSOA intensity modulators outperform considerably the SOA intensity modulators in transmission performance, which decreases significantly with reducing RSOA rear-facet reflectivity and optical input power.

Finally, to simplify the network architecture and simultaneously improve the wavelength control functionality and system performance, wavelength reused bidirectional colourless OOFDM IMDD WDM-PONs are proposed, which incorporate a SOA intensity modulator and a RSOA intensity modulator in the optical line terminal and optical network unit, respectively. Results show that 10Gb/s downstream and 6Gb/s upstream over 40km SMF transmission of conventional DSB OOFDM signals are feasible. In particular, the aforementioned transmission performances can be further improved to 23Gb/s downstream and 8Gb/s upstream over 40 km SMF when SSB-Subcarrier Modulation (SCM) is introduced in the downstream systems.

Acknowledgements

First of all, I am especially grateful to my supervisor Dr. Jianming Tang for his continuous guidance and strong support in the past years. I would also like to acknowledge my committee members, Prof. K Alan Shore, Prof. Paul S. Spencer, and especially Dr. Iestyn Pierce for important comments and suggestions on my study in Bangor, my papers and my thesis. My sincere gratitude also extends to Dr. Yanhua Hong for her constructive comments on my papers and the thesis, as well as her kind care about my life in Bangor.

I would like to express my gratitude to Dr. Cedric F. Lam in Google for his continuous encouragement, guidance, friendship, and brotherly mentorship in both my study and life since I was studying under his co-supervision in China. I am also grateful to Prof. Kun Qiu in University of Electronic Science and Technology of China who brought me into the field of optical communications and recommended me to study in Bangor University.

The time I spent with my colleagues in Bangor University was memorable. We shared experiences together in useful technical discussions and arguments, conferences, project meetings as well as leisure times. They include Dr. Xianqing Jin, Xing Zheng, Dr. Xuelin Yang, Roger P. Giddings, Dr. Emilio Hugues-Salas, Elias Giacoumidis, Muttsam A. Jarajreh, as well as Dr. Ali Hamié who was a visiting researcher from Lebanon, and Christian Sánchez who was a visiting PhD student from Spain.

My acknowledgements also extend to other people in Bangor University for their kind help that I have received and to School of Electronic Engineering at Bangor University for providing the funding for my PhD research. Also, I would like to express my sincere gratitude to the Chinese government for financial support that enabled me to live in UK.

Last but not least, I sincerely appreciate the selfless love and supports from my family. They always remind me of what "home" means. My dear friends from both China and Bangor, UK who provided me sincere support also deserve a big thank you and warm hugs. I love you all.

Abbreviations

ADC	Analog to Digital Convertor
ADSL	Asymmetric Digital Subscriber Loop
AM	Amplitude Modulation
AMOOFDM	Adaptively Modulated Optical OFDM
APON	ATM Passive Optical Network
ASE	Amplified Spontaneous Emission
ATM	Asynchronous Transfer Mode
AWG	Arrayed Wavelength Grating
BER	Bit Error Rate
BLS	Broadband Light Source
BPF	Bandpass Filter
BPON	Broadband PON
BTB	Back-to-Back
CAPEX	Capital Expenditure
CATV	Cable Television
CD	Chromatic Dispersion
CFO	Carrier Frequency Offset
CMTS	Cable Modem Termination System
CO	Central Office
CO-OFDM	Coherent Optical OFDM
CP	Cyclic Prefix
CPE	Carrier Phase Error
CWDM	Coarse WDM
DAB	Digital Audio Broadcasting
DAC	Digital to Analog Convertor
DBA	Dynamic Bandwidth Allocation
DBPSK	Differential Binary Phase Shift Keying
DBR	Distributed Bragg Grating

DFB	Distributed Feedback
(I)DFT	(Inverse) Discrete Fourier Transform
DML	Directly Modulated DFB Laser
DOCSIS	Data over Cable Service Interface Specification
DQPSK	Differential Quadrature Phase Shift Keying
DSB	Double Sideband
DSL	Digital Subscriber Line
DSLAM	DSL Access Multiplexer
DSP	Digital Signal Processing
DVB	Digital Video Broadcasting
DWDM	Dense WDM
EAM	Electro-Absorption Modulator
EDFA	Erbium Doped Fibre Amplifier
EM	External Modulator
EPON	Ethernet Passive Optical Network
ER	Extinction Ratio
FBG	Fibre Bragg Grating
FDM	Frequency Division Multiplexing
FEC	Forward Error Correction
(I)FFT	(Inverse) Fast Fourier Transform
FM	Frequency Modulation
F-P LD	Fabry-Perot Laser Diode
FSAN	Full Service Access Networks
FSK	Frequency Shift Keying
FSR	Free Spectral Range
FTTH/B/C/P	Fibre to the Home/Building/Curb/Premise
FWM	Four Wave-Mixing
GEM	GPON Encapsulation Mode
GPON	Gigabit Passive Optical Network
GTC	GPON Transmission Convergence
GVD	Group-Velocity Dispersion

HFC	Hybrid Fibre Coaxial
ICI	Inter-Carrier Interference
ID	Identifier
IEEE	Institute of Electrical and Electronics Engineers
IMDD	Intensity Modulation and Direct Detection
IP	Internet Protocol
IPTV	IP Television
I/Q	Imaginary/Quadrature
IRZ	Inverse Return-to-Zero
ISI	Inter-Symbol Interference
ITU	International Telecommunication Union
LAN	Local Area Networks
LED	Light-Emitting Diode
LPF	Low-pass Filter
LTE	Long-Term Evolution
MAC	Media Access Control
MAN	Metropolitan Area Network
MFL	Multi-Frequency Laser
MIMO	Multi-Input-Multiple-Output
MLM	Multi-Longitudinal Mode
MMF	Multi-Mode Fibre
MPMC	Multi-Point Media Access Control
NG-PON	Next Generation Passive Optical Network
NRZ	Non Return to Zero
OBPF	Optical Bandpass Filter
ODN	Optical Distribution Network
OFDM	Orthogonal Frequency Division Multiplexing
OLT	Optical Line Terminal

ONU	Optical Network Unit
OOFDM	Optical OFDM
OOK	On-Off Keying
OPEX	Operational Expenditure
OSI	Open System Interconnect
OSNR	Optical Signal-to-Noise Ratio
OSRNR	Optical Signal to RB Noise Ratio
P2MP	Point-to-Multi-Point
P2P	Point-to-Point
PAPR	Peak-to-Average Power Ratio
PLOAM	Physical Layer Operation, Administration and Maintenance
PMD	Polarization Mode Dispersion
POF	Plastic Optical Fibre
PON	Passive Optical Network
POTS	Plain Old Telephone Service
PS	Power Splitter
PSK	Phase Shift Keying
PTP	Peak-to-Peak
QAM	Quadrature Amplitude Modulation
QPSK	Quadrature PSK
RB	Rayleigh Backscattering
RF	Radio Frequency
RoF	Radio over Fibre
RSOA	Reflective Semiconductor Optical Amplifier
SBS	Stimulated Brillouin Scattering
SCM	Subcarrier Modulation
SCO	Symbol Clock Offset
SLM	Single Longitudinal Mode
SNR	Signal-to-Noise Ratio
SOA	Semiconductor Optical Amplifier

SPM	Self-phase Modulation
SRS	Stimulated Raman Scattering
SSB	Single Sideband
SMF	Single-Mode Fibre
STO	Symbol Timing Offset
TDM	Time Division Multiplexing
VCSEL	Vertical Cavity Surface Emitting Laser
VDSL	Very fast data rate Digital Subscriber Line
VOA	Variable Optical Attenuator
VoD	Video-on-Demand
VoIP	Voice over IP
WDM	Wavelength Division Multiplexing
XPM	Cross-phase Modulation

Contents

Abstract I

Acknowledgements III

Abbreviations IV

1 Introduction 1

1.1 Major Achievements in this Dissertation 5

1.2 Thesis Structure 9

2 Principles of Optical OFDM 16

2.1 Introduction 17

2.2 History of OFDM 17

2.3 OFDM Fundamentals 18

2.3.1 OFDM: Special Type of FDM 18

2.3.2 OFDM Transceivers 20

2.3.2.1 Bit Encoding 21

2.3.2.2 IFFT/FFT 21

2.3.2.3 Cyclic Prefix 25

2.3.2.4 Serialization 26

2.3.2.5 DAC/ADC 26

2.3.2.6 Pilot-Assisted Channel Estimation and Equalization 28

2.3.2.7 Synchronization 29

2.4 Principles of Optical OFDM 30

2.4.1 Optical Fibres 31

2.4.1.1 Linear Fibre Effects 31

2.4.1.1.1 Fibre Loss 31

2.4.1.1.2 Rayleigh Scattering 32

2.4.1.1.3 Chromatic Dispersion 34

2.4.1.1.4 Polarization Mode Dispersion 36

2.4.1.2 Fibre Nonlinearities 37

2.4.1.2.1 SPM, XPM and FWM 37

2.4.1.2.2 SRS and SBS 39

2.4.2 Coherent Optical OFDM (CO-OFDM) 40

2.4.3 Intensity Modulation and Direct Detection Optical OFDM 43

2.4.4 Comparison between CO-OFDM and IMDD OOFDM 48
2.4.5 Adaptively Modulated OOFDM 50
2.5 Conclusion 52
3 PON Fundamentals 57
3.1 Introduction 58
3.2 Access Network Architectures 58
3.2.1 Digital Subscriber Line (DSL) 59
3.2.2 Hybrid Fibre Coaxial (HFC) 60
3.2.3 Passive Optical Networks (PONs) 61
3.3 PON Evolution 63
3.3.1 ITU-T BPON and GPON 64
3.3.1.1 APON/BPON and ITU-T G.983 64
3.3.1.2 GPON and ITU-T G.984 65
3.3.2 EPON and IEEE 802.3ah 66
3.3.3 10Gb/s NG-PONs 67
3.3.3.1 IEEE 10G-EPON 67
3.3.3.2 ITU-T XG-PON 68
3.3.4 Beyond 10G-EPON/XG-PON 70
3.4 Promising Technologies for NG-PONs 70
3.4.1 WDM-PON 70
3.4.2 Hybrid WDM/TDM-PON 72
3.4.3 OOFDM PON 73
3.5 Electro-optic Convertors for PONs 74
3.5.1 Directly Modulated Laser 76
3.5.1.1 Fabry-Perot Laser 76
3.5.1.2 Distributed Feedback (DFB) laser 77
3.5.1.3 VCSEL 77
3.5.2 External Modulator 78
3.5.2.1 RSOA/SOA Modulator 79
3.5.2.2 Electro-Absorption Modulators (EAMs) 80
3.6 Conclusion 80
4 7dB Improvements in Optical Power Budgets of 11.25Gb/s DML-Modulated Optical OFDM PON Systems 86
4.1 Introduction 87

4.2 Theoretical OOFDM System Model 88
4.2.1 OOFDM Transceivers 89
4.2.2 DML 89
4.2.3 SMF, PIN detectors and LPF 90
4.2.4 Simulation Parameters 90
4.3 Result Comparisons and Key Limiting Factor Identification 91
4.3.1 Theoretical and Experimental Result Comparisons 91
4.3.2 Key Limiting Factors Identification 94
4.4 Tunable Narrowband OBPF-enabled Performance Improvement 99
4.5 Conclusion 101
5 DML-Modulated Carrier Suppressed Single Sideband OOFDM Signal Transmission over IMDD SMF Systems for NG-PONs 104
5.1 Introduction 105
5.2 Description of the Transmission System Model 107
5.2.1 Carrier Suppressed SSB IMDD OOFDM Model 107
5.2.2 Models for DMLs, SMFs, EDFAs and PIN Detectors 108
5.2.3 Simulation Parameters 109
5.3 The Dependence of Optimum Carrier Suppression Ratio on DML Operating Conditions 109
5.4 The Transmission Performance of Carrier Suppressed SSB IMDD AMOOFDM Signals in Optimum DML-Based SMF Systems without In-line Optical Amplification ..113
5.5 Carrier Suppressed SSB IMDD OOFDM Signal Transmission in Optimum DML-Based SMF Systems Incorporating In-line Optical Amplifiers 116
5.6 Conclusions 118
6 SOA-Enabled Intensity Modulation of AMOOFDM Signals in SMF-based IMDD Systems for WDM-PONs 121
6.1 Introduction 122
6.2 Transmission System Models 124
6.2.1 Transmission System and AMOOFDM Models 124
6.2.2 SOA-based Intensity Modulator Model 124
6.2.3 Models for SMF and PIN Detector 127
6.2.4 Simulation Parameters 127
6.3 Simulated Transmission Performance 128
6.3.1 SOA Gain Saturation Characteristics 128

6.3.2 Impact of SOA Bias Current and Optical Input Power....130
6.3.3 Impact of PTPs of Driving Currents....133
6.3.4 Optimized AMOOFDM Transmission Performance and its Physical Limitations....134
6.4 Performance Robustness....138
6.4.1 Robustness to SOA Saturation Energy....138
6.4.2 Robustness to Cavity Length....139
6.5 Conclusions....140
7 Colourless AMOOFDM Transmitters for WDM-PONs using SOAs as Intensity Modulators....144
7.1 Introduction....145
7.2 Transmission System Models....146
7.2.1 Transmission System and AMOOFDM Models....146
7.2.2 SOA Intensity Modulator Model....147
7.2.3 Models for SMF and PIN Detector....150
7.2.4 Simulation Parameters....151
7.3 SOA Characteristics....151
7.4 Transmission Performance of SOA Modulated AMOOFDM Signals....153
7.4.1 Wavelength Dependent Transmission Performance....153
7.4.2 Optimum SOA Operating Conditions for Different Wavelengths....156
7.4.3 Capacity versus Reach Performance under Optimum SOA Operating Conditions....159
7.5 Conclusions....159
8 AMOOFDM Modems Incorporating RSOAs as Intensity Modulators for WDM-PONs....162
8.1 Introduction....163
8.2 Transmission System Models....165
8.2.1 Transmission System and AMOOFDM Modems....165
8.2.2 RSOA Intensity Modulator Models....166
8.2.3 SMF and PIN Models....169
8.2.4 Simulation Parameters....169
8.3 Optical Gain Characteristics of RSOAs....170
8.4 Optimization of RSOA Operating Conditions....172
8.4.1 Optical Input Power and Bias Current Optimization....172

8.4.2 Optimization of Driving Current PTP.....174
8.4.3 Capacity versus Reach Performance.....175
8.5 Transmission Performance under Low-cost Optical Component-Enabled Practical Operating Conditions.....176
8.5.1 Verification of the RSOA Intensity Modulator Model.....177
8.5.2 Optical Input Power and Rear-facet Reflectivity Dependent Transmission Performance.....179
8.5.3 Capacity versus Reach Performance.....181
8.5.4 Impact of Negative Frequency Chirp.....182
8.6 Conclusions.....183
9 Wavelength Reused Bidirectional Transmission of AMOOFDM Signals in Colourless WDM-PONs Incorporating SOA and RSOA Intensity Modulators.....186
9.1 Introduction.....187
9.2 Theoretical Models.....188
9.2.1 Wavelength-reused Bidirectional Transmission WDM-PON Architecture and AMOOFDM Modems Incorporating SOA and RSOA Intensity Modulators.....188
9.2.2 SOA/RSOA Intensity Modulators.....190
9.2.3 RB Noise.....190
9.2.4 SMF and PIN Detector Models.....193
9.2.5 Simulation Parameters.....193
9.3 Transmission Performance.....194
9.3.1 Verification of the RB Models.....194
9.3.2 Downstream AMOOFDM Transmission Performance.....195
9.3.3 Upstream AMOOFDM Transmission Performance and Optimization of RSOA Intensity Modulator Operating Conditions.....196
9.4 SSB-SCM for Improving the Downstream and Upstream Transmission Performance 200
9.5 Conclusions.....203
10 Conclusions and Future Work.....206
10.1 Conclusions.....206
10.2 Future Work.....209
APPENDIX.....213
I. CONTRIBUTIONS TO PATENTS.....213
II. LIST OF PUBLICATIONS.....213

II-1. Journal Publications 213
II-2. Conference Contributions 215

1 Introduction

Communications have been steadily and deeply changing every aspect of our daily lives. Now, most people are directly dependent on one or more of its many facets for the efficient execution of their work, at home and in leisure. From a simple call to family, an e-mail connection with partners, to a more sophisticated on-line video chat with friends, it comes easier and easier to obtain more information from every corner of the world anytime thanks to the emergence of various communication technologies over the past few hundred years, and especially over the last decade.

The evolution of communications exhibits endless pursuit of larger bandwidths, longer distances and better quality of services. Nowadays, the high bandwidth demand arises from the rapid increase in Internet Protocol (IP) traffic and newly emerging applications such as IP Television (IPTV), Video-on-Demand (VoD) and video surveillance. Such a continuous growth of bandwidth demand places great pressures on the network infrastructures at every scale, from core to metro, access networks and even in-building networks. Present core networks have an amazing transmission capacity of 100 Pbit/s-km, which is equivalent to 400 DVDs per second over 7000km transoceanic cable according to Alcatel-Lucent Bell Labs, Sep. 2009 [1.1]. For such application scenarios, sophisticated and expensive solutions are often employed to ensure the capacity, quality and resilience needed for the networks.

In access networks, however, the presence of legacy copper pairs/cables in the home forces operators to improve their capacities by using advanced techniques such as Digital Subscriber Line (DSL) and Hybrid Fibre Coaxial (HFC). The best achievable DSL performance is symmetric 100Mbit/s transmission over 300m copper cable by using the Very fast data rate DSL2 (VDSL2: G.933.2) technique. Nevertheless, the copper cable is approaching its fundamental physical limits. This imposes a bottleneck between the end user and core network, thus limits the end users' ability to make full use of the huge capacity available in the core networks. Not surprisingly, the penetration of optical fibre directly to the home, referred to as Fibre to the Home (FTTH) or more generally FTTx (x can be H for home, B for building, and C for curb), has undergone a rapid mass

deployment to offer "future-proof" cost-effective solutions for access networks. This is because optical fibre offers potentially high and upgradable bandwidth.

Today, FTTx is in its adolescence. According to the IDATE report [1.2], in the middle of 2009 the number of FTTx subscribers around the world had reached over 54.3 million, with Asia leading the way (43.19 million representing 77.5% of global FTTx subscribers). North America and Europe came second and third (6.39 million and 4.7million subscribers, respectively). On the business side of the equation, Asian carriers have been the most active in terms of rolling out and marketing very high-speed offers, with NTT (Japan), China Telecom and KT (South Korea) being in the top 3 ranking. Moreover, the top ranking FTTx vendors are mostly from Asia with Chinese vendors ZTE and Huawei leading the global market. The strong growth momentum in Asia is remarkably accelerating the global FTTx market. It was predicted that the number of global FTTx subscribers will reach 114.4 million in 2014 with a steady average annual increase of 21% to 23%, showing a huge potential for FTTx market.

The Passive Optical Network (PON) is an attractive technology for realizing FTTx, as no active components are involved in the outside fibre plants. Currently, there are two main variants of PON technologies: Ethernet PON (EPON: IEEE standard 802.3ah) and Gigabit PON (GPON: ITU standard G.984 series). EPON is by far the most popular FTTx technology (representing 60% of the global market in 2008) and is used almost exclusively in Asia Pacific countries including Japan, South Korea and China due to its lower cost and high volume compared to GPON. While GPON is gaining momentum mainly in North America and Europe. EPON supports a symmetric bit rate of 1.25Gb/s while GPON provides 2.5Gb/s downstream and 1.25Gb/s upstream. Such bandwidths are usually shared by 32 (64 for GPON) subscribers. Consequently, a maximum downstream speed of ~30Mb/s is available for each subscriber. This speed, however, will soon reach its limit with the continuing increase in bandwidth requirement from individual and business users. Therefore, further upgrading of the current PONs has to be considered.

Indeed, IEEE and Full Service Access Networks (FSAN)/ITU-T have started the standardization work of Next Generation PON (NG-PON) targeting 10Gb/s. The IEEE 10G-EPON standard (802.3av) had already been completed in September 2009, which provides two solutions: asymmetric 10G/1G for co-existence with current 1G-EPONs and symmetric 10G/10G. The FSAN/ITU-T 10G-PON standard (G.987) is still under

discussion, offering mid-term solutions of 10G/2.5G and 10G/10G and even higher data rate for long-term solutions. The long-term solution allows the consideration of a number of emergent candidate technologies such as Wavelength Division Multiplexing (WDM) and Orthogonal Frequency Division Multiplexing (OFDM).

From the operator's point of view, cost-effectiveness is the highest priority for the deployment of NG-PONs in future, i.e., keeping the cost per bit as low as possible. Generally, the main costs involved in PONs are the costs of the electro-optic converters and other specific components. It is also greatly beneficial if the cost can be shared between as many subscribers as possible. Therefore, potential candidate technologies for NG-PONs need to have several critical features:

- Tolerance of low-cost optoelectronic components.
- Higher spectral efficiency and better tolerance to fibre dispersion, in comparison with conventional techniques used in current EPON/GPON networks.
- Improved transmission performance with an increased power split ratio and reach. This delivers services to more subscribers from potentially fewer Central Offices (COs) situated further apart geographically, leading to a reduction in power consumption and maintenance cost.
- Compatibility with the already deployed PON infrastructures. NG-PONs adopting WDM or WDM/Time Division Multiplexing (TDM) architectures allow not only accommodation of more subscribers but also compatibility with the installed PONs without significant changes.

Recently, as an advanced modulation technique that can fully use mature Digital Signal Processing (DSP), since its first proposal in 2005 [1.3], Optical OFDM (OOFDM) has been intensively investigated and demonstrated in optical fibre communication systems by industrial and academic sectors. OOFDM is also a strong candidate for NG-PONs for increasing the transmission capacity and reach without requiring high quality expensive optoelectronic components [1.4]. This is because OOFDM inherently has strong dispersion tolerance and significant system robustness, and is capable of offering, hybrid (in both the frequency and time domains) dynamic allocation of broad bandwidth among various end-users [1.4]. Moreover, OOFDM also offers the functionality of adaptive data rate to adapt the channel conditions via adjusting the modulation format taken on each individual subcarrier. This is referred to as Adaptively Modulated OOFDM (AMOOFDM) [1.5].

Such ability significantly enhances not only the networks' flexibility but also their compatibility with existing PONs, allowing transparent support for legacy services.

Generally speaking, OOFDM falls into two categories: Coherent Optical OFDM (CO-OFDM) [1.6,1.7] and Intensity Modulation and Direct-Detection OOFDM (IMDD OOFDM). Recently, 1-Tb/s CO-OFDM with a spectral efficiency of 3.3 bit/s/Hz has successfully been demonstrated over 600-km Standard Single-Mode Fibres (SSMFs) without Raman amplification or dispersion compensation [1.7]. However, CO-OFDM requires very expensive, complex and bulky equipment for signal generation and detection [1.4], thus this limits the CO-OFDM applications to long-haul transmission systems. In contrast, IMDD OOFDM uses simple signal generation and detection techniques, thus largely reduces the system complexity and subsequently improves the system cost-effectiveness. Therefore, IMDD OOFDM is more preferable to CO-OFDM for cost-sensitive application scenarios such as Multi-Mode Fibre (MMF)-based Local Area Networks (LANs) [1.3], SMF-based access networks [1.4,1.5,1.8-1.13], and Metropolitan Area Networks (MANs) [1.4,1.14,1.15]. Using low-cost, off-the-shelf optoelectronic components, the world first real-time end-to-end OOFDM transceivers over IMDD MMF systems had been successfully demonstrated by 2009 [1.16], and the highest ever 11.25 Gb/s over 25km SMF real-time end-to-end transmission performance had also been achieved [1.17], indicating great potential of OOFDM for the practical applications in PONs.

As the commercially deployed FTTx networks are overwhelmingly based on IMDD SMF links, IMDD OOFDM is therefore a natural choice for NG-PONs. In IMDD OOFDM NG-PONs, intensity modulators play critical roles in determining the system performance and cost. In addition, for WDM-PONs, to achieve cost-effectiveness, colourless (wavelength insensitive) intensity modulators are preferred. However, conventional intensity modulators have relatively strong nonlinear effects which lead to distortions on the modulated OOFDM signals. Therefore, investigations of low-cost intensity modulators with improved performance are important for maximizing the system performance.

The widely used optical intensity modulators for PONs include Directly Modulated DFB Lasers (DMLs) [1.5,1.18], Semiconductor Optical Amplifiers (SOAs)/Reflective SOAs (RSOAs) [1.8-1.13,1.19,1.20], injection-locked Fabry-Perot Laser Diodes (F-P LDs) [1.21], reflective Electro-Absorption Modulators (EAMs) integrated with SOAs [1.22], and

Vertical Cavity Surface Emitting Lasers (VCSELs) [1.23]. Among these modulators, DMLs and SOAs/RSOAs are, respectively, the most widely implemented components for EPONs/GPONs currently deployed and for WDM-PONs, as DMLs eliminate the need for an external light source thus offering highly cost-effective solutions. On the other hand, SOAs/RSOAs have strong capability of monolithic integration with electrical components and wide wavelength coverage of typically >100nm which enables colourless transmitters for WDM-PONs.

IMDD OOFDM systems using DMLs and SOAs/RSOAs as intensity modulators provide promising solutions for NG-PONs. In the meantime, these proposed solutions also bring about a number of challenges including: 1) accurate theoretical component and system models to describe accurately the generation, detection, and recovery of the DML- and SOA/RSOA-intensity modulated OOFDM signals; 2) identification of underlying physical mechanisms limiting the system data rate, transmission distance and optical power budgets of DML-modulated OOFDM PONs; and the proposal of effective approaches for alleviating these effects; 3) predictions of maximum transmission performances of SOA/RSOA-modulated OOFDM WDM-PONs and the major physical limiting factors; 4) the feasibility of achieving colourless OOFDM signal transmissions using SOA/RSOA intensity modulators; 5) comparisons between SOAs and RSOAs to identify a great diversity of RSOA and/or SOA intensity modulators in AMOOFDM WDM-PONs; and 6) the feasibility of full use of SOA and RSOA intensity modulators to realize wavelength reused bidirectional AMOOFDM signal transmission in colourless WDM-PONs, with improved cost-effectiveness and wavelength control functionality.

The research work reported in this thesis addresses the abovementioned issues.

1.1 Major Achievements in this Dissertation

To deal with the challenges outlined above, the dissertation research work has been carried out to investigate the transmission performance of OOFDM signals over IMDD SMF systems using both DMLs and SOAs/RSOAs as intensity modulators. The major achievements of the research work are summarized as follows:

- **7dB optical power budget improvements in 11.25Gb/s DML-modulated OOFDM PON systems [1.24,1.25].**

  A comprehensive DML-modulated OOFDM IMDD SMF system model is developed and rigorously verified by comparisons between simulations and 11.25Gb/s real-time OOFDM transceiver measurements. Based on the model, detailed explorations are undertaken of the various physical factors on the OOFDM system performance. The low Extinction Ratio (ER) of the DML modulated OOFDM signal is identified to be the predominant factor limiting the maximum achievable optical power budget, and the subcarrier intermixing effect upon square-law photon detection in the receiver reduces the optical power budget by at least 1dB. The use of a 0.02nm bandwidth optical Gaussian bandpass filter in the transmitter with a 0.01nm wavelength offset with respect to the optical carrier wavelength can enhance the OOFDM signal ER by approximately 1.24dB, thus resulting in a 7dB optical power budget improvement at a total channel BER of 1×10^{-3}. This work is detailed in Chapter 4.

- **DML-modulated carrier suppressed Single Sideband (SSB) OOFDM system for NG-PONs with extended reach [1.15].**

  A DML-modulated carrier suppressed SSB OOFDM IMDD SMF system is proposed to mitigate the subcarrier intermixing upon square-law detection for NG-PONs. The carrier suppression is optimized under various DML operating conditions, based on which 30Gb/s carrier suppressed SSB OOFDM signal transmission over 80km SMF without in-line optical amplification and dispersion compensation is achievable, which doubles the performance corresponding to the Double Sideband (DSB) OOFDM signals without carrier suppression. In addition, 10Gb/s over 1200km SMF incorporating in-line Erbium Doped Fibre Amplifiers (EDFAs) is also feasible, which is robust to variations in DML operating condition and optical input power. This work is detailed in Chapter 5.

- **30Gb/s over 80km SMF transmission of AMOOFDM signals by using SOA intensity modulators [1.8].**

A theoretical model describing the characteristics of a SOA intensity modulator is developed, based on which optimum SOA operating conditions are identified. Results show that the optimized SOA-based intensity modulators can support 30Gb/s AMOOFDM signal transmission over a 80km SMF, which doubles the transmission performance obtained using DMLs. In addition, excellent robustness of the optimum operating conditions and the transmission performance to variations in SOA parameters is also obtained. This work is detailed in Chapter 6.

- **SOA-enabled 30Gb/s colourless AMOOFDM signal transmissions over 60km SMF within a wavelength range of 1510nm-1590nm for WDM-PONs** [1.9,1.10].

  A theoretical model describing both optical gain saturation and gain spectral characteristics of SOA intensity modulators is developed, based on which optimum SOA operating conditions are identified for various wavelengths within a broad range of 1510nm-1590nm. It is shown that SOA intensity modulators operating at the identified optimum operating conditions are capable of achieving colourless AMOOFDM transmission. In addition, results also indicate that it is feasible to transmit >30Gb/s AMOOFDM signals over 60km SMFs within the aforementioned wavelength window. This work is detailed in Chapter 7.

- **AMOOFDM modems incorporating RSOAs as intensity modulators for WDM-PONs** [1.11,1.17,1.19,1.20].

  A comprehensive theoretical model describing the dynamic characteristics of RSOA intensity modulators is developed, taking into account counter-propagation of the forward and backward optical signals and the rear-facet reflectivity in the waveguide. Special attention is also given to performance comparisons between RSOA and SOA intensity modulators. Optimum RSOA operating conditions are identified, which are independent of RSOA rear-facet reflectivity and support 30Gb/s over 60km SMF transmission. This optimum performance is similar to those corresponding to SOAs. Whilst under low-cost optical component-enabled practical operating conditions, RSOA intensity modulators considerably outperform SOA intensity modulators in transmission performance, which decreases significantly with reducing RSOA rear-facet reflectivity and optical input power. In addition, for low optical input powers, it is shown that use can be made of the

RSOA/SOA intensity modulation-induced negative frequency chirp to improve the AMOOFDM transmission performance in IMDD SMF systems. This work is detailed in Chapter 8.

- **Wavelength reused bidirectional transmission of AMOOFDM signals in WDM-PONs incorporating SOA and RSOA intensity modulators** [1.12,1.26,1.27].

A comprehensive theoretical model describing the performance of a wavelength reused bidirectional AMOOFDM WDM-PON network architecture is developed, taking into account the dynamic optical characteristics of the SOA and RSOA intensity modulators as well as the effects of Raleigh Backscattering (RB) noise and crosstalk. It is shown that the RB noise effect and the residual downstream optical signal-induced crosstalk are the dominant factors limiting the maximum achievable downstream and upstream transmission performances. Under optimum SOA and RSOA operating conditions as well as practical downstream and upstream optical launch powers, 10Gb/s downstream and 6Gb/s upstream over 40km SMF transmission of conventional DSB AMOOFDM signals are feasible. In particular, the aforementioned transmission performances can be improved to 23Gb/s downstream and 8Gb/s upstream over 40 km SMF when SSB-Subcarrier Modulation (SSB-SCM) is introduced in the downstream systems. This work is detailed in Chapter 9.

The above-mentioned work has resulted in the publication of 6 papers in world-leading journals [1.8,1.9,1.11,1.12,1.15,1.24] and 7 papers in national/international conferences [1.10,1.19,1.25-1.29] including the world-leading conferences such as OFC and ECOC. These papers have been completed by the author of this thesis and form the major contents of this dissertation work. Apart from that, the author also contributed to other 7 journal papers and 7 conference papers that have been published by other people in the same research group in Bangor University (see Appendix: II. List of Publications). Even these co-authored papers are tightly related to this thesis [1.17,1.20,1.30-1.32], they are, however, not discussed in detail in the thesis.

It should also be noted that the author of this thesis involved in Bangor University's experimental demonstration of end-to-end real-time OOFDM systems

[1.17,1.20,1.30,1.32] in terms of the following aspects: a) the provision of an in-depth understanding of various physical mechanisms limiting the maximum achievable system performance. Such understanding is critical for system optimization in the optical domain in experiment; b) direct involvements of a number of experimental activities. The outputs of those activities have been published [1.17,1.20,1.30,1.32], but they are not reported in this thesis; c) After the PhD dissertation research, the author will be undertaking experimental research to verify the feasibility of using the novel techniques proposed in the thesis in practical systems.

1.2 Thesis Structure

The thesis comprises 10 chapters. Chapter 2 and 3 presents review work and Chapter 4 to 9 detail research results. These chapters are outlined as followings.

Chapter 1: This chapter provides a brief introduction of the research work and its major achievements.

Chapter 2: To gain a better understanding of OOFDM, this chapter deals with the principles of OFDM and OOFDM. The history of OFDM and the fundamentals of key components involved in a general OFDM system are described. SMF together with its linear and nonlinear effects is also presented, followed by discussions on two main variants of OOFDM including CO-OFDM and IMDD OOFDM, whose advantages and drawbacks are also discussed. In addition, this chapter also details AMOOFDM systems.

Chapter 3: This chapter presents fundamental principles and evolution of PONs. Various access network architectures are first overviewed. As promising access network technologies, IEEE EPON and ITU BPON/GPON together with the corresponding standards (802.3ah and G.983/G.984) are discussed, followed by the review of 10G-EPON standard 802.3av and the current status of ITU XPON and NG-PON2 standard draft G.987. Various promising architectures for NG-PON2 such as WDM-PON, hybrid WDM/TDM PON, and OOFDM PON are discussed in terms of their principles as well as strengthens and limitations. The chapter finally examines the figure of merits and defects of various optical modulators employed in current PONs.

Chapter 4: By using DML modulators in OOFDM PON systems as described in previous chapters, 11.25Gb/s over 25km SMF has been successfully demonstrated using real-time OOFDM transceiver [1.17]. However, the optical power budgets of ~20dB obtained in the real-time OOFDM systems may not satisfy the requirements for NG-PONs. To address this challenge, this chapter explores the fundamental physical mechanisms that affect the achievable optical power budget of such systems. It is identified that the low Extinction Ratio (ER) of the DML-modulated OOFDM signal is the predominant factor limiting the achievable optical power budget. The use of a wavelength-offset narrowband optical bandpass filter in the transmitter is proposed to improve the OOFDM signal ER by 1.24dB and thus system optical power budget by 7dB.

Chapter 5: Base on the analyses in Chapter 4, this chapter proposes a carrier suppressed Single Sideband (SSB) technique to realize DML-modulated (AM)OOFDM PONs with extended reach. This chapter answers three major questions regarding this novel technique: 1) what are the influences of DML operating conditions and fibre optical input powers on the optimum carrier suppression ratio; 2) what are the advantages of this technique compared to DSB AMOOFDM signal system without carrier suppression; and 3) what is the maximum achievable transmission distance for the proposed optimally carrier suppressed SSB OOFDM signal transmission over SMF links involving in-line EDFAs.

Chapter 6: Having explored DML-modulated OOFDM PON systems in Chapters 4-5, this chapter investigates the feasibility of using SOAs as intensity modulators in IMDD AMOOFDM SMF WDM-PON systems. This chapter covers the development of a theoretical model for describing the characteristics of the SOA intensity modulators, optimisation of the SOA operating conditions, identification of the key physical mechanisms determining the achievable transmission performance, and examination of the system robustness on the variation of SOA parameters.

Chapter 7: As the performance of SOA-modulated AMOOFDM WDM-PON systems at a fixed wavelength of 1550nm is explored in Chapter 6, Chapter 7 extends the topic by investigating the wavelength dependent transmission performance of SOA intensity-modulated AMOOFDM signals within a broad wavelength range of 1510nm-1590nm. Results show that, under identical SOA operating conditions, the system performance is highly dependent on the wavelength and optical input power; However, by optimizing SOA operating conditions for various wavelengths in the above-mentioned wavelength

range, colourless >30Gb/s AMOOFDM signal transmissions over 60km SMF without optical amplification and dispersion compensation are feasible within the aforementioned wavelength window.

Chapter 8: As a typical type of SOAs, RSOA is also a promising candidate for AMOOFDM WDM-PONs. Experimental demonstrations of the transmission performances of RSOA intensity-modulated AMOOFDM signals for WDM-PONs have been reported [1.13,1.20]. However, several issues have not been resolved, which include: 1) The dependence of the system performance on the RSOA rear-facet reflectivity; 2) Identification of RSOA intensity modulator-associated physical mechanisms affecting significantly the system transmission performance and optimization of RSOA operating conditions; 3) Performance comparisons between RSOA and SOA intensity modulators; and 4) the feasibility of using the RSOA/SOA intensity modulation-induced frequency chirp to compensate for the chromatic dispersion of SMFs. Solving these issues forms the main task of this chapter.

Chapter 9: After thoroughly investigating the performances of RSOA/SOA intensity modulated AMOOFDM signal transmissions in WDM-PONs in Chapters 6-8, attention in Chapter 9 is dedicated to consider the network issues related to the transmission of AMOOFDM signals in the downstream and upstream. From the cost-effectiveness point of view, it is greatly beneficial if use is made of AMOOFDM in wavelength reused bidirectional transmission over one single single-mode fibre (SMF) for WDM-PONs. This chapter therefore thoroughly investigates such AMOOFDM WDM-PONs using SOA (RSOA) intensity modulators in the downstream (upstream) transmitter, where the effects of Rayleigh Backscattering (RB) and residual downstream signal-induced crosstalk are also included. The major physical factors limiting the achievable downstream/upstream performances are identified and approaches are proposed to alleviate such effects.

Finally, Chapter 10 summarizes the thesis and suggests future research work.

References

[1.1] Available at http://www.alcatel-lucent.com.

[1.2] IDATE Consulting & Research, "FTTx 2010," 2010. Available at www.idate.org

[1.3] N. E. Jolley, H. Kee, R. Rickard, J. Tang, and K. Cordina, "Generation and propagation of a 1550 nm 10 Gb/s optical orthogonal frequency division multiplexed signal over 1000 m of multimode fibre using a directly modulated DFB," Proc. OFC/NFOEC, (OSA, 2005), Paper OFP3.

[1.4] D. Qian, N. Cvijetic, J. Hu, and T. Wang "Optical OFDM Transmission in Metro/Access networks," Proc. OFC/NFOEC, (OSA, 2009), Paper OMV1.

[1.5] J. M. Tang and K. A. Shore, "30 Gb/s signal transmission over 40-km directly modulated DFB-laser-based single-mode-fibre links without optical amplification and dispersion compensation," J. Lightwave Technol., vol.24, no. 6, pp. 2318-2327, 2006.

[1.6] W. Shieh, H. Bao and Y. Tang, "Coherent optical OFDM: theory and design," Opt. Express., vol. 16, no. 2, pp. 841-859, Jan. 2008.

[1.7] Y. Ma, Q. Yang, Y. Tang, S. Chen, and W. Shieh "1-Tb/s Single-Channel Coherent Optical OFDM Transmission With Orthogonal-Band Multiplexing and Subwavelength Bandwidth Access," J. Lightwave Technol., vol. 28, no. 4, pp. 308-315 Feb. 2010.

[1.8] J. L. Wei, A. Hamié, R. P. Giddings, and J. M. Tang, "Semiconductor optical amplifier-enabled intensity modulation of adaptively modulated optical OFDM signals in SMF-based IMDD systems," J. Lightwave Technol., vol.27, no.16, pp.3679-3689, Aug. 2009.

[1.9] J. L. Wei, X. L. Yang, R.P. Giddings and J. M. Tang, "Colourless adaptively modulated optical OFDM transmitters using SOAs as intensity modulators," Opt. Express. Vol. 17, no. 11, pp. 9012-9027, May. 2009.

[1.10] J. L. Wei, X. L. Yang, R. P. Giddings, J. M. Tang and K. A. Shore, "SOA Intensity Modulator-Enabled Colourless Transmission of Adaptively Modulated Optical OFDM Signals for WDM-PONs," presented at the *14th OptoElectronics and Communications Conf.* (*OECC*), (Hongkong, China, 2009), Paper ThLP77.

[1.11] J. L. Wei, A. Hamié, R.P. Giddings, E. Hugues-Salas, X. Zheng, S. Mansoor and J. M. Tang, "Adaptively modulated optical OFDM Modems utlizing RSOAs as intensity modulators in IMDD SMF transmission systems," Opt. express, vol. 18, no. 8, pp. 8556-8573, Apr. 2010.

[1.12] J. L. Wei, E. Hugues-Salas, R.P. Giddings, X.Q. Jin, X. Zheng, S. Mansoor and J.M. Tang, "Wavelength reused bidirectional transmission of adaptively modulated optical OFDM signals in WDM-PONs incorporating SOA and RSOA intensity modulators," Opt. express, vol. 18, no. 18, pp. 9791-9808, May 2010.

[1.13] T. Duong, N. Genay, P. Chanclou, B. Charbonnier, A. Pizzinat, and R. Brenot, "Experimental demonstration of 10 Gbit/s for upstream transmission by remote modulation of 1 GHz RSOA using Adaptively Modulated Optical OFDM for WDM-PON single fiber architecture," Proc. ECOC, (Brussels, 2008), PD paper Th.3.F.1.

[1.14] B.J.C. Schmidt, Z. Zan, L.B. Du, and A.J. Lowery, "100 Gbit/s transmission using single-band direct-detection optical OFDM," Proc. OFC/NFOEC, (OSA, 2009), Paper PDPC3.

[1.15] J. L. Wei, X.Q. Jin, and J.M. Tang, "The influence of directly modulated DFB lasers on the transmission performance of carrier suppressed single sideband optical OFDM signals over IMDD SMF systems," J. Lightwave Technol. vol. 27, no. 13, pp. 2412 – 2419, July 2009.

[1.16] G. P. Giddings, X. Q. Jin, H. H. Kee, X. L. Yang, and J. M. Tang, "Real-time implementation of optical OFDM transmitters and receivers for practical end-to-end optical transmission systems," Electron. Lett. vol. 45, no.15, pp. 800-802, 2009.

[1.17] G. P. Giddings, X. Q. Jin, E. Hugues-Salas, E. Giacoumidis, J. L. Wei, and J. M. Tang, "Experimental demonstration of a record high 11.25Gb/s real-time optical

OFDM transceiver supporting 25km SMF end-to-end transmission in simple IMDD systems," Opt. Express, vol. 18, no.6, pp. 5541-5555, 2010.

[1.18] M.-F. Huang, J. Yu, D. Qian, N. Cvijetic and G. –K. Chang, "Lightwave centralized WDM-OFDM-PON network employing cost-effective directly modulated laser, " presented at the OFC/NFOEC, (San Diego, USA, 2009), Paper OMV5.

[1.19] J. L. Wei, A. Hamié, and J. M. Tang, "Optimization and Comparison of the Transmission Performance of RSOA/SOA Intensity-Modulated Optical OFDM Signals for WDM-PONs," presented at the OFC/NFOEC, (San Diego, USA, 2010), Paper JThA53.

[1.20] R.P. Giddings, E. Hugues-Salas, X.Q. Jin, J. L. Wei and J.M. Tang, "Colourless Real-Time Optical OFDM End-to-End Transmission at 7.5Gb/s over 25km SSMF Using 1GHz RSOAs for WDM-PONs," presented at the OFC/NFOEC, (San Diego, USA, 2010), Paper OMS4.

[1.21] L. Y. Chan, C. K. Chan, D.T.K Tong, F. Tong and L. K. Chen, "Upstream traffic transmitter using injection-locked Fabry-Perot laser diode as modulator for WDM access networks," Electron. Lett., vol. 38, no. 1, pp. 43-45, Jan. 2002.

[1.22] E. K. MacHale, G. Talli, P. D. Townsend, A. Borghesani, I. Lealman, D. G. Moodie, and D. W. Smith, "Extended-reach PON employing 10Gb/s integrated reflective EAM-SOA," presented at the ECOC, (Brussels, Belgium, 2008), paper Th.2.F.1.

[1.23] T.B. Gibbon, K. Prince, C. Neumeyr, E.Rönneberg, M. Ortsiefer and I. T. Moonroy, "10Gb/s 1550nm VCSEL transmission over 23.6 km Single Mode Fiber with no dispersion compensation and no injection locking for WDM PONs," presented at the *OFC/NFOEC* (OSA, 2010), Paper JThA30.

[1.24] J. L. Wei, C. Sánches, R.P. Giddings, E. Hugues-Salas, and J. M. Tang, "Significant improvements in optical power budgets of real-time optical OFDM PON systems," Opt. Express, vol. 18, no. 20, pp. 20732-20745, Sep. 2010.

[1.25] J. L. Wei, and J.M. Tang, "7dB optical power budget improvements of OOFDM PON systems using narrow optical filters,"*ACP 2010* (Shanghai,China), Paper SuI 4.

[1.26] J. L. Wei, E. Hugues-Salas, R.P. Giddings, X.Q. Jin, X. Zheng, and J.M. Tang, "Wavelength Reused Bidirectional Adaptively Modulated Optical OFDM Transmission in Colourless WDM-PONs," Proc. ECOC 2010 (Torino, Italy).

[1.27] J. L. Wei, E. Hugues-Salas, R.P. Giddings, X.Q. Jin, X. Zheng, and J.M. Tang, "Wavelength reused bidirectional transmission of adaptively modulated optical OFDM signals in SOA/RSOA intensity modulator-based WDM-PONs," in Future Network & Mobile Summit 2010(Florence,Italy),Paper 260.

[1.28] J. L. Wei, and J. M. Tang, "Improved dispersion tolerance of coherent optical OFDM signals by adaptive modulation," presented at the Semiconductor and Integrated Opto-Electronics Conf. (IEE/SIOE' 08), Cardiff, U.K., 31st, March-2nd, Apr, 2008.

[1.29] J. L. Wei, A. Hamié, and J. M. Tang, "SOA-Enabled Intensity Modulation of Adaptively Modulated Optical OFDM Signals for PONs," present at Asian-Pacific Microwave Photonics Conference (APMP 2009), Beijing, China, April. 22-24, 2009. (An invited talk)

[1.30] R. P. Giddings, E. Hugues-Salas, X. Q. Jin, J. L. Wei and J. M. Tang, "Experimental demonstration of colourless real-time optical OFDM transmission at 7.5Gb/s over 25km SSMF using a 1GHz RSOA," IEEE Photon. Technol. Lett. vol. 22, no. 11, pp. 745-747, Jun. 2010.

[1.31] X. Zheng, J. L. Wei and J.M. Tang, "Transmission performance of adaptively modulated optical OFDM modems using subcarrier modulation over SMF IMDD links for access and metropolitan area networks," Opt. Express, vol.16, no.25, pp.20427-20440, Dec. 2008.

[1.32] R.P. Giddings, E. Hugues-Salas, X.Q. Jin, J. L. Wei and J.M. Tang, "Experimental Demonstration of Colourless Real-Time End-to-End Optical OFDM Transmission at 7.5Gb/s over 25km SSMF Using a 1GHz RSOA," in Future Network & Mobile Summit 2010 (Florence,Italy), Paper 147.

2 Principles of Optical OFDM

Contents

2.1 Introduction **17**

2.2 History of OFDM 17

2.3 OFDM Fundamentals 18

2.3.1 OFDM: Special Type of FDM 18

2.3.2 OFDM Transceivers 20

2.3.2.1 Bit Encoding 21

2.3.2.2 IFFT/FFT 21

2.3.2.3 Cyclic Prefix 25

2.3.2.4 Serialization 26

2.3.2.5 DAC/ADC 26

2.3.2.6 Pilot-Assisted Channel Estimation and Equalization 28

2.3.2.7 Synchronization 29

2.4 Principles of Optical OFDM 30

2.4.1 Optical Fibres 31

2.4.1.1 Linear Fibre Effects 31

2.4.1.1.1 Fibre Loss 31

2.4.1.1.2 Rayleigh Scattering 32

2.4.1.1.3 Chromatic Dispersion 34

2.4.1.1.4 Polarization Mode Dispersion 36

2.4.1.2 Fibre Nonlinearities 37

2.4.1.2.1 SPM, XPM and FWM 37

2.4.1.2.2 SRS and SBS 39

2.4.2 Coherent Optical OFDM (CO-OFDM) 40

2.4.3 Intensity Modulation and Direct Detection Optical OFDM 43

2.4.4 Comparison between CO-OFDM and IMDD OOFDM 48

2.4.5 Adaptively Modulated OOFDM 50

2.5 Conclusion 52

2.1 Introduction

This chapter provides an introduction to the fundamentals of OFDM and OOFDM, which forms the foundation of the work presented in the remainder of this thesis.

The OFDM technique has been intensively investigated in radio frequency wireless communications for the past 20 years. Its emergence in optical communications occurred relatively late. This chapter starts with a brief summary of the history of OFDM and its applications, then detailed discussions are made of the principles of each individual building block that forms a representative OFDM system.

An understanding of OFDM in optical fibre communications requires a good knowledge of the fibre channel characteristics. Thus both linear and nonlinear fibre effects are also discussed in this chapter, together with their impairments on today's FTTx networks. This chapter presents intensive discussions of two major variants of OOFDM namely CO-OFDM and IMDD OOFDM, whose strengths and drawbacks are also addressed. Finally, the principles of Adaptively Modulated OOFDM (AMOOFDM) systems are presented.

2.2 History of OFDM

The idea of OFDM was proposed and patented by Chang in the 1960's [2.1]. Later, the generation of OFDM signals using the Discrete Fourier Transform (DFT) algorithm was proposed in 1971 [2.2]. Signal modulation and multiplexing are achieved digitally using Inverse DFT (IDFT) in the OFDM transmitter and de-modulation and de-multiplexing using DFT in the OFDM receiver. To further improve the effectiveness of mitigating Inter-Symbol Interference (ISI), the use of Cyclic Prefix (CP) in an OFDM signal was presented in 1980 [2.3]. These three aspects form the core concepts of a general OFDM system. In 1995, Telatar reported Multi-Input-Multiple-Output (MIMO) OFDM systems [2.4], which has fuelled a new research era on OFDM. In 2001, another research wave on OFDM for optical wireless [2.5] started beginning the merging of optical and wireless access networks.

In parallel to the intensive research on OFDM, from the mid-1980s, the practical applications of OFDM also started in mobile communication systems [2.6], where the use of Forward Error Correction (FEC) was proposed and combined with OFDM. Owing to this reason, OFDM is also referred to as coded OFDM. To date, there has been a tremendous number of wireless standards incorporating OFDM as a modulation technique, such as wireless LANs (WiFi; IEEE 802.11a/g), wireless MANs (WiMAX; 802.16e), and Long-Term Evolution (LTE) – the 4G mobile communication technology [2.7]. OFDM has also been implemented in standards of cable-based transmission systems such as Asymmetric Digital Subscriber Loop (ADSL; ITU G.992.1), Digital Audio Broadcasting (DAB) [European Telecommunications Standards Institute (ETSI): DAB Eureka 147] [2.8] and Digital Video Broadcasting (DVB) (ETSI: DVB-T, DVB-H) [2.9].

The application of OFDM in optical communications occurred much later compared to its Radio Frequency (RF) counterpart. Since the first proposal of OOFDM in 2005 [2.10], it has fuelled an explosive increase of interest in simulations and experimental demonstrations of OOFDM systems. Various OOFDM systems have been explored including OOFDM in Radio over Fibre (RoF) [2.5,2.11,2.12], OOFDM over Plastic Optical Fibre (POF) systems [2.13], OOFDM for MMF-based LANs [2.6,2.14], and OOFDM for access networks and MANs using SMFs [2.15-2.17], as well as long-haul transmission systems [2.17-2.21]. It is envisioned that the standardizations of OOFDM transport at 100Gb Ethernet (100GbE) and beyond would be available in the near future due to its profound impact on optical networks [2.22].

2.3 OFDM Fundamentals

2.3.1 OFDM: Special Type of FDM

As OFDM is a special type of Frequency-Division Multiplexing (FDM) technique, descriptions are, therefore, first made of FDM. The basic idea of FDM is to transmit multiple signals simultaneously over a wideband channel by modulating the signals onto several subcarriers and multiplexing the modulated different subcarriers [2.23], as shown in Fig. 2.1. The FDM transmitter uses an oscillator array operating at different frequencies with a sufficiently wide inter-channel guard between two adjacent subcarrier frequencies, which is illustrated in Fig. 2.2(a). Each subcarrier is modulated separately by a classical

modulation format such as M-ary Quadrature Amplitude Modulation (QAM) or Phase Shift Keying (PSK). In the receiver end, different subcarrier signals are filtered by Bandpass Filters (BPFs) and demodulated by oscillators in the receiver.

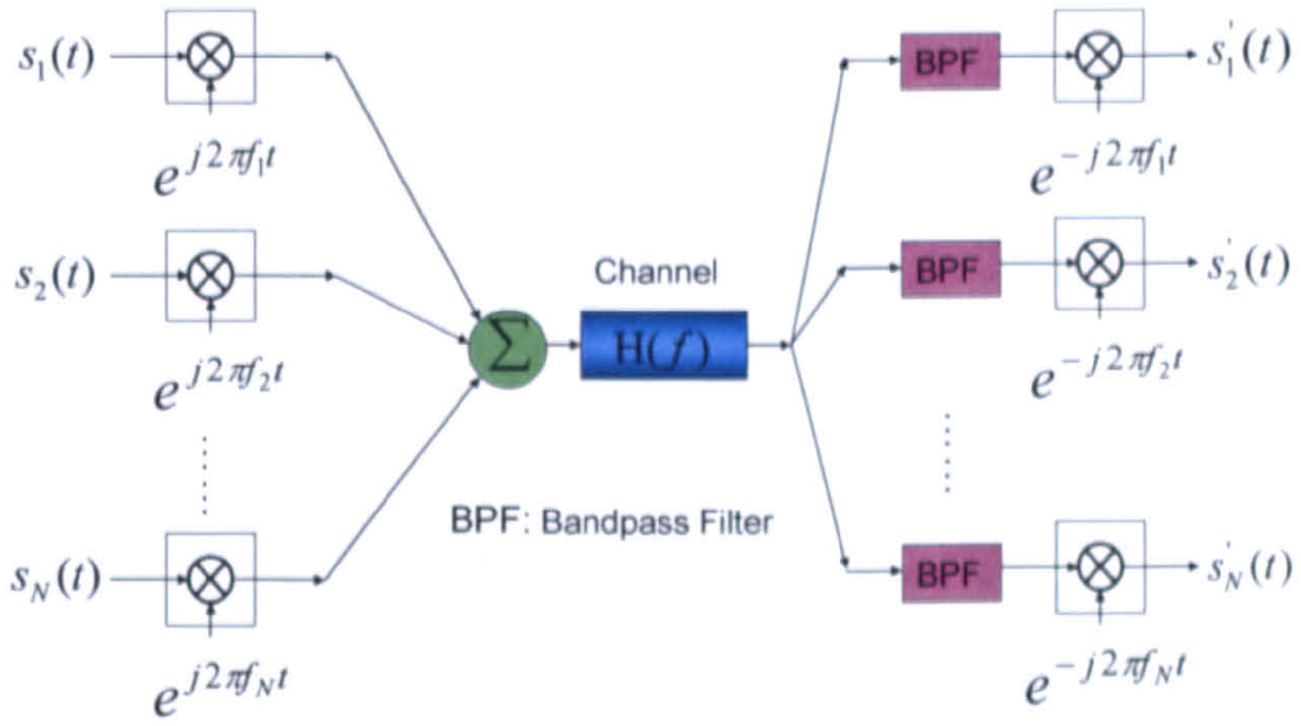

Fig. 2.1 Diagram for a generic FDM system.

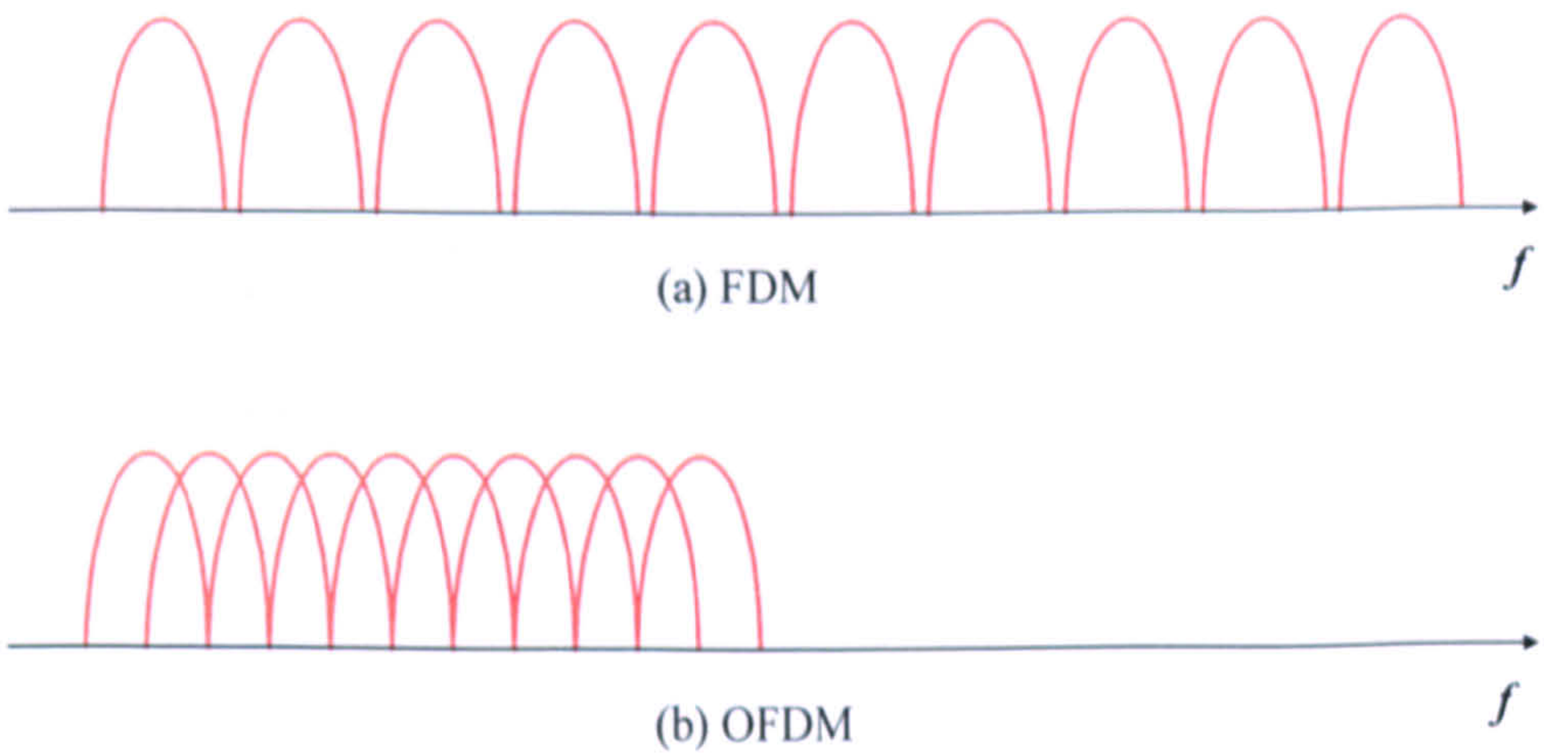

Fig. 2.2 Spectra of (a)FDM, and (b) OFDM.

Compared to FDM, OFDM precisely chooses the inter-subcarrier frequency spacing to ensure orthogonality between subcarriers, as shown in Fig. 2.2(b), so that the demodulator for one subcarrier is independent on others even though spectral overlap occurs between subcarriers. Clearly, OFDM offers significant enhancement in spectral efficiency (at least 50%) compared to FDM. On the other hand, thanks to the advances of DSP technologies, the modulation/multiplexing and de-modulation/de-multiplexing in the OFDM system can be realized by efficient Inverse Fast Fourier Transform (IFFT) and FFT, respectively. Therefore, in comparison with FDM, the OFDM systems are relatively simple, as a large number of modulators, receiver filters and demodulators required in the FDM system are

not necessary. Moreover, OFDM also has an advantage of combating frequency-selective fading effect caused by wireline or wireless channels.

2.3.2 OFDM Transceivers

A general OFDM system is composed of a transmitter, a transmission link, and a receiver, which is depicted in Fig. 2.3. The DSP in the OFDM transmitter consists of bit encoding, IFFT, Cyclic Prefix (CP) insertion, and data serialization. The generated digital signal is converted to the analog signal in a Digital-to-Analog Converter (DAC).

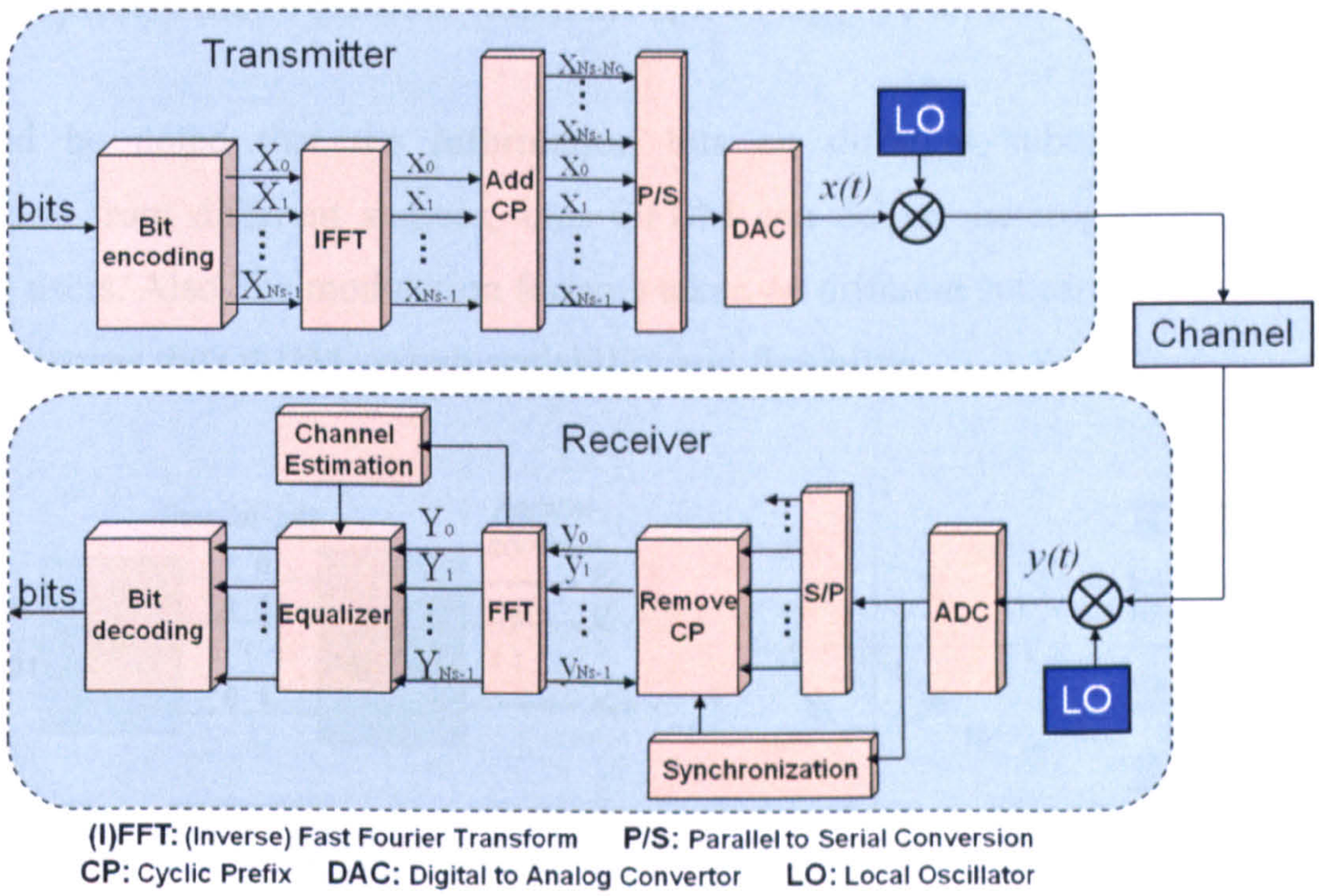

Fig. 2.3 Conceptual diagram for the OFDM transmitter and receiver as well as transmission channel

The electrical analog OFDM signal is then up-converted and transmitted through the transmission channel. The received OFDM signal is down-converted, synchronized, and then processed by the OFDM receiver signal processing procedure, which is the inverse of the transmitter as discussed above. In addition, channel estimation and equalization are performed after FFT and prior to bit decoding in the receiver.

Detailed discussions of the above-mentioned key procedures are presented in the following sections.

2.3.2.1 Bit Encoding

The bit encoding process is to map information bits into signal constellation points, as illustrated in Fig. 2.4. A serial bit stream is first converted into parallel bits corresponding to each subcarrier, and then encoded to complex numbers using a specific signal modulation format. Fig. 2.4 (b) shows two examples of multi-level modulation formats namely Quadrature PSK (QPSK) and 16-QAM. In QPSK the signal phase is keyed between four possible values (45°, 135°, 225° and 315°) to represent the four possible variations of a two-bit set. Whilst in 16-QAM both the signal amplitude and phase are keyed to represent the 16 possible variations of a 4 ($\log_2 16$)-bit set.

It should be noted that the information bits on different subcarriers may convey information from different sources, thus OFDM can deliver heterogeneous services for different users. Also, the modulation formats taken on different subcarriers can be different, which improves the OFDM system scalability and flexibility.

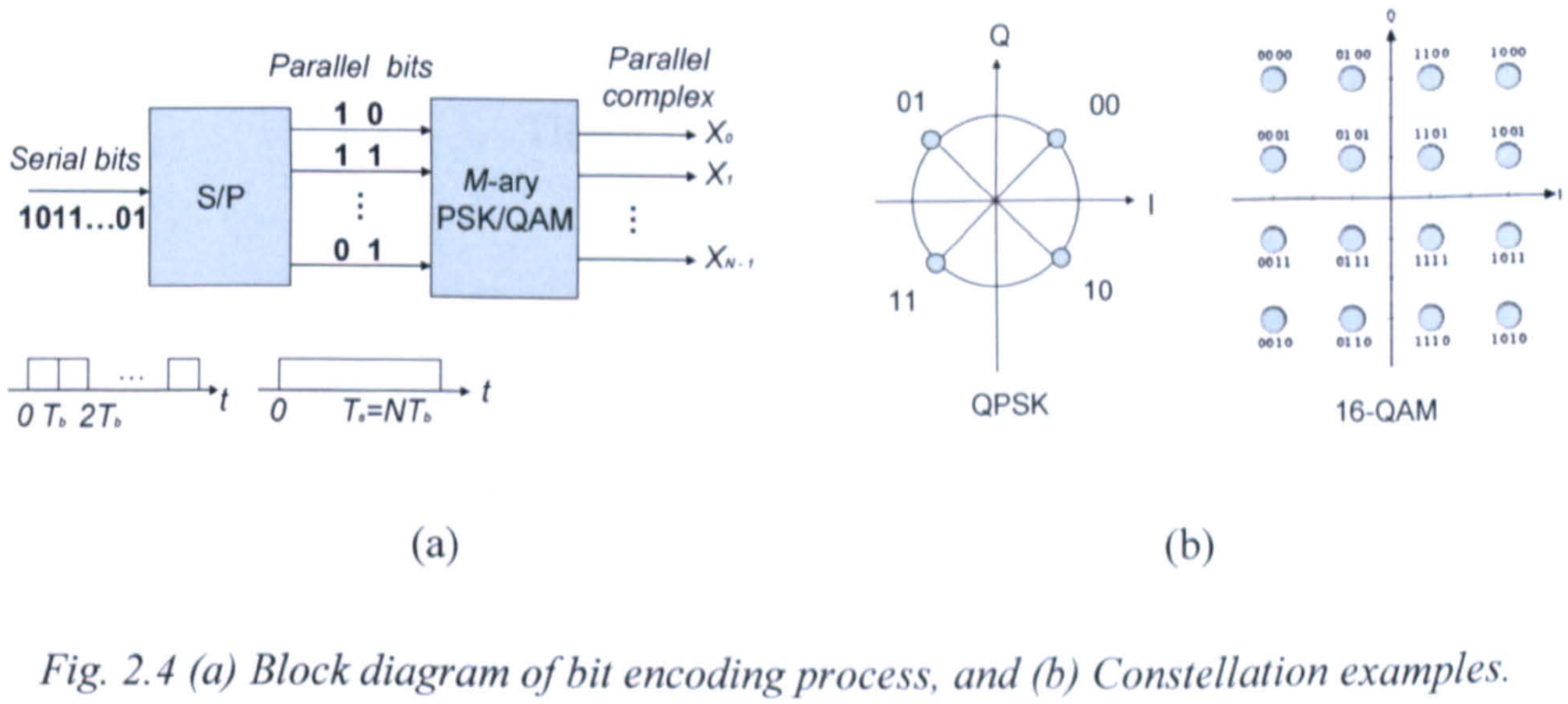

Fig. 2.4 (a) Block diagram of bit encoding process, and (b) Constellation examples.

2.3.2.2 IFFT/FFT

The encoded complex number via bit encoding needs to be up-converted to a RF subcarrier frequency and then multiplexed with other subcarriers. As mentioned in subsection 2.2, IDFT (DFT) is the core component in the transmitter (receiver) to perform the functionalities of modulation (demodulation) and multiplexing (de-multiplexing). The IDFT is defined by [2.24]

$$x(l) = \frac{1}{\sqrt{N}} \sum_{k=0}^{N-1} X(k) e^{j2\pi k \frac{l}{N}} \tag{2.1}$$

According to the discussions made in subsection 2.3.2.1, the encoded complex number of the k-th subcarrier in the n-th OFDM symbol $X_{k,n}$ can be written as

$$X_{k,n} = A_{k,n} e^{j\theta_{k,n}} \tag{2.2}$$

where $A_{k,n}$ and $\theta_{k,n}$ are the amplitude and phase of the signal constellation points. $X_{k,n}$ may not necessarily to be user information, it can also represent pilot and training signals. The k-th subcarrier waveform can be modulated independently with data $X_{k,n}$. The k-th subcarrier waveform within the n-th symbol period can be expressed as

$$x_{k,n}(t) = X_{k,n} \Pi(t - nT_s) e^{j2\pi f_k t}, \quad k=0,1,2,\ldots,N_s\text{-}1 \tag{2.3}$$

$$\Pi(t) = \begin{cases} 1, & t \in [0, T_s] \\ 0, & t \notin [0, T_s] \end{cases} \tag{2.4}$$

where N_s is the number of subcarriers, f_k is the k-th RF subcarrier frequency, T_s is the OFDM symbol period, and $\Pi(t)$ has a rectangular pulse shape of unity magnitude over the time duration of T_s. Therefore, each subcarrier spectrum has a *sinc* form (Fig. 2.5). When $X_{k,n}$ is treated as unit for simplicity, the correlation between any two subcarriers in the n-th symbol period is given by

$$\frac{1}{T_s} \int_{(n-1)T_s}^{nT_s} x_{k,n}(t) x_{l,n}^*(t) dt = e^{j2\pi(f_k - f_l)} \frac{\sin(\pi(f_k - f_l)T_s)}{\pi(f_k - f_l)T_s} \tag{2.5}$$

When the subcarrier frequency spacing satisfies

$$\Delta f = f_k - f_{k-1} = \frac{1}{T_s}, \qquad k = 1, 2, 3, \ldots, N_s\text{-}1 \tag{2.6}$$

Eq. (2.5) can be further expressed as

$$\frac{1}{T_s}\int_{(n-1)T_s}^{nT_s} x_{k,n}(t)x_{l,n}^{*}(t)dt = e^{j2\pi(k-l)/T_s}\frac{\sin(\pi(k-l))}{\pi(k-l)} = \begin{cases} 0, & k \neq l \\ 1, & k = l \end{cases} \tag{2.7}$$

Eq. (2.7) shows that mutual orthogonality between subcarriers is achieved, when subcarrier frequency spacing and symbol period satisfy Eq. (2.6). By combining Eqs. (2.3)-(2.4) and Eq. (2.6), the expression of OFDM signal associated with the k-th subcarrier within the time duration of $[(n-1)T_s, nT_s]$ is given by

$$x_{k,n}(t) = X_{k,n}e^{j2\pi\frac{k}{T_s}t} \tag{2.8}$$

It shows in Eq. (2.8) that each subcarrier waveform has an integer number of cycles within one OFDM symbol period T_s, and the number of cycles grows with the subcarrier index. Fig. 2.5(a) gives an example of the time-domain waveforms containing four subcarriers. Meanwhile, due to the rectangular pulse shape of the encoded subcarrier data $X_{k,n}$, the corresponding subcarrier spectra are *sinc* functions with a spacing of Δf, as shown in Fig. 2.5(b). Orthogonality is also maintained in the frequency domain by the way that the *sinc* function for one subcarrier has a zero at the centre of others. Thus no Inter-Carrier Interference (ICI) occurs between different subcarriers even when their spectra are overlapped.

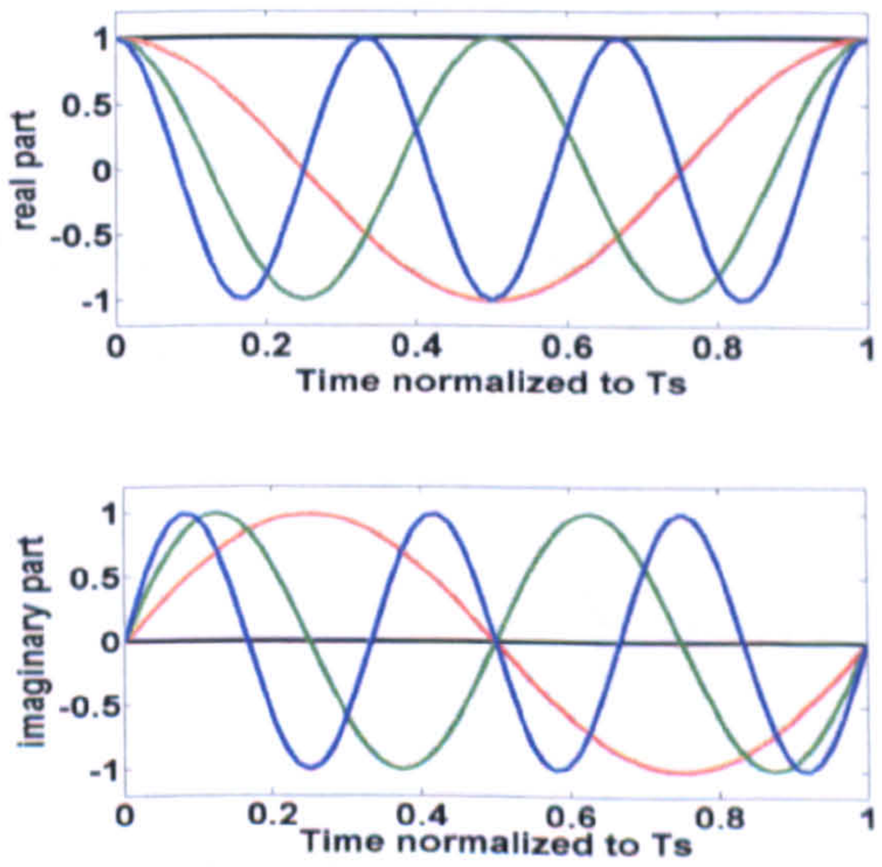

Fig. 2.5 The (a) OFDM subcarrier waveforms and (b) spectrum.

The resulting time-domain OFDM signal waveform within the time range $[(n-1)T_s, nT_s]$ can be written by

$$x_n(t) = \frac{1}{\sqrt{N_s}} \sum_{k=0}^{N_s-1} X_{k,n} e^{j2\pi \frac{k}{T_s} t} \tag{2.9}$$

When the OFDM signal given in Eq. (2.9) is sampled at a speed of $f_s = N_s / T_s$, the resulting sample at the time $t = lT_s / N_s$, $l = 0,1,2,\ldots, N_s\text{-}1$, can be expressed as

$$x_{l,n} = \frac{1}{\sqrt{N_s}} \sum_{k=0}^{N_s-1} X_{k,n} e^{j2\pi k \frac{l}{N_s}} \tag{2.10}$$

By comparing Eq. (2.10) and Eq. (2.1), it is very interesting to note that Eq. (2.10) is equivalent to $x_{l,n} = IDFT(X_{k,n})$, which means the modulation and multiplexing of a large number of OFDM subcarriers can be achieved by using IDFT. In practice the IDFT is implemented as an IFFT, an equivalent, fast method of calculating the IDFT.

When the impulse response of the transmission channel is $h(t)$, the received signal at the receiver end is given by

$$y(t) = x(t) \otimes h(t) + w(t) \tag{2.11}$$

where $w(t)$ is the channel noise and "$\otimes$" represents continuous convolution operation. In the receiver, after synchronization followed by necessary signal processing, when the FFT input sample of the n-th received OFDM symbol is $y_{l,n}$, the FFT output is expressed as

$$Y_{k,n} = \sum_{k=0}^{N_s-1} y_{l,n}(t) e^{-j2\pi k \frac{l}{N_s}}, \quad l = 0,1,2,\ldots,N_s\text{-}1 \tag{2.12}$$

For an ideal OFDM system, $Y_{k,n}$ is identical to the original data $X_{k,n}$. In a real transmission channel, a simple one-tap equalizer is usually adopted in the OFDM receiver to recover the transmitted signals, as indicated in Fig 2.3. The detailed descriptions of channel equalization are presented in Section 2.3.2.6.

2.3.2.3 Cyclic Prefix

In order to improve the resilience of OFDM signals to adverse effects such as multi-path propagation and fibre Chromatic Dispersion (CD), a Cyclic Prefix (CP) is added to the front of each OFDM symbol. The CP is a copy of the last fraction of each OFDM symbol, as shown in Fig. 2.6. After inserting the CP, the resulting samples for the n-th OFDM symbol is expressed as

$$x_n = [x_{N_s-N_c,n}, x_{N_s-N_c+1,n}, \ldots, x_{N_s-1,n}, x_{0,n}, x_{1,n}, \ldots, x_{N_s-1,n}] \tag{2.13}$$

where N_c is the number of samples of CP. The new OFDM symbol has $N_s + N_c$ samples. When the time duration corresponding to the CP is T_p, and the new symbol period is T_s, the real information occupies a time period of $T_s - T_p$ in each OFDM symbol. It should be pointed out that CP does not carry any useful information for a fixed channel bandwidth, thus it reduces the overall data rate. Throughout the thesis, the CP parameter is defined as

$$\eta = \frac{T_p}{T_s - T_p} \tag{2.14}$$

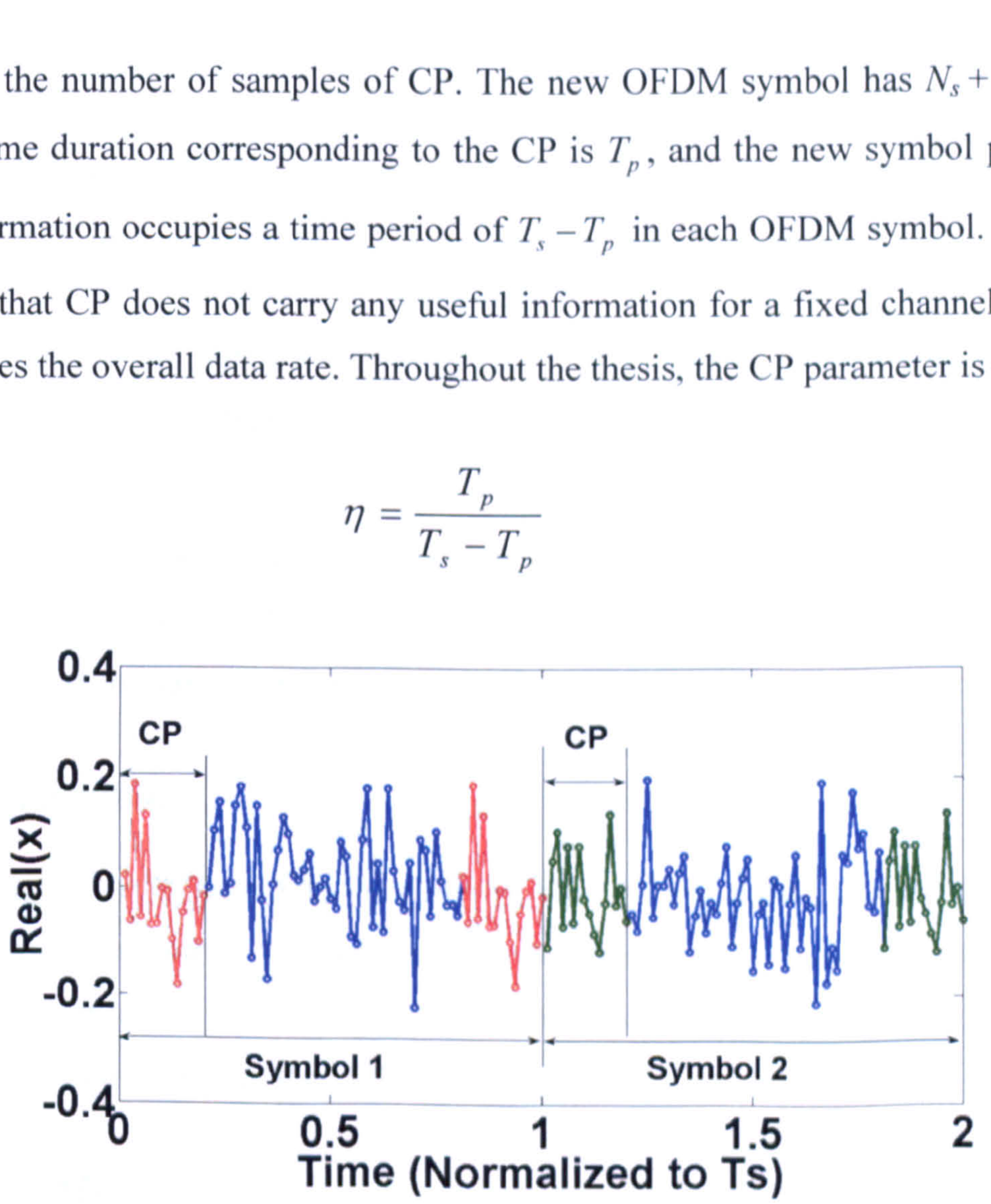

Fig. 2.6 Samples of OOFDM symbols with CP.

According to the above definition, CP quantifies the rate of the prefix duration to the duration of information-bearing part of each symbol. The CP produces a quasi-periodically extended time domain OFDM symbol, leading to the maintenance of the orthogonality between subcarriers within the symbol, as Eq. (2.7) still holds well. More importantly, due

to the CP insertion, the channel dispersive effect becomes equivalent to a cyclic convolution. If the CP length is larger than the expected maximum delay spread (the delay spread between the subcarrier with the fastest delay and the subcarrier with slowest delay [2.22]) to be encountered, after transmitting through the channel, the dispersive effect is localized within the CP region only. Prior to performing the FFT in the receiver, the distorted CP is removed, thus the OFDM symbol carrying useful information can be recovered without interference between different symbols. As the CP duration can be chosen by design, in principle, OFDM can be made free from any arbitrary delay spread.

From the above description, it is clear that, if a CP time duration is smaller than the maximum delay spread associated with the transmission link, the imperfectly compensated disperse effect limits considerably the maximum achievable transmission performance of the OFDM signals. In addition, a small CP may also affect the subcarrier orthogonality, resulting in a significant increase in the minimum required Signal-to-Noise Ratio (SNR) for a specific signal modulation format being taken on a subcarrier [2.24]. On the other hand, if the CP is longer than the maximum delay spread of the transmission link, for a fixed signal sampling speed, the CP wastes a large percentage of the transmitted signal power, giving rise to a degraded effective signal SNR. Furthermore, an excessive length of CP also prevents us from making full use of the available link bandwidth. Adaptive CPs [2.25] can be used to maximize the OFDM system performance.

2.3.2.4 Serialization

After inserting CP into each OFDM symbol, the OFDM signal is serialized through a parallel to serial convertor. On serialization, a number of low-speed parallel subcarrier signals are converted into a high-speed serial signal. This process is the inverse of the serial to parallel conversion in the OFDM receiver.

2.3.2.5 DAC/ADC

After serialization, the generated OFDM signal is fed into a DAC in the transmitter. Correspondingly, an ADC is employed in the receiver. As the processes of DAC and ADC are similar, here, only the signal processing of an ADC is discussed.

In OFDM systems, a gain-control unit that precedes the A/D stage of an ADC sets a finite dynamic amplitude range, beyond which the OFDM signal amplitudes will be clipped.

This leads to a reduction in OFDM signal Peak-to-Average Power Ratio (PAPR). For a given clipping level of ξ, also referred to as clipping ratio throughout the thesis, the clipped signal is given by

$$A_{clip}(t) = \begin{cases} A(t), & |A(t)| \leq \Lambda \\ \Lambda e^{j \arg[A(t)]}, & |A(t)| > \Lambda \end{cases} \tag{2.15}$$

where the amplitude threshold Λ is defined as $\Lambda = \sqrt{\xi P_{av}}$ with P_{av} being the average OFDM signal power. Fig. 2.7 shows clearly the OFDM signals prior to and after clipping. Clipping allows higher average signal powers to be transmitted thus improves the SNR at the receiver. However, clipping also introduces waveform distortions.

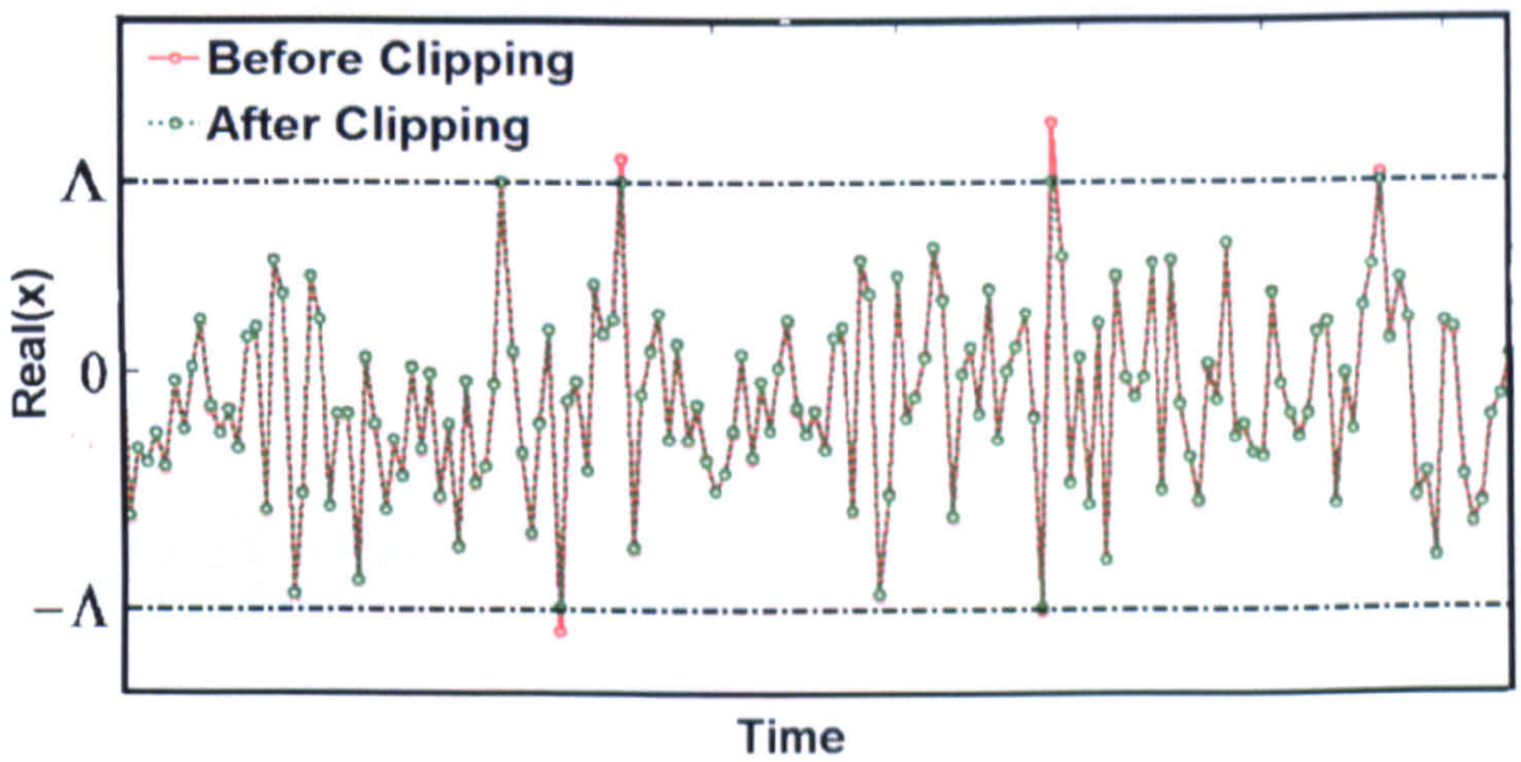

Fig. 2.7 OFDM signals before and after clipping

The clipped OFDM signal is sampled in the ADC resulting in a discrete signal with continuous-valued amplitudes. The ADC linear quantizer quantizes the sampled continuous-valued amplitude into discrete amplitude taken from a finite set of possible levels, which span the entire dynamic range of $[-\Lambda, \Lambda]$. The quantization process can be expressed as

$$Q(A_s) = \sum_{i=-\frac{L}{2}+1}^{\frac{L}{2}} \frac{\hat{A}_i + \hat{A}_{i-1}}{2} g(A_s, \hat{A}_i, \hat{A}_{i-1}) \tag{2.16}$$

where $\hat{A}_i$ and $\hat{A}_{i-1}$ represent the i-th and (i-1)-th quantization threshold value. L is the quantization levels given by $L=2^b$ where b is the quantization bits. g is the rectangular function defined as

$$g(x, x_1, x_2) = \begin{cases} 1, & x_1 \le x < x_2 \\ 0, & otherwise \end{cases} \tag{2.17}$$

Based on the above analyses, it can be seen that the system effects associated with DAC/ADC stem from two aspects: 1) Quantization error due to the finite step size of $2\Lambda / L$ for input-signal values within the dynamic range of $[-\Lambda, \Lambda]$ and 2) Amplitude clipping for input-signal values outside that range.

2.3.2.6 Pilot-Assisted Channel Estimation and Equalization

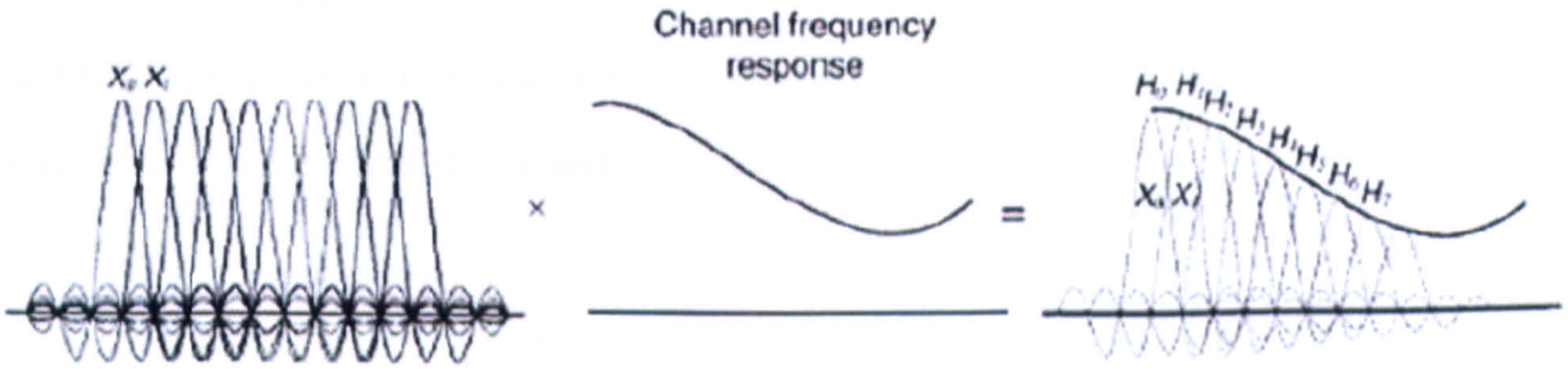

Fig. 2.8 Channel frequency response and channel fading effect on OFDM subcarriers (from [2.26]).

In OFDM systems, channel estimation can be achieved by transmitting known pilot signals that are interspersed with the user data. In the receiver, the system frequency response is estimated by extracting the pilot signals from the received signals, and is used for subsequent channel equalization so that the distortive effects can be removed and the transmitted signal can be restored prior to bit decoding.

When the k-th subcarrier channel impulse response is $h_k(t)$ and corresponding noise is $w_k(t)$, the received OFDM signal for the k-th subcarrier is

$$y_k(t) = x_k(t) \otimes h_k(t) + w_k(t) \tag{2.18}$$

where $x_k(t)$ is the transmitted OFDM signal for the k-th subcarrier. The time domain convolution between the transmitted OFDM signal and the channel response is equivalent to the multiplication of the OFDM signal spectrum with the channel frequency response, as shown in Fig. 2.8. Assuming ideal synchronization in the receiver, after performing FFT on the received signal, we have the FFT output corresponding to the k-th subcarrier

$$Y_k = X_k H_k + W_k \tag{2.19}$$

The estimated system frequency response of the k-th subcarrier can be obtained by channel estimation based on pilot signals

$$H_k = Y_{p,k} / X_{p,k} \tag{2.20}$$

where $X_{p,k}$ and $Y_{p,k}$ are the transmitted and received pilot signals of the k-th subcarrier. The OFDM receiver restores the transmitted signal by multiplying the received signal with the inverse of the estimated subcarrier channel response H_k^{-1}

$$\hat{X}_k = Y_k H_k^{-1} = X_k + W_k / H_k \tag{2.21}$$

This approach is a simple one-tap equalization. The disadvantage of the one-tap equalizer is that the channel noise can not be removed. For a channel that has strong attenuation, the noise effect imposed on the received signal is increased upon the equalizer. Practically, such an issue can be resolved efficiently by averaging the subcarrier channel frequency response estimations over a long time duration.

2.3.2.7 Synchronization

The discussions in all the above subsections are based on an assumption that ideal OFDM symbol synchronization is performed in the receiver. In practical OFDM systems, however, synchronisation errors may occur because of the following physical effects [2.27]:

- Symbol Timing Offset (STO) induced by the time delay of a transmission link.
- Sampling Clock Offset (SCO) induced by the clock mismatch between the transmitter and the receiver.

- Carrier Frequency Offset (CFO) induced by the frequency mismatch between the oscillators involved in the transmitter and receiver.
- Carrier Phase Error (CPE) induced by the constant phase shift between the transmitter and the receiver, or by the random phase noise in the local oscillators and other components.

All these synchronization errors will degrade system performance. STO-induced synchronization errors may cause a fraction of a FFT window for an OFDM symbol to occur in an extended region of an adjacent symbol, leading to system performance degradation due to the effects of ISI and ICI. SCO brings about the significant ICI effect, as the sampled values do not correspond to the peaks of the sinc [sin(x)/x] waveforms after the FFT in the receiver. CFO also introduces ICI and destroys the orthogonality of OFDM subcarriers. The influence of CPE is less important compared to the impacts of other three synchronization errors, as CPE-induced constant phase shift or phase noise can be compensated by channel estimation and equalization.

In OFDM transmission systems, there are usually two solutions for synchronization: the first is to use so-called blind approaches [2.16,2.28], which make use of the features of the repeated OFDM symbol pattern with a predetermined time period; the second are non-blind approaches [2.18,2.29] which take advantage of the features of training symbols or pilots that are interspersed with the transmitted user data. For both the abovementioned approaches, correlation calculations of incoming signals are usually performed, i.e., a sequence of samples is multiplied by a time-shifted copy of the same sequence to produce a time-dependent autocorrelation profile, which is then employed for synchronization.

2.4 Principles of Optical OFDM

In previous sections, we have discussed various key building blocks involved in OFDM transceivers. In this section, we discuss the application of OFDM in optical fibre communications.

Optical OFDM (OOFDM) can not be viewed as a simple one-to-one translation from the wireless domain into the optical domain. This is because, compared to wireless OFDM, OOFDM exhibits significant differences in several aspects: Firstly, OOFDM signals

transmit at high speed; Secondly, OOFDM signals are up-converted into high optical frequencies (~200THz) by using electro-optic convertors which introduce nonlinear effects to the modulated OOFDM signals; Finally, an optical channel is typically relatively stable over time, but has nonlinearity.

2.4.1 Optical Fibres

Optical fibres can be classified as Single-Mode Fibre (SMF) or Multi-Mode Fibre (MMF). SMFs have small core diameters and light can only propagate in one mode. MMFs have large core diameters and light can propagate in multiple modes.

In MMFs, different modes propagate at different speeds and result in mode delay. This limits link bandwidth and system performance. Therefore, MMFs are mostly installed in LANs. Compared to MMFs, SMFs support much better transmission performance thus have been used for long-haul transmissions, MANs and access networks. In this thesis, only SMF is considered.

2.4.1.1 Linear Fibre Effects

2.4.1.1.1 Fibre Loss

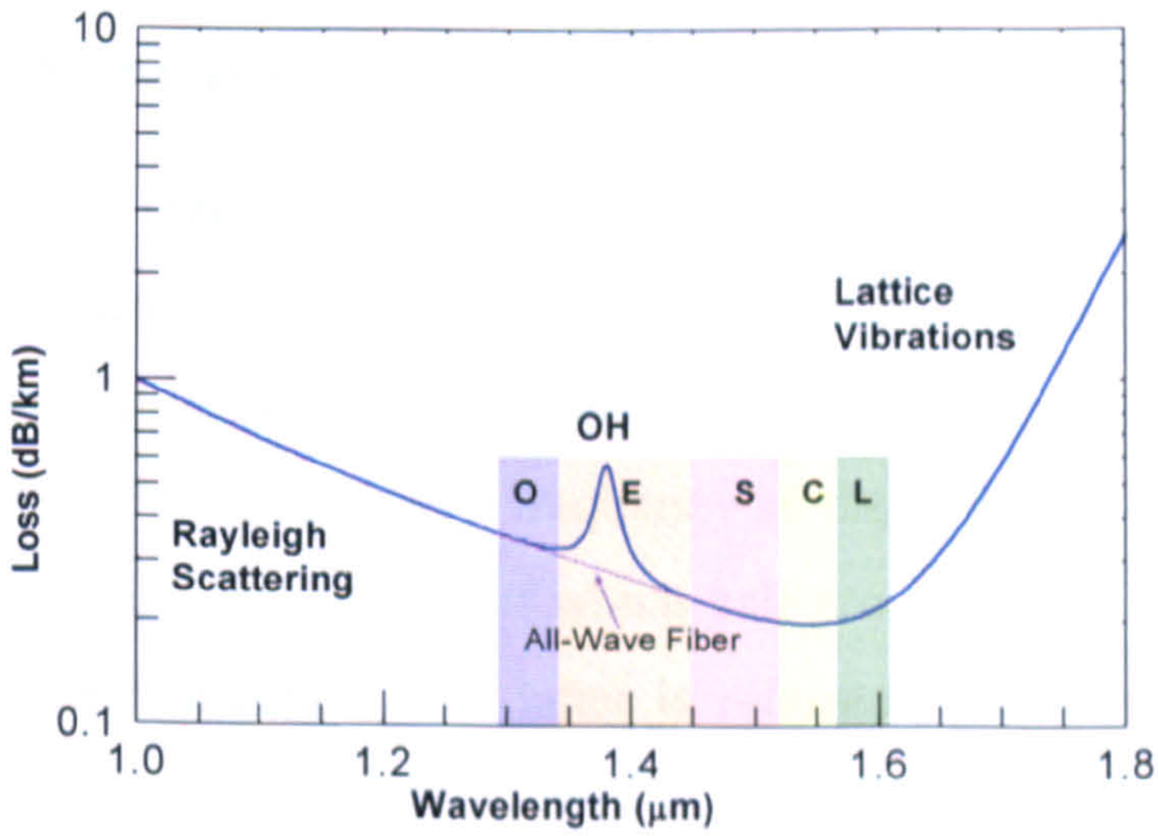

Fig. 2.9 Loss in optical fibre at different wavelengths.

In practice, fibre loss, α, is measured in dB/km and is defined by

$$\alpha = -\frac{10}{z}\log_{10}\frac{P_{in}}{P_z} \tag{2.22}$$

where P_{in} is the optical power injected into the fibre, and P_z is the optical power at a fibre distance of z. Fig. 2.9 shows the loss spectrum of a silica fibre. In the short wavelength range, wavelength dependent fibre loss is dominated by Rayleigh scattering, which will be discussed in the following section; whereas in the long wavelength range, optical scattering due to lattice vibrations is the main factor attributing to fibre loss. The attenuation peak around 1.38μm shown in Fig. 2.9 is due to absorption by OH^- impurities left upon fibre manufacturing.

As shown in Fig. 2.9, the minimum fibre loss occurs in the C-band (Conventional band: 1.53μm-1.565μm), where, optical amplification can be easily achieved with Erbium Doped Fibre Amplifiers (EDFAs). Thus it is the most popular wavelength band for long-haul WDM transmission and for analogue Cable TV (CATV) transmission where a high optical power is required. Other wavelength bands shown in Fig. 2.9 are O-band (Original band: 1.26μm-1.36μm), E-band (Extended band: 1.36μm-1.46μm), S-band (Short wavelength band: 1.46μm-1.53μm) and L-band (Long wavelength band: 1.565μm-1.625μm). Current PON systems mostly use 1.3μm (O-band) for upstream signal transmission, 1.49μm (S-band) for downstream transmission and 1.55μm for an optional analogue CATV signal overlay.

2.4.1.1.2 Rayleigh Scattering

Rayleigh scattering is the major cause of fibre loss for short wavelengths. It arises from the inhomogeneities of silica in manufacturing which leads to local fluctuations in the refractive index scattering light in all directions. Rayleigh scattering is an elastic process: the resulting scattered light has the same frequency as the incident light. A portion of the scattered light is recaptured in the fibre, of which half propagates in the forward direction and half in the backward direction. The latter is referred to as Rayleigh Backscattering (RB).

RB introduces interferometric noise fluctuations at the input facet of optical fibre. For an optical signal power launched into a SMF, P_{in}, it generates RB noise propagating at opposite direction. The RB noise power, P_{RB}, is given by [2.30]

$$P_{RB} = P_{in}B(1-e^{-2\mu\varepsilon}) \tag{2.23}$$

where $B = S\alpha_S / 2\mu$ with α_S [km^{-1}] being the fibre scattering coefficient, S being the fibre recapture coefficient, and μ [km^{-1}] being the SMF attenuation coefficient with $\mu = \frac{20}{\ln 10}\alpha$ where α is defined in Eq. (2.22). z is the fibre length. Depending upon the type of fibre and the selected wavelengths, for fibre links longer than 20km, $\zeta = B(1 - e^{-2\mu z})$ converges towards an almost constant value [2.31].

According to the above descriptions, ζ represents the backscattered power normalized to the fibre launch power. To measure ζ for SMFs at 1550nm, we used an experimental setup illustrated in Fig. 2.10(a). The measured backscattered optical power and the corresponding normalized backscattered power as a function of CW launch power are plotted in Fig. 2.10(b) for different standard SMF lengths ranging from 25km to 125km. It can be seen from Fig. 2.10(b) that, for optical launch powers of approximately <7dBm, regardless of fibre length, ζ can be taken to be -34dB. Whilst when CW launch powers exceed 7dBm, which is the threshold of the Stimulated Brillouin Scattering (SBS), SBS occurs and plays a dominant role in determining the backscattered optical power. SBS will be discussion later.

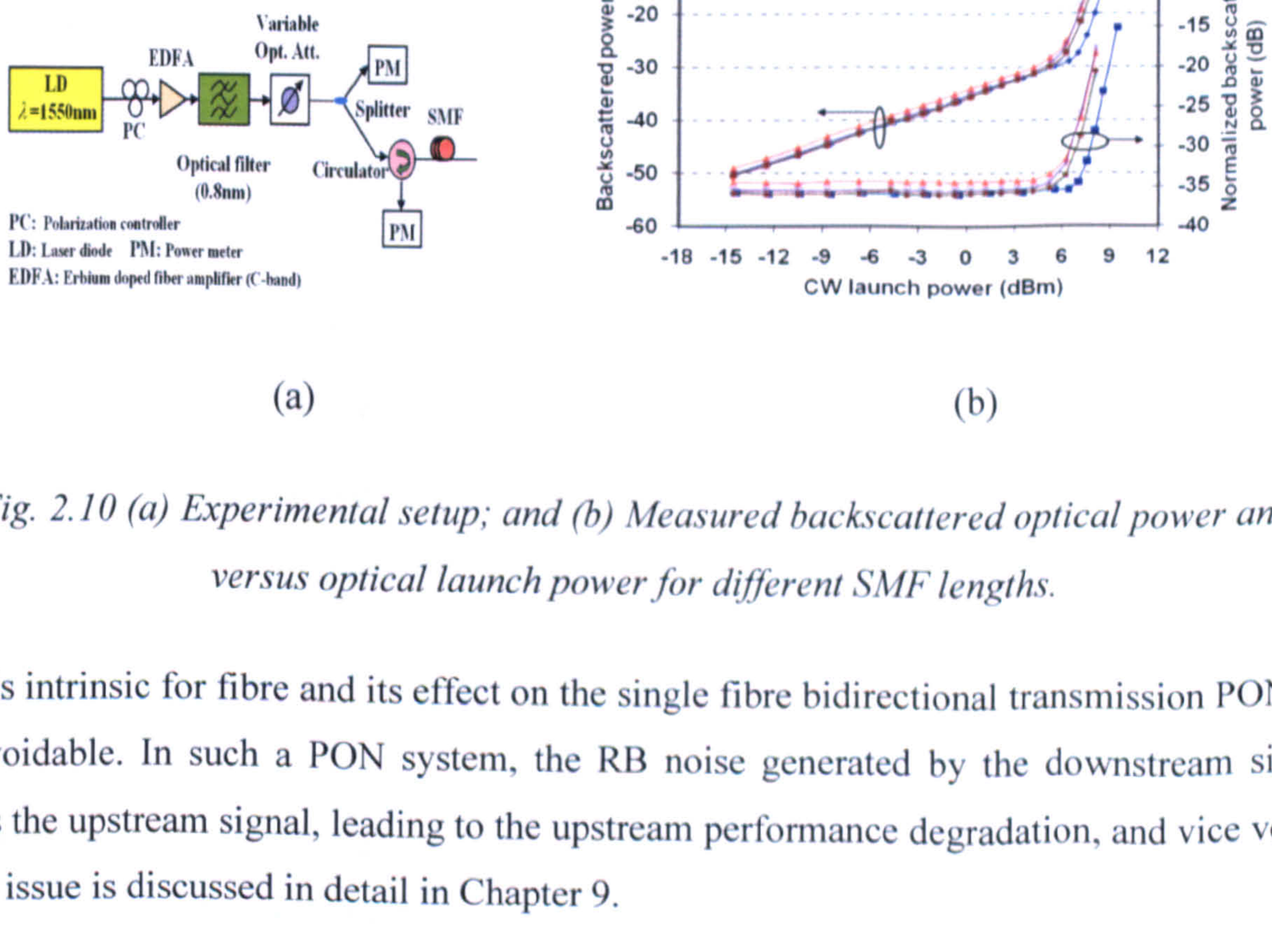

Fig. 2.10 (a) Experimental setup; and (b) Measured backscattered optical power and versus optical launch power for different SMF lengths.

RB is intrinsic for fibre and its effect on the single fibre bidirectional transmission PONs is unavoidable. In such a PON system, the RB noise generated by the downstream signal joins the upstream signal, leading to the upstream performance degradation, and vice versa. This issue is discussed in detail in Chapter 9.

2.4.1.1.3 Chromatic Dispersion

Chromatic Dispersion (CD) is caused by the frequency dependence of the refractive index $n(\omega)$ of optical fibre. As a result, light signals with different frequencies propagate in the fibre with different speeds. As signals occupy finite frequency spans, CD broadens optical signal pulses as they propagate through optical fibres, which imposes the ISI effect onto the propagating signals. For an electromagnetic waveform propagating in the z direction, the optical signal field at a distance z_0 can be expressed as

$$E(z_0,\omega) = E(0,\omega)\cdot\exp[j\beta(\omega)z_0] \tag{2.24}$$

where ω is the angular frequency and $\beta(\omega)$ is the propagation constant. Mathematically, the fiber CD effects is accounted for by expanding the mode-propagation constant in a Taylor series with respect to the central frequency ω_0 [2.32]

$$\begin{aligned}\beta(\omega) &= n(\omega)\frac{\omega}{c}\\ &= \beta_0 + (\omega-\omega_0)\beta_1 + \frac{1}{2}(\omega-\omega_0)^2\beta_2 + \frac{1}{6}(\omega-\omega_0)^3\beta_3 + \ldots\end{aligned} \tag{2.25}$$

where

$$\beta_m = \left(\frac{d^m\beta}{d\omega^m}\right)_{\omega=\omega_0} \qquad \text{for } m=0,1,2,3,\ldots \tag{2.26}$$

The group velocity $\beta_1 = c/n_g$ is the speed that the optical waveform travels in the fibre, with c being the light speed in vacuum. The parameter β_2 represents Group-Velocity Dispersion (GVD). β_3 represents the third-order dispersion. In practice, CD is characterized by the dispersion parameter D, which is defined as $D = d\beta_1/d\lambda$. By introducing this definition into to Eq. (2.26) for m=2

$$D = -\frac{2\pi C}{\lambda^2}\beta_2 \tag{2.27}$$

The CD parameter is wavelength dependent. Fig. 2.11 shows the dispersion coefficient as a function of optical wavelength for various types of optical fibre. Standard SMF has zero

dispersion around the 1.3μm region and 17ps/nm/km at 1.55μm, the wavelength of which a conventional EDFA works the best.

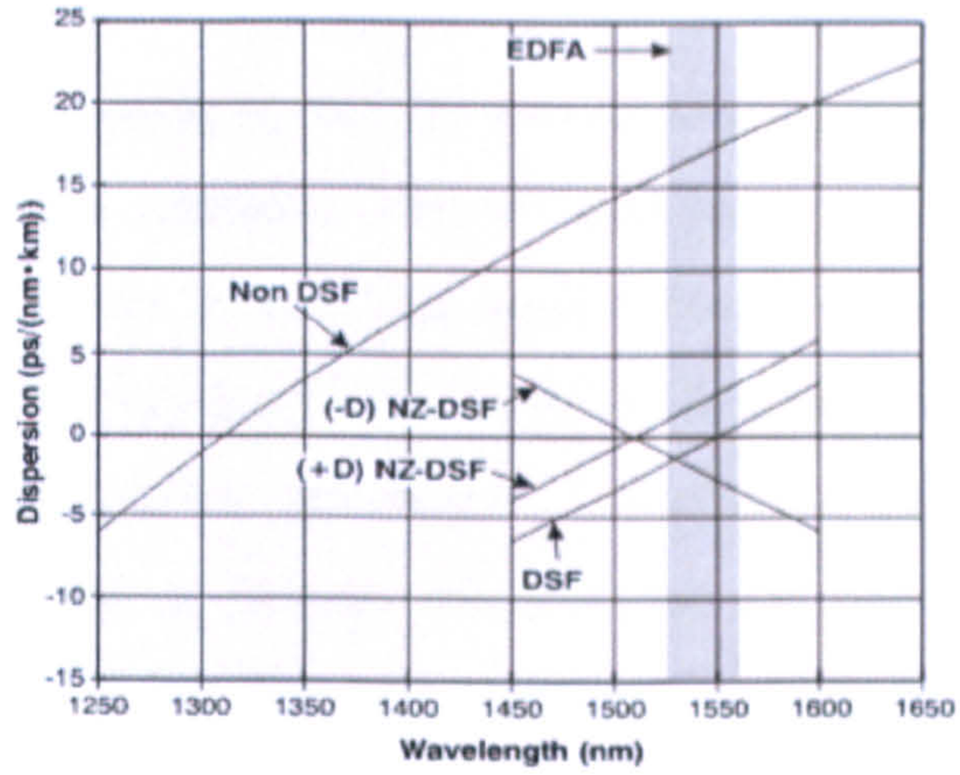

Non DSF: Non dispersion shifted fiber, which is also called standard single-mode fiber or ITU-T G.652 fiber.
(-D) NZ-DSF: negative non-zero dispersion shifted fiber
(+D) NZ-DSF: positive non-zero dispersion shifted fiber
DSF: dispersion shifted fiber with nearly zero dispersion in C-band

Fig. 2.11 Dispersion coefficient as a function as wavelength for various fibres.

The CD induced broadening of an arbitrary optical pulse propagating through SMFs is given by $\Delta T = D \cdot \delta\lambda \cdot z$, with $\delta\lambda$ being the signal bandwidth in *nm* and z being the transmission distance in *km*. Such pulse broadening brings about ISI in the received signal and thus imposes limitations for maximum achievable performance of optical communication systems. For conventional Non Return to Zero (NRZ: the binary information digit 1 is represented by a rectangular pulse of polarity A and the binary digit 0 is represented by a rectangular pulse of polarity –A [2.33]) systems, the achievable system capacity and reach are constrained by [2.34]

$$R^2 z = \frac{c}{4D\lambda_0^2} \tag{2.28}$$

where R is the signal line rate, λ_0 is the carrier wavelength and z is transmission distance. When an NRZ system operating at typically 1.55μm upgrades from 1Gb/s to 10Gb/s data rate, the achievable reach drops from 1836km to 18km, and further into only approximately 1.14km for 40Gb/s. Therefore, CD is one of the key limiting factors for high-speed optical communication systems.

2.4.1.1.4 Polarization Mode Dispersion

Polarization Mode Dispersion (PMD) is caused by the group velocity mismatch between the two polarization states of a propagating optical signal. An ideal optical fibre is a transversal isotropic waveguide so that the two orthogonal polarization modes (transversal electric TE and transversal magnetic TM) are degenerate and propagate identically in the single polarization. However, in practical optical fibres, such mode degeneracy does not hold and birefringence occurs due to the small deviations from cylindrical geometry as a result of random variations in the core shape or stress along the fibre length. Consequently, the propagation constant β is slightly different for the two polarizations. That is, one polarization state travels faster than the other one, as shown in Fig. 2.12. The resulting difference of the arriving times causes optical pulse broadening. The PMD induced time delay between two polarizations can be expressed as

$$\delta_T = D_p \sqrt{z} \tag{2.29}$$

where D_p is the PMD parameter and measured in $ps/\sqrt{km}$. The value of D_p varies from 0.1 to 1 $ps/\sqrt{km}$.

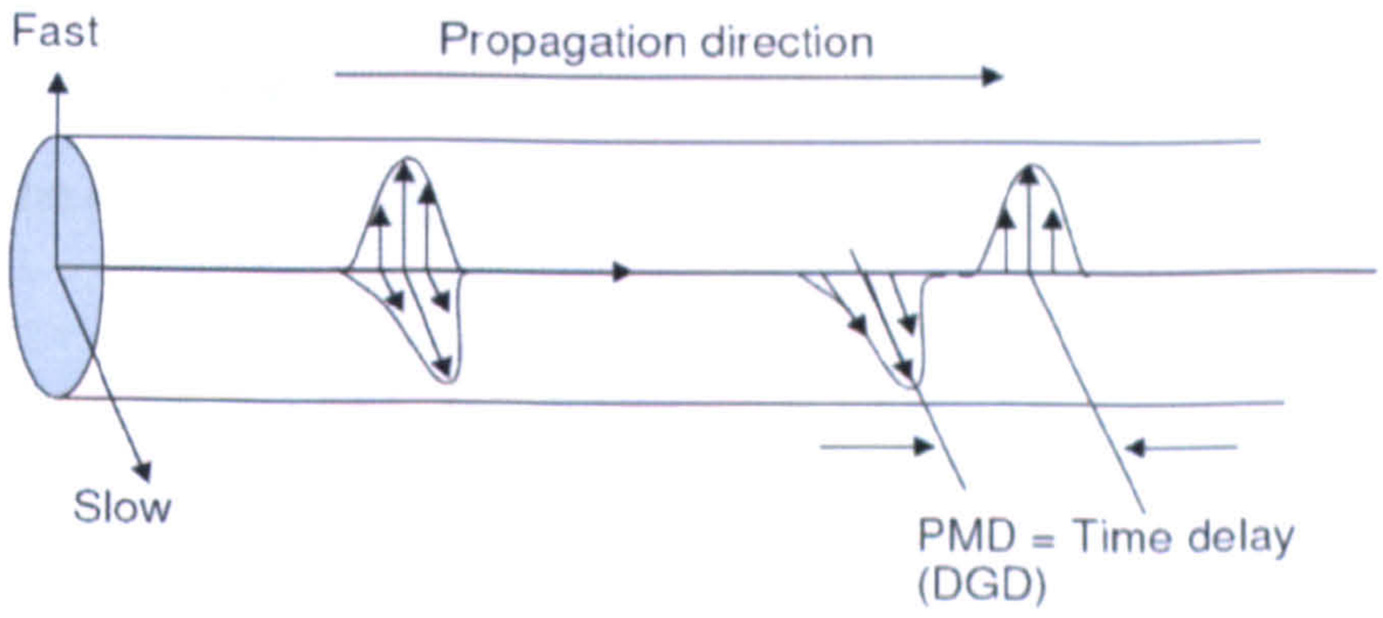

Fig. 2.12 An optical pulse propagates in the fibre with PMD arises from the differential group delay (DGD) between the two orthogonal polarization states.

Compared to CD, PMD exhibits differences in two main aspects: firstly, PMD is time dependent thus unstable due to random changes in birefringence occurring along the fibre. Secondly, the PMD-induced pulse broadening is relatively small as the PMD parameter is dependent on the square root of the distance. Therefore, for FTTx networks, PMD is not an important issue as the transmission distance is usually limited to less than 100km.

2.4.1.2 Fibre Nonlinearities

The optical fibre's response to light becomes nonlinear for intense electromagnetic fields. This property makes fibre channels different from wireless channels where nonlinearity does not exist. The fibre nonlinear effects induce changes in both the phase and power of a propagating light.

There are two major categories of optical fibre nonlinear effects. The first type of nonlinear effects arises due to the dependence of refractive index on intensity of the propagating signal. The most important nonlinear effects in this category are Self-phase Modulation (SPM), Cross-phase Modulation (XPM), and Four Wave-mixing (FWM) [2.32]. The second type of fibre nonlinearity exhibits energy transfer from the optical field to the medium via a stimulated inelastic scattering process. The nonlinear Stimulated Brillouin Scattering (SBS) and Stimulated Raman Scattering (SRS) phenomena fall in this category.

2.4.1.2.1 SPM, XPM and FWM

Self-phase Modulation

SPM refers to the self-induced phase shift experienced by an optical field during its propagation in optical fibres [2.32]. Due to the optical intensity dependence of refractive index in optical fibre, the nonlinear phase shift ϕ_{NL} imposed on the optical field is proportional to the optical intensity, which, in the absence of GVD, can be expressed as

$$\phi_{NL}(z,T) = n_2 k_0 z \mid E(z,T) \mid^2 \tag{2.30}$$

where n_2 is the nonlinear refractive coefficient, also referred to as Kerr coefficient [2.32], $k_0 = 2\pi/\lambda_0$ with λ_0 being carrier wavelength and z is the fibre length.

SPM in isolation leads to spectral broadening of optical pulses while keeping the pulse shapes unaltered. The spectral broadening generates frequency chirp thus brings about new frequencies into the optical pulse. The SPM-caused frequency chirp will gradually increase the pulse-broadening through fibre CD, which translates the phase modulation into intensity modulation.

Cross-phase Modulation

Compared to SPM, XPM induces nonlinear phase shift to an optical field which is dependent not only on the intensity of that wave but also on the intensity of a co-propagating field at a different wavelength. When two optical fields E_1 and E_2 at frequencies ω_1 and ω_2, respectively, co-propagate in optical fibre, the nonlinear phase shift for the field at ω_1 is given by

$$\phi_{NL}(z,T) = n_2 k_0 z(|E_1|^2 + |E_2|^2) \tag{2.31}$$

It is noticeable that the XPM is always accompanied by SPM, which are represented by the two terms on the right hand side of Eq. (2.31), respectively. Similar to SPM, XPM also causes a greater temporal broadening as signal propagates along the fibre due to the effect of CD.

Four-Wave Mixing

For multiple signals at different wavelengths propagating in the fibre, the intensity dependence of refractive index not only induces SPM and XPM on each signal but also causes that these signals interfere and generate refractive index gratings, such gratings interact with the signals and produce new frequencies. This nonlinear process is referred to as FWM. The multiple optical fields at frequencies ω_i, ω_j and ω_k interact to produce signals at frequencies $\omega_{ijk} = \pm\omega_i \pm \omega_j \pm \omega_k$.

FWM occurs only when phase matching between propagating signals is achieved, that is, for energy to flow effectively from one frequency to another, the signals must remain in phase. Thus FWM is dependent on fibre dispersion, since the signals at different wavelengths travel with different group velocities which gradually destroy the phase matching condition and make the FWM process less efficient.

In today's FTTx, the influences of SPM, XPM and FWM are not significant. This is because, for the upstream or downstream single-channel signal transmission, the transmission distance is normally short. On the other hand, the simultaneous transmission of downstream and upstream signals is achieved by Coarse WDM (CWDM), where the channel spacing is usually large (~180nm). However, XPM and FWM can have strong

deleterious effects when Dense WDM (DWDM) is implemented in FTTx [2.15], where it can cause crosstalk between different frequency channels, and/or an imbalance of channel powers. FWM is dependent on the channel spacing thus one efficient way to suppress this effect is to use uneven WDM channel spacing [2.35]. In practise, use is made of Non Zero-Dispersion Shifted Fibre (NZ-DSF) to avoid phase matching to suppress FWM effect in WDM optical communication systems [2.36].

2.4.1.2.2 SRS and SBS

Stimulated Raman Scattering

SRS is an inelastic process when light is scattered by material scattering centres, which causes vibrational excitation of the molecules. SRS converts a small fraction of the incident power from an optical beam to another optical beam at a downshifted frequency which is determined by vibrational modes of the medium. SRS can occur either in the forward or backward directions.

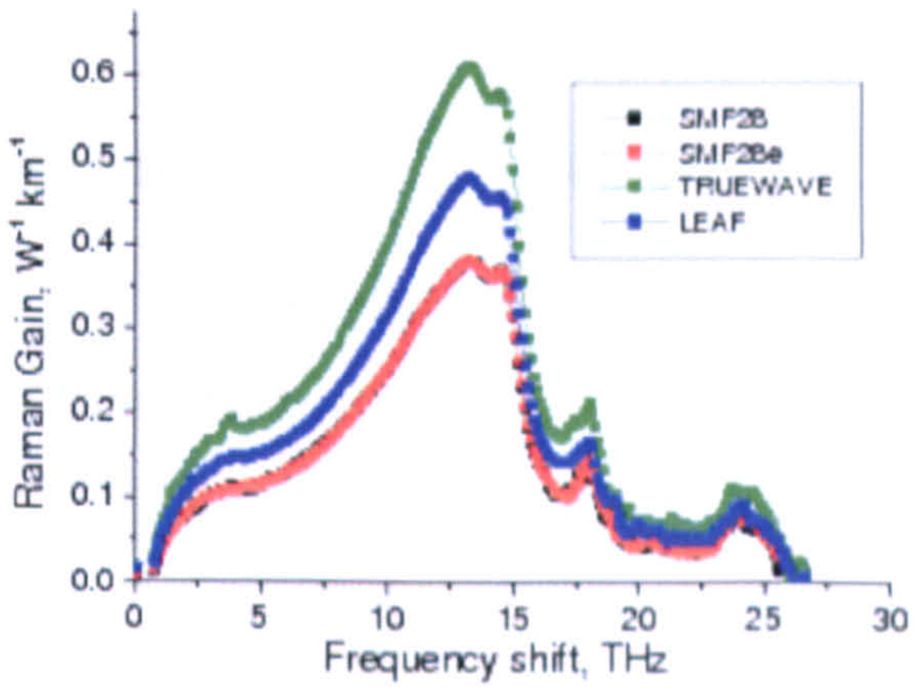

Fig. 2.13 Raman gain coefficient of various fibres measured using a 1460nm pump (from[2.37]).

SRS has an important application in WDM systems as it enables relatively high optical amplification within the transmission fibre. SRS exists at all optical frequencies and the amplification range using a single pump wavelength is as wide as 10THz, which is shown in Fig. 2.13, in which the Raman gain spectral for different fibre types is measured using a 1460-nm pump [2.37]. SRS can be detrimental as it can couple different channels in a WDM system and produce considerable inter-channel crosstalk.

Stimulated Brillouin Scattering

SBS also occurs at high optical input intensities in optical fibres but much lower than those needed for SRS. SBS manifests through reflections of the incident light wave with a downward Doppler shift caused by a travelling index grating which is generated by a sound-wave due to electrostriction. Compared to SRS, the frequency downshift in SBS is ~10GHz which is much smaller than that in SRS, and the generated optical beam propagates backward only. The effect of SBS is negligible at a lower launched power level, but becomes significant when the input power increases. Unlike SRS, the SBS strength depends only on the bandwidth and power of the incident light and is independent of the incident light frequency.

For today's FTTx systems normally using single fibre architecture, SBS may be detrimental under high launch powers (>7dBm as was seen in Fig. 2.10), as the SBS is strongest for narrow-band signals. SRS is not a major concern in FTTx since for a given incident power level, the Raman effect is three orders of magnitude weaker than the Brillouin effect.

2.4.2 Coherent Optical OFDM (CO-OFDM)

Having discussed the linear and nonlinear fibre effects, this section discusses the fundamentals of a CO-OFDM system.

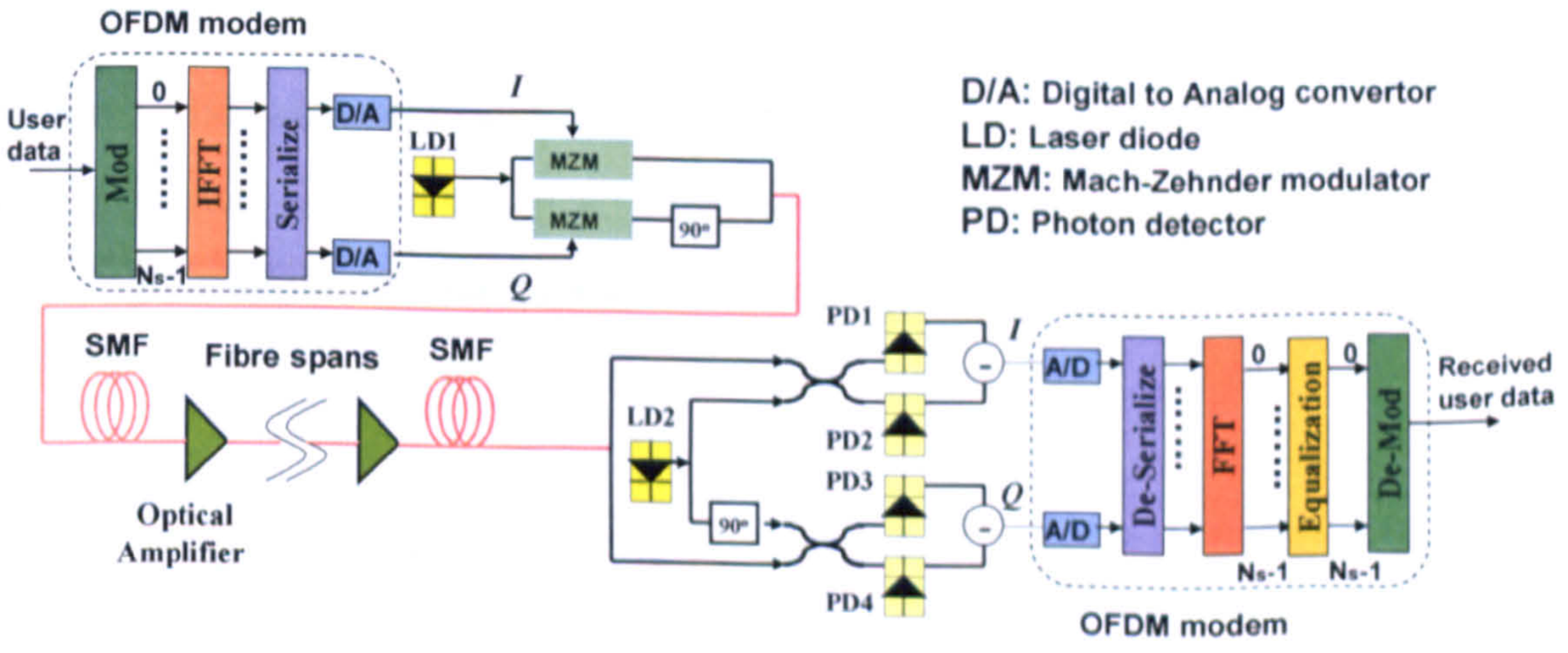

Fig. 2.14 Block diagram of CO-OFDM transmission systems

A typical CO-OFDM transmission system is illustrated in Fig. 2.14, which consists of a transmitter, a receiver and an optical fibre link. The transmitter is composed of an OFDM

modem which is similar to that shown in Fig. 2.3 and an optical Imaginary/Quadrature (I/Q) modulator. It should be pointed out that two DACs are used in the OFDM modem in transmitter to convert the real and imaginary part of the digital signal, respectively, into an analog signal. The OFDM modem generates electrical complex OFDM signal via a DSP procedure identical to that described in Section 2.3. The optical I/Q modulator comprising two Mach-Zehnder Modulators (MZMs) up-converts the real/imaginary parts of the complex OFDM signal from the electrical domain to the optical domain. Each MZM is respectively driven by the real or the imaginary parts of the electrical OFDM signal. It is well know that by biasing the MZMs at null point (bias voltage equals to the half-wave switching voltage of MZM), a linear conversion between the electrical OFDM signal and the optical field signal can be achieved [2.19,2.22]. The modulated signal can be expressed as

$$E(t) = x(t)\exp(\ j\omega_{LD1}t + \phi_{LD1}) \tag{2.32}$$

where $x(t)$ is the electrical baseband OFDM signal. ω_{LD1} and ϕ_{LD1} are the angular frequency and phase of the CW signal emitted from the Laser Diode (LD) in the transmitter, respectively.

After transmitting through the SMF link, the received optical signal is given by

$$E_r(t) = E(t) \otimes h(t) + w(t) \tag{2.33}$$

where $h(t)$ and $w(t)$ represent the channel impulse response and channel noise. The receiver uses two pairs of balanced receivers and an optical 90° hybrid to perform I/Q detection. Ignoring the imbalance and loss of the optical hybrid, the four output ports of the 90° optical hybrid E_1, E_2, E_3, and E_4 can be expressed as

$$\begin{aligned} E_1 &= \frac{1}{\sqrt{2}}[E_r + E_{LD2}], \quad E_2 = \frac{1}{\sqrt{2}}[E_r - E_{LD2}] \\ E_3 &= \frac{1}{\sqrt{2}}[E_r - jE_{LD2}], \quad E_4 = \frac{1}{\sqrt{2}}[E_r + jE_{LD2}] \end{aligned} \tag{2.34}$$

where E_{LD2} is the signal of LD2 in the receiver as shown in Fig. 2.14. The *I* component is obtained by using a pair of the photo-detectors, PD1 and PD2 in Fig. 2.14, whose photocurrent I_1 and I_2 can be described as

$$I_1 = |E_1|^2 = \frac{1}{2}[|E_r|^2 + |E_{LD2}|^2 + 2\,\mathrm{Re}(E_r E_{LD2}^*)] \tag{2.35}$$

$$I_2 = |E_2|^2 = \frac{1}{2}[|E_r|^2 + |E_{LD2}|^2 - 2\,\mathrm{Re}(E_r E_{LD2}^*)] \tag{2.36}$$

where "Re" or "Im" denotes the real or imaginary part of a complex signal. Because of the balanced detection, the *I* component of the photocurrent becomes

$$I_I(t) = I_1 - I_2 = 2\,\mathrm{Re}(E_r E_{LD2}^*) \tag{2.37}$$

From Eq. (2.33), we know that $|E_r|^2 = |E(t) \otimes h(t)|^2 + |w(t)|^2 + 2\,\mathrm{Re}\{[E(t) \otimes h(t)]w^*(t)\}$ contains three noise terms, which are suppressed upon balanced detection shown in Eq. (2.37). This is the advantage of balanced detection. Similarly, the Q component from the other pair of balanced detectors can be derived as

$$I_Q(t) = I_3 - I_4 = 2\,\mathrm{Im}(E_r E_{LD2}^*) \tag{2.38}$$

Therefore, the complex photocurrent $I(t)$ that consists of both I and Q components becomes

$$I(t) = I_I + jI_Q = 2E_r E_{LD2}^* \tag{2.39}$$

By combining Eqs. (2.32)-(2.33) and Eq. (2.39), the detected electrical OFDM signal which is given by

$$\begin{aligned} y(t) &= I(t) = x(t)\exp(j\Delta\omega t + \Delta\phi) \otimes h(t) + w(t) \\ \Delta\omega &= \omega_{LD1} - \omega_{LD2}\,,\ \Delta\phi = \phi_{LD1} - \phi_{LD2} \end{aligned} \tag{2.40}$$

where $\Delta\omega$ and $\Delta\phi$ are, respectively, the angular frequency difference and phase difference between the lasers in the transmitter and the receiver (LD1 and LD2 in Fig.2.20).

It is clear that the detected OOFDM signal is a linear replica of the received complex OOFDM signal.

The detected electrical OFDM signal is first sampled with ADCs. Then the sampled signal needs to go through sophisticated synchronization and channel estimation before decoding can be made. The synchronization includes: 1) FFT window synchronization where the OFDM symbol is properly delineated to avoid ISI; 2) frequency synchronization, namely, the frequency offset $\Delta\omega$ needs to be estimated and compensated [2.20].

From the above descriptions, CO-OFDM offers sufficient compensations for the linear effects from transmission system and components, leading to virtually unlimited dispersion tolerance. In addition, the fibre nonlinearity effects can also be compensated, to some extent, in CO-OFDM systems [2.21]. 10 × 111Gb/s-channel WDM transmission distances over 12000km with high spectral efficiency of 2bits/s/Hz has been experimentally demonstrated based on no-guard-interval CO-OFDM [2.38].

2.4.3 Intensity Modulation and Direct Detection Optical OFDM

Compared to the CO-OFDM systems, Direct Detection (DD) OOFDM systems use simple optical power detection based on a single photo-detector, greatly reducing the system complexity. In DD OOFDM systems, the up-conversion of electrical OFDM signal to optical signal can be realized either by field modulation using I/Q modulators or Intensity Modulation (IM) using intensity modulators. The latter is referred to as IMDD OOFDM systems which further reduce the transmitter complexity and cost due to the availability of cheap directly modulated laser intensity modulators.

Fig. 2.15 illustrates the block diagram of a typical IMDD OOFDM system. In the transmitter, the electrical OFDM signal generated by OFDM modem is up-converted into the optical domain by using an intensity modulator. This requires that the electrical OFDM signal has to be real-valued. Two common methods had been utilized in the OFDM modem to generate real-valued OFDM signals: the first one is to arrange the IFFT inputs to have Hermitian symmetry. The IFFT inputs can be expressed as

$$\overline{X}_{k,n} = \begin{cases} 0, & k = 0 \\ X_{k,n}, & k = 1,2,\ldots N_s/2-1 \\ 0, & k = N_s/2 \\ X^*_{N_s-k,n}, & k = N_s/2+1,\ldots, N_s-1 \end{cases} \tag{2.41}$$

where $X_{k,n}$ is the encoded complex data expressed in Eq. (2.2) and its conjugate is donated to as $X^*_{k,n}$. It can be seen from Eq. (2.41) that the last $N_s/2$ IFFT inputs have Hermitian symmetry with respect to the first $N_s/2$ inputs. Usually, the first subcarrier is dropped off [2.14]. By substituting $X_{k,n}$ in Eq. (2.10) with $\overline{X}_{k,n}$, the IFFT outputs have zero imaginary parts. In this way, however, the IMDD OOFDM system lowers spectral efficiency compared to CO-OFDM, as half of the spectra do not carry any user data.

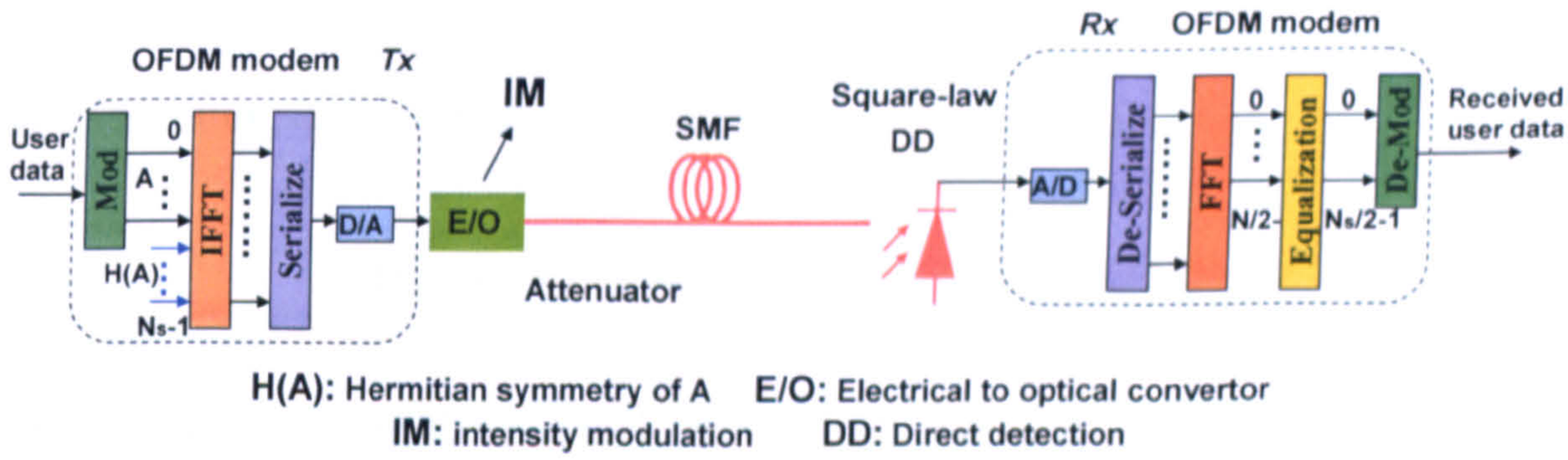

(a) Block diagram of IMDD OOFDM system

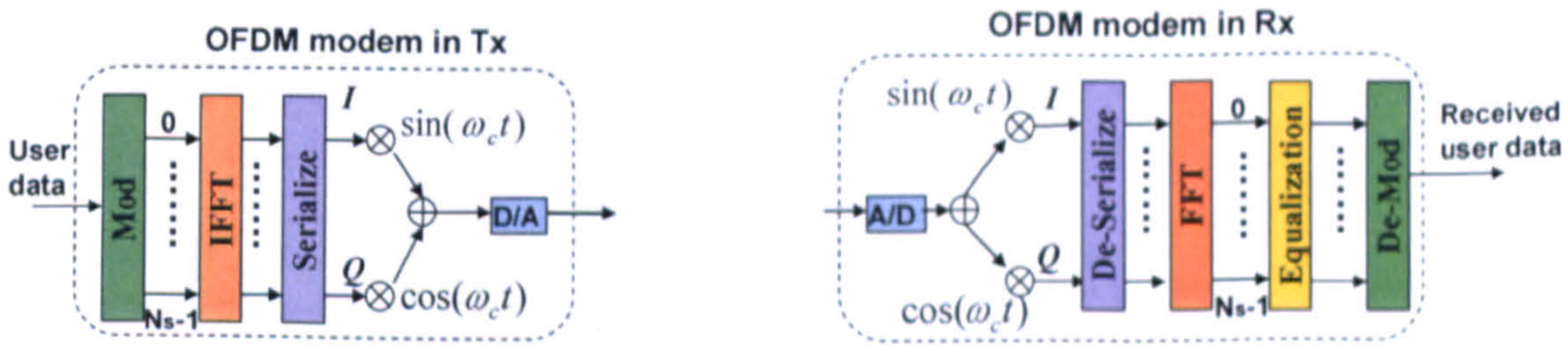

(b) Alternative OFDM modems to generate real-valued signal for IMDD OOFDM transceivers

Fig. 2.15 Block diagram of IMDD OOFDM transmission systems

The second approach is to up-convert the real and imaginary parts of the electrical OFDM signal to an intermediate RF frequency and multiplex orthogonally, resulting a real-valued electrical OFDM signal, as shown in Fig. 2.15(b). Correspondingly, the OFDM modem in the receiver performs RF down conversion after square-law detection. Compared to the first method, this approach uses RF oscillators thus increases the system complexity and makes the system vulnerable to the frequency drift and phase noise from the RF oscillators.

Due to this reason, we only deal with the IMDD OOFDM system based on the first approach throughout the thesis.

In an IMDD system, the OFDM modem-generated signal directly modulates an optical intensity modulator with a driving current of

$$i(t) = I_{dc} + x(t) \tag{2.42}$$

where I_{dc} is the required DC bias added so that the resulting driving current $i(t)$ is non-negative. Assuming an ideal intensity modulation, the optical intensity modulator generates an optical power $p(t) = i(t)$. Then the optical field can be expressed as

$$E(t) = \sqrt{p(t)} = \sqrt{I_{dc} + x(t)}e^{j\phi(t)} \tag{2.43}$$

After transmitting through SMF, the detected signal in the receiver is

$$y(t) = | \sqrt{I_{dc} + x(t)}e^{j\phi(t)} \otimes h(t) + w(t) |^2 \tag{2.44}$$

where $h(t)$ and $w(t)$ are the channel impulse response and channel noise. We can use Taylor series expansion on the square root term in Eq. (2.44). Considering $x(t)$ is real-valued and ignoring channel noise, the detected signal becomes

$$\begin{aligned} y(t) &= [(\sqrt{I_{dc}} + \frac{x(t)}{2\sqrt{I_{dc}}} - \frac{x^2(t)}{8I_{dc}^{3/2}} + ...)e^{j\phi(t)} \otimes h(t)] \\ &\quad \times [(\sqrt{I_{dc}} + \frac{x(t)}{2\sqrt{I_{dc}}} - \frac{x^2(t)}{8I_{dc}^{3/2}} + ...)e^{j\phi(t)} \otimes h(t)]^* \\ &= I_{dc} + \frac{x(t) \otimes [h(t) + h^*(t)]}{2} - \frac{x^2(t) \otimes [h(t) + h^*(t)]}{8I_{dc}} + ... \end{aligned} \tag{2.45}$$

On the right hand side of Eq. (2.45), the first term represents the DC component; the second term contains the transmitted OFDM signal that needed to be recovered; and the third term and all the following terms stand for the unwanted intermixing products due to the detector nonlinearity and the fibre effects, which are responsible for OFDM subcarrier×subcarrier intermixing [2.39].

In the OFDM receiver, the electrical signal is decoded into the original data sequence by the receiver, which is the inverse of the transmitter. The information transmitted in the positive frequency bins is then recovered. In this case, as no local LDs are required for optical signal detection, synchronization only includes FFT window synchronization and simplifies the system as compared with the CO-OFDM cases.

According to the above analyses, in spite of the merit on system simplicity and low cost, IMDD OOFDM also brings about important challenges including intensity modulation-induced low OOFDM signal Extinction Ratio (ER), nonlinear effects in the intensity modulator and direct detection-induced intermixing effects. Addressing these challenges, as discussed below, is the main emphasis of this thesis.

Intensity modulation induced issues:

1) An intensity modulated OOFDM signal contains a strong DC component [Eqs. (2.42)-(2.45)] which reduces the signal ER. The ER determines the effective Optical SNR (OSNR) of the modulated signal required to achieve a certain BER for a transmission system having fixed receiver sensitivity. Throughout the thesis, the OOFDM signal ER is defined as

$$R_{ext} = \frac{\dfrac{\sum_{j=1}^{K_1} A^2(i\Delta T)\Big|_{A^2(j\Delta T)\geq \overline{P}}}{K_1}}{\dfrac{\sum_{j=1}^{K_1} A^2(j\Delta T)\Big|_{A^2(j\Delta T)<\overline{P}}}{K_2}} \tag{2.46}$$

$$\overline{P} = \frac{\sum_{m=1}^{K_1+K_2} A^2(m\Delta T)}{K_1+K_2} \tag{2.47}$$

where $\overline{P}$ is the average optical power, $A(i\Delta T)$ ($A(j\Delta T)$) is the i-th (j-th) signal sample with its amplitude satisfying $A^2 \geq \overline{P}$ ($A^2 < \overline{P}$), ΔT is the sampling duration, K_1 (K_2) is the number of samples satisfying $A^2 \geq \overline{P}$ ($A^2 < \overline{P}$) within the entire OOFDM signal considered, and $K_1 + K_2$ is the total number of samples.

This definition considers the "noise-like" amplitude of an OOFDM waveform. Based on such a definition, the ER of an OOFDM signal emerging from an ideal intensity modulator is approximately 1.65dB; whilst in a DML-modulated OOFDM PON system, for a DML bias current of 36mA and a driving current Peak-to-Peak (PTP) of 8mA, the DML-modulated OOFDM signal has an ER as low as 0.2 dB.

2) Optical intensity modulation of OFDM signals using practical intensity modulators is nonlinear, which leads to distortions of the modulated OOFDM signals. For example, DMLs inevitably produce frequency chirp, which interact with fibre CD and introduce degradations on OOFDM signals. However, the unwanted frequency chirp-induced Frequency Modulation (FM) can be converted into useful Amplitude Modulation (AM) to enhance OOFDM signal ER by using a narrowband wavelength-offset optical filter in the transmitter. This interesting topic is investigated in Chapters 4-5. Also, SOA/RSOA intensity modulators bring about OOFDM signal waveform clipping effects due to gain saturation and limited modulation bandwidths, which significantly affect OOFDM signal transmission performance. Such signal clipping effect and SOA/RSOA modulation bandwidths are dependent on the SOA/RSOA intensity modulators' operating conditions. Therefore, optimization of SOA/RSOA operating conditions is critical for maximizing the system performance. These issues form the major task of Chapters 6-9.

Direct detection induced issues:

The direct detection gives rise to strong intermixing effects. As shown in Eq. (2.45), the equivalent channel impulse response is given by $h_{eq}(t) = h(t) + h^*(t)$. By considering fibre GVD shown in Eq. (2.25), the channel transfer function can be described by

$$H_{eq}(\omega) = (e^{j\Delta\omega^2\beta_2 z/2} + e^{-j\Delta\omega^2\beta_2 z/2})/2 = \cos(\Delta\omega^2\beta_2 z/2) \tag{2.48}$$

where $\Delta\omega = \omega - \omega_o$ is the angular frequency with respect to the angular frequency of the carrier ω_0. z is the transmission distance. It is clear from Eq. (2.48) that frequency nulls occur when $\cos(\Delta\omega^2\beta_2 z/2) = 0$ is satisfied, that is,

$$\Delta\omega^2\beta_2 z/2 = (k + 1/2)\pi, k = 0, \pm1, \pm2, \ldots \tag{2.49}$$

Consequently, upon detection of a Double Sideband (DSB) OOFDM signal, intermixing between the upper sideband and the lower sideband occurs, which introduces frequency ripples. By combining Eq. (2.49) and Eq. (2.27), the frequency ripples' locations are governed by [2.17]

$$z\Delta f^2 = \frac{(2k+1)f_c}{2\lambda_0 D}, \qquad \text{k} = 0,\pm1,\pm2,\ldots \tag{2.50}$$

Δf is the frequency difference between the optical carrier frequency, f_c, and the frequency ripple considered; λ_0 is the optical carrier wavelength, and D is the dispersion parameter defined in Eq. (2.27). As expected from Eq. (2.50), Fig. 2.16 (a) and (b) show that, frequency ripples occur within the DSB OFDM signal regime and become stronger with increasing transmission distance. This effect contaminates the fibre dispersion-induced phase shift in the electrical domain, leading to a reduced dispersion tolerance.

Apart from the intermixing between two sidebands, subcarrier×subcarrier intermixing effects also occur, as shown in the third term of the right hand side of Eq. (2.45); this induces interferences [2.39]. Such subcarrier intermixing effect associated with square-law photon detection reduces the optical power budget by at least 1dB [2.40]. Therefore, to alleviate these intermixing effects is of great importance for IMDD OOFDM systems.

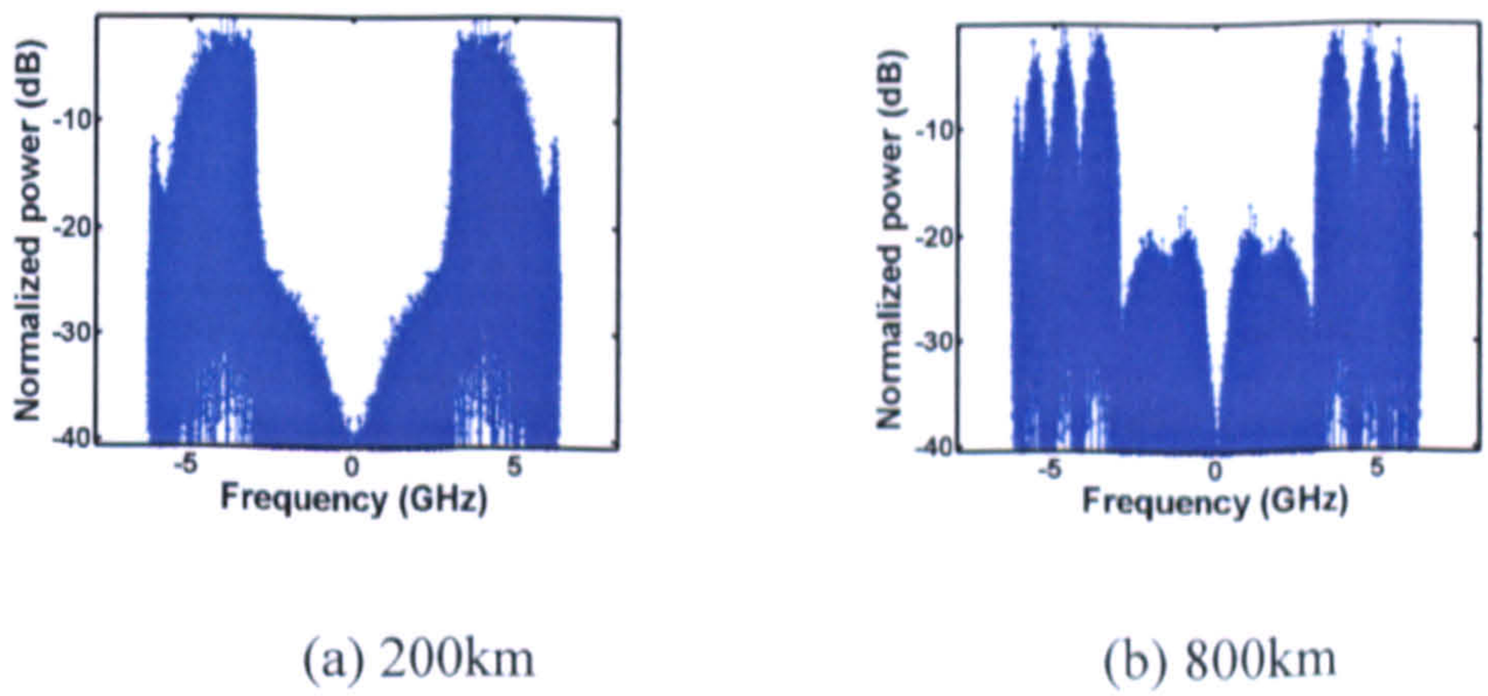

(a) 200km (b) 800km

Fig. 2.16 Electrical OFDM signal spectrum in the receiver for different SMF distances.

2.4.4 Comparison between CO-OFDM and IMDD OOFDM

As discussed in subsections 2.4.2 and 2.4.3, CO-OFDM and IMDD OOFDM each have their own strengths and drawbacks. Table 2.1 summarizes the differences between CO-

OFDM and IMDD OOFDM. Generally, CO-OFDM represents the ultimate performance in robustness to CD and PMD, as CD and PMD induced phase shifts can be well preserved upon linear coherent detection. Therefore, theoretically speaking, CO-OFDM is capable of offering virtually unlimited dispersion tolerance. On the other hand, for IMDD OOFDM, tolerance to CD and PMD is limited due to nonlinear direct detection. In addition, CO-OFDM also outperforms IMDD OOFDM on receiver sensitivity.

On the other hand, due to the coherent detection with a local laser, CO-OFDM requires frequency offset compensation, which complicates the receiver synchronization compared to IMDD OOFDM where frequency offset does not occur. More importantly, the requirements of expensive and bulky equipments for Electrical to Optical (E/O) and Optical to Electrical (O/E) conversions in CO-OFDM systems limit their applications to long-haul transmission systems. IMDD OOFDM offers promising solutions for cost-sensitive application scenarios including LAN, access networks and MANs.

Table 2.1 Comparisons between CO-OFDM and IMDD OOFDM

	CO-OFDM	IMDD OOFDM
Modulation	Field modulation	Intensity modulation
Detection	Coherent detection	Square-law direct detection
Linearity of E/O and O/E	Linear	Nonlinear
Dispersion tolerance	Unlimited (theoretically)	Limited by direct detection
Synchronization	FFT window; and frequency offset	FFT window
Receiver sensitivity	High	Relatively Low
System complexity and cost	Complex, expensive	Simple, cost-effective
Applications	Long-haul transmissions	MANs, access networks, and LANs

2.4.5 Adaptively Modulated OOFDM

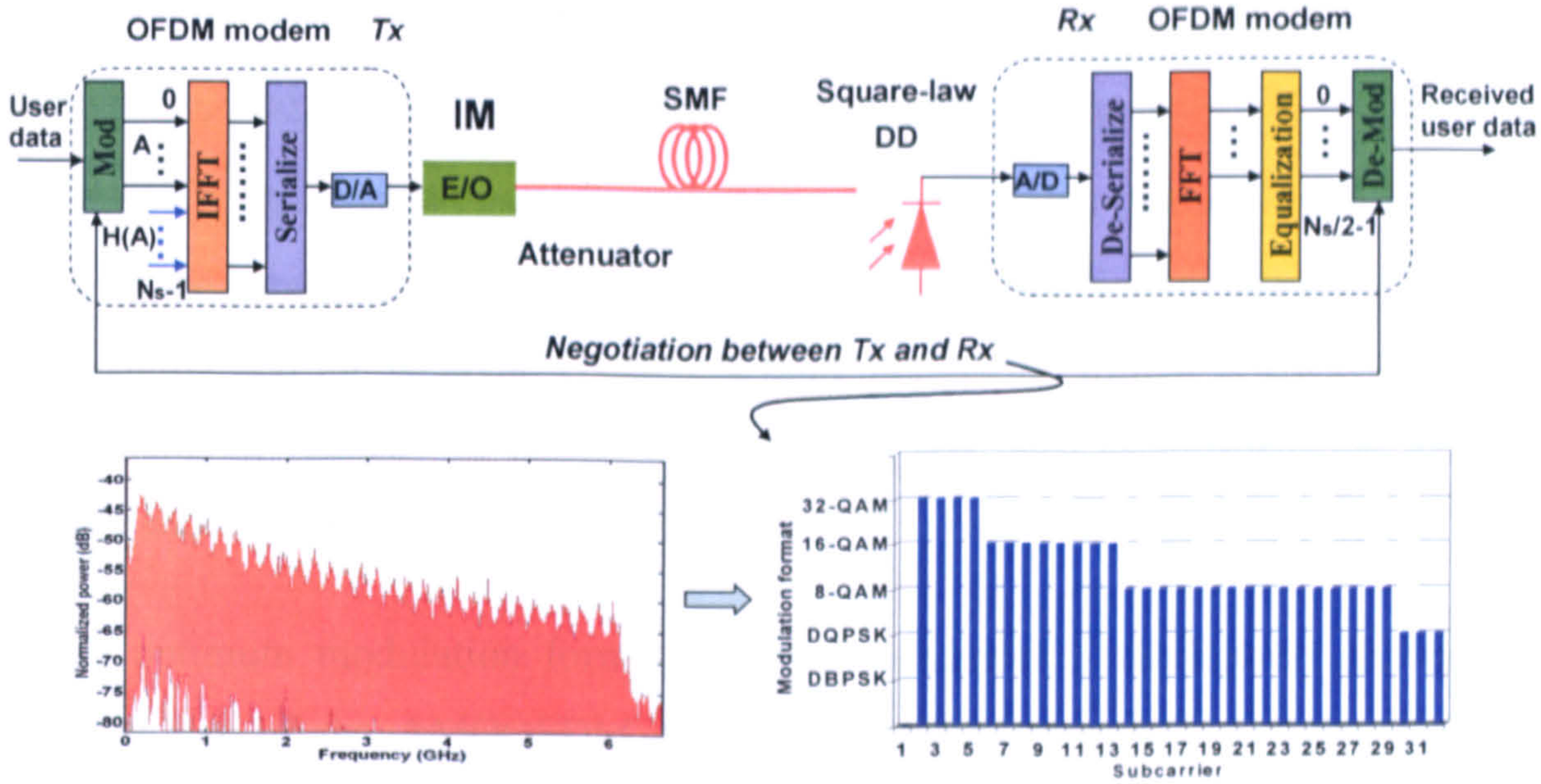

Fig. 2.17 AMOOFDM transmission system

In an IMDD OOFDM system, there is a system frequency response roll-off effect induced by optical and electrical components involved in the transmission system. To compensate this roll-off effect, AMOOFDM [2.14] was proposed to adapt channel conditions via adjusting the modulation format taken on each subcarrier. Fig. 2.17 depicts the AMOOFDM system, where the highest signal modulation format that can be used on each subcarrier is identified by negotiations between the transmitter and the receiver in the initial stage of establishing a connection over the SMF system. The modulation formats vary from Differential Binary PSK (DBPSK), Differential QPSK (DQPSK), 8-QAM, to 256-QAM. Generally speaking, a high (low) modulation format is used on a given carrier suffering a low (high) transmission loss. Any subcarrier suffering a very high loss may be dropped completely to avoid the occurrence of a large number of errors on the subcarrier.

A practical way to realize adaptive modulation is to feedback the subcarrier BERs and the total channel BER to the transmitter so that the optimum modulation format for each subcarrier can be determined. In an AMOOFDM system, the total channel BER, BER_T, is defined as

$$BER_T = \sum_{k=2}^{M_s} En_k \Big/ \sum_{k=2}^{M_s} n_k \tag{2.51}$$

where $M_s = N_s/2$ is the number of data-carrying subcarriers in the positive frequency bins, En_k is the total number of detected errors and n_k is the total number of transmitted binary bits. Both En_k and n_k are for the k-th subcarrier, whose subchannel BER, BER_k is given by $BER_k = En_k/n_k$. Based on BER_T and BER_k, the maximum modulation format adopted on each of the subcarriers within a symbol can be identified through negotiations between the transmitter and the receiver. Usually, a high modulation format is always preferred if BER_T remains at 1.0×10^{-3} or better. Once the link has been established, the modulation format on each subcarrier remains unchanged.

Once an optimum modulation format for each subcarrier is configured, the maximum signal line rate of the AMOOFDM system is obtained, which is calculated using the expression given below:

$$R_{signal} = \sum_{k=2}^{M_s} S_k = \frac{\sum_{k=2}^{M_s} n_k}{T_s} = \frac{r_s \sum_{k=2}^{M_s} n_k}{2M_s(1+\eta)} \tag{2.52}$$

where S_k is the signal bit rate corresponding to the k-th subcarrier, n_k is the total number of binary bits conveyed by the k-th subcarrier within one symbol period T_s, which is related to the ADC/DAC sampling rate r_s by $T_s = 2N_s(1+\eta)/r_s$ [2.25], and η is the cyclic prefix parameter defined previously. It should be noted that Eqs. (2.51)-(2.52) are not only valid for AMOOFDM systems but also applicable for identically modulated OOFDM systems, where identical modulation format is adopted across all the subcarriers.

The AMOOFDM technique has many advantages. AMOOFDM supports maximum data rate and improves the system flexibility. Also, compared with identical modulation, adaptive modulation is capable of reducing fibre nonlinearities including FWM and XPM due to the reduced PAPR of the DWDM AMOOFDM signals [2.15]. Therefore, AMOOFDM is a cost-effective solution for the delivery of broadband services for subscribers. In this thesis, explorations are also undertaken of the implementation of AMOOFDM in NG-PONs.

2.5 Conclusion

In this chapter, we have analysed the principles of OFDM and OOFDM. The basic idea of OFDM is to divide the serial bit stream into a number of parallel streams and transmit these low-rate parallel data simultaneously by using classical modulation formats such as M-ary QAM and (D)PSK on each parallel subcarrier. OFDM is therefore resilient to channel frequency-selective fading effects. With the aid of CP, OFDM has excellent tolerance of the channel dispersive effects. The efficient implementation of IFFT(FFT) largely reduces the OFDM system complexity. The disadvantages of OFDM are its high PAPR and sensitivity to time and frequency synchronization problems.

OOFDM enables excellent robustness against the fibre linear effects such as chromatic dispersion and PMD. Theoretically, CO-OFDM offers virtually unlimited dispersion tolerance. However, CO-OFDM is sensitive to the frequency and phase noise from the LD upon coherent detection. Moreover, the requirement of bulky and expensive equipments limits its applications in long-haul transmission systems. IMDD OOFDM uses simple intensity modulation and direct detection thus outperforms CO-OFDM on cost-sensitive application scenarios such as access networks. In addition, AMOOFDM systems can further improve the system scalability and flexibility. In the meantime, IMDD OOFDM also brings about important challenges including relatively low OOFDM signal ER induced by intensity modulation, nonlinear effects from intensity modulators and strong intermixing upon direct detection. Addressing these challenges forms the main task of this thesis.

References

[2.1] R. W. Chang, "Synthesis of band-limited orthogonal signals for multi-channel data transmission," Bell System Technical Journal, vol. 46, pp. 1775-1796, 1966.

[2.2] S. B. Weinstein and P. M. Ebert, "Data transmission by frequency-division multiplexing using the discrete Fourier transform," IEEE Tans. Commun. Technol., vol. 19, no.5, pp.628-634, Oct. 1971.

[2.3] A. Peled and A. Ruiz, "Frequency domain data transmission using reduced computational complexity algorithms," in *IEEE Proc. ICASSP 80*, Denver, CO, USA, vol. III, pp. 964-967, 1980.

[2.4] I. E. Telatar, Capacity of Multi-Antenna Gaussian Channels Tech. Memo., Bell Laboratories, Lucent Technologies, (Published in Euopean Trans. Telecommu., vol. 10, no.6, pp.585-595, Nov./Dec. 1999), Oct. 1995.

[2.5] B. J. Dixon, R. D. Pollard, and S. Iezekiel, "Orthogonal frequency-division multiplexing in wireless communication systems with multimode fiber feeds," IEEE Transactions on Microwave Theory and Techniques, vol. 49, no.8, pp. 1404-1409, Aug. 2001.

[2.6] R. Lassalle and M. Alard, "Principles of modulation and channel coding for digital broadcasting for mobile receivers," EBU Tech. Rev., pp. 168-190, 1987.

[2.7] PCC-Personal Computing and Communication, *4GW Project*, available at http://www.s3.kth.se/radio/4GW/

[2.8] ETSI ETS 300 401 (1997): "Radio broadcasting systems; DAB to mobile, portable and fixed receivers".

[2.9] Digital Video Broadcasting, available online at http://en.wikipedia.org/wiki/Digital_Video_Broadcasting.

[2.10] N. E. Jolley, H. Kee, R. Rickard, J. Tang, and K. Cordina, "Generation and propagation of a 1550 nm 10 Gb/s optical orthogonal frequency division multiplexed signal over 1000 m of multimode fibre using a directly modulated DFB," presented at the *OFC/NFOEC*, (OSA, 2005), Paper OFP3.

[2.11] J. Yu, J. Hu, D. Qian, Z. Jia, G. K. Chang and T. Wang, "Transmission of microwave-photonics generated 16Gbit/s super broadband OFDM signals in radio-over-fiber system," presented at the *OFC/NFOEC*, (OSA, 2008), Paper OThP2.

[2.12] C. –T. Lin, Y.-M. Lin, J. Chen, S.-P. Dai, P. T. Shih, P. –C. Peng, and S. Chi, "Optical direct-detection OFDM signal generation for radio-over-fiber link using frequency doubling scheme with carrier suppression," Opt. Express, vol. 16, no. 9, pp. 6056-6063, Apr. 2008.

[2.13] S. C. J. Lee, F. Breyer, S. Randel, O. Ziemann, H. P. A. van den Boom, and A. M. J. Koonen, "Low-cost and robust 1-Gbit/s plastic optical fiber link based on light-emitting diode technology," presented at the *OFC/NFOEC*, (OSA, 2008), Paper OWB3.

[2.14] J. M. Tang and K. A. Shore, "High-speed transmission of adaptively modulated optical OFDM signals over multimode fibers using directly modulated DFBs," J. Lightwave Technol., vol. 24, no. 1, pp. 429-441 Jan. 2006.

[2.15] E. Giacoumidis, J. L. Wei, X. L. Yang, A. Tsokanos and J. M. Tang, "Adaptive Modulation-Enabled WDM Impairment Reduction for Multi-Channel Optical OFDM Transmission in PONs," IEEE Photonics J., vol. 2, no. 2, pp. 130-140, Apr. 2010.

[2.16] X. Q. Jin, R. P. Giddings, E. Hugues-Salas and J. M. Tang, "Real-time experimental demonstration of optical OFDM symbol synchronization in directly modulated DFB laser-based 25km SMF IMDD systems," Opt. Express, vol.18, no. 20, pp. 21100-21110, Sep. 2010.

[2.17] J. L. Wei, X.Q. Jin, and J.M. Tang, "The influence of directly modulated DFB lasers on the transmission performance of carrier suppressed single sideband optical OFDM signals over IMDD SMF systems," J. Lightwave Technol. vol. 27, no. 13, pp. 2412 – 2419, July 2009.

[2.18] W. Shieh, "Maximum-Likelihood Phase and Channel Estimation for Coherent Optical OFDM," IEEE Photon. Technol. Letters, vol. 20, no. 8, pp. 605-607, Apr. 2008.

[2.19] W. Shieh, H. Bao, and Y. Tang, "Coherent optical OFDM: theory and design," Opt. Express, vol. 16, no. 2, pp. 841-859, Jan. 2008.

[2.20] W. Shieh, X. Yi, Y. Ma and Q. Yang, "Coherent optical OFDM: has its time come? [invited]," J. Optical Netw., vol.7, no. 3, pp.234-255, Mar. 2008.

[2.21] A. J. Lowery, "Fiber nonlinearity pre- and post-compensation for long-haul optical links using OFDM," Opt. Express, vol. 15, no. 20, pp. 12965-12970, Oct. 2007.

[2.22] W. Shieh, and I. Djordjevic, *Orthogonal Frequency Division Multiplexing for Optical Communications*, Academic Press, Inc., 2010.

[2.23] L. W. Couch, *Digital and Analog Communication Systems*, (Prentice Hall, 2006)

[2.24] L. Hanzo, S. X. Ng, T. Keller, and W. Webb, *Quadrature Amplitude Modulation: From Basics to Adaptive Trellis-Coded, Turbo-Equalised and Space-Time Coded OFDM, CDMA and MC-CDMA Systems.* (Hoboken, NJ: Wiley, 2004).

[2.25] E. Giacoumidis, J. L. Wei, X. Q. Jin and J. M. Tang, "Improved transmission performance of adaptively modulated optical OFDM signals over directly modulated DFB laser-based IMDD links using adaptive cyclic prefix," Opt. Express, vol. 16, no. 13, pp. 9840-9494, Jun. 2008.

[2.26] T.-D. Chiueh and P.-Y. Tsai, *OFDM Baseband Receiver Design for Wireless Communications*, Wiley, 2007.

[2.27] R. Prasad, OFDM for Wireless Communications Systems. London: Boston, 2004.

[2.28] M. Sandell, J. J. Van de Beek, and P. O. Börjesson, "Timing and frequency synchronization in OFDM systems using the cyclic prefix," in Int. Symposium Synchronization, (Essen, Germany, 1995), pp. 16–19.

[2.29] T. Wakutsuand and M. Serizawa, "A novel carrier frequency offset estimation scheme for OFDM systems utilizing correlation with a pilot symbol without sub-

carrier.," in Proc. of IEEE 49th Vehicular Technology Conference, VTC'99, vol. 1, (Houston, Texas, USA, May 1999), pp. 113–117.

[2.30] P. Gysel and R. K. Staubli, "Statistical properties of Rayleigh backscattering in single-mode fibers," J. Lightwave Technol., vol. 8, no. 4, pp. 561-567 Apr. 1990.

[2.31] C. Arellano, K.-D. Langer, and J. Prat, "Reflection and multiple Rayleigh backscattering in WDM single-fiber loopback access networks," J. Lightwave Technol., vol. 27, no. 1, pp. 12-18 Jan. 2009.

[2.32] G. P. Agrawal, *Nonlinear Fibre Optics*, Academic Press, Inc., 1995.

[2.33] J. G. Proakis, *Digital Communication*, McGraw-Hill, Inc., 1995.

[2.34] A. Ghatak and K. Thyagarajan, *Introduction to Fibre Optics*. Cambridge: University Press, 1998.

[2.35] K.-D Chang, G.-C. Yang, and W. C. Kwong, "Determination of FWM products in unequal-spaced-channel WDM lightwave systems," J. Lightwave Technol., vol. 18, no. 12, pp. 2113-2122 Dec. 2000.

[2.36] T.Katagiri, T. Naito, A. Miura, K. Amemiya, R. Funane, "FWM crosstalk suppression using wavelength grouping in 25-GHz-spaced 10Gbps-based WDM transmission over NZ-DSF in C-band," OFC 2003, Paper FE6.

[2.37] N.R. Newbury, "Pump-wavelength dependence of Raman gain," *OAA 2002*, Paper OME9.

[2.38] E. Yamazaki, et al., "Multi-staged nonlinear compensation in coherent receiver for 12015km WDM transmission of 10ch × 111Gb/s no-guard-interval CO-OFDM," Electronic Lett. , vol. 45, no. 13. pp. 635-645, 2009.

[2.39] A. J. Lowery, "Amplified-spontaneous noise limit of optical OFDM lightwave systems," Opt. Express, vol. 16, no. 2, pp. 860-865, Jan. 2008.

[2.40] J. L. Wei, C. Sánches, R.P. Giddings, E. Hugues-Salas, and J. M. Tang, "Significant improvements in optical power budgets of real-time optical OFDM PON systems," Opt. Express, vol. 18, no. 20, pp. 20732-20745, Sep. 2010.

3 PON Fundamentals

Contents

3.1 Introduction 58

3.2 Access Network Architectures 58

3.2.1 Digital Subscriber Line (DSL) 59

3.2.2 Hybrid Fibre Coaxial (HFC) 60

3.2.3 Passive Optical Networks (PONs) 61

3.3 PON Evolution 63

3.3.1 ITU-T BPON and GPON 64

3.3.1.1 APON/BPON and ITU-T G.983 64

3.3.1.2 GPON and ITU-T G.984 65

3.3.2 EPON and IEEE 802.3ah 66

3.3.3 10Gb/s NG-PONs 67

3.3.3.1 IEEE 10G-EPON 67

3.3.3.2 ITU-T XG-PON 68

3.3.4 Beyond 10G-EPON/XG-PON 70

3.4 Promising Technologies for NG-PONs 70

3.4.1 WDM-PON 70

3.4.2 Hybrid WDM/TDM-PON 72

3.4.3 OOFDM PON 73

3.5 Electro-optic Convertors for PONs 74

3.5.1 Directly Modulated Laser 76

3.5.1.1 Fabry-Perot Laser 76

3.5.1.2 Distributed Feedback (DFB) laser 77

3.5.1.3 VCSEL 77

3.5.2 External Modulator 78

3.5.2.1 RSOA/SOA Modulator 79

3.5.2.2 Electro-Absorption Modulators (EAMs) 80

3.6 Conclusion 80

3.1 Introduction

To gain some knowledge of PON fundamentals, this chapter first reviews various access network technologies including DSL, HFC, and PON. As PONs are dominant technologies for today's access networks due to their mature standards and massive global deployment, the evolution of PON technologies and standards is also overviewed in this chapter, which include ITU-T B/GPON, IEEE EPON as well as NG-PON technologies such as IEEE 10G-EPON and ITU-T NG-PON1 (also referred to as XG-PON) and NG-PON2. ITU-T NG-PON2 provides a long-term solution beyond 10G-EPON/XG-PON, and allows more emerging technology candidates to be considered, namely WDM-PONs, hybrid WDM/TDM-PON and OOFDM PON, which are also discussed in this chapter.

The FSAN/ITU-T emphasizes on keeping optoelectronic components of NG-PONs as common as possible in order to achieve cost-effectiveness. Considering the fact that there are plenty of dark fibres that have already been installed in practice, and that electro-optic convertors take a majority part of the cost of PON transceivers, therefore, various PON optical modulators are discussed in this chapter in terms of their operating principles, advantages and disadvantages. Among all those modulators, the widely used DMLs and RSOAs/SOAs have demonstrated to be cost-effective solutions for NG-PONs.

3.2 Access Network Architectures

A generic structure of a modern telecommunication network is shown in Fig. 3.1, which comprises inter-connected core networks, Metro networks and access networks. The core network is a central part of the network, which provides long distance and high capacity services via WDM to customers connected to it through Metro networks or access networks. Metro/regional networks lie in a city or region responsible for traffic grooming and multiplexing functions. While access networks distribute signals downstream to end subscribers and transmit the aggregated traffic upstream to the service providers' Central Offices (COs).

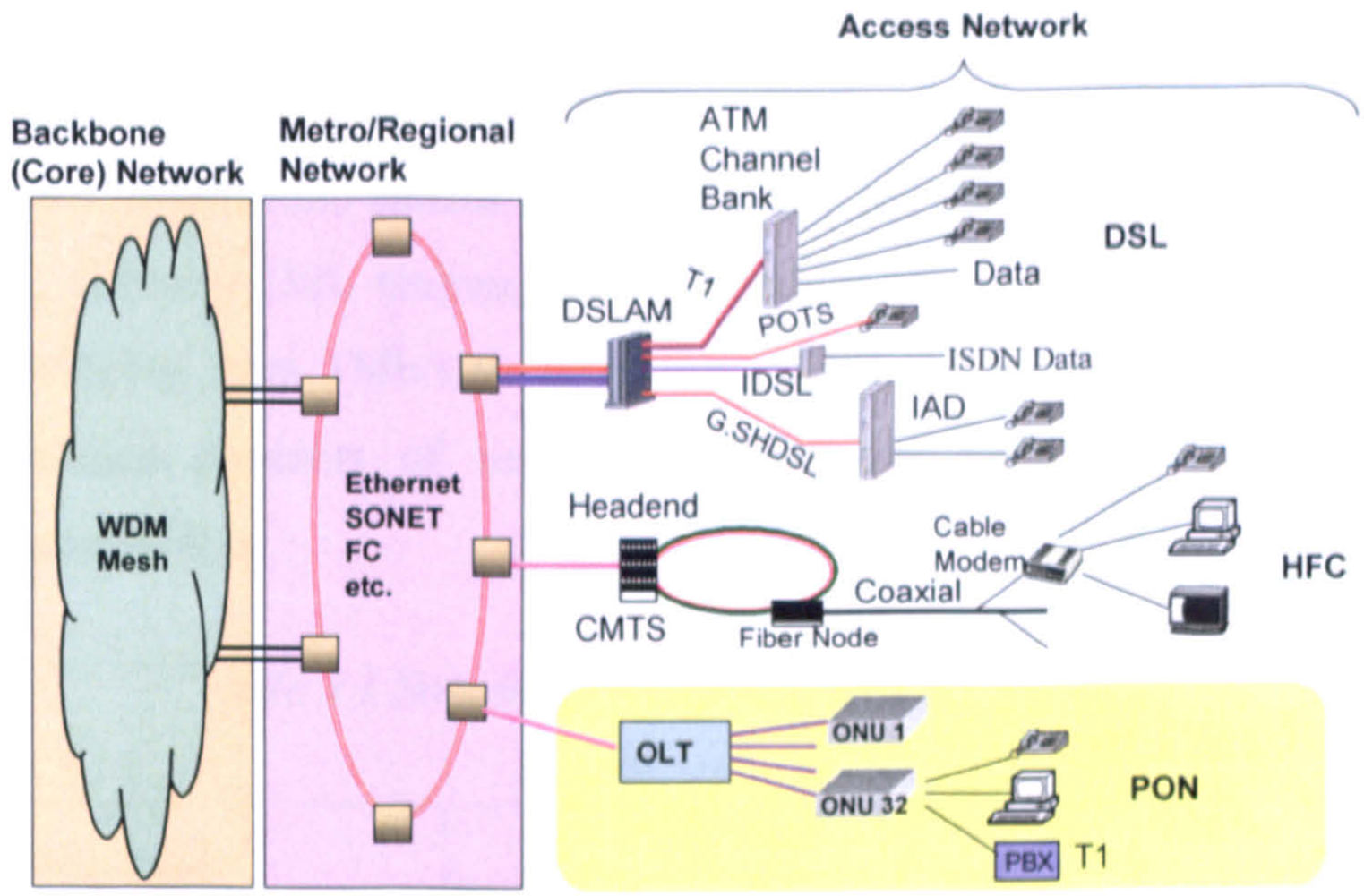

Fig. 3.1 Generic structure of a modern telecommunication network (from [3.1]).

Initially, the most widely deployed transmission media in access networks are twisted-pair copper cables that have been used for telephone lines for more than 100 years. Over a long history, analogue voice services were transmitted over 4 kHz bandwidth. As Internet was first invented in 1960s, the voice grade bandwidth was also used to transmit digital Internet signals, however, the best data rate available was only 56kbps [3.1]. In order to deal with the growing bandwidth requirement, solutions including new modulation techniques for legacy copper cables and deployment of optical fibre were proposed. This leads to the co-existence of today's major wired access network technologies including DSL, HFC, and PONs.

3.2.1 Digital Subscriber Line (DSL)

DSL, or collectively called xDSL, uses multi-level modulation technique such as QAM in twisted-pair copper cables, leading to maximized throughput. In DSL networks, a DSL modem is employed at the user end to connect the user to the service provider through a DSL Access Multiplexer (DSLAM) located at a remote node or central office as shown in Fig.3.1. The DSL modem acts as a filter to separate the voice signals from data signals. The DSLAM provides a Point-to-Point (P2P) dedicated bandwidth between the service provider and each end user.

In DSL systems, the 0 to 4kHz band carries the traditional Plain Old Telephone Service (POTS) line, and the 25kHz to 160kHz band carries the upstream (user to carrier) data and the 240KHz to 1.5MHz band carries the downstream (carrier to user) data. As summarized in Table 3.1, different DSL techniques provide symmetric or asymmetric transmission bandwidths, ranging from 1Mb/s to 100 Mb/s. VDSL (VDSL2) provides the maximum bandwidth-distance products of roughly 50 Mb/s-km (30Mb/s-km) for downstream (upstream) transmission.

Table 3.1 Summery of different DSL technologies

DSL Type	Maximum speed		Max. Trans. distance	Number of lines	ITU Standard
	Downstream	Upstream			
ADSL (Asymmetric DSL)	8Mb/s	700Kb/s	5.5km	1	G.992(1999)
HDSL (High data rate DSL)	1.54Mb/s	1.54Mb/s	3.65km	2	G.991.1(1998)
IDSL (ISDN)	144Kb/s	144Kb/s	10.7km	1	
MSDSL (Multirate Symmetric DSL)	2Mb/s	2Mb/s	8.8km	1	
RADSL (Rate Adaptive DSL)	7Mb/s	1Mb/s	5.5km	1	
SDSL (Symmetric DSL)	2.3Mb/s	2.3Mb/s	6.7km	1	
VDSL (Very high data rate DSL)	52Mb/s	16Mb/s	1.2km	1	G.993.1 (2004)
VDSL2 (30-MHz)	100Mb/s	100Mb/s	300m		G.993.2(2006)

3.2.2 Hybrid Fibre Coaxial (HFC)

HFC implements a hybrid optical fibre and coaxial copper cable architecture to deliver Cable Television (CATV), voice, and Internet services to end users and transmit aggregated data from users. As shown in Fig. 3.1, cable modems at individual households are connected to a Cable Modem Termination System (CMTS) at a headend office. Downstream data signals from head ends are transmitted to remote fibre node where they are converted back to the RF domain and broadcast to individual cable modems through the coaxial cable plant. Each individual cable modem recognizes its data by the Identifier (ID) embedded in downstream data. Customer data are multiplexed using TDM. The CMTS acts a Media Access Control (MAC) master which assigns upstream time slots for each cable modem.

The downstream and upstream signals are transmitted simultaneously through the same cable between the home and the remote fibre node through FDM. The coaxial cable has a useable frequency range of up to 1GHz, which is much broader than that corresponding to

twisted pairs. Broadcast TV signals normally occupy a frequency band from 50MHz to 500MHz or 750MHz. Each CATV channel occupies a 6-MHz or 8-MHz bandwidth, and 5 MHz to 42 MHz are used for upstream data transmission.

Table 3.2 Summary of DOCSIS modulation format and data rate

DOCSIS Versions	Downstream		Upstream	
	Modulation format	Max. data rate	Modulation format	Max. data rate
1.0	64-QAM,256-QAM	38Mb/s	QPSK, 16-QAM	10Mb/s
2.0		40Mb/s	QPSK, 16-QAM, 32-QAM, 64-QAM, 128-QAM	30Mb/s
3.0		160Mb/s		120Mb/s

Data over Cable Service Interface Specification (DOCSIS) specifies the modulation formats for both HFC downstream and upstream transmissions. Table 3.2 lists the available downstream/upstream modulation formats, and the corresponding maximum achievable data rate specified by the three versions of DOCSIS. However, such a large bandwidth is shared by hundreds of households per fibre node, the per user bandwidth is only 3Mb/s to 8 Mb/s downstream and 200kbps to 800kbps upstream.

3.2.3 Passive Optical Networks (PONs)

PONs are promising solutions for access networks. A typical TDM-PON system is illustrated in Fig. 3.2, which consists of an Optical Line Terminal (OLT) located in the CO, multiple Optical Network Units (ONUs), a fibre link and a Power Splitter (PS). The section between OLT and ONUs is referred to as Optical Distribution Network (ODN).

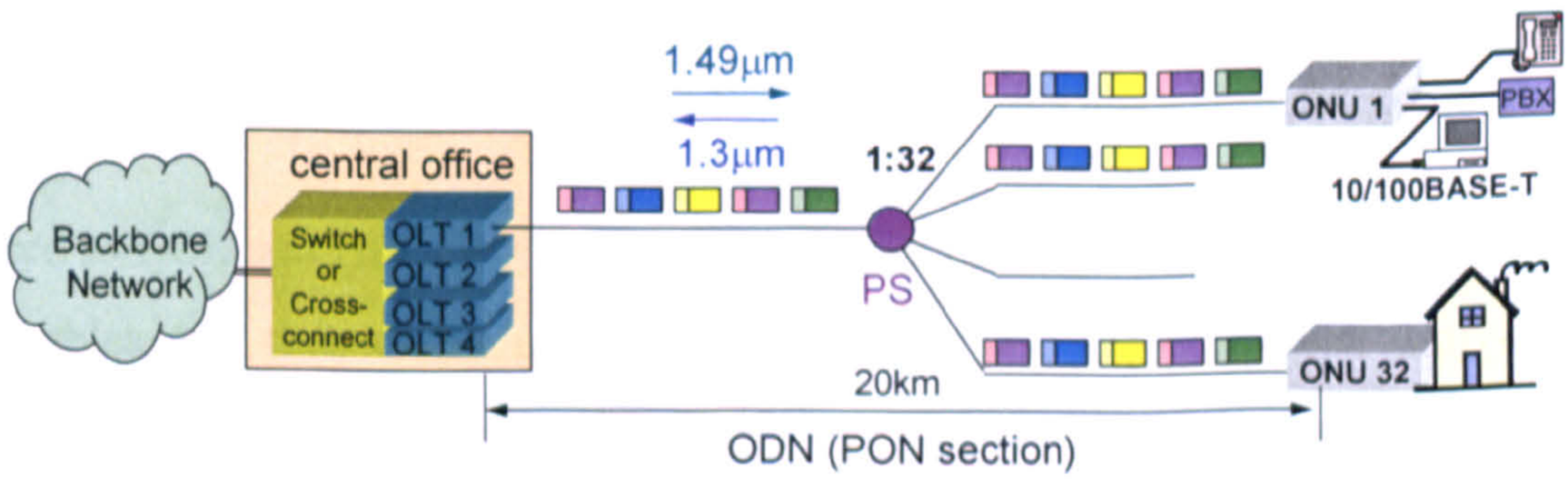

Fig. 3.2 A typical TDM-PON architecture (from [3.1])

Multiple OLTs in the CO are interconnected with a backbone switch or cross-connect, which provides the cross-connection and switching among different OLTs, ONUs and the backbone network. OLT also provides the translation between the backbone signal formats

(e.g. SONET/SDH, or Ethernet) and ODN signal ones [3.1]. Similar to the OLT, the ONU performs translation between ODN signal formats and signal formats used by the end user equipments.

The PON architecture generally supports 32 ONUs with a maximum covered transmission distance of usually 10 to 20km. The bidirectional transmission of downstream and upstream signals is realized by Coarse WDM (CWDM) with 1.49μm and 1.3μm wavelengths being assigned to downstream and upstream, respectively.

The PON is a shared network due to the use of the Point-to-Multi-Point (P2MP) topology. In downstream, the OLT broadcasts signals to all ONUs by interleaving frames destined for different ONUs as a continuous stream. Each ONU extracts its own frames based on its own ID. In upstream, since there is only one receiver in the OLT and a single feeder fibre, ONUs take turns to send their data in a TDM schedule. Moreover, when an ONU is not sending data, it has to turn off its laser to avoid interference with other ONUs' upstream transmission. As a result, the use of burst mode ONU transmitters and OLT receivers is critical in PON.

The PON has numerous advantages which are summarized as followings:

- PON eliminates the need for active optoelectronic and electronic devices located in the cabinet in the harsh outside environment. No power consumption equipment leads to low maintenance cost and better system performance stability.
- The system cost including OLT devices, fibre installation and maintenance is shared by a number of customers. This makes PONs cost-effective.
- PON offers topological flexibility by placing the PS anywhere along the fibre link.

Compared to DSL and HFC, PON eliminates the bandwidth "bottleneck" caused by legacy copper cables and thus offers much larger capacity and reach to each individual user. PONs have been deployed all over the world. In a global view, Asia Pacific gains the most success in PONs. Take Japan for example, the number of PON subscribers has exceeded that of DSL and HFC, thus PON becomes the dominant access network technology [3.2]. The success of PON relies on not only the strong user demand of broadband services but also government and regulatory support and competitive market. In Japan, the government set up "e-Japan" plan targeting 30 million PON subscribers by 2010. South Korea

government established the "e-Korea" (2002) plan and later "U-Korea" (ubiquitous integration) to build broadband convergence networks as core networks for U-Korea. China also announced to deploy the world's largest PON deployment [3.3]. It is envisioned that PON will experience a golden time in the next a few decade.

Standardized PON has several variants including ITU-T Asynchronous Transfer Mode (ATM) PON (APON)/Broadband PON (BPON)/GPON and IEEE EPON, as well as NG-PONs including IEEE 10G-EPON and ITU-T XG-PON and NG-PON2. The next section reviews the evolution of PON technologies.

3.3 PON Evolution

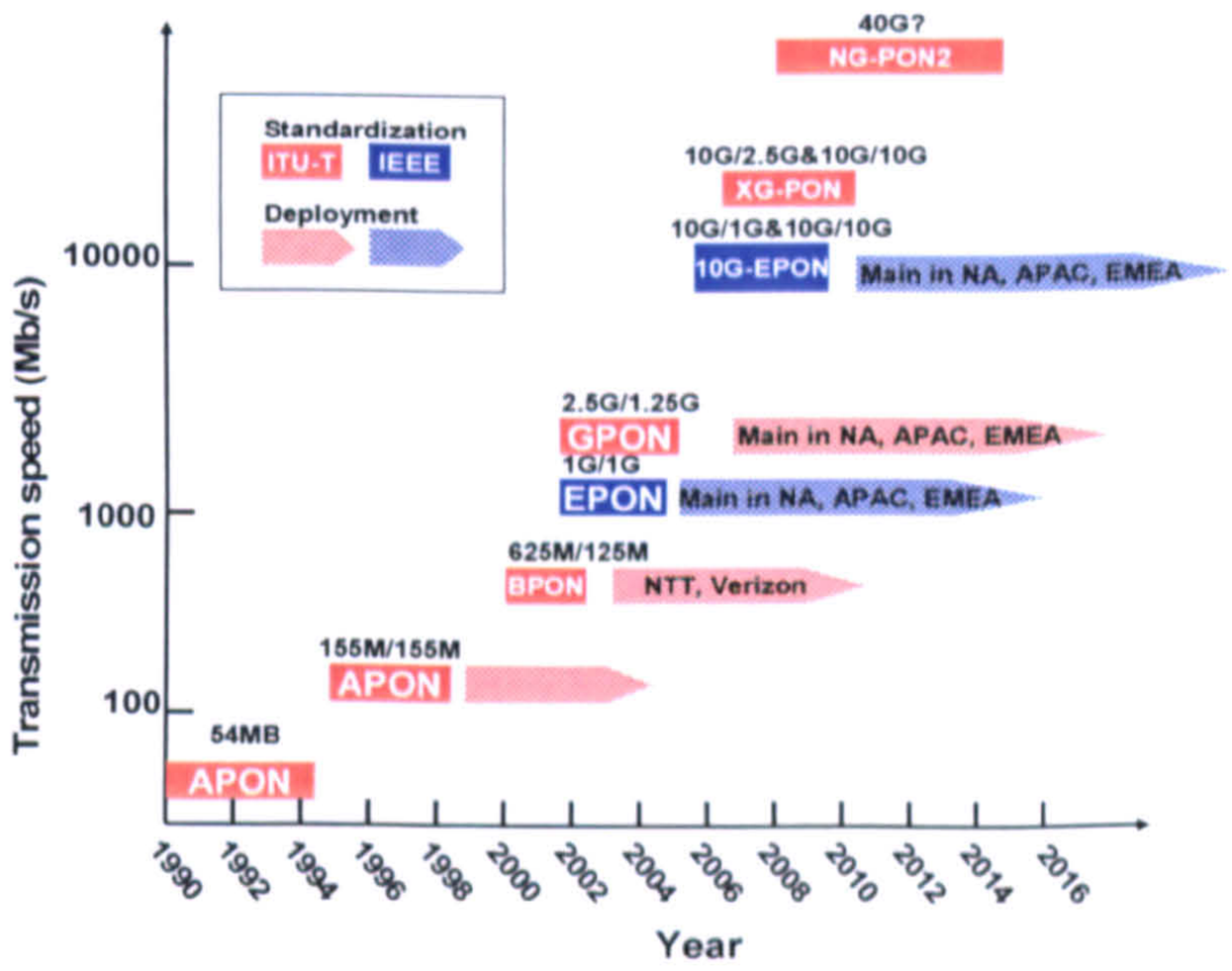

Fig. 3.3 History of PON development

Fig. 3.3 illustrates the evolution of PON technologies together with reference to actual deployments in major global areas. The first generation of PON is ITU-T APON (G.983.1) supporting a data rate from a few tens of Mb/s to hundreds of Mb/s, which gained small scale deployment. Later, ITU-T specified BPON (G.983.3) and further GPON (G.984) which supports data rate of up to 2.5Gb/s thus were widely deployed over the world. In the meantime, to compete with GPON, IEEE also specified EPON standard (802.3ah) offering 1Gb/s data rate. To deliver ever increasing broadband services, both ITU-T and IEEE started NG-PON standardization work of 10G-EPON (802.3av) and XG-PON (X is the

Rome sign of 10: G.987), respectively, targeting 10Gb/s data rate. Moreover, ITU-T also considers long-term solutions with even higher data rates, which is referred to NG-PON2.

PON standards cover the data link layer (MAC layer) and physical (PHY) layer of the Open System Interconnect (OSI) reference model. This subsection reviews various PON technologies shown in Fig. 3.3, together with their standards.

3.3.1 ITU-T BPON and GPON

3.3.1.1 APON/BPON and ITU-T G.983

The work of APON was started by Full Service Access Network (FSAN)/ITU-T and later transferred to ITU-T G.983.1 standard in 1998. BPON is a higher speed version of APON and was specified in G.983.3 in 2001. For this reason, we simply use BPON to refer to this class of PON subject to G.983 series [3.4]. Here, a general summery of BPON in terms of the PHY layer and MAC layer is presented. The PHY layer covers data rate, transmission distance, power split ratio, wavelength plan and optical link budget.

PHY Layer

Table 3.3 BPON downstream/upstream data rate combinations

	Downstream	**Upstream**
1.	155.52Mbps	155.52Mbps
2.	622.08Mbps	155.52Mbps
3.	622.08Mbps	622.08Mbps
4.	1244.16Mbps	155.52Mbps
5.	1244.16Mbps	622.08Mbps

Data rates: BPON supports both symmetric and asymmetric downstream/upstream data rates, as listed in Table 3.3.

Power split ratio: Typically 1:32 or 1:64, restricted by path loss.

Transmission distance: Maximum 20km.

Wavelength plan: ITU-T G.983.3 specifies CWDM wavelength overlay for both BPON and GPON systems, as shown in Fig. 3.4. The upstream transmission uses the 1260-1360nm window and downstream uses the 1480-1500nm window. The C-band as an enhanced band is used for carrying either CATV signals or additional digital services

such as SONET/SDH links. Other two bands including the 1360-1480nm band and 1565 nm beyond are reserved for future applications.

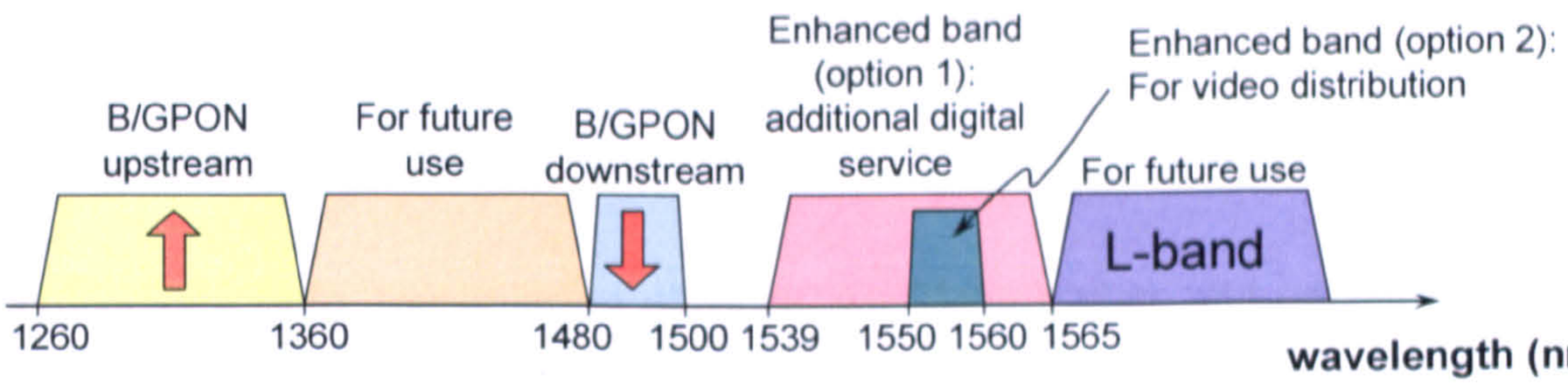

Fig. 3.4 Wavelength plan for B/GPON systems.

Optical link budget: All ITU PON standards feature three classes of optical link budgets for different ODN attenuations between ONU and OLT. The three classes are Class A (5 to 20dB), Class B (10 to 25dB) and Class C (15 to 30dB), which are specified in ITU-T G.982 [3.5]. Later, Class B+ with 28dB attenuation was also introduced by most PON transceiver vendors due to cost reasons.

MAC Layer

BPON is based on the ATM communication protocol in the MAC layer. BPON signals are transported in timeslots. Each timeslot contains an ATM cell or a Physical Layer Operation, Administration and Maintenance (PLOAM) cell. PLOAM cells are used to carry physical layer management information. The downstream frame is composed of 56 ATM cells for the basic rate of 155Mb/s, in which two dedicated PLOAM cells are inserted at the beginning and the middle of the frame, and the remaining 54 ATM cells carry the data. The downstream frame can scale up to 224 and 448 ATM cells for the rates of 622Mbit/s and 1244 Mbit/s, respectively. The upstream frame is similar but can be divided into mini-slots to support Dynamic Bandwidth Allocation (DBA) mechanisms (G.983.4).

3.3.1.2 GPON and ITU-T G.984

GPON is an evolution of BPON with a high data rate. The GPON standard G.984 series [3.6] inherited many ideas covered in the G.983 standards.

PHY Layer

Data rate: Similar to BPON, the downstream and upstream bit rates defined in G.984 are also combinations of several possible rates, which are

- Downstream: 1244.16Mbps / 2488.32Mbps
- Upstream: 155.52Mbps / 622.08Mbps / 1244.16Mbps / 2488.32Mbps

The power split ratio, transmission distance, wavelength plan, and optical link budget of GPON are identical to those of BPON.

MAC Layer

GPON MAC layer is described as GPON Transmission Convergence (GTC), which supports two operation modes: ATM and GPON Encapsulation Mode (GEM). GEM allows adaptation of various protocols, including Ethernet and TDM. Therefore, GPON is not only back compatible to BPON but also capable of carrying different applications. Additionally, G.984.3 defines an optional Forward Error Correction (FEC) capability using RS(255, 239) code in GTC framing to improve the optical link budget in GPON.

3.3.2 EPON and IEEE 802.3ah

The work of EPON was started in March 2001 by the IEEE 802.3ah study group and finished in June 2004 [3.7]. EPON provides 1.25Gb/s symmetric downstream and upstream bandwidth, which are shared by 16 or 32 ONUs. Two different reaches of 10km and 20km between the OLT and ONU are defined in EPON. EPON also inherits the wavelength allocation plan of GPON, as shown in Fig. 3.4. However, EPON does not specify a wavelength for CATV broadcast. Moreover, EPON adopts 8B/10B line coding but the use of FEC is optional in EPON.

In EPON MAC layer, all services are framed in the Ethernet format thus EPON inherently support IP-based applications such as Voice over IP (VoIP) and IPTV. Different from conventional Ethernet technique based on P2P, EPON supports P2MP by adopting a new sub-layer Multi-Point Media access Control (MPMC) in the data link layer. P2P emulation function is introduced in EPON in order to operate with the 802.1 based Ethernet switching.

3.3.3 10Gb/s NG-PONs

Both FSAN/ITU-T and IEEE have endeavoured targeting on NG-PONs at 10Gb/s data rates. The IEEE 802.3av 10G-EPON standards was ratified in September 2009. However, the FSAN group has a more open-ended charter, considers a range of solutions, thus with a much longer timeline for NG-PON standardization.

3.3.3.1 IEEE 10G-EPON

10G-EPON is a smooth evolution of 802.3ah 1G-EPON. The 802.3av standard places significant emphasis on enabling simultaneous operation of 1 Gb/s and 10 Gb/s EPON systems on the same outside plant. Such a co-existed EPON is illustrated in Fig. 3.5, where the downstream 1 Gb/s and 10 Gb/s channels are separated in the wavelength domain; while the upstream 1 Gb/s and 10 Gb/s channels share spectrum in the low chromatic dispersion region and are separated in time domain by using a dual rate burst mode OLT receiver which automatically switches between 1Gb/s and 10Gb/s based on the scheduled ONU transmission bursts.

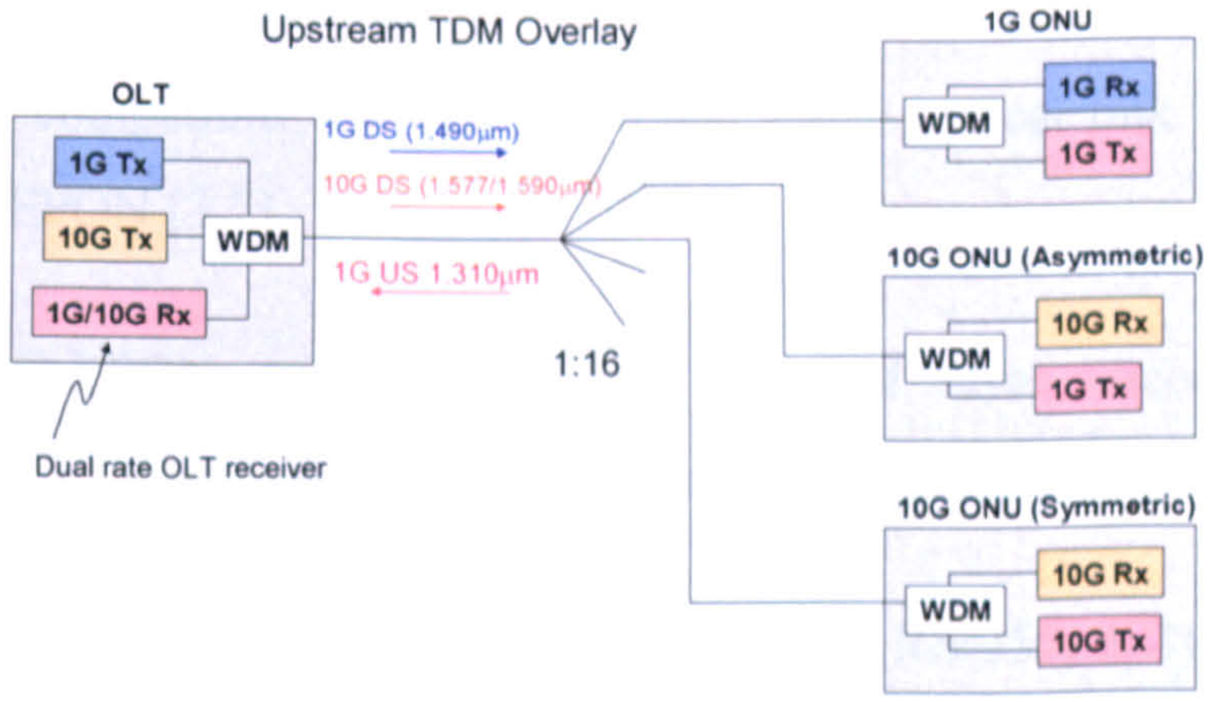

Fig. 3.5 Co-existence of 10G-EPON and 1G-EPON

IEEE 802.3av preserves the back compatibility with 1G-EPON (IEEE. 802.3ah) in a wide scale. The former is the extension of the latter. Compared to 802.3ah, 802.3av has a small change in MAC layer which occurs in the MPCP sub-layer: the auto-recovery process will be needed to distinguish 1G and 10G registration, which supports the dual rate operations in OLT. The differences between them in the PHY layer contain four main aspects: wavelength plan, optical link budget, line coding and FEC.

Wavelength plan: IEEE 802.3av preserves the wavelength plan for EPON for 1Gb/s downstream and upstream transmissions. Meanwhile, there are additional two bands: 1575-1580nm for 10Gb/s downstream transmission and 1260-1280nm for 10Gb/s upstream transmission.

Optical link budget: The 802.3av defines the power budget for symmetric-rate PHY for PON operating at 10Gb/s downstream/10G/s upstream which is denoted as PR; and for asymmetric-rate for 10G downstream/1G upstream which is designated to PRX. The three classes of optical link budget are listed as followings:

- PR(X)10: 5-20dB for 10km transmission distance.
- PR(X)20: 10-24dB for 20km transmission distance.
- PR(X)30: 15-29dB for 20km transmission distance. This power budget is expected to be compatible with the existing "B+" class as mentioned in Section 3.3.1.1.

The values "10", "20", and "30" immediately following "PR(X)" represents low, medium, and high power budgets, respectively. The PR(X)10 and PR(X)20 are, respectively, compatible with the PX10 and PX20 optical link budgets defined for 802.3ah 1G-EPON [3.7].

Line coding: 10G-EPON employs 66B/64B physical layer encoding, providing an overhead of 3% which is much smaller than that of 8B/10B used in 802.3ah EPON.

FEC: 10G-EPON employs a FEC mechanism based on RS(255, 223). FEC is mandatory for all channels operating at 10 Gb/s, including 10Gb/s downstream/10Gb/s upstream EPON and 10Gb/s downstream/1Gb/s upstream EPON. While FEC using RS(255,239) is optional for symmetric 802.3ah 1G-EPON.

3.3.3.2 ITU-T XG-PON

Fig. 3.6 shows the evolution roadmap of ITU-T GPON. ITU-T has a near-term plan for its 10Gb/s NG-PON technology evolution: the plan aims at asymmetric/symmetric 10Gb/s GPON with the co-existence with the current GPON. This is referred to as NG-PON1 (also known as XG-PON). The standard documents of XG-PON were expected to be completed in later 2010 or early 2011.

XG-PON allows smooth upgrade of individual customers into future PON on the current ODN without disrupting the services of other users in the same PON [3.8]. To achieve the co-existence between XG-PON and current GPON, a WDM filter is installed to combine (separate) G-PON and XG-PON signals into (out of) the common ODN [3.8]. Compared to GPON, XG-PON keeps changes to the Transmission Convergence (TC)/MAC layer to the minimum. The major differences between current GPON and XG-PON consist in the PHY layer, which mainly include the wavelength plan, link power budget, PON split ratio and physical reach.

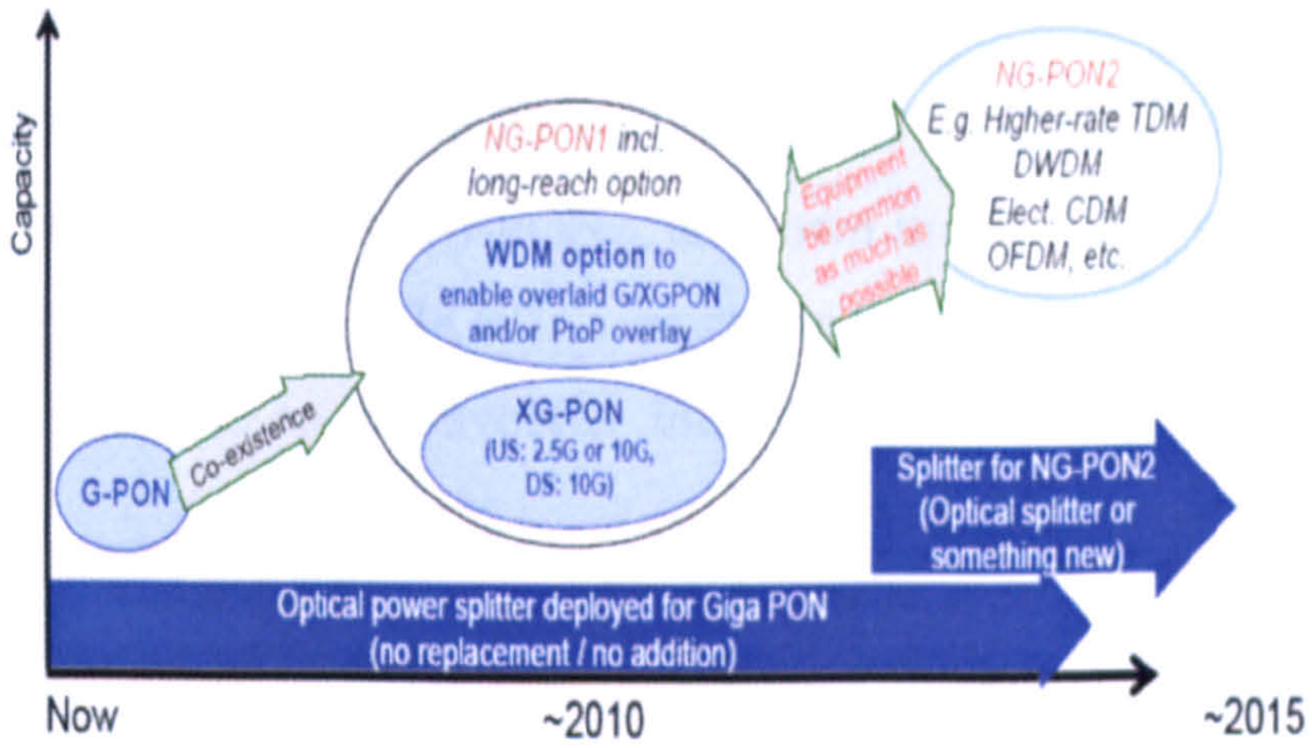

Fig. 3.6 NG-PON technology evolution pathway from FSAN

XG-PON includes two generations: XG-PON1 and XG-PON2. XG-PON1 supports asymmetric 10G downstream/2.5G upstream transmissions; while XG-PON2 offers symmetric 10G downstream/10G upstream transmissions.

XG-PON1

FSAN/ITU-T proposed wavelength band plan enhancements specified in Recommendation G.984.5, which respects the wavelength allocation for GPON (Fig. 3.4) and adds new wavelength bands of 1575-1580nm for the XG-PON1 downstream and 1260-1280nm for XG-PON1 upstream. Such a wavelength plan is similar to that defined in IEEE802.3av. The power budget for XG-PON1 is compatible with the "B+" class in current GPON with additional losses from an optical filter. This results in a total power budget of approximately 28.5dB to 31dB. Moreover, XG-PON1 supports a minimum power split ratio of 1:64 and a minimum physical reach of 20km.

XG-PON2

The wavelength plan for XG-PON2 has not been defined yet, most assume that it will adopt a similar wavelength plan to XG-PON1. XG-PON2 may require increase in the system performance by extending the power budget, which is defined as the class "C+" power budget in addition with the insertion loss from the optical filter. Therefore the total insertion loss for the transmission link will achieve approximately 33dB to 35.5dB depending on the deployment requirements from operators.

3.3.4 Beyond 10G-EPON/XG-PON

ITU-T also offers the long-term plan beyond XG-PON/10G-EPON targeting even higher data rates, which is referred to as NG-PON2, as shown in Fig. 3.6. Though the processing of NG-PON2 is in parallel to XG-PON1, a much longer time period till 2015 was set for NG-PON2 standardization as it involves intensive research on the emergent novel technologies.

Different from XG-PON, NG-PON2 takes into account the long-term solutions that do not necessarily co-exist with GPON on the same ODN. NG-PON2 may use separate splitters and fibres rather than those shared by GPON and XG-PON. Furthermore, NG-PON2 may also use a different device such as wavelength router to substitute the power splitter currently used. Therefore, NG-PON2 accounts for a number of technology candidates with potential excellence, such as WDM-PON, hybrid WDM/TDM-PON, and OOFDM PONs.

3.4 Promising Technologies for NG-PONs

As ITU-T NG-PON2 would not be restricted to the G.984.5 enhancement wavelength band operation and optical characteristics of current ODN system components, it offers opportunity to consider novel technologies. In this section, the potential technologies including WDM-PON, hybrid WDM/TDM-PON and OOFDM PON are discussed.

3.4.1 WDM-PON

It is agreed that PONs based on pure TDM cannot cope with the requirements of future networks with aggregated bandwidth and the allowable power budget. A promising

solution to address this challenge is to adopt WDM-PON. A general WDM-PON architecture is shown in Fig. 3.7. In the downstream direction, OLT uses a mixed-wavelength laser array or a Multi-Frequency Laser (MFL) to generate a downstream signal, which is multiplexed to form a WDM signal. An Arrayed Wavelength Grating (AWG) is adopted in the remote node to route the wavelengths to a proper ONU. While in the upstream direction, each ONU uses an individual wavelength to carry its signal and these ONU signals are aggregated into a WDM signal after passing through the AWG. The OLT receiver de-multiplexes the received WDM signal using filters and a photo-detector array. A Band Splitter (BS) or circulator is used in both the OLT and ONU to separate the upstream/downstream signals so that bidirectional transmission is performed.

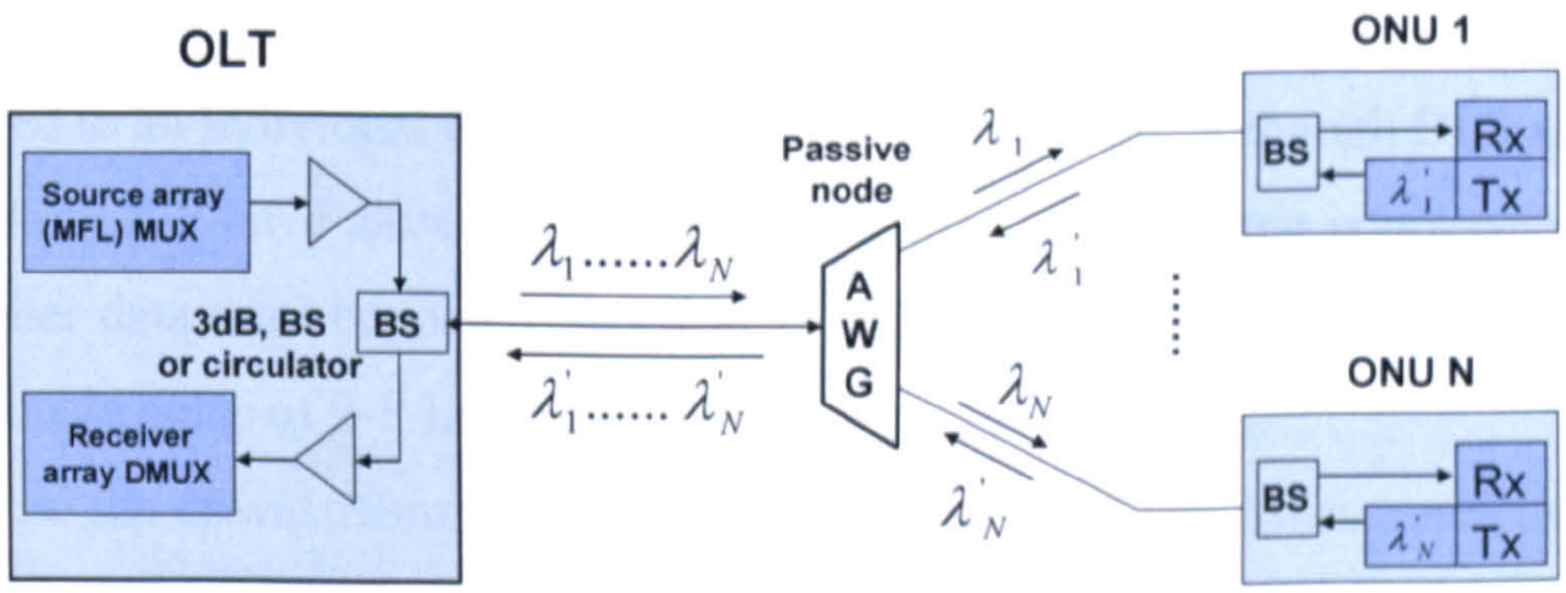

Fig. 3.7 A general WDM-PON architecture

WDM-PONs exhibit advantages in many aspects:

- As ONU is assigned with a dedicated wavelength, which provides a tremendous bandwidth and excellent privacy to an individual customer.
- WDM-PONs preserve a passive ODN thus maintenance cost is low.
- Each ONU and OLT has an independent P2P connection thus largely simplifies the MAC layer (no P2MP media access control) and enables the achievement of system protocol transparency.
- Easy to scale. Each wavelength can operate at different data rate and run different protocol so an easy pay-as-you-grow upgrade is possible.

The disadvantages of WDM-PONs are the high cost of WDM components and wavelength specific ONU. This may limit its wide practical applications. Therefore, colorless ONU

operation is highly preferred to minimize stock and wavelength management problems and thus the cost for operators. Generally, there are three colorless ONU solutions:

1) Use of a tunable laser and an external modulator in each ONU [3.9,3.10]. This approach offers, in the long-term, the highest performance for WDM-PON by allowing the highest potential number of channels. It makes economic sense because of the availability of commercial tunable semiconductor lasers at prices of potentially a few ten U.S. dollars.
2) Broadband Light Source (BLS) from CO and optical injection-locked Laser Diode (LD) such as F-P LD [3.11,3.12] and VCSEL [3.9] in ONU. The BLS can be from Amplified Spontaneous Emission (ASE) generated by an EDFA [3.13], or Light-Emitting Diodes (LEDs) [3.14], which is sliced by the AWG and each sliced carrier is fed to an individual ONU for upstream transmission. Although BLS and injection locking F-P have already been commercialized, this scheme is not easy to provide higher data rates beyond 1Gb/s due to high power loss in spectrum slicing and the intrinsic noise of F-P LD [3.9].
3) Reuse the downstream wavelength. In this approach, the downstream optical signal received by ONU is split into two: one is detected by the ONU receiver and the other is re-modulated by the upstream signal and sent back to OLT receiver. The modulators in ONU can be injection-locked F-Ps [3.15], EAMs [3.15], or RSOA/SOA intensity modulators [3.15,3.16]. The major challenge for this scheme is the crosstalk effect between the residual downstream signal and the re-modulated upstream signal. Moreover, RB noise is also an issue if bi-directional transmission is used in the WDM-PON.

As NG-PONs based on WDM architecture operate at high bit rates (>10Gb/s) per wavelength, the tunable ONU and the downstream wavelength reuse approaches discussed above seem survive easily in NG-PONs. Therefore, in this thesis, these two colorless ONU methods are thoroughly investigated of using RSOAs/SOAs as intensity modulators in WDM-PON using the OOFDM technique.

3.4.2 Hybrid WDM/TDM-PON

In real cases, WDM-PONs are often combined with TDM-PONs to increase transmission distance, power split ratio and system scalability. A typical example of such hybrid

WDM/TDM-PONs is the WDM Ethernet PON (WE-PON), developed by Electronics and Telecommunications Research Institute, Korea (ETRI) and Korea Telecom [3.17], by combining WDM PON and EPON together. The WE-PON system is shown in Fig. 3.8, where 32 wavelengths and 1:32 power splitters are used, allowing a total split ratio of approximately 1:1000.

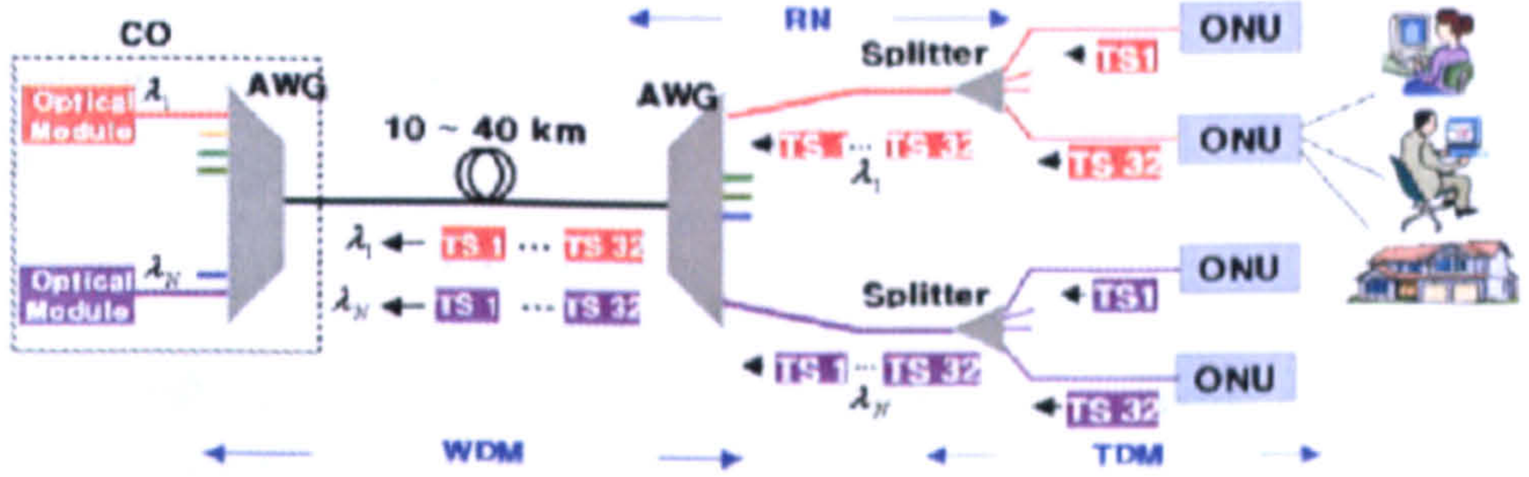

Fig. 3.8 WE-PON architecture (from [3.17]).

The hybrid WDM/TDM PON possesses the advantages of both WDM-PON and TDM-PON, and also effectively eliminates the limitations of pure TDM-PON. With the increase of number of customers and transmission distance enabled by WDM/TDM-PON, the number of CO can also be reduced leading to considerable power and maintenance cost savings. Similar to WDM-PONs, colorless ONUs are also preferred in WDM/TDM-PONs.

3.4.3 OOFDM PON

As discussed in Chapter 2, OOFDM is an advanced signal modulation technique for PONs due to its high spectral efficiency, high chromatic dispersion tolerance, excellent system scalability and flexibility [3.10,3.18-3.20]. Integrated circuit implementations of OFDM modems are feasible for affordable mass-produced transmitters and receivers. Apart from these advantages, OOFDM PON also offers, in particular, multiple access capability that allows different OFDM subcarriers to be assigned to different customers/services [3.21,3.22]. Fig. 3.9 shows a typical architecture and multiple access strategy of OOFDM PON.

For downstream transmission, different services such as Ethernet data, RoF signals share the same laser and downstream wavelength. The signal is broadcast to all ONUs by using a PS. Each ONU recovers its signal at the allocated subcarriers. For upstream transmission, each ONU maps its data and/or signal to the allocated subcarriers, sets all the other

subcarriers to zero, and completes the modulation to generate an electrical OFDM frame. The OFDM frame is then converted into OOFDM symbols with low cost DMLs and transmitted over fibre. The OOFDM symbols from multiple ONUs will be combined at the optical coupler, forming a single OOFDM frame, and detected by a single photo-detector at the OLT receiver.

Compared to conventional TDM-PON technologies, OOFDM PON not only provides improved performance but also the possibility of convergence between optical, wireless, and copper access networks.

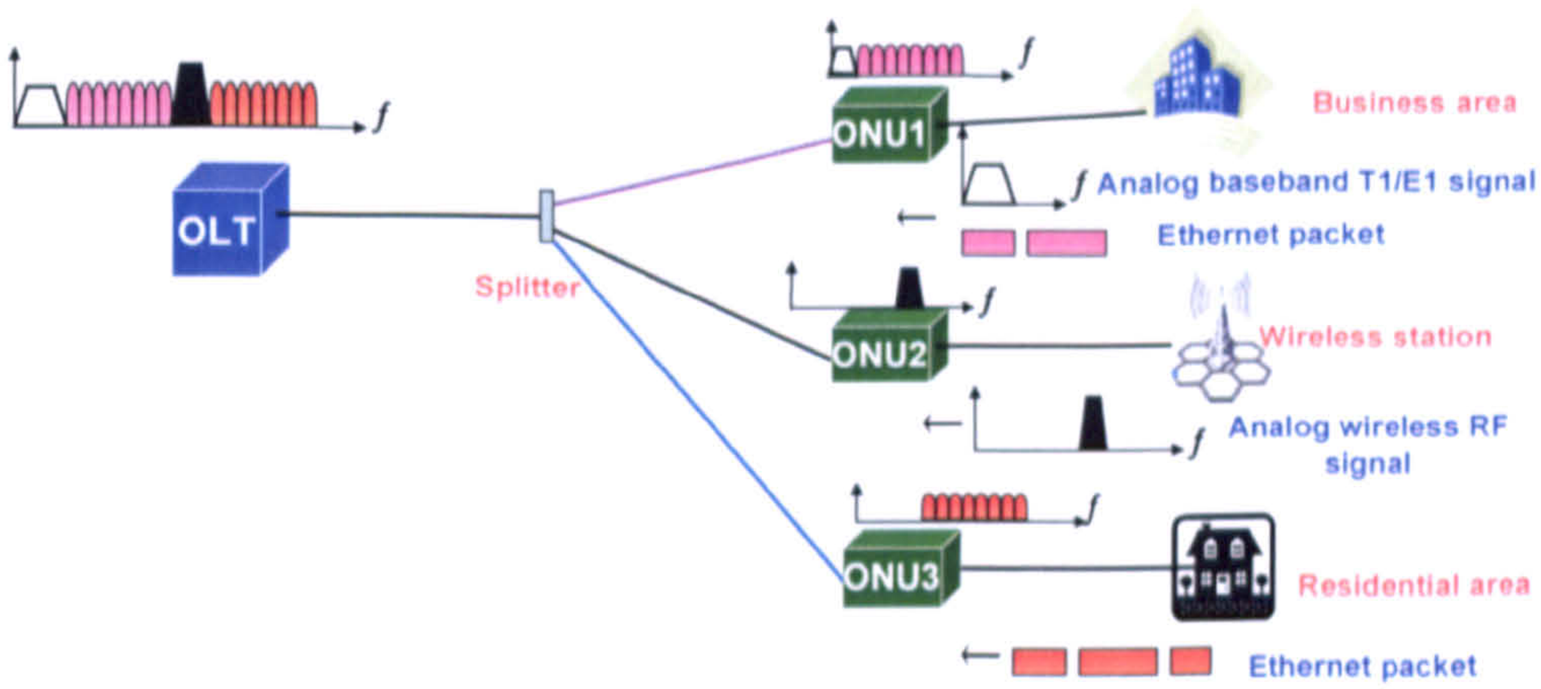

Fig. 3.9 A typical architecture and multiple access strategy of OOFDM PON.

The above mentioned WDM-PON, WDM/TDM PON and OOFDM PON are widely viewed as promising technologies for NG-PONs. WDM-PON is a "future-proof" solution to support the required bandwidth and scalability for NG-PONs due to the mature WDM technology. WDM-PON was also considered as the base technology for NG-PON2 by FSAN group [3.23]. While WDM/TDM PON provides better flexibility than pure WDM-PONs do, which allows delivery of services to more subscribers and the efficient use of bandwidth of each wavelength. OOFDM PON brings about high transmission performance, high spectral efficiency, strong dispersion tolerance as well as flexibility.

3.5 Electro-optic Convertors for PONs

The ITU-T/FSAN work group places an emphasis on ensuring electro-optic components to be as common as possible in the process of migration to NG-PON2. This is very important for CAPEX and OPEX saving for operators, as PONs are cost-sensitive application

scenarios. This chapter reviews the electro-optic convertors adopted in current PONs, which are the major contributors to the cost of PON transceivers. To be consistent with the definition in other published literatures, throughout this thesis, use is made of "optical modulator" instead of electro-optic convertors to highlight the role of the laser devices in PON systems.

Optical modulators used in PONs vary with PON architectures. EPON/GPON standards do not specify explicitly the optical modulators, while the most commercially deployed EPON/GPON systems implement DMLs for downstream transmission at 1549nm due to its Single Longitudinal Mode (SLM) output with a high optical power, and F-P lasers with Multi-Longitudinal Mode (MLM) output for upstream transmission at 1310nm where fibre dispersion is minimum. For WDM-PONs, a diversity of optical modulators have been used for the upstream colourless transmission together with various upstream light source schemes. Table 3.4 summarizes various optical modulators and light supply schemes presented for PONs in literatures.

Table 3.4 Summery of optical modulators used in PONs

PON Type	Optical modulators		ONU light source	Refs
	Downstream	Upstream		
TDM-PON	DML			[3.24]
	VCSEL			[3.24,3.25]
WDM-PON		EM	Tunable laser	[3.9,3.10]
	VCSEL array	VCSEL		[3.26]
		RSOA	Central CW light	[3.27-3.29]
		Reflective EAM-SOA		[3.30]
		RSOA	Central BLS	[3.13][3.14]
		EM	CO F-P spectrum	[3.11]
	EAM/DML	EAM, RSOA, SOA, Injection-locked F-P LD, Injection-locked VECSEL	downstream wavelength reuse	[3.15,3.16,3.31]

It can be seen from Table 3.4 that semiconductor optical modulators including DMLs, F-P lasers, VCSELs, RSOA/SOA modulators, and EAMs are widely used for PONs. This is due to their inherent advantages including compactness, small footprint, monolithic integration with electrical components and the capability of signal modulation at high

frequencies. For simplicity, these convertors can be classified into two main categories: directly modulated lasers and External Modulators (EMs). The former is widely used in TDM-PONs and also for WDM-PON downstream transmissions; while the latter is the main scheme for WDM-PON colourless ONU transmitters.

3.5.1 Directly Modulated Laser

3.5.1.1 Fabry-Perot Laser

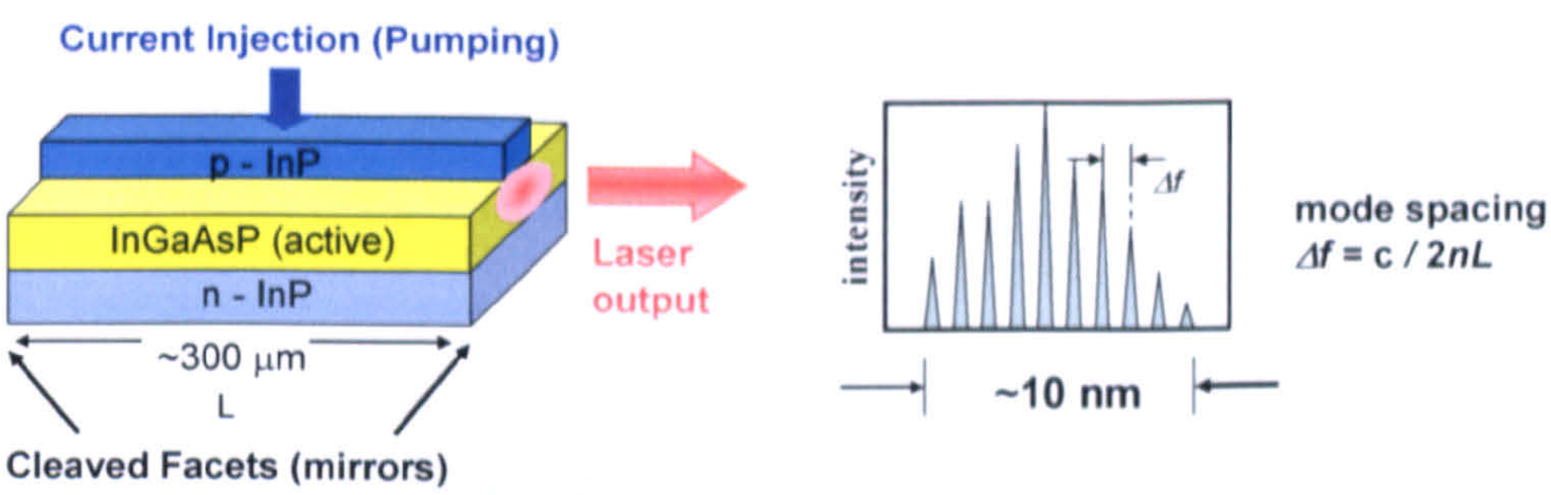

Fig. 3.10 F-P laser and its output spectrum.

Fig. 3.10 illustrates a Fabry-Perot (F-P) laser usually consisting of a semiconductor optical gain medium and two cleaved facets as mirrors. When the laser is pumped by an injection current above its threshold, the laser oscillation occurs and emits an optical beam containing multiple frequency modes $f_m = \frac{mc}{2nL}$ with f_m being the m-th longitudinal mode (frequency), n being the index of refraction of the gain medium and L being the cavity length. The frequency spacing between two adjacent modes, as referred to as Free Spectral Range (FSR), is $\Delta f = \frac{c}{2nL}$ depending on the optical gain material and the cavity length. Due to its Multi-Longitudinal Mode (MLM) output, F-P laser is widely used in TDM-PONs for upstream transmission at 1310nm where fibre dispersion is minimum. Moreover, a F-P LD has an important property that, when an external light is injected, the F-P cavity mode will be locked at the injected wavelength. As a direct result, F-P LDs can also be used in WDM-PON to facilitate colourless ONUs [3.11,3.15].

F-P laser is the simplest and low-cost laser. The main drawback of F-P lasers lies in the MLM output which has an output spectrum width of 2-10nm, which leads to undesirable pulse broadening due to fibre chromatic dispersion (Section 2.4.1.1.3). Due to the data

rate/distance limitations, the F-P lasers are not recommended to be used in ITU G.987.2 Recommendation for XG-PONs.

3.5.1.2 Distributed Feedback (DFB) laser

Compared to F-P lasers, DFB lasers provide feedback only at a certain frequency rather than multiple frequencies. In DFB lasers, the feedback at a chosen wavelength is realized by using corrugated gratings on the semiconductor substrate. The grating structure provides feedback which is distributed along the cavity length rather than at the end facets only, as shown in Fig. 3.11. The DFB laser has very narrow spectral linewidth of as low as 1MHz [3.32].

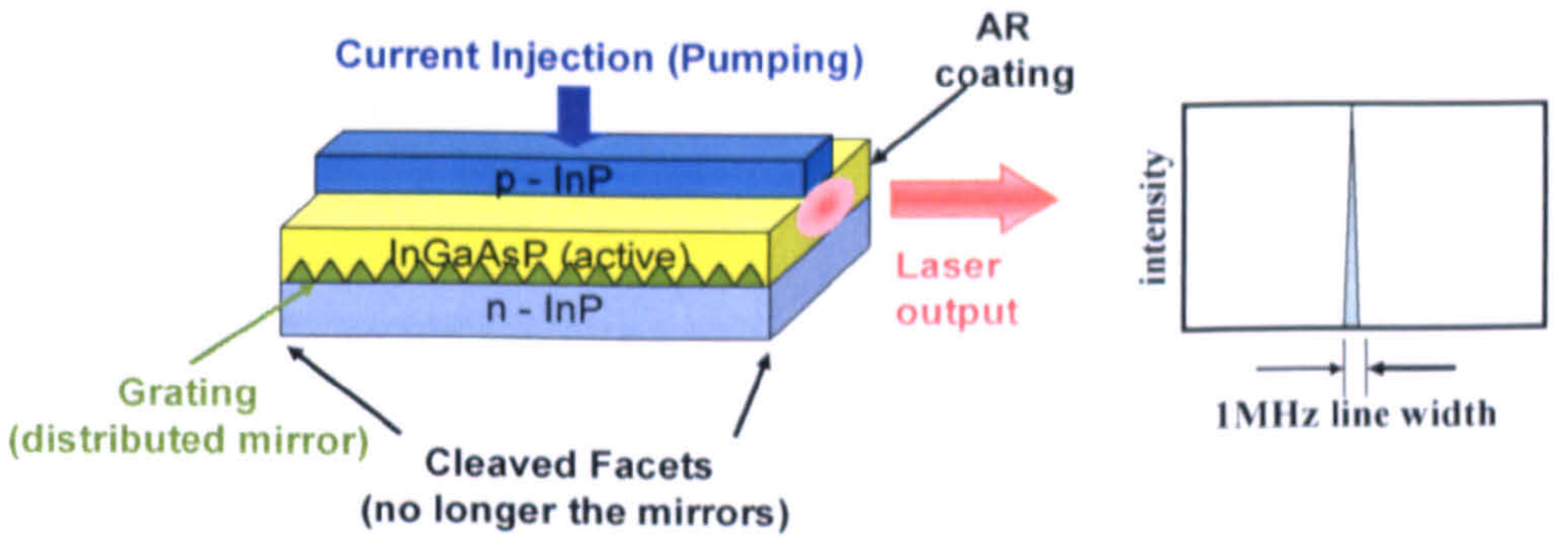

Fig. 3.11 DFB laser and its output spectrum.

Due to the single longitudinal mode operation, DFB lasers are used in many 1.55-μm optical communication systems operating at bit rates of 2.5Gb/s or more. Commercially available DFB lasers offer a typical high output optical power of 13dBm, thus DMLs are promising for NG-PONs with allowable large optical budget.

Despite the wide acceptance of DMLs in modern telecommunications, the direct modulation of DFB lasers produce nonlinear frequency chirp which is imposed onto the optical field. Such laser chirp interacts with fibre chromatic dispersion resulting in distortions on the optical signal transmitting through fibre. This brings about challenges for high speed optical fibre communications involving DMLs.

3.5.1.3 VCSEL

Vertical Cavity Surface Emitting Laser (VCSEL) differentiates from F-P lasers and DFB lasers in terms of that the laser beam is perpendicular with its top surface, as shown in Fig. 3.12. A VCSEL consists of semiconductor optical gain medium located in the vertical

cavity and Distributed Bragg Grating (DBR) mirrors at both the bottom and top of the cavity. The DBR mirrors consist of layers alternating high and low refractive index yielding high intensity reflectivity. VCSEL is SLM laser because the short cavity length leads to large FSR among different modes and only one mode has a net optical gain larger than "1".

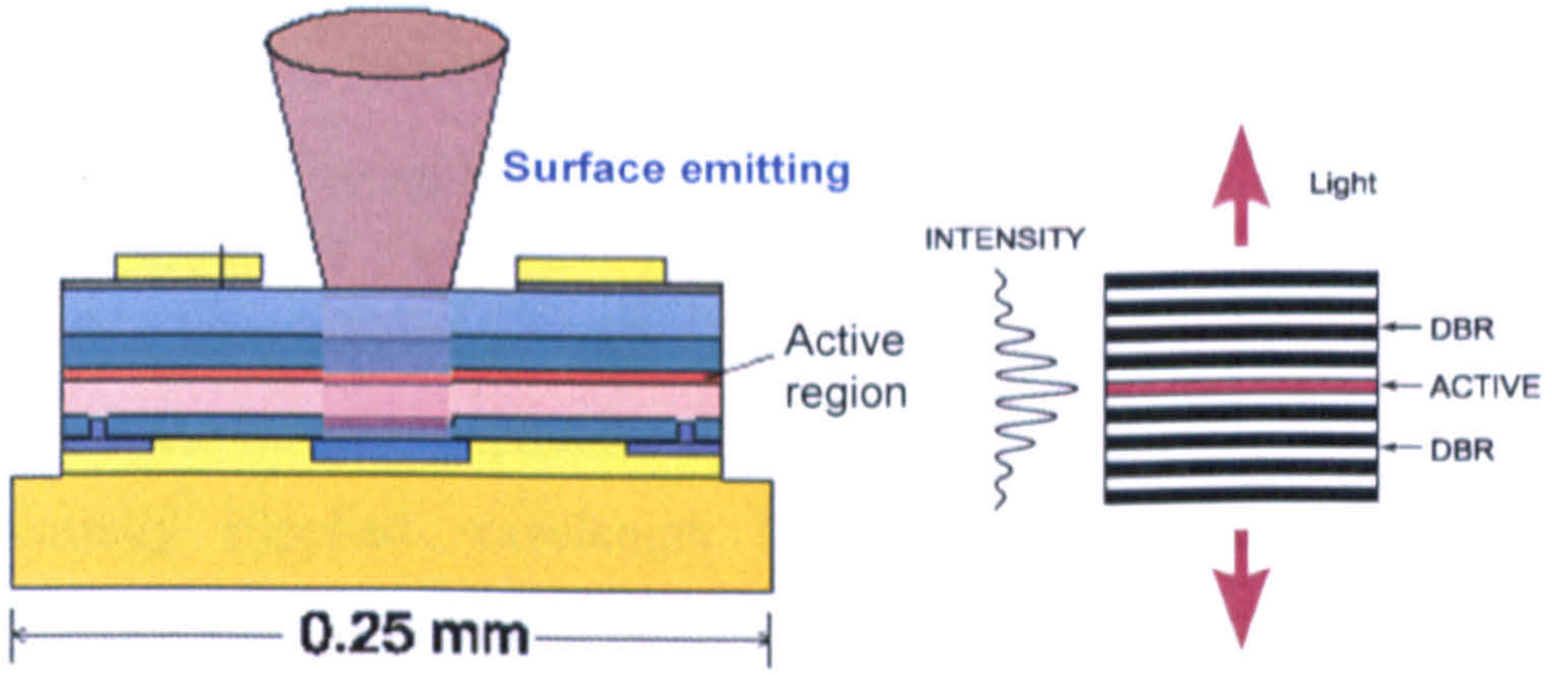

Fig. 3.12 Diagram of a VCSEL laser and its optical intensity distribution (from [3.33]).

Compared to conventional edge-emitting lasers, a VCSEL has advantages of low cost and easy manufacturing and packaging thus good for mass production. The SLM output is also better for dispersion reduction. Moreover, long wavelength VCSELs were under research for WDM-PONs [3.24,3.26,3.31] as cost-effective transmitters.

However, the main disadvantage of VCSELs is the relatively low output power of typically 0dBm, its polarization instability and multi-transversal model operations. Moreover, most of the commercially available VCSELs operate at short wavelength around 850nm where the fibre loss and dispersion are high. Recently, experimental investigations in Bangor University have shown that these disadvantages can be overcome to some extent by using adaptive modulation.

3.5.2 External Modulator

External modulators implemented in WDM-PONs or hybrid WDM/TDM-PONs are divided into two types: electro-optic modulators where the injected light properties such as intensity vary with the applied electric field. RSOA/SOA intensity modulators fall into this category. The other is electro-absorption modulator where the amount of light absorbed varies with the applied electric field. EAM modulator belongs to this category.

3.5.2.1 RSOA/SOA Modulator

An SOA has a similar structure as a F-P laser, except that anti-reflection facets are coated at both ends. An RSOA is a special type of an SOA with a high reflective coating at its rear-facet. With this design, an RSOA exhibits increased optical gain compared to an ordinary SOA due to the double signal propagation through the active region. One of the salient properties of RSOAs/SOAs is the wide wavelength coverage, which enables colourless ONUs in WDM-PONs. Colourless ONU using RSOA/SOA intensity modulators in WDM-PONs can be realized by three approaches:

- A tuneable laser located in each ONU to provide the light source for colourless RSOAs/SOAs intensity modulation [3.10].
- A centrally supplied wavelength for remote modulation. This means two wavelengths are transmitted to an ONU; one carries downstream data and the other is reserved for upstream modulation [3.9, 3.13, 3.27-3.29].
- Re-modulation of the downstream signal so that a single wavelength can be used by both downstream and upstream signals. Typically, this scheme uses the RSOA/SOA gain saturation to erase the downstream signal waveform, which is then re-modulated to transmit signal upstream [3.15,3.16].

By using the OOFDM technique, 7.5Gb/s and 10Gb/s colourless upstream transmission in WDM-PONs have been experimentally achieved by using RSOAs [3.28,3.29]. The RSOAs used in the experiments have 3-dB bandwidths of approximately 1GHz, which are much smaller than the OFDM bandwidth. It is well known that the RSOA/SOA modulation bandwidth is proportional to the inverse of the effective carrier lifetime, τ_e , which is defined by [3.34]

$$\tau_e = \frac{1}{1/\tau_c + P_{out}/E_{sat}} \tag{3.1}$$

where E_{sat} is the saturation energy, τ_c is the carrier lifetime, P_{out} is the RSOA/SOA output power. It is clear in Eq. (3.1) that τ_e can be adjusted by altering the output optical power, meaning that τ_e is dependent on the RSOA/SOA operating conditions. For RSOAs/SOAs operating at strongly saturated optical gain regions, their τ_e can be reduced to values of an order of less than 50 ps [3.35], which means that RSOAs/SOAs can have modulation

bandwidths of as large as 20GHz. This indicates that higher OOFDM signal data rate is achievable by optimizing RSOA/SOA operating conditions. Such an interesting subject will be investigated in this thesis.

3.5.2.2 Electro-Absorption Modulators (EAMs)

EAM is a semiconductor device modulating the intensity of a laser beam with an electric voltage based on the electro-absorption effect. EAMs can be easily integrated with driver circuits and/or laser sources to form data transmitters. Most importantly, EAM occupies large wavelength coverage as RSOA/SOA does, which make it suitable for the remote ONU colourless modulation for WDM-PONs.

However, EAM modulators are expensive components. Moreover, due to electroabsorption, the insertion loss of EAM is very high (~10dB). This brings about challenges for WDM-PONs as the total optical power budget considering the forth and back of the centrally supplied light becomes very stringent. To solve this problem, optical amplification of the EAM modulated optical signal using a SOA had been proposed [3.30] and integrated EAM-SOA modulators are commercially available offered by manufacturers such as CIP technologies.

According to the above analyses, optical intensity modulators are critical components for practical implementation of PONs, as they not only determine the achievable transmission performance but also take the major part of the cost of PON system. Among the abovementioned modulators, DMLs and RSOA/SOA intensity modulators that are widely used in today's TDM-PONs and WDM-PONs provide cost-effective solutions for NG-PONs. Therefore, these modulators will be investigated in OOFDM IMDD PON systems of interest of this thesis.

3.6 Conclusion

This chapter first reviewed various existing technologies for access networks as well as their strengthens and limitations. The technologies include DSL, HFC, and PON. PON plays the dominate role in today's access network due to its mature standards (IEEE EPON and ITU-T B/GPON) and massive global deployment. A general review of EPON and

GPON standards was made, followed by the discussions on 10G-EPON standard as well as the current status of ITU NG-PON1 (also XG-PON) and NG-PON2.

ITU NG-PON2 is a long-term solution beyond 10G-EPON/XG-PONs with higher data rates, which considers a number of technology candidates. These candidates including promising technologies such as WDM, hybrid WDM/TDM and OOFDM which were discussed in terms of principles as well as the advantages and drawbacks.

To improve the cost-effectiveness of NG-PONs, ITU-T requires the electro-optic components as common as possible. This chapter discussed various electro-optic convertors and for PONs that contribute the majority part of the cost of PON transceivers, together with their merits and disadvantages. These electro-optic convertors include F-P lasers, DMLs, VCSELs, RSOAs/SOAs and EAMs. DMLs and RSOA/SOA intensity modulators that widely implemented in today's TDM-PONs and WDM-PONs offer cost-effective solutions for NG-PONs. The remainder chapters in this thesis aim to investigate the performances of OOFDM IMDD NG-PONs using DML and RSOAs/SOAs as intensity modulators.

References

[3.1] C. F. Lam, *Passive Optical Networks: Principles and Practice*, Academic Press, Oct. 2007

[3.2] K. Tanaka, A. Agata, and Y. Horiuchi, "IEEE 802.3av 10G-EPON dtandardization and its research and development status," J. Lightw. Technol., vol. 28, no. 4, pp. 651-661, Feb. 2010.

[3.3] IDATE Consulting & Research, "FTTx market report," July 2009. Available at www.idate.org

[3.4] ITU-T G.983.x, available at http://www.itu.int/rec/T-REC-G/e

[3.5] ITU-T G.982, Optical access networks to support services up to the ISDN primary rate or equivalent bit rates, 1996

[3.6] ITU-T G.984.x, available at http://www.itu.int/rec/T-REC-G/e

[3.7] IEEE Standard 802.3, *Carrier sense multiple access with collision detection (CSMA/CD) access method and physical layer specifications*, 2005 Edition.

[3.8] J.-I, Kani, F. Bourgart, A. Cui, A. Rafel, M. Campbell, R. Davey, and S. Rodrigues, "Next-Generation PON – Part I, II and III," IEEE Commun. Magazine, pp. 43-64, Nov. 2009.

[3.9] CIP White Paper: WDM-PON Technologies, available at: http://www.ciphotonics.com/New_PDFs/WPON_White_Paper_v1%200.pdf

[3.10] J. L. Wei, X. L. Yang, R. P. Giddings, J. M. Tang and K. A. Shore, "SOA Intensity Modulator-Enabled Colourless Transmission of Adaptively Modulated Optical OFDM Signals for WDM-PONs," presented at the *14th OptoElectronics and Communications Conf. (OECC)*, (Hongkong, China, 2009), Paper ThLP77.

[3.11] S. L. Woodward, P. P. Iannone, K. C. Reichmann, and N. J. Frigo, "A spectrally sliced PON employing Fabry-Perot lasers," IEEE Photon. Technol. Lett. 10, 1337-1339 (1998).

[3.12] K. Y. Park and C.H. Lee, "Intensity noise in a wavelength-locked Fabry-Perot laser diode to a spectrum sliced ASE," IEEE J. Quant. Electronics, vol. 44, no. 3, pp. 209-215, March 2008.

[3.13] D. K. Jung, H. Kim, K. H. Han, and Y. C. Chung, "Spectrum-sliced bidirectional passive optical network for simultaneous transmission of WDM and digital broadcast video signals," Electron. Lett. 37, 308-309 (2001).

[3.14] K. H. Han, E. S. Son, H. Y. Choi, K. W. Lim, and Y. C. Chung, "Bidirectional WDM PON using light-emitting diodes spectrum-sliced with cyclic arrayed-waveguide grating" IEEE, Photon. Technol. Letters, vol. 16, no. 10, pp. 2380-2382, Oct. 2004.

[3.15] C.W. Chow, C. H. Yeh, C. H. Wang, F. Y. Shih, and S. Chi, "Demonstration of signal remodulation long reach carrier distributed passive optical network using OFDM-QAM signal," at the *ECOC* (Vienna, Austria, 2009), paper 8.5.2.

[3.16] H. Takesue, and T. Sugie, "Wavelength channel data rewrite using saturated SOA modulator for WDM networks with centralized light sources," J. Lightwave Technol. vol. 21, no. 5, pp. 2546-2556 Mar. 2003.

[3.17] J. Yoo, H. Yun, T. Kim, K. Lee, M. Park, B. Kim, B. Kim, "A WDM-Etherent hybrid passive optical network architecture," at the *8th International Conference on Advanced Communication Technology (ICACT),* (Korea,2006), Feb 2006.

[3.18] J. Yu, M.-F. Huang, D. Qian, L. Chen, and G.-K. Chang, "Centralized lightwave WDM-PON employing 16-QAM intensity modulated OFDM downstream and OOK modulated upstream signals," IEEE Photon. Technol. Lett. vol. 20, no.18, pp.1545-1547, Sep. 2008.

[3.19] T. Duong, N. Genay, B. Charbonnier, P. Urvoas, P. Chanclou, and A. Pizzinat, "Experimental demonstration of 10 Gbit/s transmission over 110 km SMF by direct

modulation of 2 GHz bandwidth DFB laser using discrete multi-tone modulation for passive optical network," at the OFC/NFOEC, (San Diego, USA, 2008), Paper NMB3.

[3.20] C.-W. Chow, C.-H. Yeh, C.-H. Wang, F.-Y. Shih, C.-L. Pan, and S. Chi, "WDM extended reach passive optical networks using OFDM-QAM," Opt. Express. vol. 16, no. 16, pp.12096-12101, Aug. 2008.

[3.21] D. Qian, J. Hu, P.N. Ji and T. Wang, "10Gb/s OFDMA-PON for delivery of heterogeneous services," at the *OFC/NFOEC*, (San Diego, USA, 2008), Paper OWH4.

[3.22] N. Cvijetic, D. Qian, J. Hu, and T. Wang, "44-Gb/s/λ upstream OFDMA-PON transmission with polarization-insensitive source-free ONUs," at the *OFC/NFOEC* (San Diego, US, 2010), Paper OTuO3.

[3.23] J.-P. Elbers, "Optical access solutions beyond 10G-EPON/XG-PON," at the *OFC/NFOEC* (San Diego, USA, 2010), Paper OtuO1.

[3.24] T. N. Duong, N. Genay, P. Chanclou, B. Charbonnier, J. L. Masson, and M. Ouzzif, "Maximizing the Transmission Performance of DMT signal for Next Generation PON system by Direct Modulation of Cost-effective and Low Bandwidth Lasers," at the *OFC/NFOEC* (San Diego, CA, US, 2009), Paper NME1.

[3.25] P.A. Gamage, A. Nirmalathas, et al, "Multi-Services Distribution using Power-Efficient Low-Cost VCSELs" at International topical meeting on Microwave Photonics, Jointly held with the Asia-Pacific Microwave Photonics Conference (MWP/APMP, 2008). pp. 169-172.

[3.26] T. B. Gibbon, K. Prince, C. Neumeyr, E. Rönneberg, M. Ortsiefer and I. T. Monroy, "10 Gb/s 1550 nm VCSEL transmission over 23.6 km Single Mode Fiber with no Dispersion Compensation and no Injection Locking for WDM PONs," at the *OFC/NFOEC* (San Diego, CA, US, 2010), Paper JThA30.

[3.27] P. Chanclou, F. Payoux, T. Soret, N. Genay, R. Brenot, F.Blache, M. Goix, J. Landreau, O. Legouezigou, and F. Mallécot, "Demonstration of RSOA-based remote modulation at 2.5 and 5 Gbit/s for WDM-PON," at the *OFC/NFOEC* (San Diego, USA, 2007), paper OWD1.

[3.28] R.P. Giddings, E. Hugues-Salas, X.Q. Jin, J. L. Wei and J.M. Tang, "Colourless Real-Time Optical OFDM End-to-End Transmission at 7.5Gb/s over 25km SSMF Using 1GHz RSOAs for WDM-PONs," at the *OFC/NFOEC*, (San Diego, USA, 2010), Paper OMS4.

[3.29] T. Duong, N. Genay, P. Chanclou, B. Charbonnier, A. Pizzinat, and R. Brenot, "Experimental demonstration of 10 Gbit/s for upstream transmission by remote modulation of 1 GHz RSOA using Adaptively Modulated Optical OFDM for WDM-PON single fiber architecture," at the *ECOC*, (Brussels, Belgium, 2008), PD paper Th.3.F.1.

[3.30] E.K. MacHale, G. Talli, P.D. Townsend, A. Borghesani, I. Lealman, D.G. Moodie, D.W. Smith, "Extended-reach PON employing 10Gb/s integrated reflective EAM-SOA," at the *ECOC* (Brussels, Belgium, 2008), Paper Th.2.F.1.

[3.31] D. Parekh, W. Yang, W. Hofmann, M. C. Amann, and C. J. C.-Hansnain, "Isolator-less Optically Injection-Locked 1.55-μm VCSELs for Upstream Transmitters in WDM-PONs," at the *OFC/NFOEC* (San Diego, CA, US, 2009), Paper OThA4.

[3.32] C. F. Lam, "Optical Ethernet," at the *OFC/NFOEC* (Anaheim, CA, US, 2005), Short Course 134.

[3.33] M.-C. Amann, "Long-Wavelength VCSELs," ECOC 2001 Tutorial Tu.M.2.1.

[3.34] R. Gutiérrez-Castrejón, L. Schares, L. Occhi, and G. Guekos,"Modeling and measurement of longitudinal gain dynamics in saturated semiconductor optical amplifiers of different length," IEEE J. Quantum Electron., vol. 36, no. 12, pp.1476-1484, Dec. 2000.

[3.35] R. J. Manning, D. A. O. Davies, and J. K. Lucek, "Recovery rates in semiconductor laser amplifiers: optical and electrical bias dependencies," Electron. Lett., vol. 30, no.15, pp. 1233–1235, Jul. 1994.

4 7dB Improvements in Optical Power Budgets of 11.25Gb/s DML-Modulated Optical OFDM PON Systems

Contents

4.1 Introduction 87
4.2 Theoretical OOFDM System Model 88
4.2.1 OOFDM Transceivers 89
4.2.2 DML 89
4.2.3 SMF, PIN detectors and LPF 90
4.2.4 Simulation Parameters 90
4.3 Result Comparisons and Key Limiting Factor Identification 91
4.3.1 Theoretical and Experimental Result Comparisons 91
4.3.2 Key Limiting Factors Identification 94
4.4 Tunable Narrowband OBPF-enabled Performance Improvement 99
4.5 Conclusion 101

4.1 Introduction

Having discussed OOFDM and PON in previous chapters, this chapter deals with detailed technical issues associated with DML-modulated OOFDM PON systems using SSMFs. In such systems, as discussed in Section 2.4.3, the practical achievable system performance is mainly limited by the following three factors [4.1-4.3]: i) the positive transient frequency chirp associated with the involved DML; ii) the low signal ER of the DML modulated OOFDM signal, and iii) subcarrier intermixing upon square-law photon detection in the receiver. To compensate for the DML-induced frequency chirp effect, use can be made of negative dispersion fibres [4.3,4.4] and mid-span spectral inversion [4.5], which, however, require significant changes to installed PON systems. For conventional signal modulation techniques, narrowband wavelength-offset optical filtering [4.6,4.7] has been proposed to improve the DML-modulated signal ER via converting unwanted chirp-induced frequency modulation (FM) into useful amplitude modulation (AM). In comparison with negative dispersion fibres and mid-span spectral conversion, the optical filtering approach is more advantageous, as it is capable of reusing the existing PON systems without introducing significant alterations to the installed fibre plants. However, as far as we are aware, detailed investigations of the influence of both narrowband wavelength-offset optical filtering and subcarrier intermixing on the DML-based IMDD OOFDM PON system performance have not been reported.

Recently, in DML-based IMDD OOFDM PON systems without incorporating chromatic dispersion compensation and in-line optical amplification, experimental demonstrations have been reported of end-to-end real-time OOFDM transceivers at record-high signal bit rates of up to 11.25Gb/s [4.1]. In addition, optical power budgets of approximately 20dB have been proved to be feasible in chromatic dispersion compensation-free real-time OOFDM systems without in-line optical amplification [4.1]. This optical power budget may, however, not be sufficiently high to satisfy the requirements of NG-PONs.

To further improve the optical power budget of the DML-based IMDD OOFDM PON system, an in-depth understanding of some fundamental issues is of great importance.

These issues include: i) what are the key physical mechanisms limiting the maximum achievable optical power budget? and ii) can the identified effects be alleviated effectively by a simple approach without complicating both the real-time OOFDM transceiver designs and the PON system architecture? Addressing these two critical challenges in detail forms the main scope of this chapter.

In this chapter, extensive numerical investigations are undertaken of fitting our 11.25Gb/s end-to-end real-time OOFDM experimental results obtained in DML-based IMDD 25km SMF systems [4.1]. Excellent agreement between theoretical results and experimental measurements is observed in terms of system frequency response, error distribution across subcarriers, subcarrier constellation diagrams and total channel BER performance. This verifies the validity of the comprehensive theoretical OOFDM system model adopted here. Based on the system model, the impact of different physical mechanisms is explored on the obtainable optical power budgets. The low ER of the DML intensity modulated OOFDM signal is identified to be the predominant factor limiting the achievable optical power budget. More importantly, the use of a wavelength-offset narrowband Optical Bandpass Filter (OBPF) in the transmitter is proposed to considerably improve the DML-modulated OOFDM signal ER and thus the optical power budget. It is shown that a 0.01nm offset OBPF having a 3dB bandwidth of 0.02nm enables a 7dB increase in optical power budget at a total channel BER of 1×10^{-3}.

4.2 Theoretical OOFDM System Model

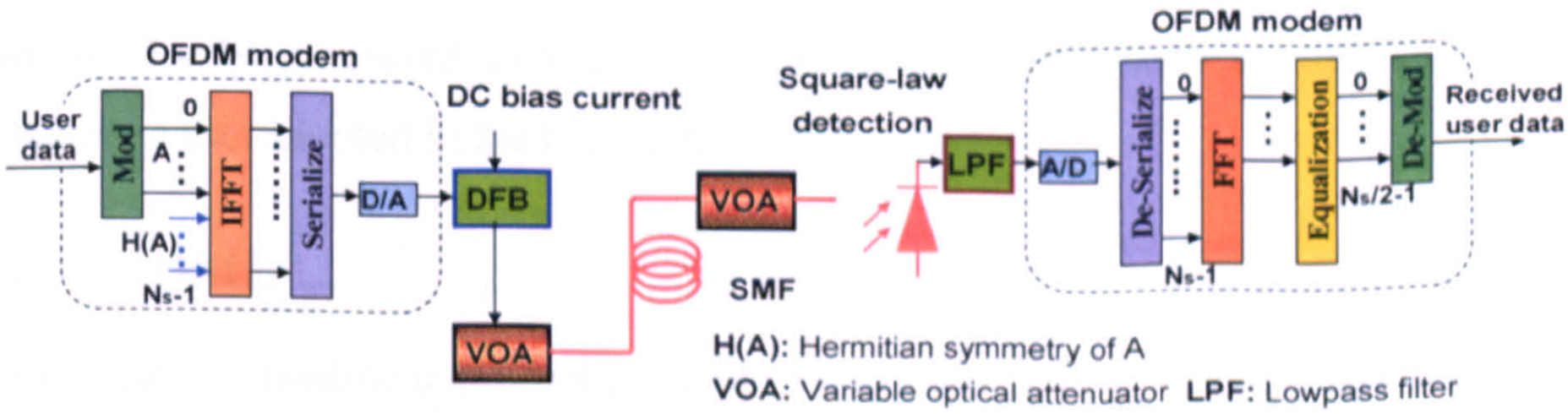

Fig. 4.1 Diagram of the transmission system and the OOFDM transceiver architectures.

Fig. 4.1 depicts the OOFDM transmission system considered in this chapter, which consists of an OOFDM transmitter, an SMF link without involving in-line optical amplification and chromatic dispersion compensation and an OOFDM receiver. The

OOFDM transmitter is composed of an electrical OFDM modem, a DML and a Variable Optical Attenuator (VOA). The OOFDM receiver has a square-law photon detector, an electrical LPF and an electrical OFDM modem.

4.2.1 OOFDM Transceivers

In the transmitter, the generation of an electrical OFDM signal in the OFDM modem is modelled following the procedure presented in Section 2.3. The major operations in the modem include data mapping using 64-QAM, IFFT, CP insertion, OFDM symbol serialization and DAC. To generate real-valued IFFT outputs, the IFFT inputs are arranged to satisfy the Hermitian symmetry, as shown in Eq. (2.41). Here it is also worth pointing out, in particular, that, to pre-compensate for the system frequency response roll-off effect induced by optical and electrical components involved in the transmission system, variable power loading [4.1] is applied to the subcarriers prior to the IFFT. Similar to the approach described in [4.1], each individual 64-QAM-encoded subcarrier power is first normalized using a common scaling factor, and then multiplied with a controllable gain factor to obtain evenly distributed errors across all the subcarriers within a symbol. Having amplified/attenuated the electrical OFDM current to an optimum level, the generated electrical OFDM signal is then combined with an optimum DC current to directly drive the DFB laser. Finally, the output OOFDM signal from the DML is fed into a VOA to fix the launched optical signal power at an optimum level.

After transmitting through the SMF link, the OOFDM signal is first attenuated by a VOA and then detected by a square-law photon detector. An electrical LPF is employed to remove the noise outside the useful OFDM signal band. The received electrical OFDM signal is finally processed in the receiver OFDM modem with an inverse procedure compared to that adopted in the transmitter OFDM modem.

4.2.2 DML

To simulate the nonlinear properties of the DFB-based DML, here a lumped DFB laser theoretical model developed in Bangor University [4.8] is adopted, taking into account a wide range of nonlinear effects namely longitudinal-mode spatial hole-burning, linear and nonlinear carrier recombination as well as nonlinear gain. It is assumed that the influence of the laser linewidth on the link performance is negligible. Such an assumption holds well

for the transmission systems considered here [4.9]. The validity of the DML model has been verified rigorously and used successfully in [4.2,4.3,4.8].

4.2.3 SMF, PIN detectors and LPF

A standard theoretical SSMF model based on the widely used split-step Fourier method [4.10] is adopted here. The model has been successfully used in [4.2,4.3], in which the effects of loss, chromatic dispersion and optical power dependence of refractive index are taken into account. The effect of fiber nonlinearity-induced phase noise to intensity noise conversion is also included.

A square-law photon detector is employed in the receiver to detect the optical signals emerging from the transmission systems. Both shot noise and thermal noise are considered, which are simulated following the procedure similar to that presented in [4.11].

A LPF is considered, which has amplitude and phase responses similar to those employed in the real-time experiments [4.1]. The LPF introduces the system frequency response roll-off and the frequency dependent phase variation to the received electrical OFDM signal.

4.2.4 Simulation Parameters

In numerical simulations, all parameter values that are made known in the real-time experiments [4.1] are treated as default constants, which are listed as following:

- For the OOFDM transceivers, the total number of subcarriers is 32, of which 15 subcarriers in the positive frequency bins are used to carry user data and one subcarrier close to the optical carrier frequency is dropped completely. The modulation format taken on all the 15 data-carrying subcarriers is 64-QAM. The sampling rates of the DAC/ADC are taken to be 4GS/s. The cyclic prefix parameter defined in Eq. (2.14) is 25%. These parameters give a raw signal line rate of 11.25Gb/s. The number of quantization bits and the optimum signal clipping level is 8-bits and 12.7dB, respectively. The above-mentioned parameters give a signal bandwidth in the positive frequency bins of 2GHz, a bandwidth of each individual subcarrier of 125MHz, and a cyclic prefix length of 2ns within each OFDM symbol having a time duration of 10ns. The subcarrier power distribution prior to the FFT in the transmitter is also identical to that optimized in the experiments [4.1].

- For the 1550nm DML, the optimum driving current Peak-to-Peak (PTP) value is 8mA and the optimum bias current is 36mA. Under such DML operating conditions, a signal extinction ratio is approximately 0.2dB based on the OOFDM signal extinction ratio definition presented in Eqs. (2.46)-(2.47)

- The optical power launched into the SMF link is fixed at 7dBm.

- A PIN detector with a quantum efficiency of 0.8 and a receiver sensitivity of -17dBm (corresponding to a 10Gb/s NRZ at a BER of 1.0×10^{-9}) is adopted.

- The LPF has a 3dB bandwidth of 2.4 GHz and representative frequency dependent group delays: for example, 0.52ns (0.86ns) at 125MHz (1875MHz).

For simulating DFB lasers operating at 1550nm, the parameters identical to those reported in [4.8] are considered: a cavity length of 300μm; a cross-section area of the active region of $0.066\mu m^2$; a photon lifetime of 3.6ps; a nonlinear gain coefficient of $7.4\times10^{-23}m^3$; a linewidth enhancement factor of 3; a transparency carrier density of $1.5\times10^{24}m^{-3}$; a carrier lifetime of 10ns; a bimolecular recombination coefficient of $1.0\times10^{-16}m^3/s$; an Auger recombination coefficient of $6.5\times10^{-41}m^6/s$; a linear gain coefficient of $7.5\times10^{-20}m^2$; an optical width (vertical) of 0.47μm; an optical width (horizontal) of 1.80μm; a confinement factor of 0.07; a group refractive index of 3.7; a phase refractive index of 3.2203 and a 38% coupling efficiency from the laser chip to the SMF.

The SMF parameters are detailed as followings: an effective area of $80\mu m^2$, a dispersion parameter of 18.0ps/nm/km, a dispersion slope of $0.07ps/nm^2/km$, a loss of 0.20dB/km and a Kerr coefficient of $2.35\times10^{-20}m^2/W$.

4.3 Result Comparisons and Key Limiting Factor Identification

4.3.1 Theoretical and Experimental Result Comparisons

To perform fair comparisons with experimental results presented in [4.1], apart from the parameters listed in Section 4.2.4, a system frequency response that is responsible for the entire transmission system from the IFFT input in the transmitter to the FFT output in the receiver is also considered, whose frequency dependent roll-off profile is finely adjusted to

provide the best fits with all the key experimental results presented in [4.1]. In numerical simulations, a total number of 1600 OFDM symbols are employed, which gives rise to 524888 samples after oversampling.

Fig. 4.2 shows the system frequency response comparisons for optical BTB and 25km SMF transmission. It can be seen in Fig. 4.2 that excellent agreements between the numerical simulations and experimental measurements are obtained across the whole OOFDM signal spectral region. The observed system frequency response roll-off of approximately 11dB for the optical BTB case is mainly contributed by: inherent sin(x)/x response in the DAC, the DML response and the LPF filtering effects. The SMF further lowers the system frequency response due to the IMDD fibre link frequency response.

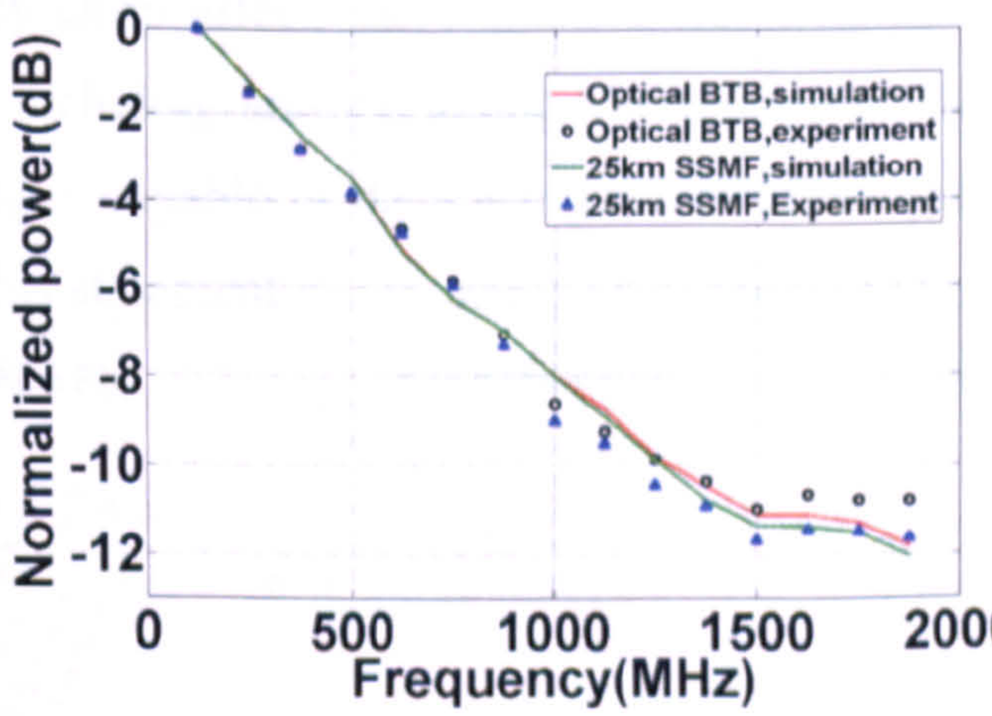

Fig. 4.2 Comparisons of system frequency response between numerical simulations and experimental measurements for different link configurations.

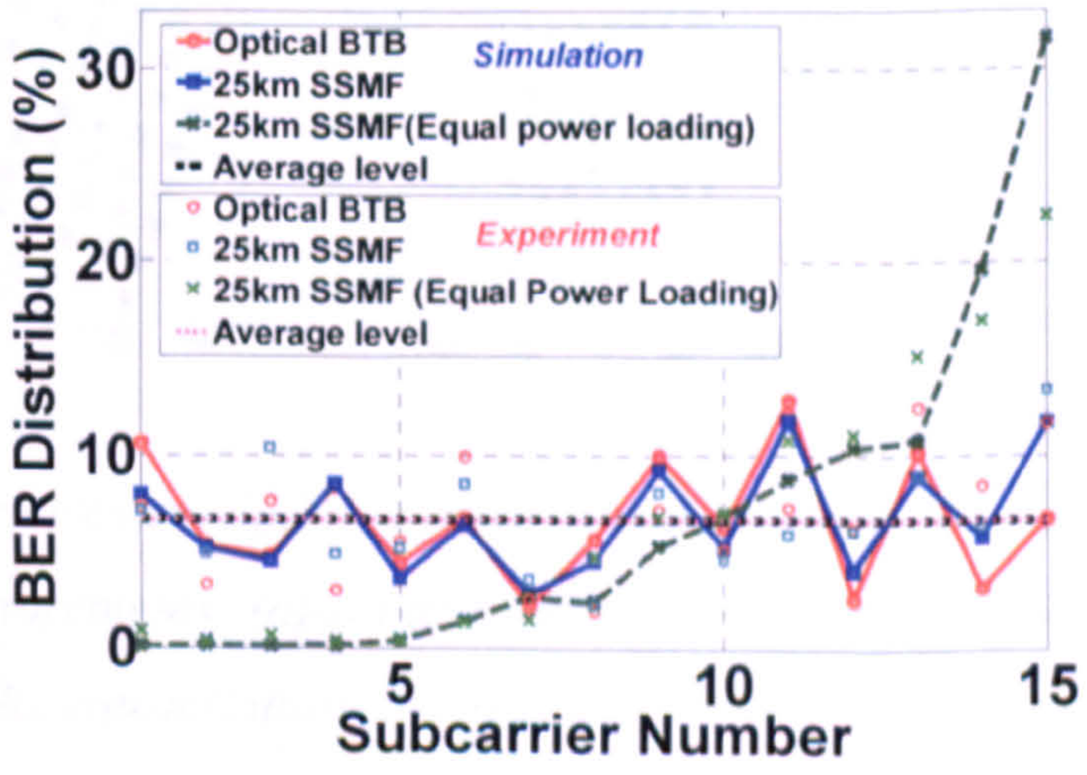

Fig. 4.3 Comparisons of bit error distribution across all the subcarriers between numerical simulations and experimental measurements for equal and variable power loading under various system configurations.

When equal power loading is applied across all the subcarriers, the presence of the deep system frequency response roll-off shown in Fig. 4.2 inevitably causes a large variation in received subcarrier power and thus the occurrence of a large number of bit errors on high frequency subcarriers, as seen in Fig. 4.3. This leads to a total channel BER as large as 5.0×10^{-3} for a received optical power of -6.5dBm. However, by making use of variable power loading with a subcarrier power profile similar to that reported in [4.1], bit errors are distributed almost evenly across all the subcarriers, as shown in Fig. 4.3, and the total channel BER is reduced to 8.8×10^{-4}. It is also interesting to note that the simulated bit error distribution and the corresponding average error level are almost identical to those measured in the experiments [4.1]. For the last four high frequency subcarriers that experience a similar system frequency response roll-off and suffer from the relatively strong DML frequency chirp effect, there exists a significantly large bit error difference between the cases of including and excluding variable power loading. This implies that variable power loading is capable of decreasing the DML frequency chirp-induced signal spectral distortions. This statement is confirmed once again in Fig. 4.5 and Fig. 4.7.

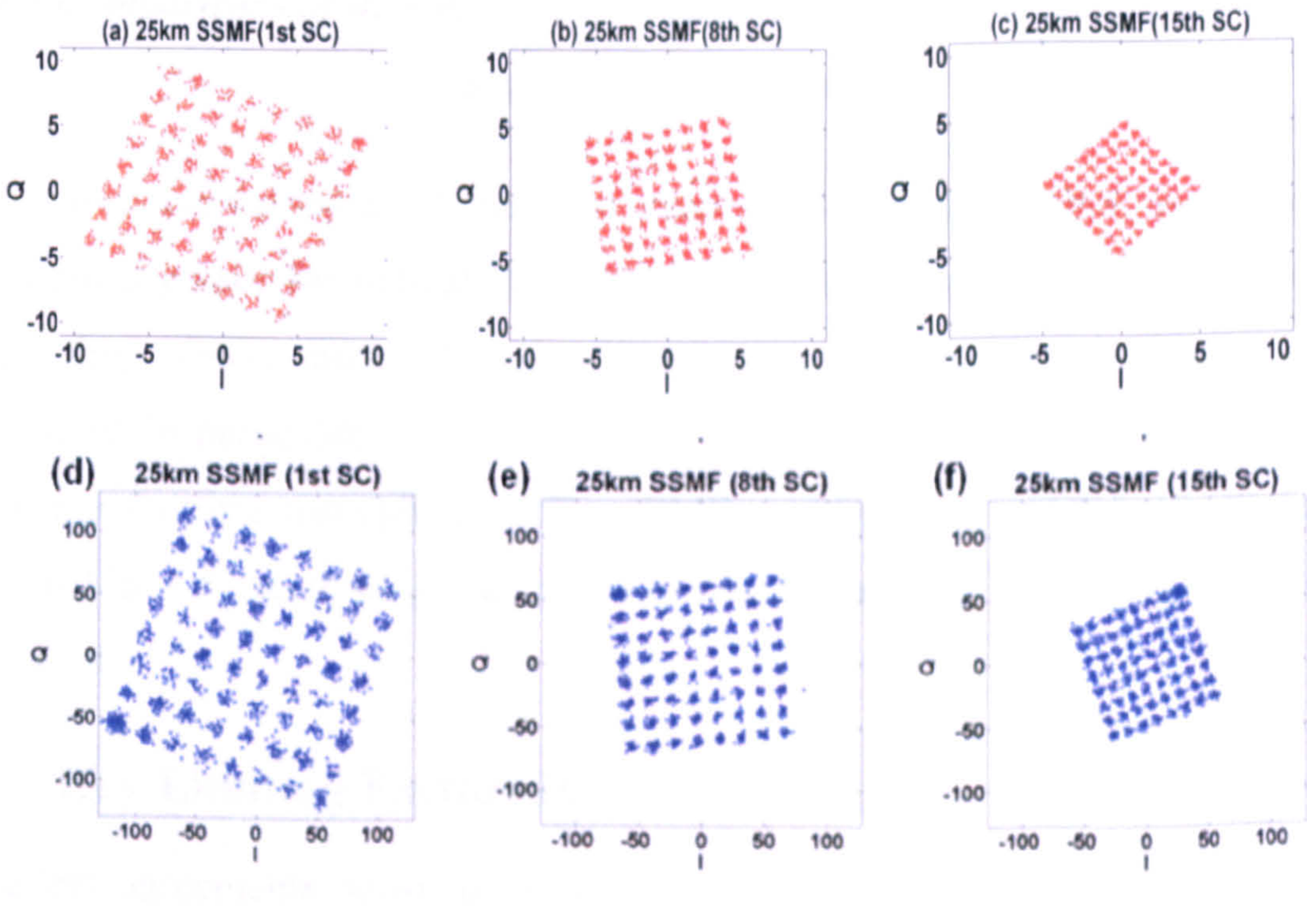

Fig. 4.4 Subcarrier constellation comparisons between numerical simulations and experimental measurements: (a)-(c) are simulated results and (d)-(f) are experimental results. The constellations are recorded before channel equalization.

Based on the variable power loading profile adopted in simulating Fig. 4.3, after transmitting through a 25km SMF, the representative subcarrier constellations recorded prior to channel equalization in the receiver are presented in Fig. 4.4, where the

numerically simulated constellations are shown in Fig. 4.4(a)-(c) and the corresponding experimentally measured constellations are given in Fig. 4.4(d)-(f). Once again, the simulated results agree very well with the experimental measurements. These constellations also show the residual system frequency roll-off effect for high frequency subcarriers.

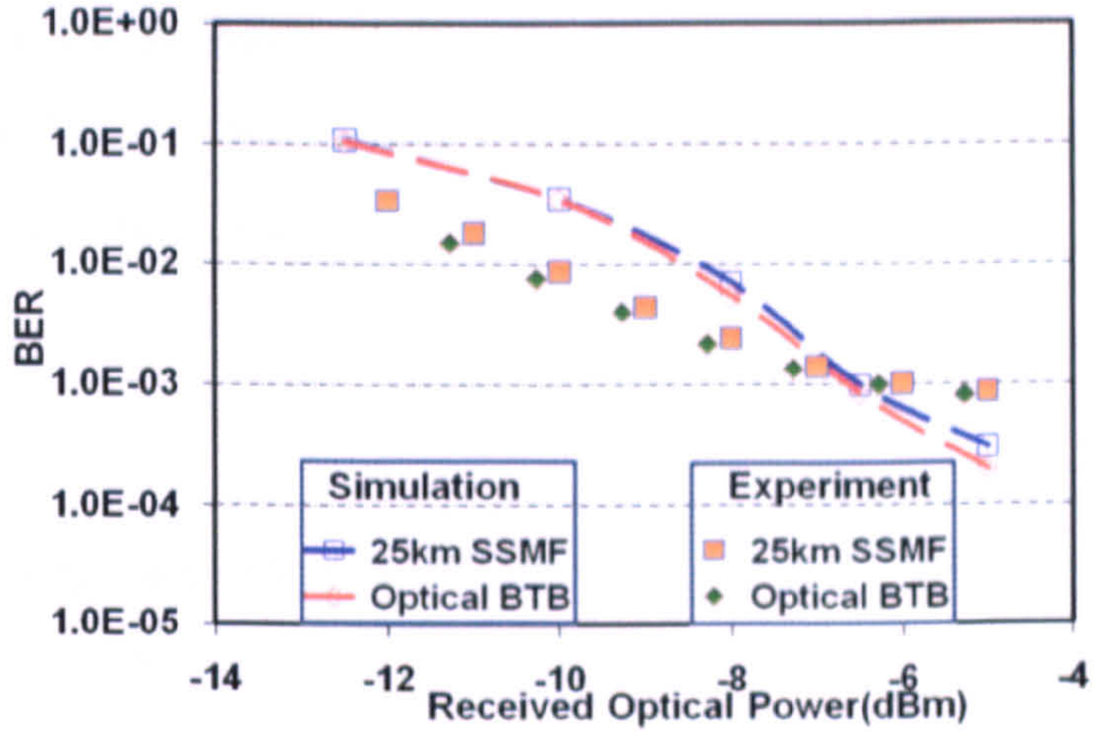

Fig. 4.5 Comparisons of BER versus received optical power performance for different system configurations.

Fig. 4.5 shows comparisons of the total channel BER performance as a function of received optical power for optical BTB and 25km SMF transmission subject to variable power loading. Once more, the simulated results are similar to those measured experimentally, in particular, in the vicinity of a BER of 1.0×10^{-3}. As expected from Fig. 4.3, after transmitting through the 25km SMF, a negligible optical power penalty is observed in Fig. 4.5, suggesting that both linear and nonlinear optical-domain distortions are very small.

4.3.2 Key Limiting Factors Identification

The excellent agreements between the simulated results and experimental measurements presented in Section 4.3.1 confirm the validity of the theoretical OOFDM system model adopted here. Based on the OOFDM system model and utilizing variable power loading, numerical investigations are extended in this subsection to explore the impacts of various physical mechanisms on the optical power budget to identify key factors limiting the OOFDM performance. Here special attention is focused on three factors, namely OOFDM

signal ER, DML frequency chirp and subcarrier intermixing upon square-law detection in the receiver. The simulated results are plotted in Figs. (4.6)-(4.8).

The intensity modulated optical field emerging from a DML can be expressed as $S(t) = A(t)e^{j\phi(t)}$ with $A(t)$ and $\phi(t)$ being the amplitude and phase of the output optical field. By taking into account the time-domain "noise-like" OOFDM waveform with an approximately Gaussian probability density function, the ER of an OOFDM signal is defined explicitly in Eqs. (2.46)-(2.47). To alter the signal ER but without considerably affecting both $A(t)$ and $\phi(t)$, the optical field can be rewritten as

$$S'(t) = K\sqrt{A^2(t) - C}e^{j\phi(t)} \tag{4.1}$$

where K (>0) is a factor for adjusting the output optical power at the input facet of the transmission link, $C(< A^2(t))$ is the factor for varying the signal ER via vertically shifting the signal waveform.

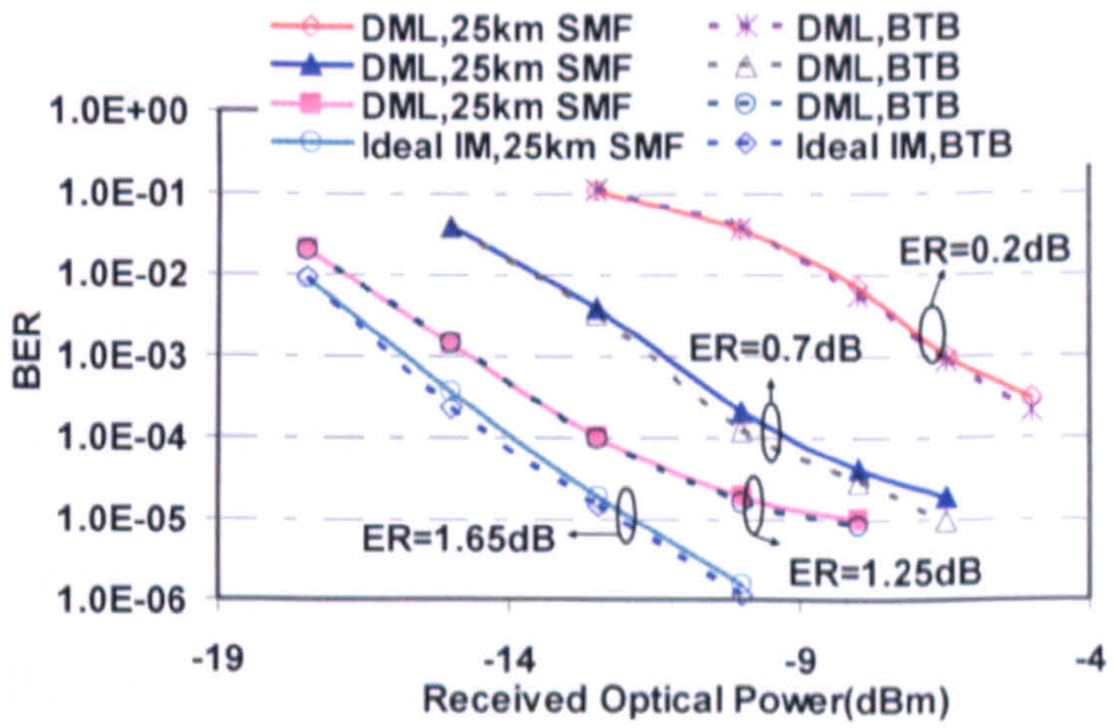

Fig. 4.6 Impact of OOFDM signal ER on the received optical power dependent total channel BER performance for optical BTB and 25km SMF transmission. The BER performance for ideal intensity modulator (IM)-modulated OOFDM signals is also plotted for comparison.

Numerical simulations are undertaken to explore the impact of the OOFDM signal ER on the received optical power dependent BER performance. The simulated results are plotted in Fig. 4.6 for optical BTB and 25km SMF transmission. For comparison, the BER performance of a DML modulated OOFDM signal (corresponding to C=0 and a signal ER of 0.2dB) is also plotted, together with the BER performance of an ideal intensity

modulator-modulated OOFDM signal (corresponding to a signal ER of 1.65dB). It can be seen in Fig. 4.6 that the received optical power required for achieving a total channel BER of 1.0×10^{-3} decreases significantly with increasing signal ER. For a fixed optical launch power, an 8dB improvement in optical power budget is feasible when the signal ER is increased from 0.2dB to 1.25dB [the maximum signal ER according to Eq. (4.1) for the adopted DML operating conditions]. Such significant improvement is due to the fact that the effective OSNR of the transmitted OOFDM signal increases with signal ER for a transmission system having a fixed receiver sensitivity. Moreover, Fig. 4.6 also shows that the optical power budget improvement is transmission link independent, suggesting that the signal ER variation does not change the signal phase for the system considered.

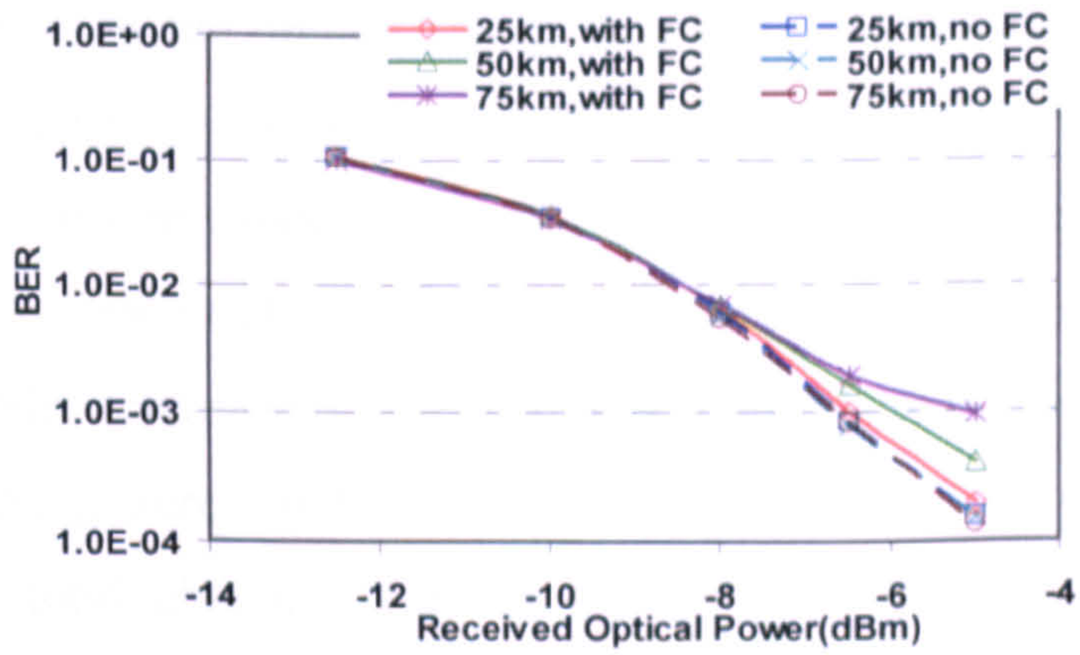

Fig. 4.7 Impact of the DML frequency chirp (FC) on the received optical power dependent BER performance for different transmission distances. The signal ER of 0.2dB is adopted.

The influence of the DML frequency chirp on the total channel BER performance is also explored theoretically and the simulated results are shown in Fig. 4.7 for various transmission distances of up to 75km. In obtaining Fig. 4.7, C=0 is utilized for all the cases and the cases of excluding the DML frequency chirp is realized by replacing $\phi(t)$ in Eq.(4.1) with a constant value. It can be seen in Fig. 4.7 that, for received optical powers of >-8dBm and the cases of including the DML frequency chirp, the received optical power corresponding to a total channel BER of 1.0×10^{-3} increases with increasing transmission distance. This is due to the combined effects of chromatic dispersion and DML frequency chirp. Whilst for received optical powers of <-8dBm with the DML frequency chirp still being present, no BER performance differences are observed for different transmission distances. This is because thermal noise associated with the PIN photo-detector becomes the dominant factor limiting the system performance. The above analysis is confirmed by

the BER performance obtained for the cases of excluding the DML frequency chirp, as shown in Fig. 4.7. For such cases, no BER differences between different transmission distances are shown over the whole received optical power range. It should also be noted in Fig. 4.7 that, the DML frequency chirp effect is not as significant as those presented in [4.3] where equal power loading is applied. This implies that variable power loading can not only compensate for, to some extent, the system frequency response roll-off effect, as discussed in Fig. 4.3, but also effectively reduce the DML frequency chirp effect.

Theoretical explorations of the impairments of subcarrier intermixing on the received optical power dependent BER performance are undertaken and the numerical results are shown in Fig. 4.8. In obtaining Fig. 4.8, for the cases where zero-padding is considered, the first 8 subcarriers close to the optical carrier frequency are zero-mapped and no changes are made to all the remaining subcarriers. Given the fact that the subcarrier intermixing effect introduces the strongest spectral distortions to the first subcarrier and becomes weak for higher frequency subcarriers, such a zero-padding approach can, therefore, partly eliminate the subcarrier intermixing effect. Fig. 4.8 reveals that, compared to the cases of excluding zero-padding, zero-padding brings about at least 1dB reduction in received optical power at a total channel BER of 1.0×10^{-3} for all the transmission distances considered.

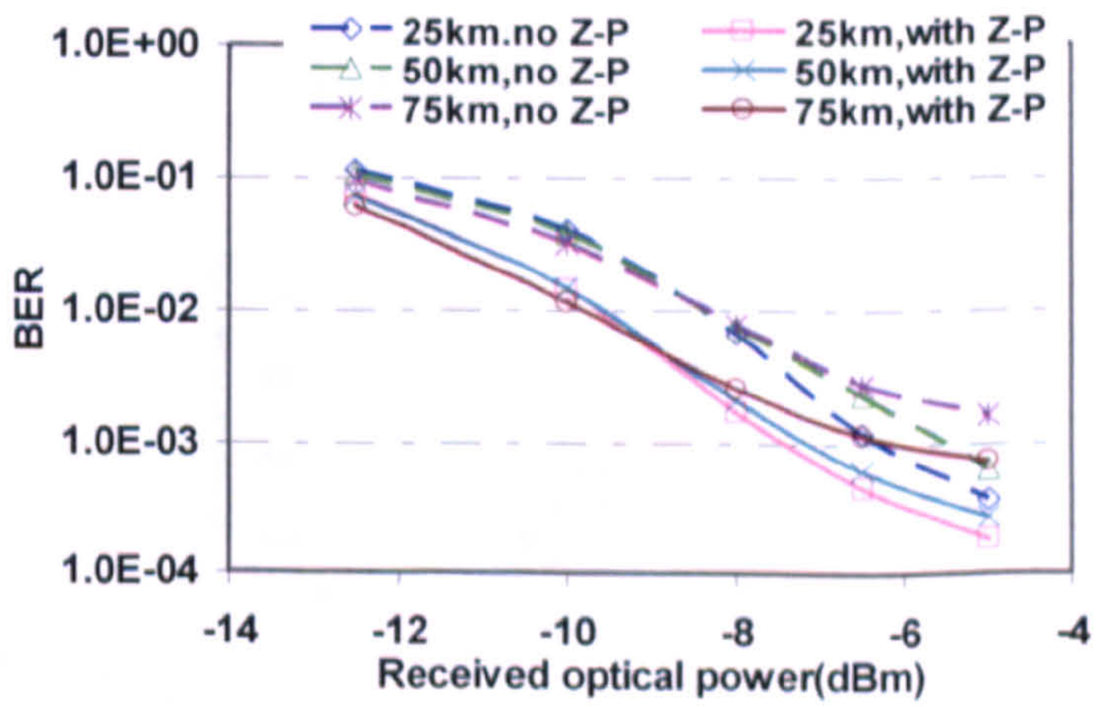

Fig. 4.8 Impairments of received optical power dependent total channel BER performance for the cases with zero-padding (Z-P) and without Z-P. Different SMF transmission distances are considered for both these cases.

From the above analyses, it is concluded that the low ER of the DML modulated OOFDM signal is the predominant factor limiting the achievable system performance. The

subcarrier intermixing effect associated with direct photon detection reduces the optical power budget by at least 1dB. Variable power loading can effectively eliminate the DML-induced frequency chirp effect. Therefore, it is greatly advantageous if a simple and effective approach capable of improving the ER of the DML intensity-modulated OOFDM signal can be identified. This forms the major task of Section 4.4.

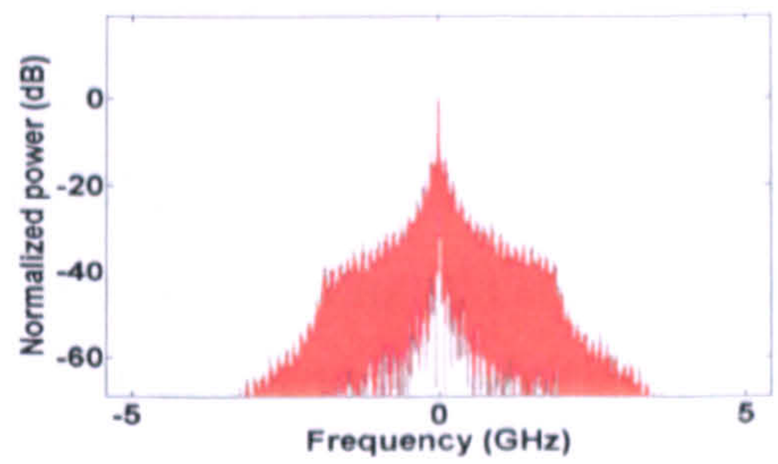

(a) Before filtering.

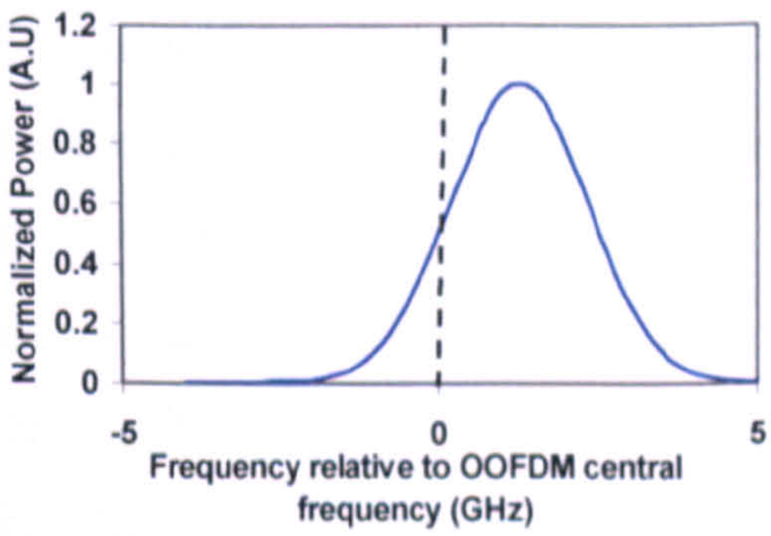

(b) Gaussian filter spectral profile.

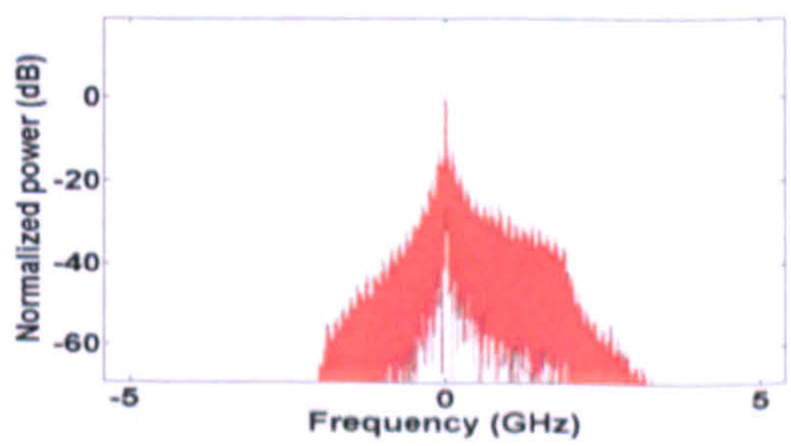

(c) After filtering

Fig. 4.9 (a) OOFDM signal spectrum before filtering; (b) OBPF profile with a wavelength offset of 0.01nm (1.25GHz) with respect to the OOFDM carrier wavelength. The 3dB bandwidth is 2.5GHz (0.02nm); (c) filtered OOFDM signal spectrum.

4.4 Tunable Narrowband OBPF-enabled Performance Improvement

In this section, numerical investigations are undertaken of the feasibility of using a tunable narrowband OBPF to considerably improve the ER of the DML intensity-modulated OOFDM signal and thus the system performance.

The signal ER improvement technique can be easily implemented by inserting a tunable narrowband OBPF between the DML and the VOA in the OOFDM transmitter illustrated in Fig. 4.1. For a transmission system operating at a specific optical carrier wavelength, the narrowband OBPF should be finely detuned to provide an optimum wavelength offset with respect to the optical carrier wavelength. Such wavelength offset can enhance the conversion from the unwanted FM components into the useful AM components, thus giving rise to a maximized OOFDM signal ER without significantly distorting the OOFDM signal spectrum. For simplicity, in the following numerical simulations, the tunable narrowband OBPF is assumed to have a Gaussian spectral profile and a flat phase response. As an example, Fig. 4.9 presents the OOFDM signal spectra before and after the OBPF, as well as the Gaussian filtering profile with its peak wavelength being detuned away from the optical carrier wavelength. Generally speaking, for a given wavelength offset, a narrow 3-dB OBPF bandwidth produces a high signal ER.

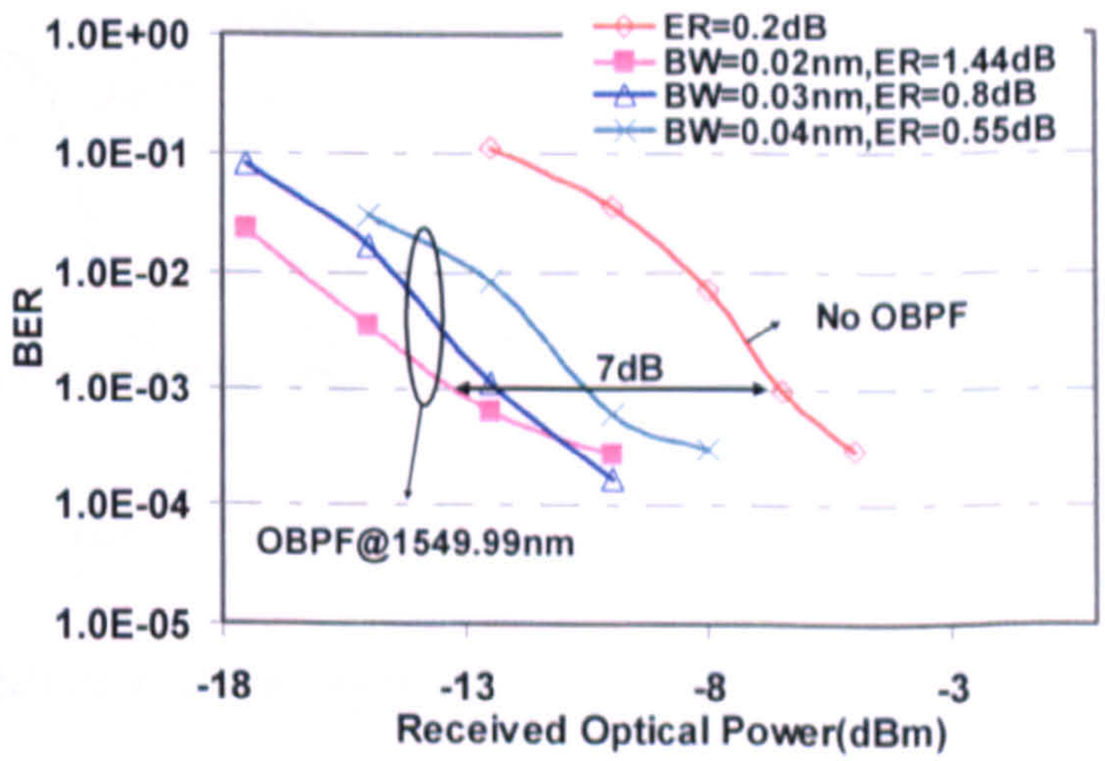

Fig. 4.10 Total channel BER as a function of received optical power for various bandwidth OBPFs with 0.01nm wavelength detuning.

The effectiveness of the technique is examined numerically in Fig. 4.10, where the total channel BER versus received optical power is plotted for various OBPF bandwidths of

0.02nm (1.44dB ER), 0.03nm (0.8dB ER) and 0.04nm (0.55dB ER). In obtaining Fig. 4.10, the wavelength offset is set at 0.01nm (1.25GHz) and the transmission distance is taken to be 25km. For comparisons, the BER performance of the DML intensity-modulated OOFDM signal without applying the optical filtering technique is also shown in the same figure. In addition, the filtered OOFDM signal is launched into the SMF link at a fixed optical power of 7dBm.

It can be seen in Fig. 4.10 that a reduction in OBPF bandwidth considerably decreases the received optical power required for achieving a total channel BER of 1.0×10^{-3}. Compared to the unfiltered case, for a 0.01nm wavelength offset, an OBPF with a 0.02nm bandwidth can increase the signal ER from 0.2dB to 1.44dB, this results in an optical power budget improvement as large as 7dB. It should be pointed out that, when the same OBPFs are used for ideal intensity modulator-modulated OOFDM signals and/or DML intensity-modulated OOFDM signals with $\phi(t)$ being replaced by constant phases, in comparison with the unfiltered cases, no improvements in signal ER are observed and the BER performance becomes worse. This can be understood by considering the fact that these chirp-free signals have flat top spectra, therefore, the use of the OBPF distorts the signal spectra without increasing the signal ER.

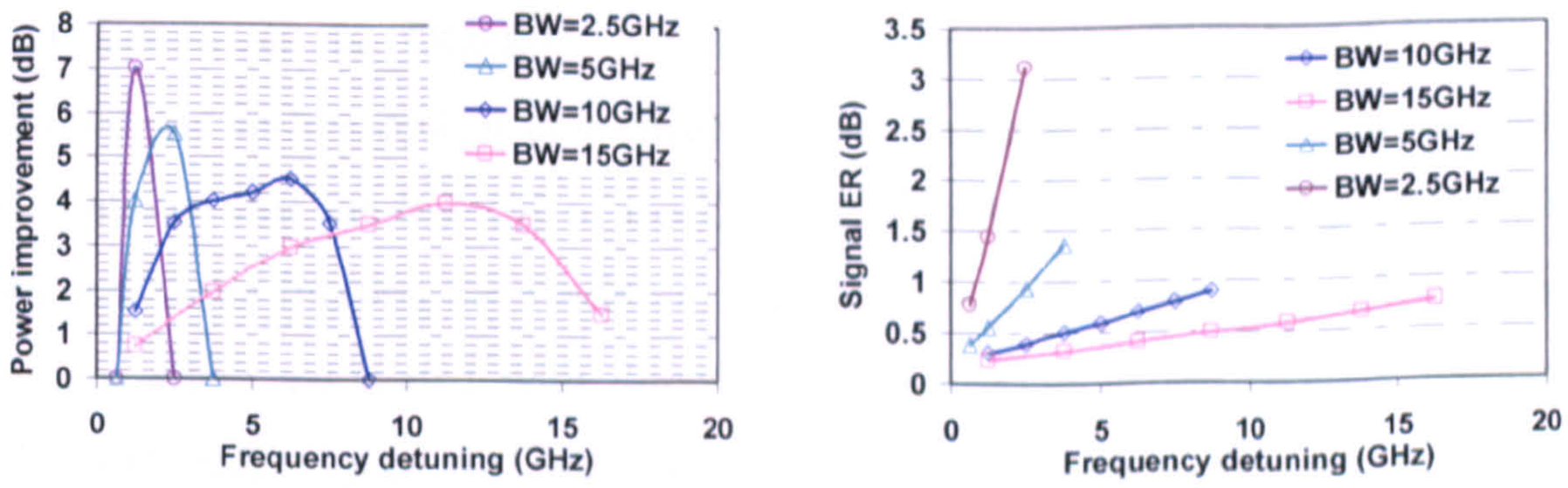

Fig. 4.11 (a) Optimum wavelength offsets for different 3-dB bandwidth OBPFs. (b) Obtained OOFDM signal ER as a function of frequency offset for different OBPFs. The SMF length is 25km.

Fig. 4.11 explores theoretically the optimum wavelength offsets for various OBPFs with different 3-dB bandwidths of 2.5GHz, 5GHz, 10GHz and 15GHz. Fig. 4.11(a) shows that for a fixed OBPF bandwidth, there exists an optimum wavelength offset, corresponding to

which a maximum improvement in optical power budget can be obtained at a total channel BER of 1.0×10^{-3}. Below the optimum wavelength offset value, the observed increase in optical power budget with increasing wavelength offset is mainly due to the growth of the OOFDM signal ER, as shown in Fig. 4.11(b); Whilst for wavelength offsets exceeding the optimum value, the BER performance degradation occurs mainly due to the strongly distorted OOFDM spectra. Fig. 4.11(a) also shows that the optimum wavelength offset increases with increasing OBPF bandwidth, and that the maximum achievable optical power budget improvement decreases with increasing OBPF bandwidth. For instance, for a 2.5GHz bandwidth OBPF, a 7dB optical power budget improvement is obtainable, which, however, drops to 4dB when a 15GHz bandwidth OBPF is used. This originates from the fact that a wide bandwidth OBPF gives less steep spectral profile edges, thus leading to small OOFDM signal ERs, as shown in Fig. 4.11(b).

4.5 Conclusion

Based on a comprehensive theoretical OOFDM system model rigorously verified by comparing numerical results with 11.25Gb/s end-to-end real-time experimental measurements, detailed explorations have been undertaken of the impacts of various physical factors on the OOFDM system performance over DML-based IMDD SMF systems without in-line optical amplification and chromatic dispersion compensation. It has been shown that the low ER of the DML intensity-modulated OOFDM signal is the predominant factor limiting the maximum achievable optical power budget. The subcarrier intermixing effect associated with direct photon detection in the receiver reduces the optical power budget by at least 1dB, and variable power loading can eliminate the DML-induced frequency chirp effect. Results have also shown that, immediately after the DML in the transmitter, the use of a 0.02nm 3-dB bandwidth OBPF with a 0.01nm wavelength offset can increase the OOFDM signal ER by 1.24dB, thus leading to a 7dB optical power budget improvement at a total channel BER of 1×10^{-3}.

References

[4.1] G. P. Giddings, X. Q. Jin, E. Hugues-Salas, E. Giacoumidis, J. L. Wei, and J. M. Tang, "Experimental demonstration of a record high 11.25Gb/s real-time optical OFDM transceiver supporting 25km SMF end-to-end transmission in simple IMDD systems," Opt. Express, vol. 18, no.6, pp. 5541-5555, 2010.

[4.2] J. M. Tang and K. A. Shore, "30 Gb/s signal transmission over 40-km directly modulated DFB-laser-based single-mode-fibre links without optical amplification and dispersion compensation," J. Lightw. Technol., vol. 24, no.6, pp. 2318-2327 Jun. 2006.

[4.3] X. Zheng, X. Q. Jin, R. P. Giddings, J. L. Wei, E. Hugues-Salas, Y. H. Hong and J. M. Tang, "Negative Power Penalties of Optical OFDM Signal Transmissions in Directly Modulated DFB Laser-Based IMDD Systems Incorporating Negative Dispersion Fibres", IEEE Photonics J., vol. 2, no. 4, pp. 532-542, Jun. 2010.

[4.4] H.S. Chung, Y. G. Jang, and Y. C. Chung, "Directly modulated 10-Gb/s signal transmission over 320km of negative dispersion fiber for regional metro networks," IEEE Photon. Lett. Technol., vol. 15, no. 9, pp. 1306-1308, Sept. 2003.

[4.5] M. C. Tatham, X. Cu, L. D. Westbrook, G. Sherlock, and D. M. Spirit, "Transmission of 10 Gbit/s directly modulated DFB signals over 200-km standard fiber using mid-span spectral inversion," Electron. Lett., vol. 30, no. 16, pp. 1335–1336, Aug. 1994.

[4.6] D. H. Sim, Y. Takushima, and Y. C. Chung, "MMF transmission of directly-modulated 40-Gb/s signal using mode-field matched center-launching technique," presented at OFC/NFOEC09, (San Diego, USA, 2009), Paper JThA37.

[4.7] L.-S. Yan, Y. Wang, B. Zhang, C.Yu, J. McGeehan, L. Paraschis, and A. E. Willner, "Reach extension in 10-Gb/s directly modulated transmission systems using asymmetric and narrowband optical filtering, " Opt. Express, vol. 13, no. 13, pp. 5106-5115, Jun. 2005.

[4.8] J. M. Tang, P. M. Lane and K. A. Shore, "High speed transmission of adaptively modulated optical OFDM signals over multimode fibers using directly modulated DFBs," J. Lightw. Technol., vol. 24, no.1, pp. 429-441, Jan. 2006.

[4.9] Z. Zan, M. Premaratne and A. J. Lowery, "Laser RIN and linewidth requirements for direct detection optical OFDM," presented in Conference on Lasers and Electro-Optics/Quantum Electronics and Laser Science Conference and Photonic Applications Systems Technologies 2008 Technical Digest., Washington, DC, 2008, Paper CWN2.

[4.10] G. P. Agrawal, *Nonlinear Fiber Optics*, 2nd ed. New York: Academic, 1995.

[4.11] G. P. Agrawal, *Fibre-Optic Communication Systems*, 2nd ed. Hoboken, NJ: Wiley, 1997.

5 DML-Modulated Carrier Suppressed Single Sideband OOFDM Signal Transmission over IMDD SMF Systems for NG-PONs

Contents

5.1 Introduction **105**

5.2 Description of the Transmission System Model 107

5.2.1 Carrier Suppressed SSB IMDD OOFDM Model 107

5.2.2 Models for DMLs, SMFs, EDFAs and PIN Detectors 108

5.2.3 Simulation Parameters 109

5.3 The Dependence of Optimum Carrier Suppression Ratio on DML Operating Conditions 109

5.4 The Transmission Performance of Carrier Suppressed SSB IMDD AMOOFDM Signals in Optimum DML-Based SMF Systems without In-line Optical Amplification 113

5.5 Carrier Suppressed SSB IMDD OOFDM Signal Transmission in Optimum DML-Based SMF Systems Incorporating In-line Optical Amplifiers 116

5.6 Conclusions 118

5.1 Introduction

In Chapter 4, we have identified the impacts of various physical effects on DML-modulated OOFDM PON systems. These effects include the low DML-modulated OOFDM signal ER, DML-induced positive frequency chirp and subcarrier intermixing upon direct detection in the receiver. The use of a wavelength-offset narrowband OBPF has been shown to be effective in improving the OOFDM signal ER and thus the system optical power budget.

However, the reduction of the subcarrier intermixing effect upon square-law detection has not been discussed. Moreover, as discussed in Section 2.4.3, the square-law detection also introduces frequency ripples originating from the intermixing between the upper sideband and the lower sideband of a DML-intensity modulated signal with DSB spectrum. Clearly, this effect contaminates the fiber dispersion-induced phase shift in the electrical domain, leading to a reduced dispersion tolerance [5.1]; and therefore limits the achievable transmission distance of the DML-modulated OOFDM signals. Optical Single Sideband (SSB) has been widely considered as an effective approach to eliminate such an effect [5.2,5.3]. In addition, a guard band between the optical carrier and the OFDM signal band can also be inserted to prevent the unwanted subcarrier×subcarrier beating terms from occurring in the useful OFDM signal band.

However, the use of optical SSB IMDD OOFDM signals results in a large power ratio between the optical carrier and the optical SSB signal band, leading to a low OSNR sensitivity. Carrier suppression [5.2] is thus obligatory to obtain a proper OSNR sensitivity in the receiver. As discussed in Chapter 4, for a DSB optical signal emerging from a DML operating at representative conditions, a typical optical signal ER is approximately <1dB, implying that the majority of the optical signal power is carried by the optical carrier wave. In particular, the optical signal ER is strongly dependent upon DML operating conditions [5.4,5.5]. From the practical operation point of view, the carrier suppression-induced variation in power ratio between the optical carrier wave and the optical SSB signal band is very easy to use in designing the transmission systems involving DMLs subject to various

operating conditions. Therefore, throughout this chapter, the optical carrier suppression ratio, C_s, is defined as

$$C_s = \frac{P_{C0}/P_{S0}}{P_{C1}/P_{S1}} \tag{5.1}$$

where P_{C0} (P_{C1}) and P_{S0} (P_{S1}) are the optical carrier wave power and the SSB optical signal band power prior to (after) applying carrier suppression, respectively.

As mentioned above, at the output facet of a DML, the signal ER, the output signal power and its corresponding frequency chirp depend strongly on DML operating conditions [5.4-5.6]. It is expected that the carrier suppression ratio is DML dependent and plays a crucial role in optimizing the transmission performance of the carrier suppressed SSB IMDD OOFDM systems involving DMLs. It is therefore desirable to investigate the impact of DMLs on the transmission performance of the carrier suppressed SSB IMDD OOFDM signals. It should be pointed out that, DMLs have been employed in [5.4-5.7], in which carrier suppression is, however, not required as all the transmission systems are based on DSB IMDD.

The thrust of this chapter is to explore thoroughly the influence of the DMLs on the transmission performance of carrier suppressed SSB IMDD OOFDM signals over SMF systems involving DMLs. The optimum DML operating conditions are identified, based on which detailed discussions are made of the feasibility of such signals for practical implementation in NG-PON without in-line optical amplifications. It is shown that, for DML-based NG-PONs excluding in-line optical amplifications, 30Gb/s signal transmission over 80km SMF is achievable, which doubles the performance corresponding to the DSB IMDD OOFDM signals without carrier suppression [5.4]; and for DML-based NG-PONs incorporating inline EDFAs, 10Gb/s carrier suppressed SSB IMDD OOFDM transmission over 1200km SMF is feasible. In addition, results also indicate that the systems considered here have excellent flexibility and great robustness to variations in both DML operating condition and optical input power.

5.2 Description of the Transmission System Model

In this section, a comprehensive system model is developed to simulate the generation, transmission and detection of carrier suppressed SSB IMDD OOFDM signals in DML-based SMF systems excluding (or including) EDFAs. The transmission system is illustrated in Fig. 5.1, where the block diagrams of the transmitter and the receiver are also given.

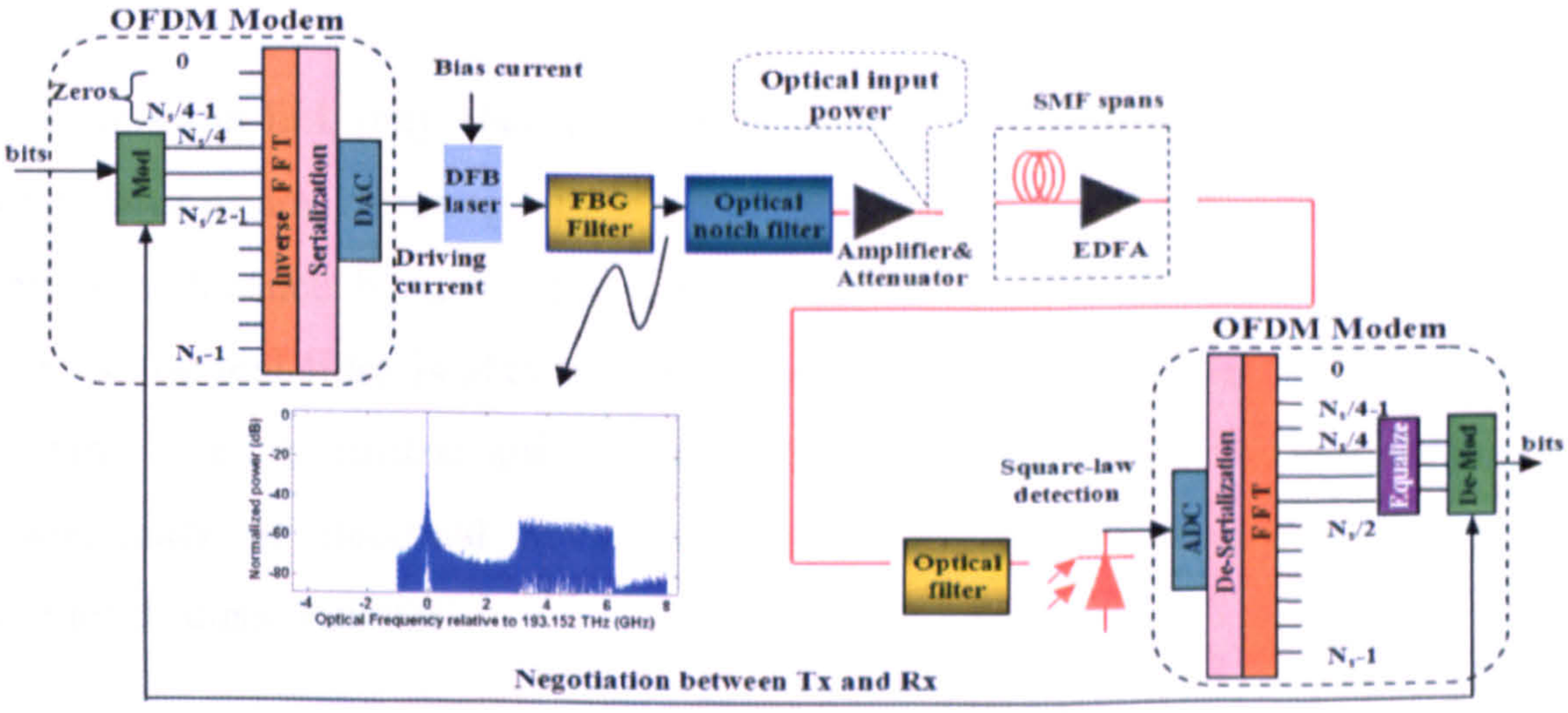

Fig. 5.1 Transmission link diagram together with block diagrams of the transmitter and receiver.

5.2.1 Carrier Suppressed SSB IMDD OOFDM Model

In the transmitter, the OFDM modem is similar to that described in Section 4.2.1, except that, at the IFFT input, the first $N_s/4$ subcarriers are padded with zeros to introduce a guard band between the carrier wave and the OFDM signal band, and after the guard band, another group of $N_s/4$ subcarriers is followed, which are used to carry user's data. The remaining $N_s/2$ subcarriers are arranged to satisfy the Hermitian symmetry with respect to the first $N_s/2$ subcarriers, as expressed in Eq. (2.41). In addition, equal power loading is applied across all the subcarriers as the roll-off effects from DAC/ADC are ignored here. Finally, the electrical signal emerging from the OFDM modem is ready to directly modulate a DFB laser.

To generate a SSB OOFDM signal having an optimum carrier suppression ratio, a Fibre Bragg Grating (FBG) filter and a F-P tunable filter used as an optical notch filter [5.2] are inserted between the DFB laser and the input port of the amplifier/attenuator in the

transmission system, as shown in Fig. 5.1. The FBG filter removes the lower sideband of the OOFDM signal generated by the DML. By finely detuning the central frequency of the FP tunable filter, the optical carrier power is adjusted without affecting the SSB signal band power. Therefore, an optimum carrier suppression ratio can be achieved for an arbitrary transmission system. It should be noted that the variation in carrier suppression ratio also brings about alteration in carrier suppressed SSB optical signal power. Thus the carrier suppressed SSB optical signal has to be amplified/attenuated to provide the required optical input power coupled into the transmission system.

The transmission link may also incorporate in-line EDFAs to boost the OOFDM signals for long transmission distances; such a configuration is to exam the maximum achievable transmission distance by using the carrier suppressed SSB OOFDM technique. In the receiver, an optical filter is also introduced to remove all the noises outside the OOFDM signal band. The transmitted optical signal is then detected by a square-law photo-detector. The procedures of electrical signal processing in the receiver are the inverse of the transmitter discussed above.

It should be pointed out that identical or adaptive signal modulation formats may be adopted on individual subcarriers within an OOFDM symbol. The latter technique is known as AMOOFDM [5.4-5.7], which has been described in detail in Section 2.4.5. For both the identical modulation technique and the AMOOFDM technique, the total channel BER, BER_T, and the system signal line rate are defined as in Eq. (2.51) and Eq. (2.52), respectively.

5.2.2 Models for DMLs, SMFs, EDFAs and PIN Detectors

The models for DMLs, SMFs and PIN detectors employed in Chapter 4 are used here, whose validities have been confirmed by well agreements with experimental measurements.

The EDFA model performs the function of a simple saturating optical amplifier, which is characterized as a gain block followed by a Gaussian optical filter. The associated noise figure is defined as the ratio of the SNR at the input to the SNR at the output of the amplifier [5.8].

5.2.3 Simulation Parameters

It should be pointed out that all the parameter values given below are used as default ones in this chapter, unless addressed explicitly in the corresponding text when necessary.

In simulating the OOFDM modems, the sampling speeds of the DAC and ADC are fixed at 12.5GS/s in both the transmitter and the receiver. The total number of subcarriers, N_s, is taken to be 128, which is an optimum value obtained in [5.7]. The above-mentioned parameters give a signal bandwidth in the positive frequency bins of 12.5/2 = 6.25GHz. The bandwidth for each subcarrier is 6.25/64 ≈ 97.5MHz. As defined in Eq. (2.14), here a CP parameter of η=25% is considered, which gives a CP length of 2.56ns within each OFDM symbol having a total time duration of 12.8ns. The dispersion tolerance of the OOFDM technique, $D_{dispersion}$, is a function of CP parameter, η, and number of subcarriers, N_s, and their relationship can be written as [5.7]

$$D_{dispersion} \propto \frac{4}{r_s^3}\eta N_s \tag{5.2}$$

with r_s being the ADC/DAC sampling speed. The quantization bits and clipping ratio are set to be 7 bits and 13dB, respectively, which are the optimum values identified in [5.9].

For simulating DFB lasers operating at 1550nm, the corresponding DML model parameters listed in Section 4.2.4 are adopted here. Each SMF span is assumed to have a length of 80km. The parameters associated with SMFs can be found from Section 4.2.4 except that a dispersion parameter of 17.0ps/nm/km is adopted here.

The EDFA parameters are taken to be an optical gain of 16dB and a noise figure of 5 dB. A PIN detector with a quantum efficiency of 0.8 and sensitivity of -19dBm (corresponding to a 10Gb/s NRZ with a BER of 1.0×10^{-9}) is adopted in simulations.

5.3 The Dependence of Optimum Carrier Suppression Ratio on DML Operating Conditions

As already mentioned in Section 5.1, the generation of an optical SSB signal causes a significant reduction in the effective signal OSNR due to the removal of half of the

OOFDM signal band, carrier suppression is therefore necessary to enhance the system transmission performance when system nonlinearities and noises are present. In this section, special attention is given to exploring the dependence of the optimum carrier suppression ratio on DML operating conditions. As the influence of variation in signal modulation format is negligible on optimum DML operating conditions [5.4,5.5], for simplicity but without losing generality, identical modulation formats across all the subcarriers are employed in this section. For an 80 km SMF transmission link without optical amplification, Fig. 5.2(a)-(c) show the dependence of carrier suppression ratio upon optical input power (coupled into the transmission link), DFB laser bias current and PTP driving current. Such dependence is also explored for a system consisting of 12 spans (960km) with EDFA and PIN noises being considered, to evaluate not only the potential of the proposed technique but also the dependence of carrier suppression ratio on transmission distance. In obtaining Fig. 5.2, 16-QAM signal modulation format is employed across all the 32 data-carrying subcarriers, this gives a signal line rate of 10Gb/s. A zero BER_T is obtained when BTB transmission is considered for all the operating conditions discussed in Fig. 5.2.

As mentioned in Section 5.2.1, a variation in carrier suppression ratio also changes the optical signal power. To set the carrier suppressed SSB optical signal at a desired power, an optical attenuator/amplifier is used between the notch filter and the input facet of the SMF link, as shown in Fig. 5.1.

When the DML bias current and PTP driving current are fixed, both the output optical signal power from the DML and the optical signal ER remain constant. For a DML bias current of 30mA and a PTP driving current of 15mA, Fig. 5.2(a) and Fig. 5.2(d) show that, for a given optical input power, there exists an optimum carrier suppression ratio, corresponding to which a minimum BER is observed. For carrier suppression ratios lower than the optimum value, the increase in BER is due to the low carrier suppression ratio-induced reduction in effective signal OSNR; whilst for carrier suppression ratios higher than the optimum value, the growth in BER is because of the high carrier suppression ratio-induced increase in signal clipping noise. It can be seen from Fig. 5.2 (a) and Fig. 5.2(d) that, a low optical input power corresponds to a high optimum carrier suppression ratio, as the low optical input power suffers from the relatively strong noise effect, which

can be partially mitigated if the effective signal OSNR is boosted by using a high carrier suppression ratio.

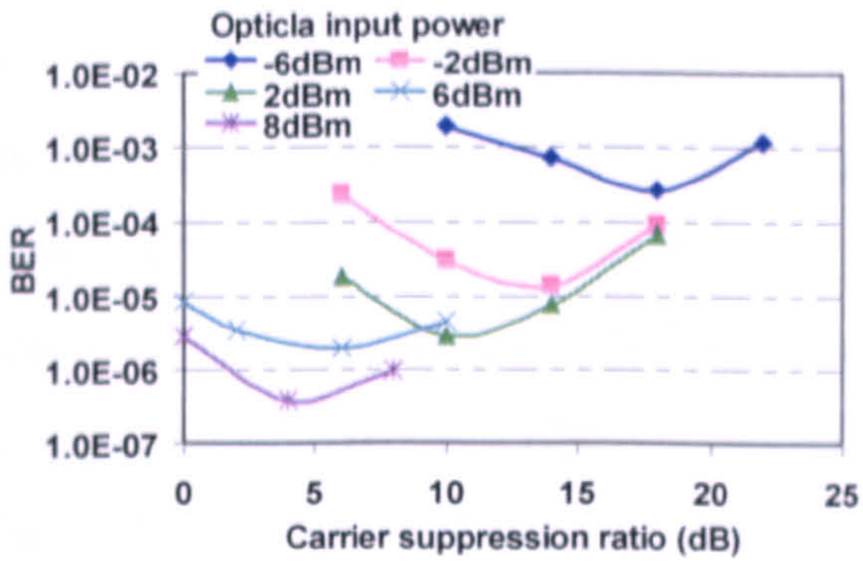

(a)

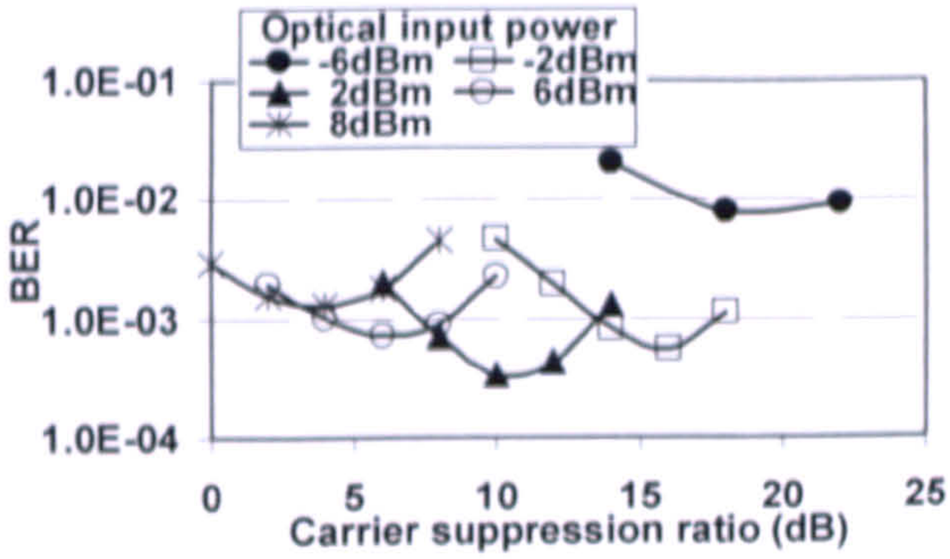

(d)

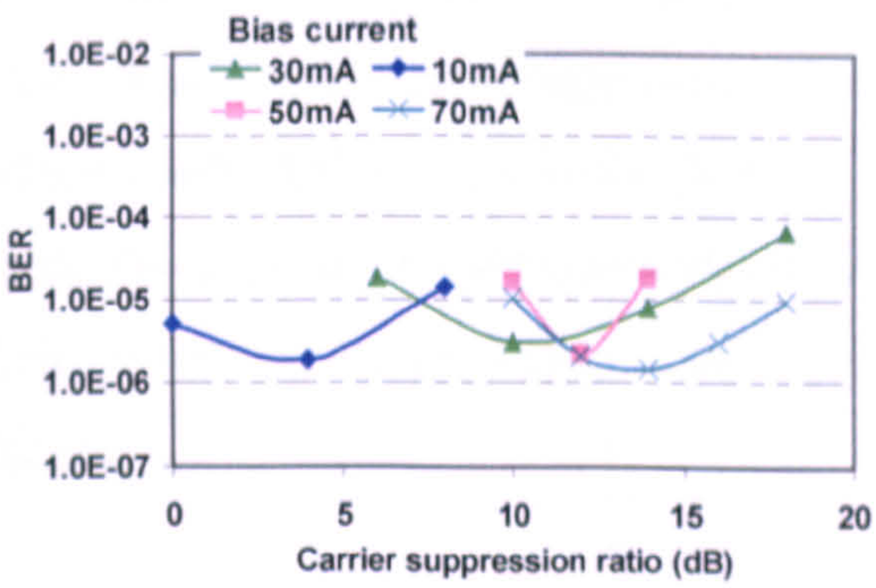

(b)

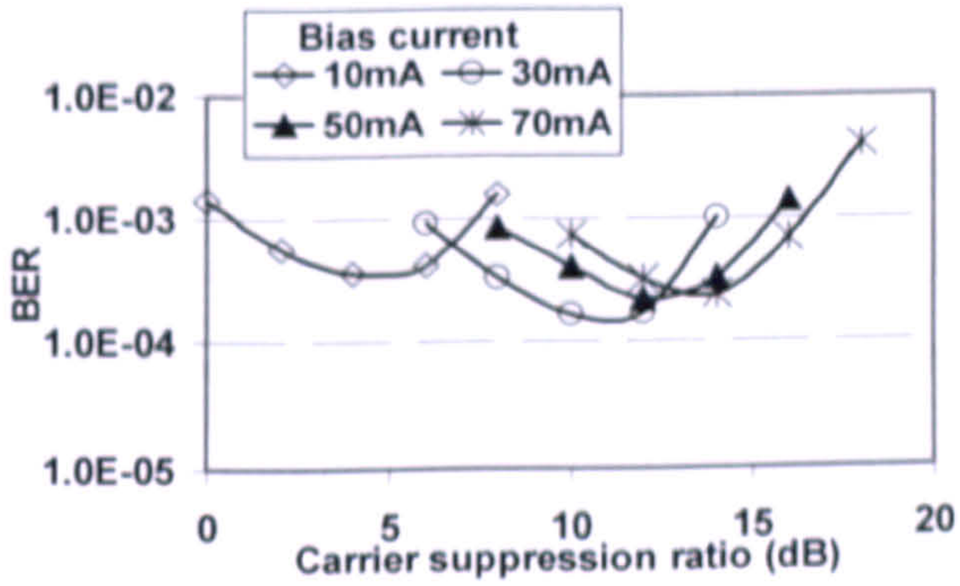

(e)

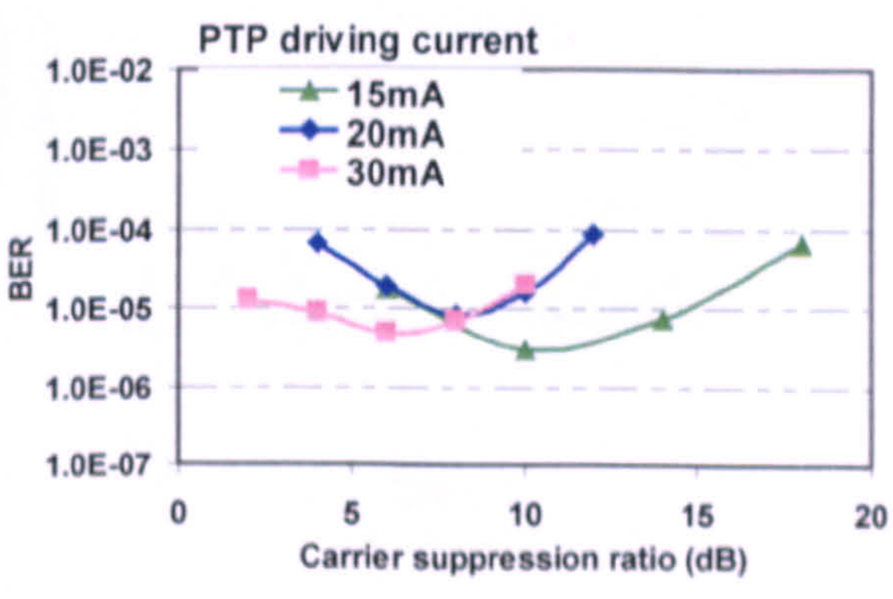

(c)

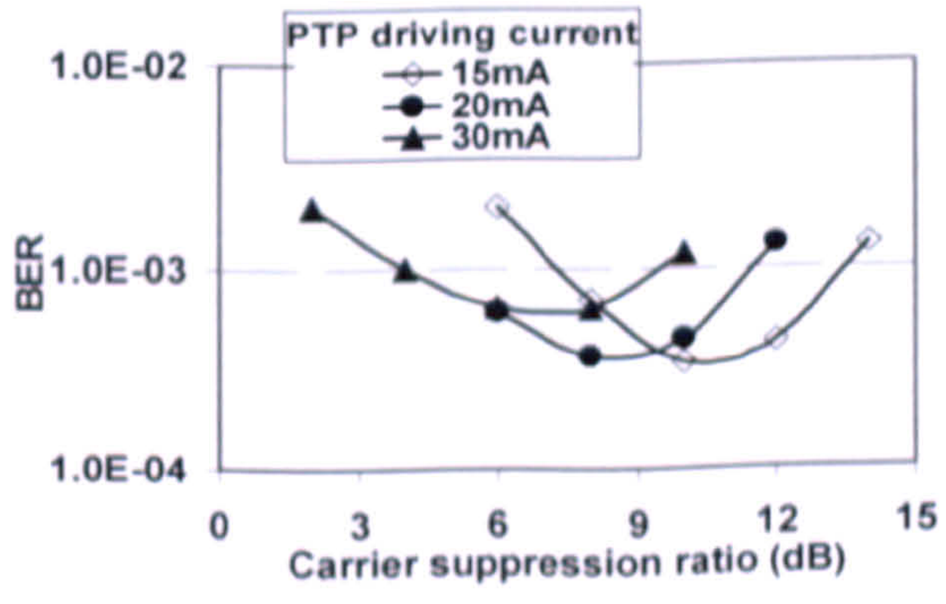

(f)

Fig. 5.2 BER_T versus carrier suppression ratio: (a) and (d) The PTP driving current is 15mA and the bias current is 30mA; (b) and (e) The optical input power is 2dBm and the PTP driving current is 15mA, (c) and (f) The optical input power is 2dBm and the bias current is 30mA. (a)-(c) are for SMF of 80km, while (d)-(f) are for 960km.

For a fixed optical input power of 2dBm and a fixed PTP driving current of 15mA, the dependence of carrier suppression ratio on DML bias current is shown in Fig. 5.2(b) and Fig. 5.2(e), from which, it can be seen that, a high DFB laser bias current requires a high optimum carrier suppression ratio. This is because a high DFB laser bias current gives rise to a low signal ER, thus requiring a high carrier suppression ratio for achieving the desired signal effective OSNR. As expected from the discussions in Fig. 5.2(b) and Fig. 5.2(e), a low PTP driving current leads to a small signal ER, thus a high carrier suppression is required to maintain the effective signal OSNR required, as demonstrated in Fig. 5.2(c) and Fig. 5.2(f).

By comparing Fig. 5.2(a)-(c) with Fig. 5.2(d)-(f), it is also interesting to note that, the identified optimum carrier suppression ratio for a fixed DML operating conditions and SMF input power is independent of transmission distance. However, for the cases of 960km SMF links with inline EDFA, the system exhibits worse BER performances in comparison to those corresponding to of 80km SMF links without inline EDFA. This is a direct result of the increased noise and fibre nonlinearity effects in the long transmission distances.

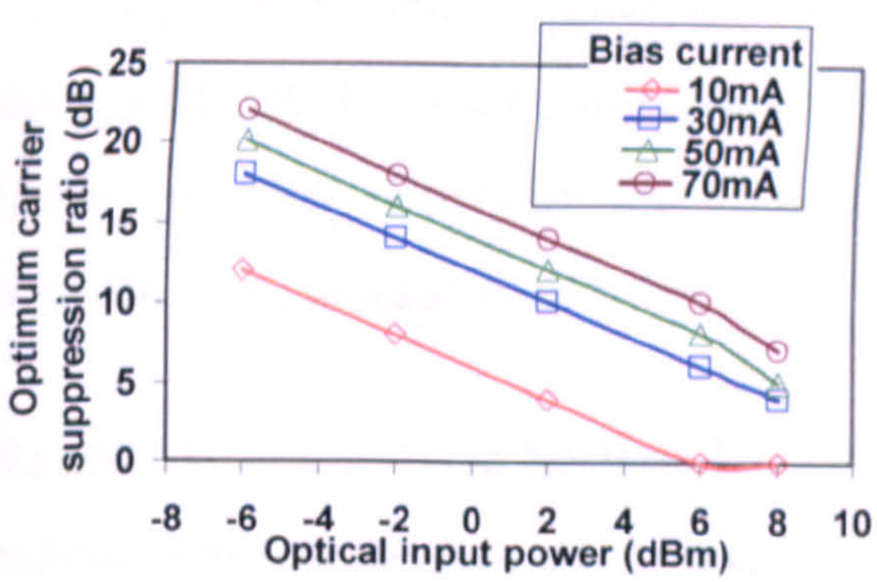

(a)

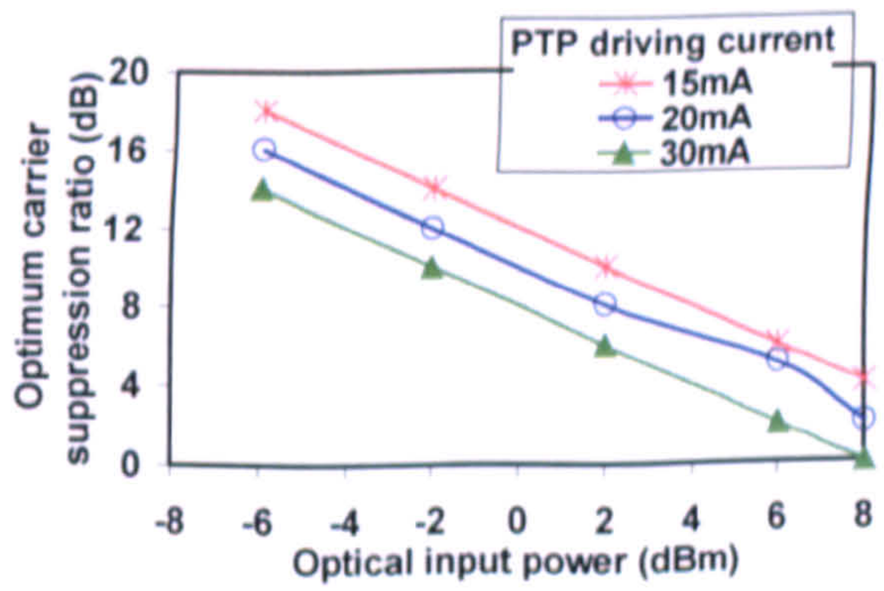

(b)

Fig. 5.3 Optimum carrier suppression ratio versus optical input power for different DFB operating conditions: (a) The PTP driving current is 15mA, (b) The bias current is 30mA.

To ease the practical system design, the optimum carrier suppression ratio as a function of optical input power is plotted explicitly in Fig. 5.3(a) and Fig. 5.3(b) for various DFB laser operating conditions that may be encountered in practice. It can be seen from Fig. 5.3 that the optimum carrier suppression ratio increases almost linearly with decreasing the optical input power, regardless of the DFB laser operating conditions. Such an evolution trend can

be explained by using the physical mechanism similar to that used in explaining Fig. 5.2(a). In addition, the linear lineshapes observed in Fig. 5.3 can also be understood by considering the fact that, for a specific transmission system, the required effective OSNR is fixed for achieving a BER_T of 1×10^{-3}. As the signal extinction ratio remains constant for a given DFB operating point, therefore, a relatively small carrier suppression ratio is sufficient to produce the required effective OSNR when the optical input power is large.

5.4 The Transmission Performance of Carrier Suppressed SSB IMDD AMOOFDM Signals in Optimum DML-Based SMF Systems without In-line Optical Amplification

To evaluate the validity of the optimum DML parameters identified in Section 5.3, and to demonstrate the effectiveness of the carrier suppressed SSB technique for use in DML-based NG-PONs without optical amplification and dispersion compensation, the AMOOFDM signal line rate as a function of transmission distance is plotted in Fig. 5.4. To make a fair performance comparison with the DSB case [5.4], adaptive modulation is used here, and the simulation parameters adopted are the same as those used in [5.4], except that 1) an optimum carrier suppression ratio of 6dB is adopted, and 2) the ADC/DAC sampling speeds of 25GS/s is employed to give a maximum signal line rate of 40Gb/s when 256-QAM are taken across all the 32 data-carrying subcarriers. An optical launch power of 6.3dBm is considered here.

As already discussed in Section 2.4.5, for a specific transmission system, the highest signal modulation format that can be used on each subcarrier can be identified according to the frequency response associated with that transmission system, through negotiations between the transmitter and the receiver. As a direct result of such a signal modulation format manipulation, AMOOFDM improves significantly the obtainable signal transmission capacity in comparison with OOFDM using identical signal modulation [5.4]. In addition, as predicted by Eq. (5.2), for a given optical signal spectral property, AMOOFDM has a dispersion tolerance similar to that associated with OOFDM without adaptive modulation.

It can be seen from Fig. 5.4 that, in DML-based IMDD systems without involving optical amplifiers, 30Gb/s carrier suppressed SSB signal transmission over 80km SMF can be achieved, which doubles the performance corresponding to the DSB AMOOFDM signals

without carrier suppression [5.4]. By comparing the transmission performances of the AMOOFDM signals without carrier suppression between the cases of including and excluding the SSB technique, it can be found from Fig. 5.4 that, the SSB technique is a major contributor to the above-mentioned transmission performance improvement for transmission distances of <60km. This is because, over that transmission distance region, the fibre chromatic dispersion effect is a dominant factor determining the maximum achievable transmission performance [5.4]. The use of the SSB technique is capable of offering a better preservation of the fibre dispersion-induced phase shift in the electrical domain, thus enables AMOOFDM to take a full advantage of its strong dispersion compensation capability.

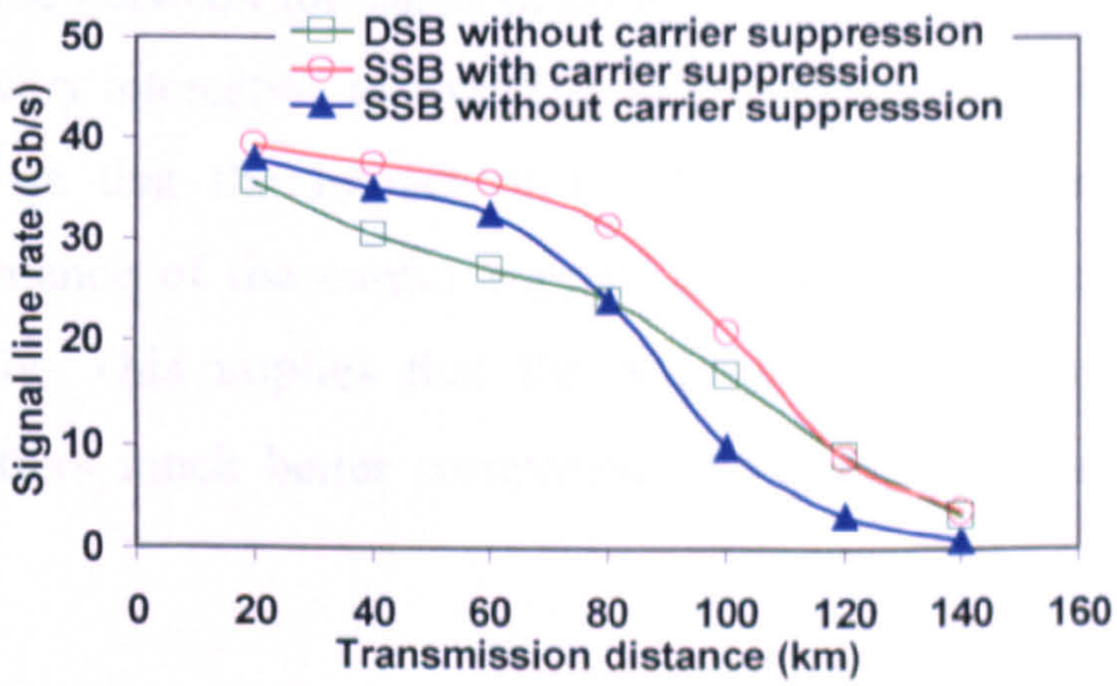

Fig. 5.4 Signal line rate versus transmission distance for different optical OFDM signals in DML-based IMDD transmission systems without including EDFAs.

However, for transmission distances of >80km, over which the fibre loss is a dominant factor limiting the maximum achievable transmission performance [5.4], employing only the SSB technique degrades considerably the transmission performance, as shown in Fig. 5.4. This originates from the SSB-induced decrease in OSNR sensitivity. The cross point of the two curves corresponding to these two cases without carrier suppression is a direct result of the offset between the SSB-induced dispersion tolerance improvement and OSNR sensitivity decrease. Such an OSNR sensitivity decrease can be reduced when the carrier suppression technique is applied. This can be clearly seen in Fig. 5.4 by comparing the transmission performances of the SSB AMOOFDM signals between the cases of including and excluding the carrier suppression technique. For transmission distances of >120km, the carrier suppression-induced improvement in transmission capacity is offset almost completely by the SSB-induced performance degradation, giving rise to the identical

transmission performance of the carrier suppressed SSB AMOOFDM signals, compared to that achieved by the DSB AMOOFDM signals without carrier suppression, as shown in Fig. 5.4.

Owing to the co-existence of both SSB and carrier suppression, the use of the proposed technique is, therefore, more prominent in enhancing the transmission performance for transmission distances of < 100km, and this technique is less prominent for transmission distances of >100km, as demonstrated in Fig. 5.4.

The impact of the DML-induced nonlinear effect on the transmission performance of the carrier suppressed SSB AMOOFDM signals is examined in Fig. 5.5, in which performance comparisons are made between the cases of considering an ideal intensity modulator and the DFB laser. It is very interesting to note that, in comparison with the results presented in [5.4], Fig. 5.5 shows that the impact of the DML-induced nonlinear effect on the transmission performance of the carrier suppressed SSB IMDD AMOOFDM signals is reduced considerably. This implies that the SSB technique with an optimum carrier suppression ratio offers much better compensation for the DML-induced optical signal distortions.

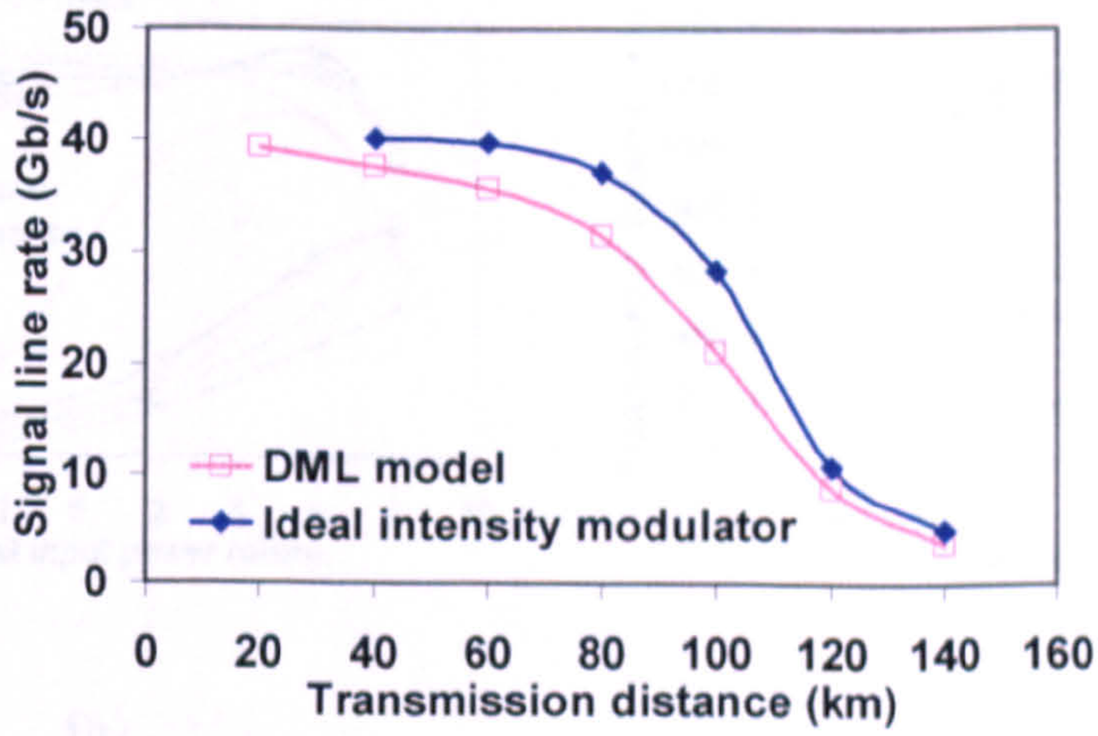

Fig. 5.5 Signal line rate versus transmission distance for carrier-suppressed SSB optical OFDM signals in DML- and ideal intensity modulator- based IMDD transmission systems without including EDFAs.

5.5 Carrier Suppressed SSB IMDD OOFDM Signal Transmission in Optimum DML-Based SMF Systems Incorporating In-line Optical Amplifiers

To further explore the potential of DML-based carrier suppressed SSB IMDD OOFDM technique, in this section, investigations are undertaken of the maximum achievable transmission distance over SMF systems consisting of in-line EDFAs. Such extended reach is promising for NG-PONs in rural scenario. In this subsection, the 16-QAM signal modulation format is used across all the data-carrying subcarriers. The optimum parameters identified in Section 5.3 are considered here. There are two main reasons underpinning the adoption of the above-mentioned identical signal modulation format in simulations performed in this section: a) this treatment allows fair performance comparisons to be made between the simulated results and experimental measurements [5.10]; b) The use of identical signal modulation format enables us to distinguish easily the carrier suppression SSB-induced performance improvement from that caused by adaptive modulation, as our simulations indicate that both two techniques can improve the transmission performance of the systems of interest of this subsection.

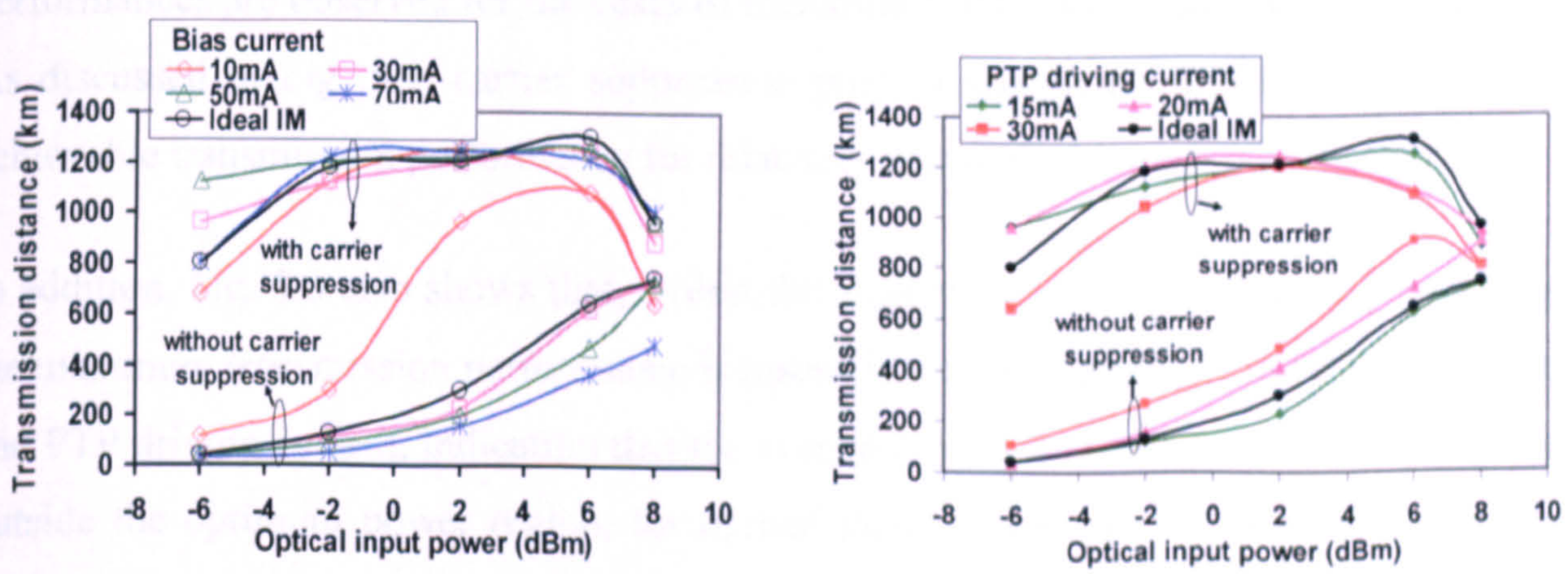

Fig. 5.6 Achievable transmission distance versus optical input power for different DML operating conditions: (a) the PTP driving current is 15mA, (b) the bias current is 30mA. The black curves in (a) and (b) are obtained using ideal intensity modulators (IM).

The transmission distance versus optical input power is plotted in Fig. 5.6(a) and Fig. 5.6(b) for different DFB bias currents and PTP driving currents, respectively. For comparison, in these two figures, the transmission performances are also given for the

cases of excluding carrier suppression and using ideal intensity modulators. The transmission distance considered is the maximum fibre length that gives the transmitted signal a total channel BER_T of 1.0×10^{-3}. In simulating each of the curves illustrated in Fig. 5.6, firstly, the DML is set at the specified operating conditions. Secondly, based on the results presented in Section 5.3, an appropriate adjustment of the optical carrier wave power is made to produce an optimum carrier suppression ratio that corresponds to the DML operating conditions and the chosen optical launch powers. And finally, optical amplification/attenuation is applied to the signal to set the signal power at a required level.

It is very interesting to note that, 10Gb/s over about 1200km signal transmission is achievable over a broad range of optical input powers varying from -2 – 6dBm. Such performance agrees very well with the experiments [5.10], in which 10Gb/s over 1000km SMF is achieved using external modulators. The performance similarity between the optimum DML-based systems and external modulators-based systems, indicates that the influence of the DMLs under the optimized operating conditions is negligible on the transmission performance of the carrier suppressed SSB IMDD OOFDM signals. This statement is also verified by considering Fig. 5.6, where almost the same transmission performances are observed for the cases of including DMLs and ideal intensity modulators. As discussed in Fig. 5.4, carrier suppression plays a significant role in determining the achievable transmission performance for relatively low optical launch powers (Fig. 5.6).

In addition, Fig. 5.6 also shows that, within the aforementioned optical input power range, the maximum transmission performance is insensitive to the variations in DFB bias current and PTP driving current, indicating that the system is very robust. For optical input powers outside the optimum power region, for optical input powers of < -2dBm, the significant reduction in transmission distance shown in Fig. 5.6 is due to the decrease in the effective signal OSNR caused by large EDFA noise, whilst for optical input powers of > 6dBm, the transmission distance reduction is due to the strong fibre nonlinear effect, as no significant performance degradations have been observed for optical input powers of <4dBm when the fibre nonlinear effect is not considered.

5.6 Conclusions

The transmission performance of carrier suppressed SSB IMDD OOFDM signals over DML-based transmission systems has been investigated thoroughly for applications in NG-PONs without and with incorporating in-line optical amplifications, respectively. The impact of DMLs has been explored on the transmission performance of such signals. The dependence of optimum carrier suppression ratio has been identified on DML operating condition and optical input power. It has been shown that, for DML-based in-line optical amplification-free NG-PONs, 30Gb/s carrier suppressed SSB IMDD AMOOFDM signals over 80km SMF is achievable, which doubles the performance obtained by using DSB AMOOFDM signals without carrier suppression, and that, 10Gb/s carrier suppressed SSB IMDD OOFDM signals over about 1200km SMF is also feasible in DML-based NG-PONs incorporating in-line EDFAs. In addition, the obtained transmission performance is very insusceptible to variations in both DML operating condition and optical input power. Furthermore, the SSB technique with optimum carrier suppression ratio reduces considerably the DML-induced nonlinear effect.

References

[5.1] M. Sieben, J. Conradi and D. E. Dodds, "Optical single sideband transmission at 10 Gb/s using only electrical dispersion compensation," J. Lightw. Technol., vol. 17, no. 10, pp. 1742–1749, Oct. 1999.

[5.2] R. Hui, B. Zhu, R. Huang, C. T. Allen, K. R. Demarest and D. Richards, "Subcarrier multiplexing for high-speed optical transmission," J. Lightw. Technol., vol. 20, no. 3, pp. 417–427, Mar. 2002.

[5.3] M. Schuster, S. Randel, C.A. Bunge, S. C. J.Lee, F. Breyer, B. Spinnler and K. Petermann, "Spectrally efficient compatible single-sideband modulation for OFDM transmission with direct detection," IEEE Photon. Technol. Lett. Vol.20, no.9, pp.670-672, May 2008.

[5.4] J. M. Tang and K. A. Shore, "30 Gb/s signal transmission over 40-km directly modulated DFB-laser-based single-mode-fibre links without optical amplification and dispersion compensation," J. Lightw. Technol., vol. 24, no.6, pp. 2318-2327 Jun. 2006.

[5.5] J. M. Tang, P. M. Lane and K. A. Shore, "High speed transmission of adaptively modulated optical OFDM signals over multimode fibers using directly modulated DFBs," J. Lightw. Technol., vol. 24, no.1, pp. 429-441, Jan. 2006.

[5.6] E. Giacoumidis, J.L. Wei, X.Q. Jin and J.M. Tang, "Improved transmission performance of adaptively modulated optical OFDM signals over directly modulated DFB-laser based IMDD links using adaptive cyclic prefix," Opt. Express., Vol. 16, no.13, pp.9480-9494, June 2008.

[5.7] X. Q. Jin, J. M. Tang, P. S. Spencer and K. A. Shore, "Optimization of adaptively modulated optical OFDM modems for multimode fiber-based local area networks", J. of Opt. Netw., vol. 7, no.2, pp. 198-214, Feb. 2008.

[5.8] J. J. Pan, Y. Shi and K. Zhang, "Optical amplifier noise figure reduction using a variable polarisation beam splitter" Electron. Lett., vol. 31, no. 12, pp. 979-980, Jun. 1995.

[5.9] J. M. Tang and K. A. Shore, "Maximizing the transmission performance of adaptively modulated optical OFDM signals in multimode-fiber links by optimizing analog-to-digital converters," J. Lightw. Technol., vol. 25, no. 3, pp. 787-798, Mar. 2007.

[5.10] D. Qian, J. Yu, J. Hu, L. Zong, L. Xu and T. Wang, "10Gb/s WDM-SSB-OFDM transmission over 1000km SSMF using conventional DFB lasers and direct-detection," Electron. Lett., vol. 44, no. 3, pp. 223-225, Jan. 2008.

6 SOA-Enabled Intensity Modulation of AMOOFDM Signals in SMF-based IMDD Systems for WDM-PONs

Contents

6.1 Introduction 122

6.2 Transmission System Models 124

6.2.1 Transmission System and AMOOFDM Models 124

6.2.2 SOA-based Intensity Modulator Model 124

6.2.3 Models for SMF and PIN Detector 127

6.2.4 Simulation Parameters 127

6.3 Simulated Transmission Performance 128

6.3.1 SOA Gain Saturation Characteristics 128

6.3.2 Impact of SOA Bias Current and Optical Input Power 130

6.3.3 Impact of PTPs of Driving Currents 133

6.3.4 Optimized AMOOFDM Transmission Performance and its Physical Limitations 134

6.4 Performance Robustness 138

6.4.1 Robustness to SOA Saturation Energy 138

6.4.2 Robustness to Cavity Length 139

6.5 Conclusions 140

6.1 Introduction

In Chapters 5-6, investigations have been carried out of DML-converted IMDD OOFDM signal transmission performance for NG-PONs. However, for WDM-PONs, the use of a wavelength specified DML in each individual ONU is not preferred due to high system cost and lack of efficient wavelength control. As discussed in Chapter 3, SOAs/RSOAs are promising solutions to facilitate cost-effective colourless transmitters due to their compactness, strong capability of monolithic integration with electrical components and wide wavelength coverage. In this chapter, investigations are, therefore, undertaken of the feasibility of using SOAs as intensity modulators in IMDD AMOOFDM PONs.

The idea of using SOAs to perform intensity modulation of AMOOFDM signals is illustrated in Fig. 6.1, whereby a real-valued OFDM signal in the electrical domain drives directly an SOA with a high CW optical wave being injected simultaneously. The power of the injected optical wave mimics the SOA gain variation induced by the electrical OFDM signal. Thus intensity modulation can be realized using the SOA-based intensity modulator. For SOAs operating at strongly saturated optical gain regions, their effective carrier lifetimes can be reduced to values of an order of less than 50ps [6.1]. As the SOA modulation bandwidths are proportional to the inverse of their effective carrier lifetimes [Eq. (3.1)], therefore, SOAs can have modulation bandwidths of as large as 20GHz. Such modulation bandwidths are much wider than both typical AMOOFDM spectral widths and those corresponding to DMLs, implying that the significantly reduced frequency chirp effect is possible, as shown in Fig. 6.4, if the DMLs are replaced by the SOA-based intensity modulators.

Apart from the reduction in the frequency chirp effect, SOA-based intensity modulators also offer a number of other unique features listed as followings:

- Extremely wide spectral coverage from 1200nm-1650nm. This enables the delivery of true colourless AMOOFDM transmitters in a cost-effective manner.
- Considerable transmission performance improvement compared to DMLs.

- Excellent system flexibility and great performance robustness to variations in SOA component parameters.
- Controllable bandwidths. An SOA bandwidth can be engineered easily by reducing its effective carrier lifetime through altering the power of an injected CW optical wave, adjusting the SOA bias current [6.1], and selecting appropriately device design parameters such as cavity length [6.2].

It should be pointed out that, a reduction in SOA's effective carrier lifetime is always accompanied with a decay of ER of the modulated optical signal. This offsets the large SOA bandwidth-induced transmission performance improvement.

The thrust of this chapter is to explore thoroughly, for the first time, the impact of the SOA-based intensity modulators on the transmission performance of AMOOFDM signals over SMF IMDD systems without involving optical amplification and dispersion compensation. A theoretical model for describing the characteristics of the SOA-based intensity modulators is developed, based on which optimum SOA operating conditions are identified. It is shown that the optimized SOA-based intensity modulators can support a 30Gb/s AMOOFDM signal transmission over a 80km SMF, which doubles the transmission performance obtained using DMLs. In addition, key physical factors limiting the maximum achievable transmission performance of the AMOOFDM technique are also identified. Finally, rigorous examinations are made of the robustness of the optimum operating conditions and the transmission performance to variations in SOA parameters.

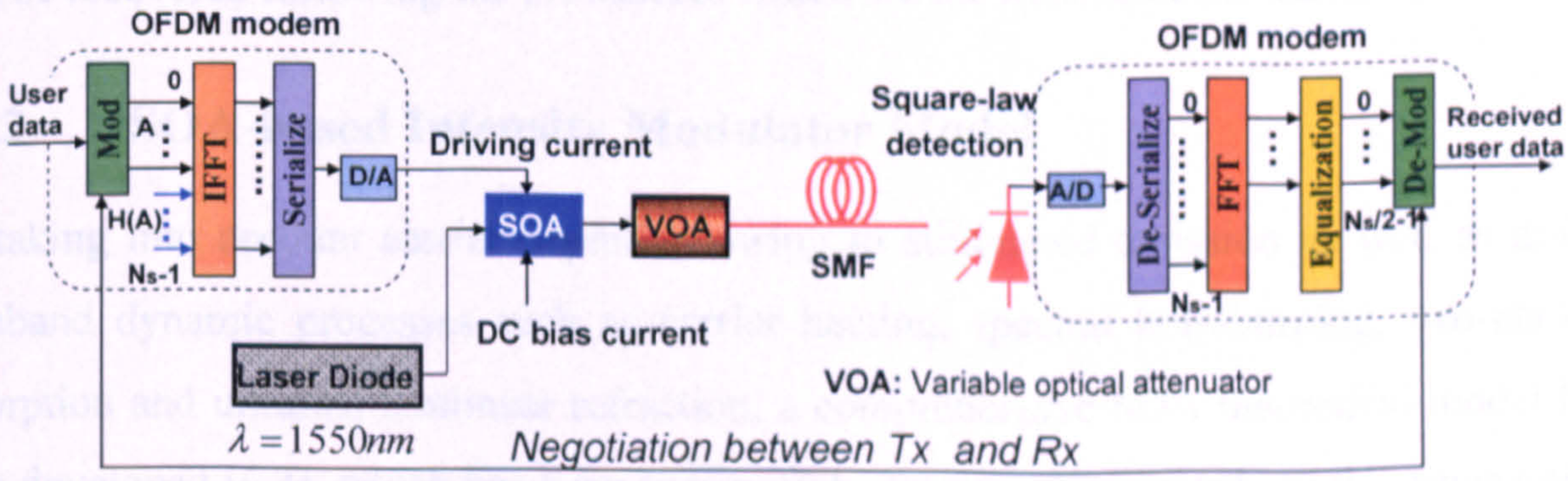

Fig. 6.1 Transmission system diagram together with block diagrams of the transmitter and the receiver

6.2 Transmission System Models

6.2.1 Transmission System and AMOOFDM Models

In Fig. 6.1, the transmission system considered in this chapter is illustrated, which includes a transmitter involving an SOA performing intensity modulation, a single-channel optical amplification- and dispersion compensation-free SMF IMDD transmission link, a square-law photon detector and a receiver. The DSP procedure of the electrical OFDM signal in the OFDM modem is identical to those presented in Section 2.3. It should be mentioned that equal power loading is applied across all the subcarriers and the IFFT inputs are arranged to satisfy the Hermitian symmetry, as expressed in Eq. (2.41), so that the IFFT outputs are real-valued. The real-valued electrical OFDM signal generated by the OFDM modem in the transmitter is combined with a DC bias current. Finally, the up-shifted electrical OFDM signal drives directly the SOA to modulate the injected CW optical wave by varying the optical gain of the SOA.

To enable the SOA to operate at desired conditions, the input power of the injected CW optical wave, the DC bias current and the driving current are adjusted. Such adjustments may alter the output power of the modulated optical signal. An optical attenuator is thus inserted between the SOA and the input facet of the SMF link to fix the coupled optical power at a required level.

In the receiver, the optical signal is detected by a square-law photon detector. The data can then be recovered following the procedures which are the inverse of the transmitter.

6.2.2 SOA-based Intensity Modulator Model

By taking into account carrier depletion owing to stimulated emission as well as major intraband dynamic processes such as carrier heating, spectral hole-burning, two-photon absorption and ultrafast nonlinear refraction, a comprehensive SOA theoretical model has been developed [6.3], which has been successfully employed in describing the propagation of strong picosecond optical pulses in SOAs [6.3], ultrafast switching characteristics of terahertz optical asymmetric demultiplexers [6.4], phase conjugation of picosecond optical pulses [6.5] and active picosecond optical pulse reshaping in SOAs [6.6].

In the SOA-based intensity modulator illustrated in Fig. 6.1, the adopted DACs/ADCs have sampling rates of typically less than 20GS/s, which correspond to sampling durations of greater than 50ps, which is at least 50 times higher than the response times associated with all the above-mentioned intraband dynamic processes [6.3]. In addition, as discussed in Section 6.3, the optical gain saturation properties of the SOA are mainly determined by the strong DC component of an optical signal propagating in the SOA. For example, at the output facet of the SOA, the modulated optical signal with a noise-like waveform has a relatively small signal ER of about 1dB, as shown in Section 6.3. The above facts indicate that it is sufficiently accurate to neglect the influence of the intraband dynamic processes on the optical gain saturation characteristics of the SOA.

The exclusion of the intraband carrier processes simplifies significantly the SOA theoretical model developed in [6.3]. When a transformation of the wave propagation equation [6.3] is made to the retarded reference frame, $T = t - z/v_g$ with t, z and v_g being the time, the transmission distance and the group velocity, respectively, and the optical field is defined as

$$A(z,T) = \sqrt{P(z,T)}\exp[j\phi(z,T)] \tag{6.1}$$

with $P(z,T)$ and $\phi(z,T)$ being the optical power and phase, respectively, a set of equations which govern the propagation of the optical signal travelling through the SOAs are obtained:

$$\frac{dg(z,T)}{dT} = \frac{g_0(T) - g(z,T)}{\tau_c} - \frac{g(z,T)}{E_{sat}}P(z,T) \tag{6.2}$$

$$\frac{\partial P(z,T)}{\partial z} = g(z,T)P(z,T) \tag{6.3}$$

$$\frac{\partial \phi(z,T)}{\partial z} = -\frac{1}{2}\alpha g(z,T) \tag{6.4}$$

where $g(z,T)$ is the optical gain defined as $g(z,T) = \Gamma a[N(T) - N_0]$ with $N(T)$ and N_0 being the carrier density and the carrier density at transparency, Γ is the confinement factor and a is the differential gain. $g_0(T)$ is the small signal gain of the SOA, which can

be expressed as $g_0(T) = \Gamma a N_0[I(T)/I_0 - 1]$, here $I(T)$ is the total injected current including the DC bias current and the driving current, and I_0 is the current required at transparency. τ_c is the carrier lifetime. $E_{sat} = \hbar\omega_0 wd/\Gamma a$ is the SOA saturation energy with ω_0, w and d being the frequency of the optical signal, the width and depth of the SOA active region, respectively. α is the linewidth enhancement factor. In deriving Eq. (6.3), the SOA linear internal loss effect is incorporated into a slight increase in carrier density required at transparency.

By integrating Eqs. (6.2)-(6.4) over the entire SOA cavity length, L, a set of equations can be obtained:

$$\frac{dh(T)}{dT} = \frac{g_0(T)L - h(T)}{\tau_c} - \frac{P_{in}(T)}{E_{sat}}\{\exp[h(T)] - 1\} \tag{6.5}$$

$$P_{out}(T) = P_{in}(T)\exp[h(T)] \tag{6.6}$$

$$\phi_{out}(T) = \phi_{in}(T) - \frac{1}{2}\alpha h(T) \tag{6.7}$$

with
$$h(T) = \int_0^L g(z,T)dz \tag{6.8}$$

where $P_{out}(T)$ and $\phi_{out}(T)$ are the power and phase of the modulated optical signal, $P_{in}(T)$ and $\phi_{in}(T)$ are the power and phase of the optical input wave. Eqs. (6.5)-(6.7) can be easily solved numerically when $I(T)$, $P_{in}(T)$ and $\phi_{in}(T)$ are made known.

Apart from intensity modulation, the SOA also imposes ASE noise onto the modulated optical signal. The total ASE power, P_{ASE}, can be calculated by [6.7]

$$P_{ASE} = (N_f G - 1)B_0\hbar\omega_0 \tag{6.9}$$

where N_f is the SOA noise figure, $G = \exp[h(T)]$, B_0 is the optical bandwidth and $\hbar\omega_0$ is the photon energy. In deriving Eq. (6.9), it is assumed that the ASE noise does not affect the SOA gain dynamics.

Eqs. (6.5)-(6.7) and Eq. (6.9) are the final set of equations, which are used in numerical simulations in Section 6.3. After adding the ASE noises into $P_{out}(T)$ and $\phi_{out}(T)$, and subsequently introducing them into Eq. (6.1), the intensity modulated optical signal can be obtained. In the receiver, the transmitted optical signal can be detected using a square-law photon detector when a CW optical input wave is selected. It should be pointed out, in particular, that the validity of the SOA intensity modulator model developed here is confirmed by the excellent agreement between the theoretical results and experimental measurements [6.8], as discussed in Section 6.3.4.

6.2.3 Models for SMF and PIN Detector

The SMF model successfully used in Chapters 4-5 is adopted here. In the receiver, a square-law photon detector is utilized to detect the optical signals emerging from the transmission system. Shot noise and thermal noise are considered. These effects are simulated following the procedures similar to those presented in [6.9].

6.2.4 Simulation Parameters

In simulating the AMOOFDM modems, the total number of subcarriers, N_s, is taken to be 64. In the positive frequency bins, 31 subcarriers are used to carry original data and the remaining one subcarrier close to the optical carrier frequency is dropped. The sampling rates of the DAC/ADC are fixed at 12.5GS/s in both the transmitter and the receiver. The above-mentioned parameters give a signal bandwidth in the positive frequency bins of 12.5/2 = 6.25GHz. The bandwidth for each subcarrier is 6.25/32 ≈ 195.3MHz. The cyclic prefix parameter defined in Eq. (2.14) is taken to be 25%, which gives a cyclic prefix length of 1.28ns within each OFDM symbol having a total time duration of 6.4ns. Other parameters associated with the AMOOFDM modems are identical to those presented in Section 5.2.3.

The parameters used in simulating SOA-based intensity modulators are representative for InGaAsP semiconductor materials operating at a wavelength of ~1550nm, as listed in Table 6.1, where both the SOA parameters and their corresponding references are shown. The SOA parameters without any references being listed are chosen within their typical variation ranges [6.3,6.4,6.9,6.10]. By attenuating/amplifying the modulated optical output signals from the SOAs, the optical power coupled into the SMF system is fixed at 6.3dBm.

The simulation parameters of PIN detectors are also listed in Table. 6.1, together with their corresponding references. The parameters associated with SMF are identical to those presented in Section 5. 2.3.

Table 6.1 SOA and PIN Parameters

SOA		
Symbol	**Value**	**Reference**
L	500μm	
w	1.5μm	[8]
d	0.27μm	
τ_c	0.3ns	[11]
Γ	0.35	
a	$3\times10^{-20}m^2$	[13]
α	5	[9]
N_0	$1.05\times10^{24}m^{-3}$	[13]
v_g	8.43×10^{7}m/s	[8]
ω_0	1550nm	
N_f	8dB	
PIN		
Parameter	**Value**	**Reference**
Quantum efficiency	0.8	[3]
Noise current density	8pA/√Hz	[14]

It should be pointed out that, in numerical simulations in this chapter, all the parameter values mentioned above and listed in Table. 6.1 are treated as default ones, unless addressed explicitly in the corresponding text where necessary.

6.3 Simulated Transmission Performance

6.3.1 SOA Gain Saturation Characteristics

To gain an in-depth understanding of the transmission performance of AMOOFDM signals over SMF IMDD systems using SOA-based intensity modulators, it is necessary to discuss first the optical gain saturation characteristics of the SOAs. The dependence of SOA optical gain upon CW optical input power and bias current is presented in Fig. 6.2, where a 10GHz sinusoidal electrical driving current having a fixed PTP value of 80mA is applied to the SOA to ensure that the SOA operating conditions considered here are similar to those adopted in other figures of this chapter.

As expected, Fig. 6.2(a) shows that the optical gain of the SOA depends strongly upon both CW optical input power and bias current: an increase (a decrease) in CW optical input power (in bias current) brings about a small SOA optical gain. In addition, the SOA optical input saturation power increases significantly with decreasing bias current.

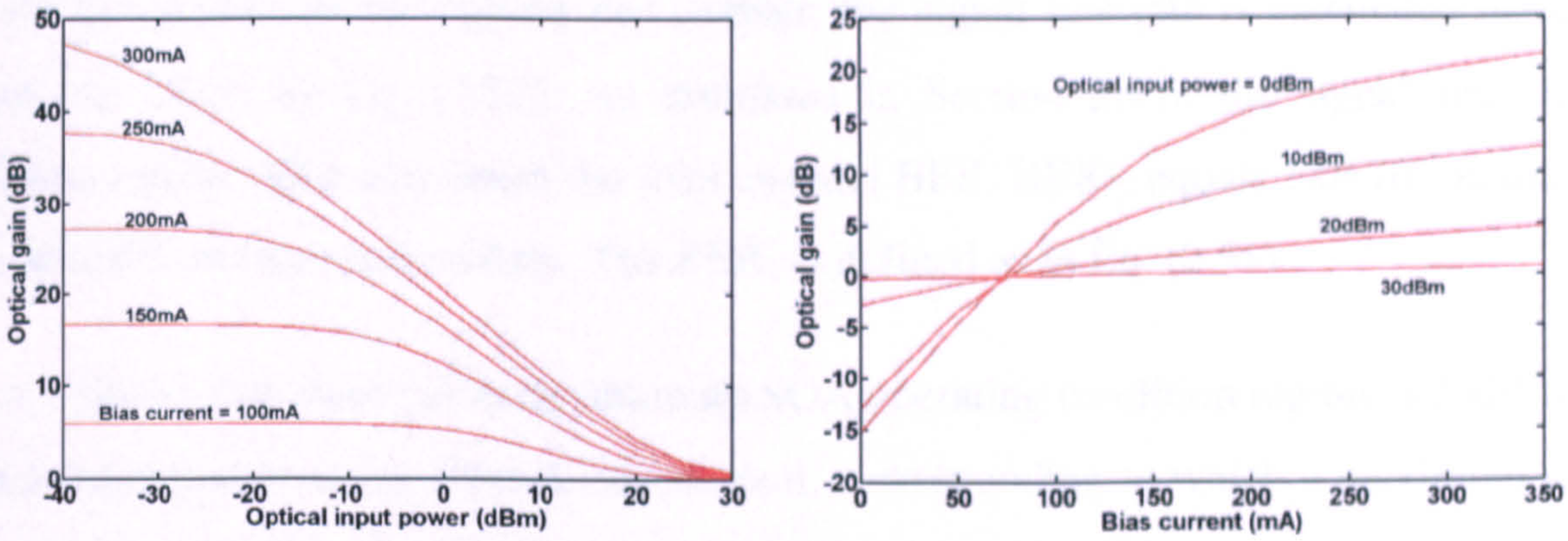

(a) (b)

Fig. 6.2 SOA gain saturation characteristics for different operating conditions. (a) Optical gain versus optical input power and (b) Optical gain versus bias current.

Given the central role of the electrical current-induced SOA optical gain variation in determining the quality of the modulated AMOOFDM signals, Fig. 6.2(b) is plotted to show the SOA optical gain as a function of bias current for different CW optical input powers. It can be seen from Fig. 6.2(b) that, to obtain a desired linear current-gain lineshape, the bias currents and the CW optical input powers need to be set at approximately 100mA and greater than 10dBm, respectively. Under such operating conditions, it can be easily found from Fig. 6.2 (a) that, the SOAs are strongly saturated, resulting in significantly reduced effective carrier lifetimes and thus wide SOA bandwidths. On the other hand, as shown in Fig. 6.2(b), a large CW optical input power broadens considerably the bias current variation range corresponding to the linear current-gain region, and simultaneously declines the slope of the linear current-gain curve. This implies that the above-mentioned SOA operating conditions may clip the modulated AMOOFDM signals and also affect their ERs. Therefore, detailed explorations of the impact of SOA operating conditions on the transmission performance of the AMOOFDM signals are crucial for optimizing the transmission systems consisting of SOA-based intensity modulators.

6.3.2 Impact of SOA Bias Current and Optical Input Power

For a 60km SMF IMDD transmission system, a contour plot of maximum achievable signal line rate as a function of CW optical input power and bias current is shown in Fig. 6.3, where a driving current with a constant PTP value of 80mA is considered. In numerical simulations throughout this chapter, the signal line rate is calculated using the expression given by Eq. (2.52). As discussed in Section 2.4.5, the signal line rate is considered to be valid only when the total channel BER, BER_T, equals 1.0×10^{-3} is satisfied for a specific transmission system. The BER_T is defined as in Eq. (2.51).

Fig. 6.3 shows that there exists an optimum SOA operating condition region: a 20dBm CW optical input power and a 100mA bias current, corresponding to which a maximum signal line rate is observed. Considering Fig. 6.2, it is clear that under the optimum operating conditions, the SOA is highly saturated. In addition, it is also interesting to note that, when the transmission distance is increased from 60km to 100km, the above-mentioned optimum SOA operating conditions still retain, except that the corresponding signal transmission capacities are reduced.

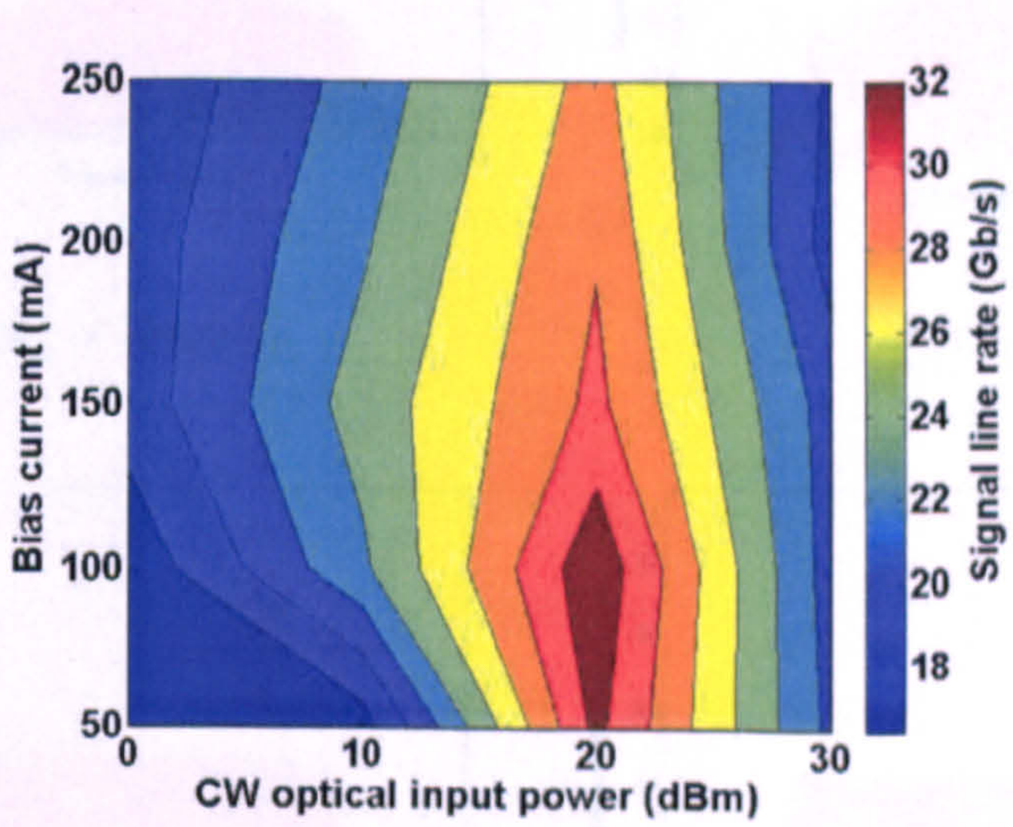

Fig. 6.3 Contour plot of signal line rate as a function of CW optical input power and bias current for a 60km SMF IMDD transmission system.

The occurrence of the optimum CW optical input power shown in Fig. 6.3 can be explained as followings: For CW optical input powers of less than the optimum value of approximately 20dBm, the improvement in signal transmission capacity for high CW optical input powers is mainly due to the reduction in SOA effective carrier lifetime. The

optical power dependent SOA effective carrier lifetime, τ_e , is expressed in Eq. (3.1). As an example, when the CW optical input power is taken to be 20dBm, the SOA effective carrier lifetime is approximately 40ps, which is shorter than the ADC/DAC sampling durations. This indicates that the SOA operating at a highly saturated optical gain region has a short effective carrier lifetime, thus is capable of offering a sufficiently wide bandwidth for use in modulating the AMOOFDM signal. This statement is confirmed by Fig. 6.4, which shows that, at the output facet of the SOA, the spectrum of the modulated AMOOFDM signal is significantly distorted for CW optical input powers of less than 15dBm, whilst rectangular-shaped spectra occur for CW optical input powers of greater than 20dBm. Therefore, it is clear that the broadening of the SOA bandwidth due to the injection of high CW optical input powers gives rise to reduced signal spectral distortions, thus leading to the improved transmission performance, as observed in Fig. 6.3.

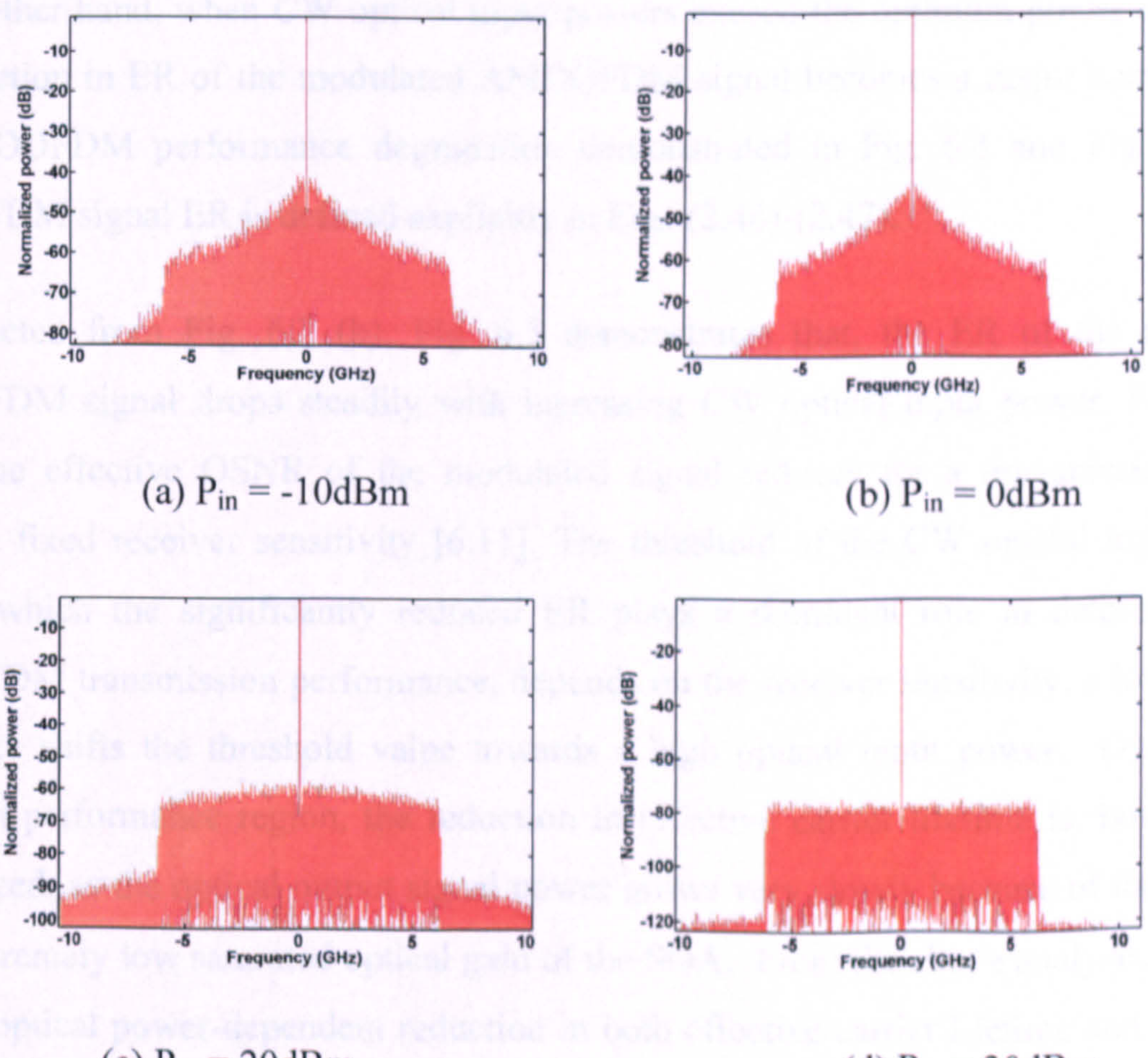

(a) P_{in} = -10dBm

(b) P_{in} = 0dBm

(c) P_{in} = 20dBm

(d) P_{in} = 30dBm

Fig. 6.4 Spectrum of modulated AMOOFDM signal at the output facet of the SOA subject to different CW optical input powers. The adopted bias current is 100mA.

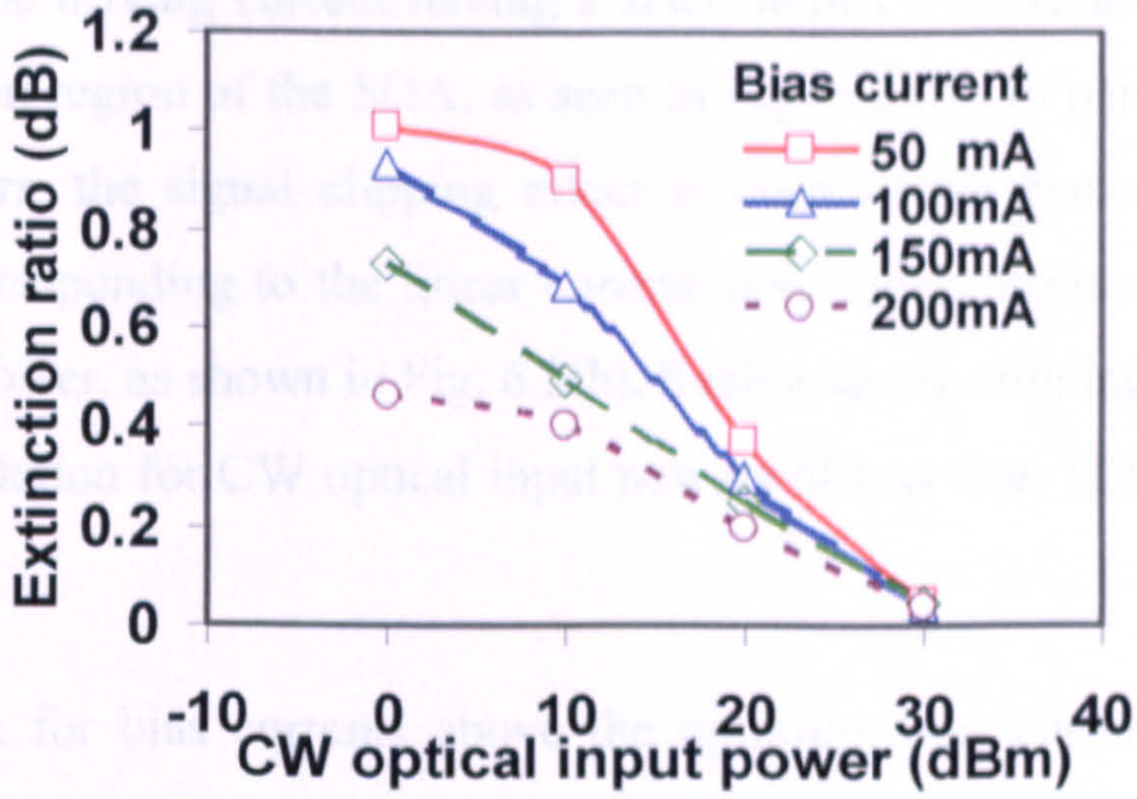

Fig. 6.5 Extinction ratio of modulated AMOOFDM signal as a function of optical input power for different bias currents. IM: intensity modulation.

On the other hand, when CW optical input powers exceed the optimum power of 20dBm, the reduction in ER of the modulated AMOOFDM signal becomes a major contributor to the AMOOFDM performance degradation demonstrated in Fig. 6.3 and Fig. 6.5. The AMOOFDM signal ER is defined explicitly in Eqs. (2.46)-(2.47).

As expected from Fig. 6.2 (b), Fig. 6.5 demonstrates that, the ER of the modulated AMOOFDM signal drops steadily with increasing CW optical input power. As a direct result, the effective OSNR of the modulated signal reduces for a transmission system having a fixed receiver sensitivity [6.11]. The threshold of the CW optical input power, beyond which the significantly reduced ER plays a dominant role in determining the AMOOFDM transmission performance, depends on the receiver sensitivity: a low receiver sensitivity shifts the threshold value towards a high optical input power. Over the ER dominant-performance region, the reduction in effective carrier lifetime is, however, not pronounced, as the optical output signal power grows very slowly because of the presence of an extremely low saturated optical gain of the SOA. From the above analysis, it is clear that the optical power-dependent reduction in both effective carrier lifetime and signal ER is the major physical process underpinning the occurrence of the optimum CW optical input power observed in Fig. 6.3.

In Fig. 6.3, there also exists an optimum bias current of approximately 100mA. For bias currents below the optimum value, the decrease in signal line rate is because the lower part of the electrical driving current applied to the SOA is clipped upon intensity modulation, as

the lower part of the driving current having a fixed 80mA PTP value penetrates into the negative optical gain region of the SOA, as seen in Fig. 6.2 (b). In particular, for low CW optical input powers, the signal clipping effect is even severe because the bias current variation range corresponding to the linear current–gain region decreases with decreasing CW optical input power, as shown in Fig. 6.2(b). Such a strong clipping effect causes rapid performance degradation for CW optical input powers of less than 15dBm, as seen in Fig. 6.3.

On the other hand, for bias currents above the optimum bias current, the transmission performance degradation originates mainly from two factors including decreased ER and increased signal clipping. The impact of the first factor is very easy to understand by considering Fig. 6.5; whilst the second factor takes place when the upper part of the electrical driving current experiences an almost flat optical gain of the SOA, as shown in Fig. 6.2(b). It should be pointed out that, a high bias current also gives a low effective carrier lifetime [6.1], thus leading to less spectral distortions of the modulated AMOOFDM signals. The later effect offsets the effects of the above-mentioned two factors, thus causing that the optimum operating region extends towards the high bias current direction, as seen in Fig. 6.3.

6.3.3 Impact of PTPs of Driving Currents

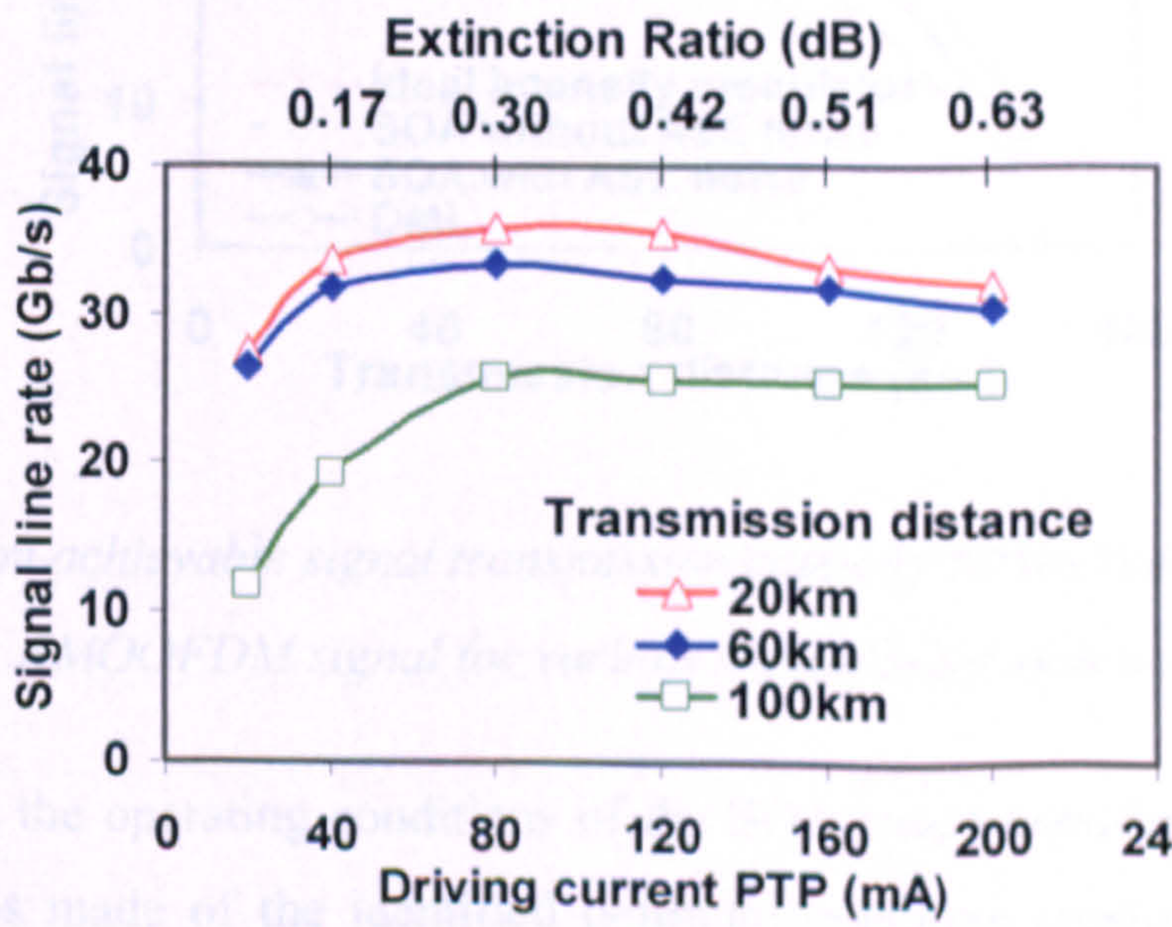

Fig. 6.6 Signal line rate versus driving current PTP and corresponding signal extinction ratio at the output facet of the SOA intensity modulator for different transmission distances. The optical input power and bias current are fixed at 20dBm and 100mA, respectively.

Apart from CW optical input power and DC bias current, from the system design point of view, it is also very important if optimization of the PTP value of a driving current is also undertaken. The impact of a driving current PTP value on the maximum achievable AMOOFDM transmission performance is shown in Fig. 6.6, in obtaining which the optimum CW optical input power of 20dBm and the optimum bias current of 100mA are adopted. Fig. 6.6 exhibits an optimum PTP value of 80mA, which corresponds to a maximum signal line rate. For PTPs lower than the optimum value, the sharp decline in signal line rate is due to the small signal ER, whose impact is discussed in Fig. 6.3. On the other hand, for PTPs higher than the optimum value, the slight reduction in signal line rate is because of the increased signal clipping effect, as discussed in Fig. 6.3. In addition, Fig. 6.6 also shows that the optimum PTP value is independent of transmission distance, which is consistent with the developing trend of the optimum operating region identified in Section 6.3.2.

6.3.4 Optimized AMOOFDM Transmission Performance and its Physical Limitations

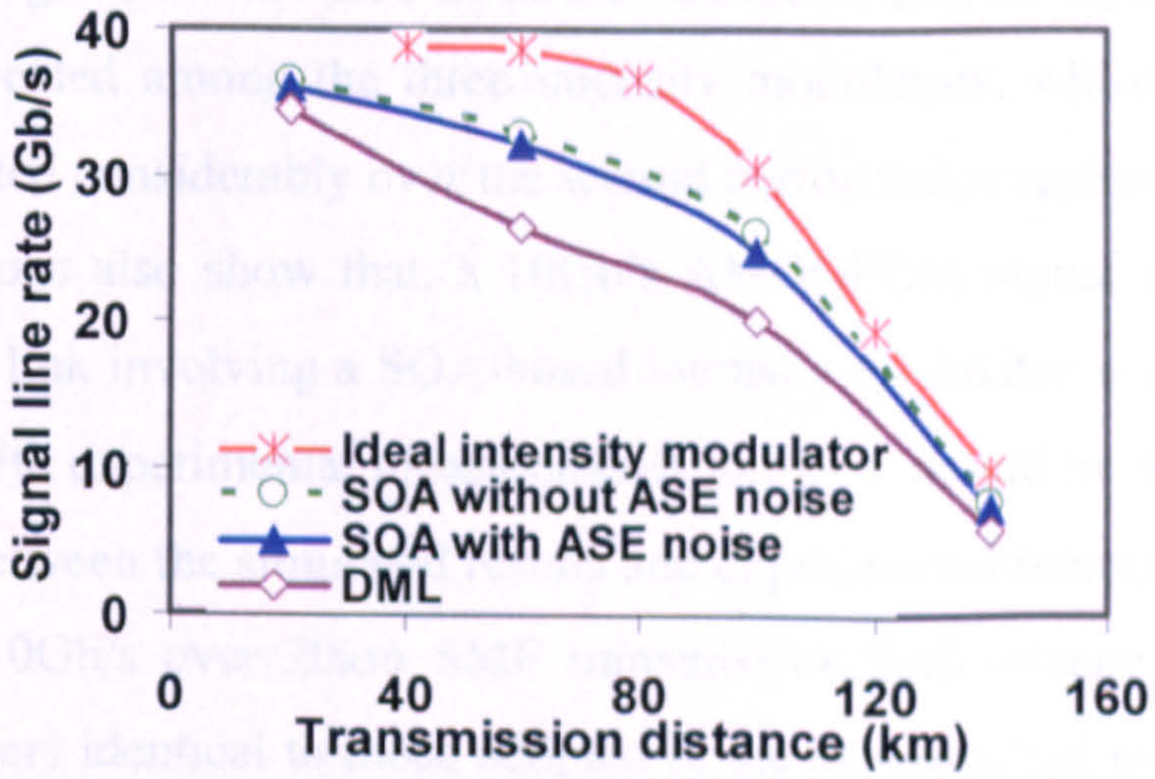

Fig. 6.7 Maximum achievable signal transmission capacity versus reach performance of AMOOFDM signal for various transmission systems.

Having optimized the operating conditions of the SOA-based intensity modulator, in this section, full use is made of the identified optimum operating conditions to explore the maximum achievable AMOOFDM transmission performance and its physical limitations in SMF IMDD systems without involving optical amplification and chromatic dispersion compensation. The numerically simulated results are shown in Fig. 6.7. In computing this

figure, the adopted optimum SOA operating conditions are listed as followings: a CW optical input power of 20dBm, a DC bias current of 100mA and a driving current with a PTP of 80mA. To identify the key physical factors limiting the maximum achievable transmission performance, comparisons of signal capacity versus reach performance are also made in Fig. 6.7 among the cases of employing the SOA-based intensity modulators, DML-based intensity modulators and ideal intensity modulators. In simulating the DML-based intensity modulator, a DML theoretical model developed in [6.12], which had been used in Chapters 4-5 is employed, together with its optimum operating conditions and all other DML parameters presented in [6.11,6.12]. On the other hand, in simulating the ideal intensity modulator, a simple square root operation is applied to the sum of the driving and DC bias currents.

Very similar to those observed in the DML-based SMF IMDD transmission systems [6.11] (also plotted in Fig. 6.7), for the SOA-based systems, Fig. 6.7 shows a chromatic dispersion-dominant performance region and a link loss-dominant performance region for transmission distances of less than 100km and greater than 100km, respectively. Over the first performance region, as expected from discussions in [6.11], significant performance differences are revealed among the three intensity modulators, whilst their performance differences are abated considerably over the second performance region. More importantly, numerical simulations also show that, a 10Gb/s AMOOFDM signal transmission over a 20km SMF IMDD link involving a SOA-based intensity modulator is also feasible, which agrees very well with experimental measurements [6.8]. It should be noted that, to ensure fair comparisons between the simulated results and experimental measurements, only is the above-mentioned 10Gb/s over 20km SMF transmission performance obtained based on simulation parameters identical to those adopted in the experimental measurements. These parameters are: a CW optical input power of -10dBm at the input facet of the SOA, a -1dBm optical power coupled into the transmission link, and a -19dBm optical power at the input facet of the photon detector. All the aforementioned characteristics verify firmly the validity of the system models developed here.

It is very interesting to note from Fig. 6.7 that, in comparison with the DML-based intensity modulator, the SOA-based intensity modulator enhances the AMOOFDM transmission performance across the entire transmission distance range of interest of this chapter. In particular, such an enhancement is more pronounced over the chromatic

dispersion-dominant performance region. For instance, the SOA-based intensity modulator supports a 30Gb/s AMOOFDM signal transmission over a 80km SMF, which doubles the performance corresponding to the DML-based intensity modulator.

The physical origin of the above-mentioned performance improvement lies mainly in the considerably reduced frequency chirp effect, resulting from the strong SOA gain saturation-induced decrease in SOA effective carrier lifetime. The statement is evaluated in Fig. 6.8, which shows almost identical transmission performances between the SOA- and DML-based systems if the fibre chromatic dispersion effect is set to zero. As the treatment of removing the chromatic dispersion effect eliminates effectively the impact of the DML-induced frequency chirp effect, therefore, the SOA intensity modulator's capability of reducing the frequency chirp effect is confirmed in Fig. 6.8. In comparison with the case of excluding fibre chromatic dispersion, for long transmission distances, Fig. 6.8 shows an improved transmission performance for the case of including fibre chromatic dispersion. This is due to the fact that SOA modulated AMOOFDM signal has a chirp parameter with an opposite sign compared to the GVD parameter of a standard fibre.

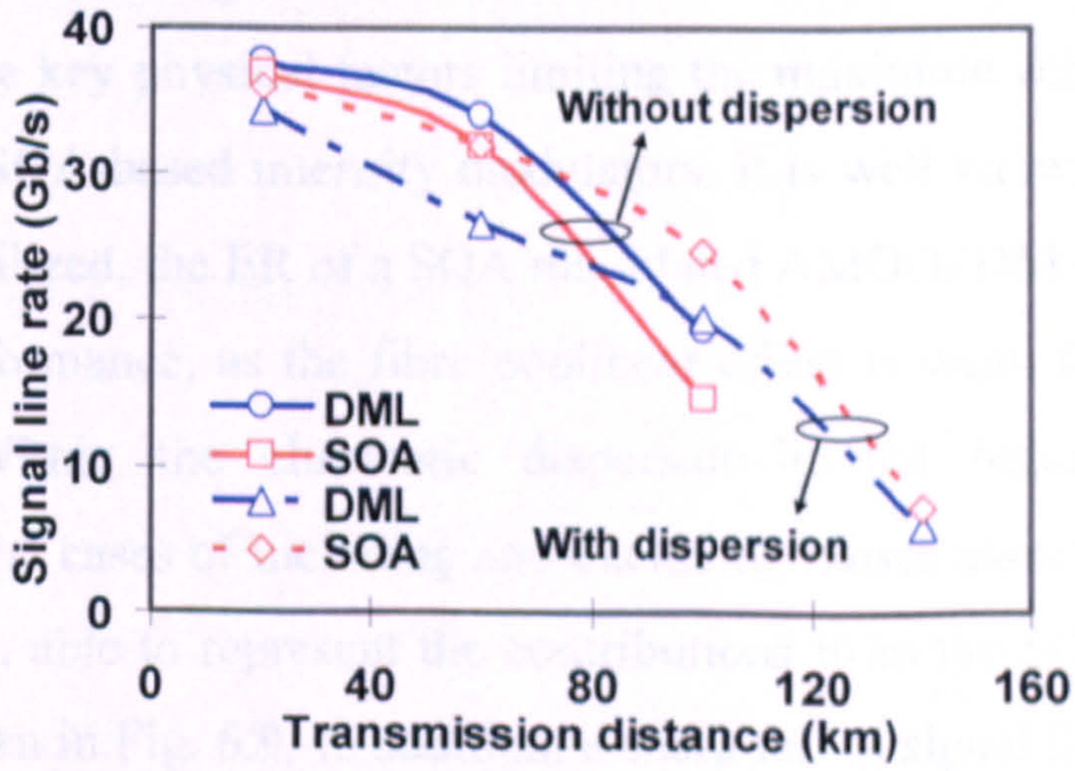

Fig. 6.8 Comparison of AMOOFDM signal transmission capacity versus reach performance for SOA- and DML-based SMF transmission systems including/excluding the chromatic dispersion effect.

In addition, by comparing performances between the cases of including and excluding the SOA associated ASE noises, it can also be found in Fig. 6.7 that, the impact of the ASE noises is negligible on the AMOOFDM transmission performance. This is due to the fact

that the SOA operating at a highly saturated optical gain region offers a very small optical gain and subsequently produces a low ASE power, as indicated in Eq. (6.9).

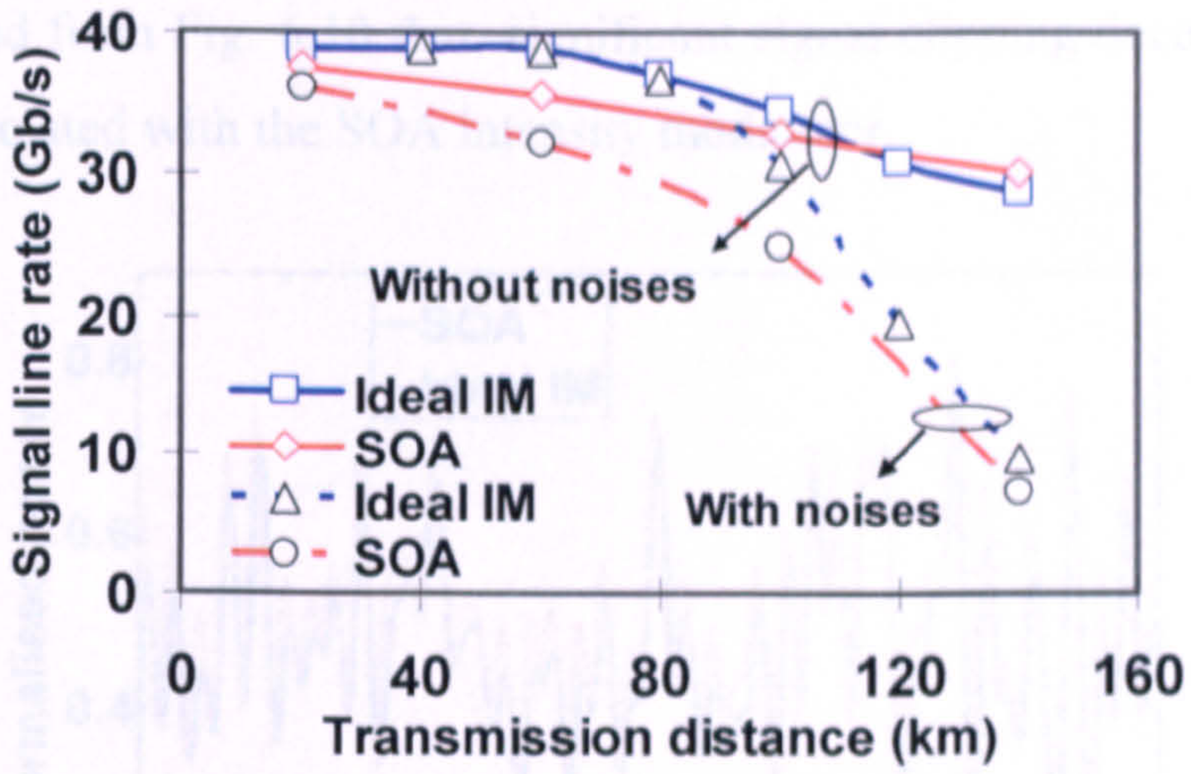

Fig. 6.9 Comparison of AMOOFDM signal transmission capacity versus reach performance for SOA intensity modulator- and ideal intensity modulator(IM)-based SMF transmission systems including/excluding photon detector associated noises.

From Fig. 6.6, Fig. 6.9 and Fig. 6.10, it can be understood that, low signal ER and signal clipping noise are the key physical factors limiting the maximum achievable transmission performance of the SOA-based intensity modulators. It is well known that, if a noise-free photon-detector is utilized, the ER of a SOA modulated AMOOFDM signal does not affect its transmission performance, as the fibre nonlinear effect is weak for short transmission distances [6.11]. Within the chromatic dispersion–limited region, the performance difference between the cases of including and excluding noises associated with the photon detector is, therefore, able to represent the contributions from the SOA-induced reduction in signal ER, as shown in Fig. 6.9. In addition, a sharp fall of signal line rate is observed in Fig. 6.6 for signal ERs of smaller than 0.2dB. The above-mentioned facts indicate that low signal ER is, indeed, one of the most important physical factors limiting the maximum achievable transmission performance. Furthermore, for transmission systems consisting of noise-free photon detectors only, as seen in Fig. 6.9, over the chromatic dispersion-limited performance region there still exists performance differences between the SOA-based intensity modulator and the ideal intensity modulator. Such differences are a direct result of the signal clipping effect. To demonstrate explicitly the SOA-induced signal clipping effect, comparisons of normalized waveforms of the AMOOFDM signals at the input facet of the transmission link are made in Fig. 6.10 between the cases of including a SOA

intensity modulator and an ideal intensity modulator. In obtaining Fig. 6.10, for both cases, the same distribution of signal modulation formats taken across the entire subcarriers are employed, which are identical to those used in Fig. 6.9 for a transmission distance of 60 km. It can be found from Fig. 6.10 that, significant signal clipping occurs in the peaks of the waveform associated with the SOA intensity modulator.

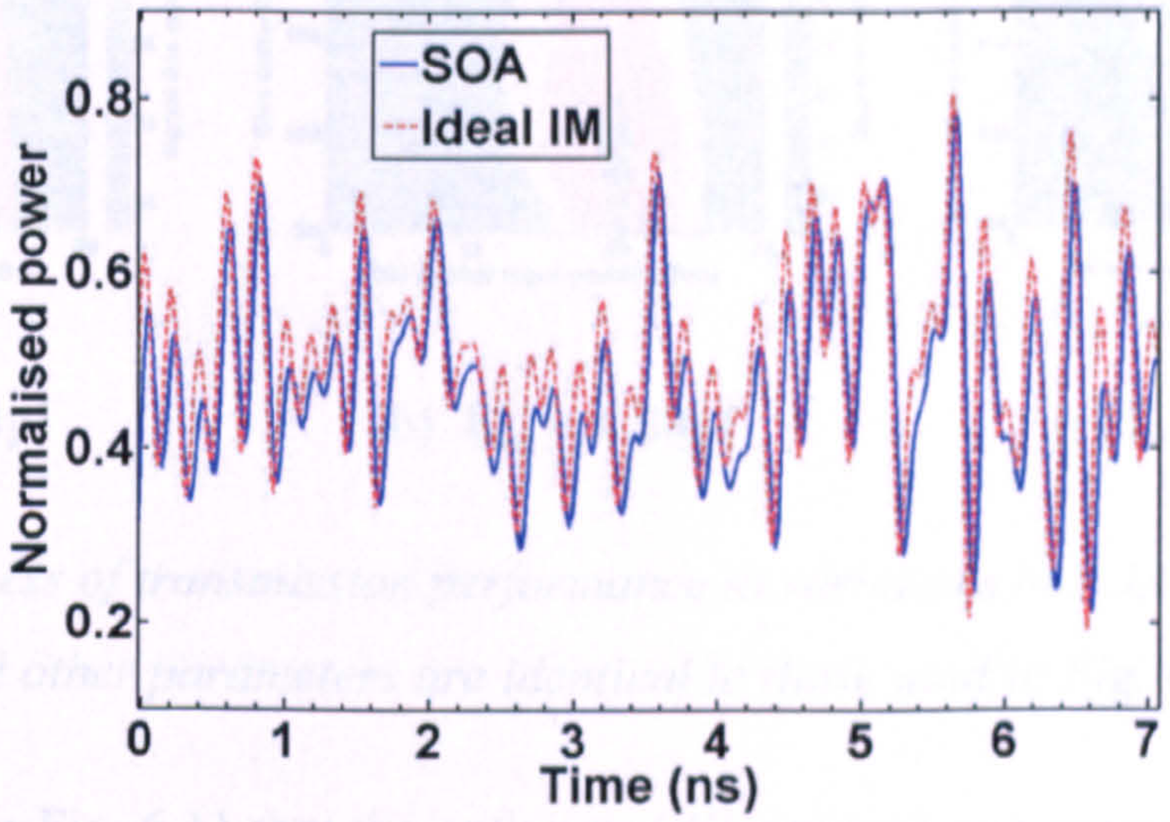

Fig. 6.10 Comparison of normalized AMOOFDM signal waveforms generated by a SOA intensity modulator and an ideal intensity modulator. IM: intensity modulator.

6.4 Performance Robustness

Given the great diversity of the characteristics of the SOAs commercially available in practice, from the system design point of view, it is crucial to investigate the robustness of both optimum SOA operating conditions and AMOOFDM transmission performance to different SOA components. As seen from Table 6.1, a SOA has a large number of parameters, which are closely related. Thorough explorations of all these parameters are practically impossible. To provide an insight into the above important issue, in this section, use is made of two of the most important SOA parameters: saturation energy and cavity length. It is also worth addressing that, each of these two parameters is taken within its appropriate variation range to ensure the accuracy of the simulated results.

6.4.1 Robustness to SOA Saturation Energy

Fig. 6.11 shows three contour plots of maximum achievable signal line rate as a function of CW optical input power and bias current for three SOA saturation energies. These

saturation energies are obtained by setting the cross section area of the active region at three different values of $0.2\mu m^2$, $0.4\mu m^2$ and $0.6\mu m^2$. All other parameters used in simulating Fig. 6.11 are identical to those adopted in Fig. 6.3.

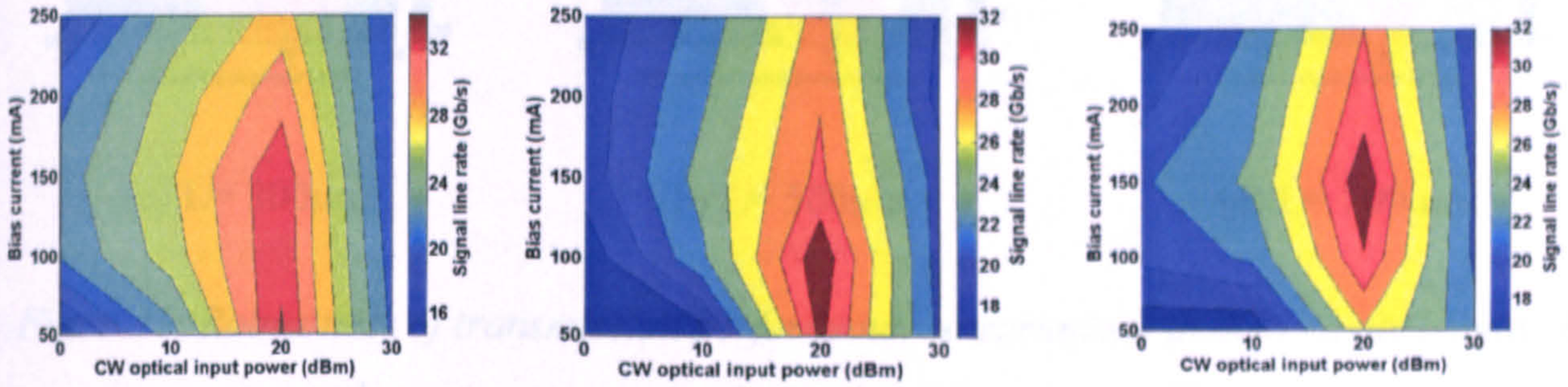

(a) E_{sat} = 2.44pJ (b) E_{sat} = 4.88pJ (c) E_{sat} = 7.32pJ

Fig. 6.11 Robustness of transmission performance to variations in SOA saturation energy. All other parameters are identical to those used in Fig. 6.3.

It can be seen from Fig. 6.11 that the optimum CW optical input power is insusceptible to variations in SOA saturation energy. Such insusceptibility can be explained by considering Fig. 6.2(a), where an approximately 40dB variation in SOA optical input saturation power alters the optical gain by less than 5dB when the SOA is highly saturated due to the injection of a 20dBm CW optical input power. In addition, an SOA with a high saturation energy shifts the corresponding linear current-gain region, as discussed in Section 6.3.1, towards high bias currents, thus an increase in bias current is observed in Fig. 6.11 with increasing saturation energy.

It is very interesting to note that, under the optimum operating conditions, excellent tolerance of maximum achievable transmission performance is shown in Fig. 6.11 to variations in SOA saturation energy. A 3-fold increase in saturation energy corresponds to approximately less than 8% variations in signal line rate.

6.4.2 Robustness to Cavity Length

Fig. 6.12 shows the robustness of maximum achievable transmission performance to variations in SOA cavity length. In calculating Fig. 6.12, all the simulation parameters are identical to those used in Fig. 6.3, except that appropriate changes are made to SOA cavity length. This treatment affects the small signal gain and optical input saturation power of the SOA.

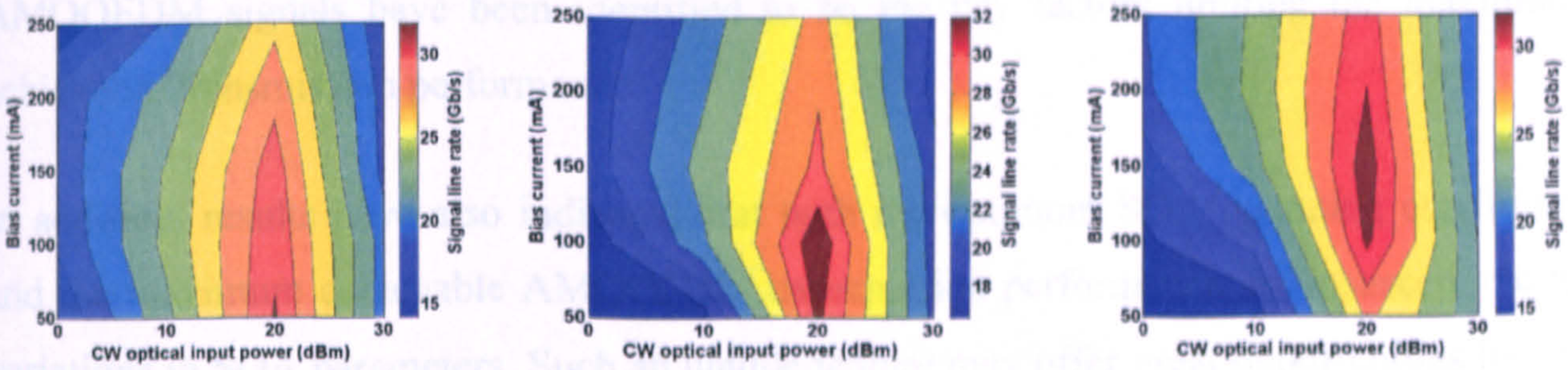

(a) L= 300μm (b) L= 500μm (c) L= 700μm

Fig. 6.12 Robustness of transmission performance to variations in SOA cavity length. All other parameters are identical to those used in Fig. 6.3

Very similar to those illustrated in Fig. 6.11, Fig. 6.12 shows that the optimum CW optical input power is independent of cavity length, and that an increase in cavity length increases optimum bias current because of a corresponding reduction in current density. It is also shown in Fig. 6.12 that negligible changes are introduced to the maximum achievable transmission performance for an increase in cavity length by a factor of 2.3. All the above-mentioned performance robustness to variations in SOA parameters indicates that the optimum AMOOFDM transmission performance claimed in this chapter is likely feasible for a very wide range of SOAs commercially available.

6.5 Conclusions

Detailed investigations of the transmission performance of AMOOFDM signals modulated using SOA-based intensity modulators have been undertaken in SMF IMDD systems without consisting of optical amplification and chromatic dispersion compensation. A theoretical model describing the characteristics of the SOA-based intensity modulator has been developed, based on which optimum SOA operating conditions have been identified. It has been shown that the optimized SOA-based intensity modulators support a 30Gb/s signal transmission over a 80km SMF, which doubles the transmission performance offered by DMLs in the transmission systems of similar configuration. The above-mentioned performance enhancement is mainly due to the considerably reduced frequency chirp effect resulting from the strong SOA gain saturation-induced decrease in SOA effective carrier lifetime. Relatively low ER and clipping of the SOA modulated

AMOOFDM signals have been identified to be the key factors limiting the maximum achievable transmission performance.

In addition, results have also indicated that both the optimum SOA operating conditions and the maximum achievable AMOOFDM transmission performance are insusceptible to variations in SOA parameters. Such an unique feature may offer great opportunities for: a) easing practical system designs, b) enhancing flexibility and robustness of transmission systems to component perturbation and extreme environmental conditions, and finally c) further reducing cost in system installation and maintenance.

References

[6.1] R. J. Manning, D. A. O. Davies, and J. K. Lucek, "Recovery rates in semiconductor laser amplifiers: optical and electrical bias dependencies," Electron. Lett., vol. 30, no.15, pp. 1233–1235, Jul. 1994.

[6.2] F. Girardin, G. Guekos, and A. Houbavlis, "Gain recovery of bulk semiconductor optical amplifiers," IEEE Photon. Tech. Lett., vol. 10, no. 6, pp.784-786, Jun. 1998.

[6.3] J. M. Tang and K. A. Shore, "Strong picosecond optical pulse propagation in semiconductor optical amplifiers at transparency," IEEE J. Quantum Electron., vol. 34, no. 7, pp. 1263-1269, July 1998.

[6.4] J. M. Tang and K. A. Shore, "Analysis of the characteristics of TOAD's subject to frequency-detuned control and signal picosecond pulses," IEEE J. Quantum Electron., vol. 35, no. 11, pp.1704-1712, Nov. 1999.

[6.5] J. M. Tang and K. A. Shore, "Characteristics of optical phase conjugation of picosecond pulses in semiconductor optical amplifiers," IEEE J. Quantum Electron., vol. 35, no. 7, pp.1032-1040,July. 1999.

[6.6] J. M. Tang and K.A. Shore, "Active picoseconds optical pulse compression in semiconductor optical amplifiers," IEEE J. Quantum Electron., vol. 35, no. 1, pp.93-100, Jan. 1999.

[6.7] N.A. Olsson, "Lightwave systems with optical amplifiers," J. Lightw. Technol., vol. 7, no. 7, pp. 1071-1082, July 1989.

[6.8] T. Duong, N. Genay, P. Chanclou, B. Charbonnier, A. Pizzinat, and R. Brenot, "Experimental demonstration of 10 Gbit/s for upstream transmission by remote modulation of 1 GHz RSOA using Adaptively Modulated Optical OFDM for WDM-PON single fiber architecture," presented at the European Conference on Optical Communication (ECOC), Brussels, Belgium, 2008, PD Paper Th.3.F.1.

[6.9] G. P. Agrawal, *Fibre-Optic Communication Systems*, 2nd ed. Hoboken, NJ: Wiley, 1997.

[6.10] M. J. Connelly, *Semiconductor Optical Amplifiers*, London: Kluwer, 2002.

[6.11] J. M. Tang and K. A. Shore, "30 Gb/s signal transmission over 40-km directly modulated DFB-laser-based single-mode-fibre links without optical amplification and dispersion compensation," J. Lightw. Technol., vol. 24, no.6, pp. 2318-2327 Jun. 2006.

[6.12] J. M. Tang, P. M. Lane, and K. A. Shore, "High speed transmission of adaptively modulated optical OFDM signals over multimode fibers using directly modulated DFBs," J. Lightw. Technol., vol. 24, no.1, pp. 429-441, Jan. 2006.

[6.13] J. Mørk, A. Mecozzi, and G. Eisenstein, "The modulation response of a semiconductor laser amplifier," J. Selected. Topics. Quantum. Electron., vol. 5, no. 3, pp. 851-860, May/June 1999.

[6.14] P. Fay, W. Wohlmuth, A. Mahajan, C. Caneau, S. Chandrasekhar, and I. Adesida, "Low-noise performance of monolithically integrated 12-Gb/s p-i-n/HEMT photoreceiver for long-wavelength transmission systems," IEEE Photon. Tech. lett., vol. 10, no. 5, pp. 713-715, May. 1998.

7 Colourless AMOOFDM Transmitters for WDM-PONs using SOAs as Intensity Modulators

Contents

7.1 Introduction **145**

7.2 Transmission System Models 146

7.2.1 Transmission System and AMOOFDM Models 146

7.2.2 SOA Intensity Modulator Model 147

7.2.3 Models for SMF and PIN Detector 150

7.2.4 Simulation Parameters 151

7.3 SOA Characteristics 151

7.4 Transmission Performance of SOA Modulated AMOOFDM Signals 153

7.4.1 Wavelength Dependent Transmission Performance 153

7.4.2 Optimum SOA Operating Conditions for Different Wavelengths 156

7.4.3 Capacity versus Reach Performance under Optimum SOA Operating Conditions 159

7.5 Conclusions 159

7.1 Introduction

Having investigated the feasibility of employing SOAs as intensity modulators in AMOOFDM PON systems at a fixed wavelength of 1550nm in Chapter 6, this chapter extends the topic by investigating the wavelength dependent transmission performance of SOA modulated AMOOFDM signals over IMDD SMF links.

As discussed in Section 3.4.1, colourless ONU operation is critical for minimizing stack and wavelength management problems. To realize colourless ONUs, one promising solution is to use a tunable laser in each ONU, which makes economic sense because of the availability of commercial tunable semiconductor lasers at prices of potentially a few ten U.S. dollars. The major challenge in practical implementation of this strategy is, therefore, the provision of cost-effective colourless optical transmitters in ONUs to ensure that the uplink transmission performance is independent of the wavelengths assigned dynamically by COs. A wide range of optical modulators have been proposed to realize colourless transmitters for WDM-PONs. These modulators include, as summarized in Table 3.4, injection-locked Fabry-Perot lasers [7.1], RSOAs/SOAs [7.2,7.3], and reflective EAMs integrated with SOAs [7.4]. Given the fact that the volumes of optical modulators required by WDM-PONs are potentially very high, it is considerably beneficial if use can be made of monolithically integrated semiconductor modulators to reduce significantly the installation and maintenance cost.

In Chapter 6, it has been shown that AMOOFDM modems using SOAs as intensity modulators are capable of supporting 30Gb/s transmission over 80km SMF in IMDD links for PONs without optical amplification and chromatic dispersion compensation. It is therefore greatly advantageous if the feasibility of employing SOAs as intensity modulators in AMOOFDM modems can be exploited for achieving colourless AMOOFDM transmitters for WDM-PONs. Based on a SOA that is not saturated strongly, a 10Gb/s AMOOFDM signal transmission over a 20km SMF has been demonstrated experimentally in an upstream link of a WDM-PON [7.3].

As an SOA has a wide spectral coverage of >100nm and its optical gain saturation characteristics vary significantly with SOA operating conditions and optical signal properties, detailed explorations of the wavelength dependent transmission performance of the AMOOFDM signals modulated using SOAs are, therefore, very crucial for evaluating the feasibility of utilizing SOAs to achieve colourless AMOOFDM transmitters for WDM-PONs. However, previous work reported in Chapter 6 was undertaken using a fixed wavelength of 1550nm only. Although the transmission performance of SOA modulated AMOOFDM signals for a few wavelengths have been presented in [7.3], very limited discussions have, however, been made. To address the important issue and to provide valuable insights for practical system designs, this chapter is a significant extension of the work in Chapter 6, because, here, special attention is focused on exploring the wavelength dependent transmission performance of SOA modulated AMOOFDM signals, based on a comprehensive SOA model capable of describing wavelength dependent SOA characteristics.

The focus of this chapter is to investigate extensively, for the first time, the wavelength dependent transmission performance of AMOOFDM signals modulated by SOAs over IMDD SMF link without optical amplification and dispersion compensation. A theoretical SOA model describing both optical gain saturation and gain spectral characteristics is developed, based on which optimum SOA operating conditions are identified for various wavelengths within a broad range of 1510nm-1590nm. It is shown that SOA intensity modulators operating at the identified optimum operating conditions are capable of achieving colourless AMOOFDM transmitters. In addition, results also indicate that it is feasible to transmit >30Gb/s AMOOFDM signals over 60km SMFs.

7.2 Transmission System Models

7.2.1 Transmission System and AMOOFDM Models

The transmission system considered here is similar to that illustrated in Fig. 6.1, which consists of a transmitter, an optical amplification- and chromatic dispersion compensation-free IMDD SMF link, a photodiode and a receiver. The difference is that a tunable semiconductor laser rather than a laser operating at a fixed wavelength is used here. As the AMOOFDM modem and the SOA-enabled intensity modulation of AMOOFDM signals

have been explained in detail in Chapter 6, here light is only shed on the wavelength dependence of the intensity modulation of AMOOFDM signals.

A tunable semiconductor laser is employed to provide a CW light source with the desired optical power and optical carrier wavelength. The DC bias current and the driving current are also adjusted appropriately to enable the SOA to operate at optimum operating conditions. Such adjustments may also alter the output power of the modulated optical signal. An optical attenuator is therefore inserted at the input facet of the SMF link to fix the coupled optical power at a required level.

At the receiver end, the optical signal is detected using a photodiode. The data is finally recovered following an inverse procedure of the AMOOFDM modem in the transmitter.

7.2.2 SOA Intensity Modulator Model

Based on the assumptions made in Section 6.2.2, in developing the SOA intensity modulator model here, various SOA intraband dynamic processes are not considered, which include carrier heating, spectral hole-burning, two-photon absorption and ultrafast nonlinear refraction [7.5]. The exclusion of the intraband dynamic processes simplifies significantly the comprehensive theoretical SOA model developed in [7.5]. When a transformation of the coupled wave propagation equations [7.5] is made to the retarded reference frame, $T=t-z/v_g$ with t, z and v_g being the time, the transmission distance and the group velocity, respectively, and when the optical field is defined as

$$A(z,T)=\sqrt{P(z,T)}\exp[j\phi(z,T)] \tag{7.1}$$

with $P(z,T)$ and $\phi(z,T)$ being the optical power and the optical phase, respectively, the output optical signal from the SOA is governed by

$$\frac{dh_i(T)}{dT}=\frac{g_{s,i}(T)L-h_i(T)}{\tau_c}-\frac{P_{in,i}(T)}{E_{sat,i}}\{\exp[h_i(T)]-1\} \tag{7.2}$$

$$P_{out,i}(T)=P_{in,i}(T)\exp[h_i(T)] \tag{7.3}$$

$$\phi_{out,i}(T)=\phi_{in,i}(T)-\frac{1}{2}\alpha h_i(T) \tag{7.4}$$

with $$h_i(T) = \int_0^L g_i(z,T)dz \tag{7.5}$$

where the subscript i is referred to the wavelength λ_i . $P_{in,i}(T)$ and $\phi_{in,i}(T)$ are the power and phase of the input optical signal. $P_{out,i}(T)$ and $\phi_{out,i}(T)$ are the power and phase of the modulated output optical signal. $h_i(T)$ represents the integrated optical gain along the entire SOA length L. $g_i(z,T)$ is the saturated optical gain defined as $g_i(z,T)=\Gamma a_i[N(T)-N_{0i}]$ with $N(T)$ and N_{0i} being the carrier density and the carrier density at transparency, Γ is the confinement factor and a_i is the differential gain. For a specific optical gain spectrum, $g_{s,i}(T)$ is the small-signal gain of the SOA at a fixed wavelength λ_i , which can be expressed as $g_{s,i}(T)=\Gamma a_i N_{0i}[I(T)/I_{0i}-1]$, here $I(T)$ is the total injected electrical current including the DC bias current and the driving current, and I_{0i} is the transparency current. τ_c is the carrier lifetime. $E_{sat,i}=\hbar\omega_i wd/\Gamma a_i$ is the SOA saturation energy, where ω_i, w and d are the optical signal frequency, the width and depth of the SOA active region, respectively. α is the linewidth enhancement factor. It can be seen from Eq. (7.4) that, α varies the phase of the modulated AMOOFDM signal only. Owing to direct detection in an IMDD link, such a phase variation does not affect the transmission performance of the SOA modulated signal. Therefore, the wavelength dependence of the α parameter is not considered in this chapter. Eqs. (7.2)-(7.4) can be easily solved numerically when $g_{s,i}(T)$, $P_{in,i}(T)$ and $\phi_{in,i}(T)$ are made known.

In order to simulate the optical wavelength dependence of small-signal gain $g_{s,i}(T)$, a theoretical gain spectral model should be as realistic as possible without requiring too many parameters and easily calibrated against experimental measurements of an actual SOA. Here a widely used SOA optical gain spectral model is adopted [7.6]. The wavelength- and injected current-dependent small-signal gain in dB, $G_{dB,i}(\lambda_i,T)$, can be expressed as

$$G_{dB,i}(\lambda_i,T)=[a_g(\lambda_i)-b_g(\lambda_i)]G_{dB}(\lambda_{\max})+b_g(\lambda_i)G_{dB,i}(\lambda_{\max},T) \tag{7.6}$$

where $G_{dB}(\lambda_{max})$ is the small-signal peak gain corresponding to a wavelength λ_{max} and a current I_{max}. In this chapter, these parameters are treated as a reference point and their corresponding values are listed in Table 7.1 [7.6]. $G_{dB,I}(\lambda_{max},T)$ is the small-signal gain at λ_{max} for an injected current $I(T)$ and satisfies

$$G_{dB,I}(\lambda_{\max},T)=\Gamma a(\lambda_{\max})N_0(\lambda_{\max})[I(t)/I_0(\lambda_{\max})-1]$$

Therefore, $G_{dB,I}(\lambda_l,T)$ and $G_{dB,I}(\lambda_{max},T)$ are time-variant due to the injection of a time-dependent driving current $I(T)$. $a_g(\lambda_l)$ and $b_g(\lambda_l)$ are the normalized small-signal gain coefficient and normalized differential gain, respectively. They are defined as $a_g(\lambda_l)\equiv g_{s,l}(T)/g_{\max}(T,\lambda_{\max})$ and $b_g(\lambda_l)\equiv a_l/a(\lambda_{\max})$, where $g_{max}(T,\lambda_{max})$ and $a(\lambda_{max})$ are the small-signal gain and the differential gain at λ_{max}, respectively. The spectral dependence of $a_g(\lambda_l)$ and $b_g(\lambda_l)$ can be written as [7.6]

$$a_g(\lambda_l)=m_2(\lambda_l-\lambda_{\max})^2+1 \tag{7.7}$$

$$b_g(\lambda_l)=n_2(\lambda_l-\lambda_{\max})^2+n_1(\lambda_l-\lambda_{\max})+1 \tag{7.8}$$

The coefficients m_2, n_2 and n_1 can be obtained by quadratic and parabolic fittings of experimental measurements [7.6]. Their values taken from [7.6] are listed in Table 7.1.

Apart from performing intensity modulation, the SOA also imposes simultaneously ASE noise onto the modulated optical signal. The total ASE power $P_{ASE,I}$ at λ_l can be calculated by [7.7]

$$P_{ASE,I}=\{N_f\exp[h_l(T)]-1\}B_0\hbar\omega_l \tag{7.9}$$

where N_f is the SOA noise figure, B_0 is the optical bandwidth and $\hbar\omega_l$ is the photon energy. In deriving Eq. (7.9), it is assumed that ASE noise does not affect the SOA gain dynamics. This assumption is valid because the saturated optical gain is typically small (<5dB) when the SOA operates in a deeply saturated gain region, as discussed in Section

7.3 and Section 7.4. In addition, the small saturated optical gain also gives rise to the negligible SOA self-saturation effect.

After adding the ASE noise into $P_{out,l}(T)$ and $\phi_{out,l}(T)$, by using Eq. (7.1), the modulated optical signal can be obtained. In the receiver, the transmitted optical signal is detected using a photodiode when a CW optical input wave is chosen in the transmitter.

Table 7.1 SOA and SMF parameters

SOA	
Symbol	**Value**
L	500μm
w	1.5μm
d	0.27μm
τ_c	0.3ns
Γ	0.35
α	5
v_g	8.43×10^{7}m/s
λ_{max}	1550nm
$a(\lambda_{max})$	3×10^{-20}m^2
$N_0(\lambda_{max})$	1.05×10^{24}m^{-3}
$G_{dB}(\lambda_{max})$	32dB
m_2	-2.4×10^{-4} nm^{-2}
n_2	1.27×10^{-4} nm^{-2}
n_1	-1.9×10^{-2} nm^{-1}
N_f	8dB
SMF	
Parameter	**Value**
Effective area	80μm^2
Dispersion	17.0ps/nm/km
Dispersion slope	0.07ps/nm/nm/km
Dispersion wavelength	1550nm
Attenuation	0.2dB/km
Attenuation slope	-0.0005dB/nm/km (for $\lambda_1 < \lambda_{max}$)
	0.0005dB/nm/km (for $\lambda_1 > \lambda_{max}$)
Kerr coefficient	2.35×10^{-20}m^2/W

7.2.3 Models for SMF and PIN Detector

A SMF model successfully used in Chapters 4-6 is adopted here. In particular, the wavelength dependence of fiber loss and chromatic dispersion is also considered to accommodate optical signals having wavelengths within a broad wavelength window. The effect of Kerr nonlinearity-induced phase noise to intensity noise conversion is

incorporated upon photon detection in the receiver. The PIN detector model used in Chapter 6 is considered here.

7.2.4 Simulation Parameters

In simulating the performance of the AMOOFDM modems, parameters identical to those presented in Section 6.2.4 are adopted here. The parameters used in simulating the SOA intensity modulator are representative for InGaAsP semiconductor materials [7.6], which are listed in Table 7.1. By attenuating/amplifying the modulated optical signal from the SOA, the optical power coupled into the SMF link is fixed at 6.3dBm.

The simulation parameters for SMFs are also given in Table 7.1. The parameters for PIN detectors can be found in Table 6.1. It should be noted that SMF attenuation and dispersion parameters are wavelength dependent. As an example, the attenuation and dispersion parameters are 0.22dB/km and 14.2ps/nm/km (0.22dB/km and 19.8ps/nm/km) at 1510nm (1590nm), whilst the corresponding parameters at 1550nm are 0.2dB/km and 17ps/nm/km.

7.3 SOA Characteristics

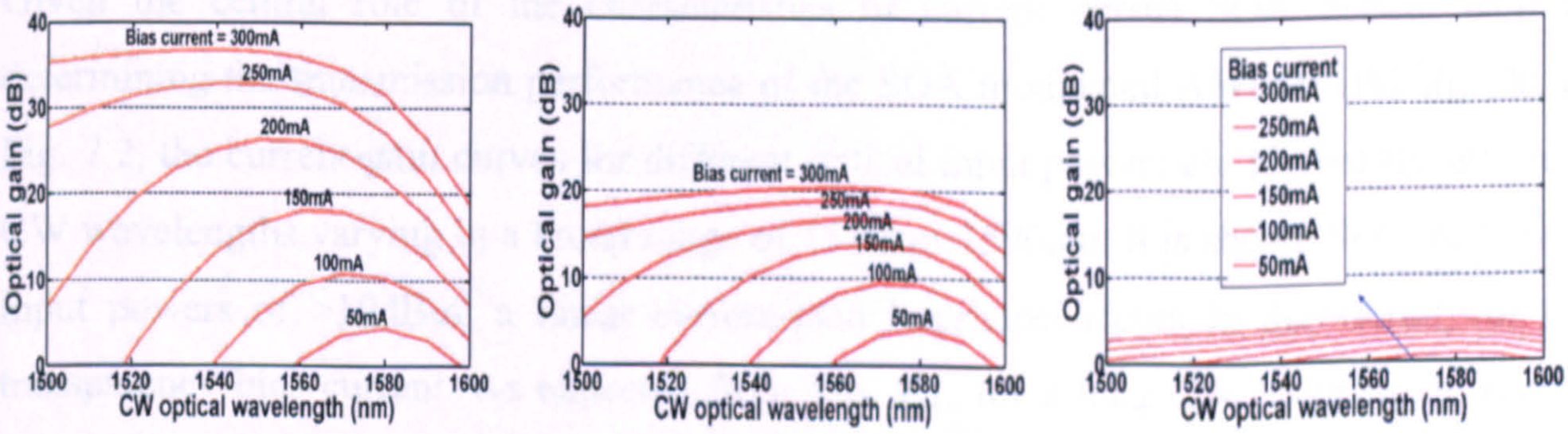

Fig. 7.1 SOA optical gain spectra for different bias currents and optical input powers. (a)An optical input power of -20dBm, (b) An optical input power of 0dBm and (c) An optical input power of 20dBm.

To gain an in-depth understanding of simulation results presented in Section 7.4, in this section brief discussions are made of the wavelength dependent SOA optical gain properties. Fig. 7.1 shows the SOA optical gain spectra for different bias currents and

optical input powers. In obtaining Fig. 7.1, a 10GHz sinusoidal electrical driving current having a fixed PTP value of 80mA is applied to the SOA to ensure that the SOA operating conditions considered here are similar to those adopted in other figures of the chapter.

Fig. 7.1 shows that, for a specific optical input power, the SOA gain spectral peak shifts towards a long wavelength with decreasing bias current. This agrees very well with experimental measurements [7.6]. In addition, as seen in Fig. 7.1, a rapid decline in bias current required at transparency with increasing CW wavelength also shows good agreement with results reported in [7.8]. The above-mentioned behaviours confirm strongly the validity of the wavelength dependent SOA model developed here.

As expected, it can be seen in Fig. 7.1 that, the SOA gain spectra vary considerably with optical input power. For optical input powers of <10dBm, strong wavelength dependent SOA gain spectra occur, implying that the AMOOFDM transmission performance is sensitive to CW wavelength. Whilst for optical input powers of >10dBm, the SOA operates in a deeply saturated gain region, resulting in a flat gain spectrum with a significantly reduced optical gain. This indicates that a wavelength independence of the AMOOFDM transmission performance is expected over such operating conditions.

Given the central role of the characteristics of current versus SOA optical gain in determining the transmission performance of the SOA modulated AMOOFDM signals, in Fig. 7.2, the current-gain curves for different optical input powers are plotted for different CW wavelengths varying in a broad range of 1510nm-1590nm. It is shown that, for optical input powers of >10dBm, a linear current-gain lineshape occurs in the vicinity of the transparency bias current. As expected from Fig. 7.1, for a long CW wavelength, such a linear region broadens and simultaneously shifts towards a low bias current. This implies that, to maximize the transmission performance of the AMOOFDM signals, the SOA has to be set at a low bias current for a long CW wavelength. Outside the linear current-gain region, the modulated AMOOFDM signals suffer from the signal clipping effect, as discussed in Chapter 6. To minimize the effect, it is necessary to optimize the PTP value of the driving current. Moreover, Fig. 7.2 also shows that, a long CW wavelength corresponds to a decreased slope of the current-gain curve, leading to a degraded ER of the modulated optical signals.

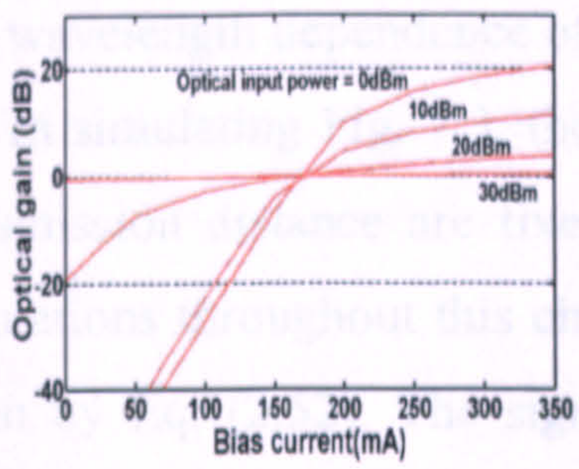

(a) 1510nm

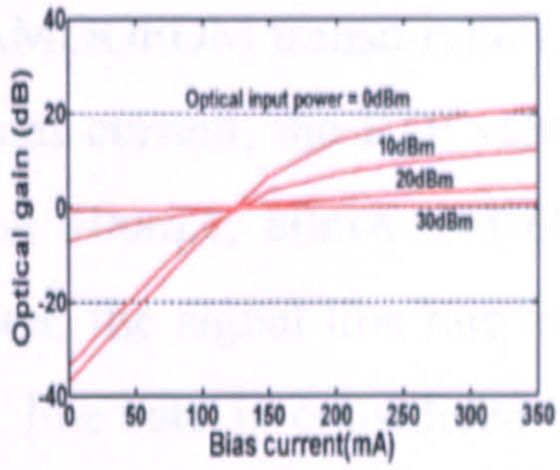

(b) 1530nm

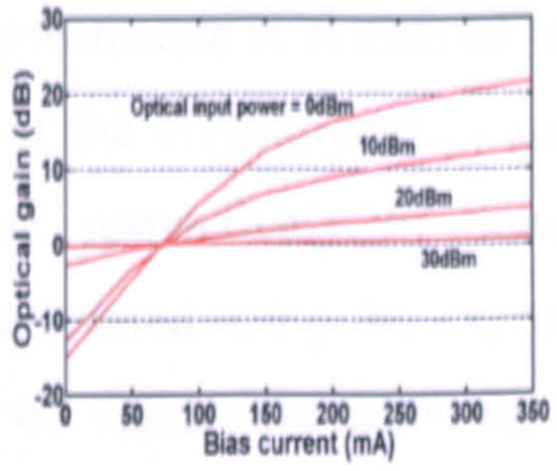

(c) 1550nm

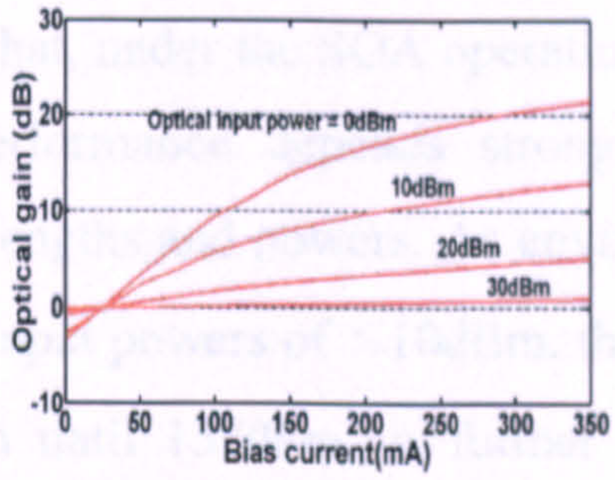

(d) 1570nm

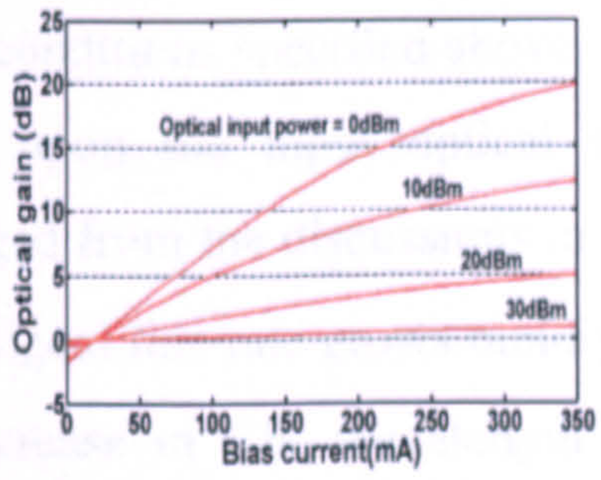

(e) 1590nm

Fig. 7.2 SOA optical gain versus bias current for different optical input powers and CW wavelengths.

7.4 Transmission Performance of SOA Modulated AMOOFDM Signals

7.4.1 Wavelength Dependent Transmission Performance

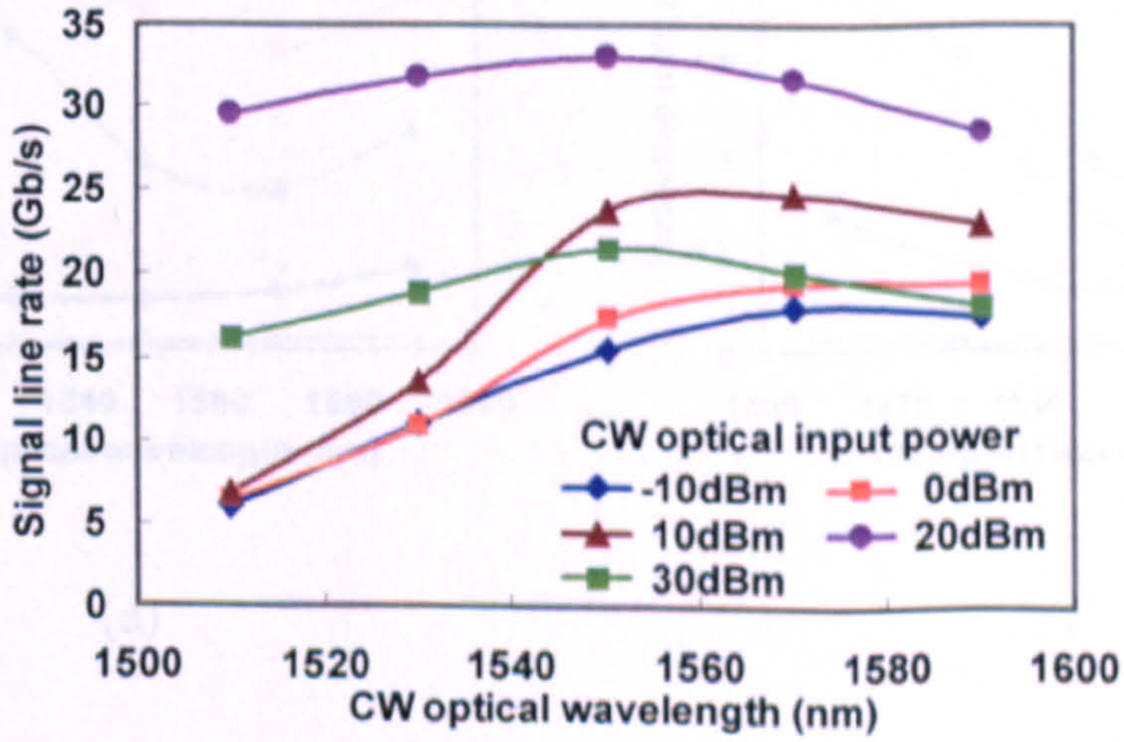

Fig. 7.3 Signal line rate as a function of CW wavelength for different optical input powers.

The wavelength dependence of AMOOFDM transmission performance is examined in Fig. 7.3. In simulating Fig. 7.3, the bias current, the PTP value of the driving current and the transmission distance are fixed at 100mA, 80mA and 60km, respectively. In numerical simulations throughout this chapter, the signal line rate is calculated using the expression given by Eq. (2.52). The signal line rate is considered to be valid only when the total channel BER, BER_T, equals 1.0×10^{-3} is satisfied for a specific transmission system. The BER_T is defined in Eq. (2.51).

Fig. 7.3 shows that, under the SOA operating conditions specified above, the AMOOFDM transmission performance depends strongly upon the input optical signal properties including wavelengths and powers. As envisaged from the discussions in Fig. 7.1 and Fig. 7.2, for optical input powers of ≤10dBm, the signal line rate grows rapidly with increasing CW wavelength until 1570nm. A further increase in CW wavelength brings about an almost flattened signal line rate developing trend. Such wavelength dependent performance behaviours are consistent with experimental measurements [7.3]. On the other hand, for optical input powers of >10dBm, the signal capacity differences for different CW wavelengths are reduced considerably, and an almost symmetric signal capacity lineshape occurs with respect to a CW wavelength of 1550nm. Moreover, for a fixed CW wavelength, the signal line rate increases with increasing optical input power for optical input powers of <20dBm, beyond this value, the achievable signal line rate drops sharply, which suggests the optimum optical input power is approximately 20dBm.

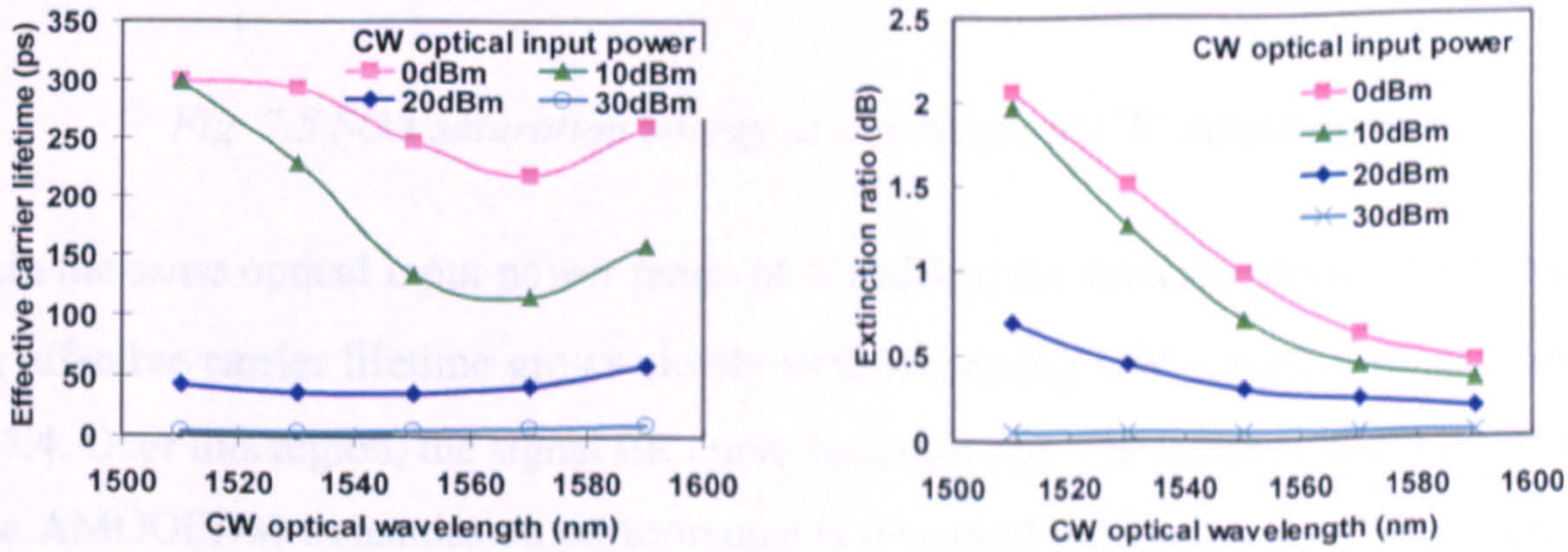

Fig. 7.4 SOA effective carrier lifetime (a) and AMOOFDM signal extinction ratio (b) versus CW wavelength for different optical input powers.

The physical mechanisms behind the above-mentioned transmission performance behaviors are the co-existed effects of SOA effective carrier lifetime [defined in Eq. (3.1)] and ER of the modulated signal [defined in Eqs. (2.46)-(2.47)], as discussed in Chapter 6.

As seen in Fig. 7.4, for optical input powers of ≤10dBm and CW wavelengths of <1570nm, both the SOA effective carrier lifetime and the modulated signal ER decrease quickly with increasing CW wavelength. A short effective carrier lifetime corresponds to a large SOA bandwidth, leading to the reduced frequency chirp effect and thus an improved transmission performance, as discussed in Chapter 6. Whilst a small signal ER increases the minimum OSNR required for achieving a specific transmission performance, resulting in a reduction in signal transmission capacity. Comparisons between Fig. 7.4 and Fig. 7.3 indicate that, under the aforementioned optical input power and CW wavelength range, the reduction in SOA effective carrier lifetime dominates the wavelength dependent AMOOFDM performance illustrated in Fig. 7.3.

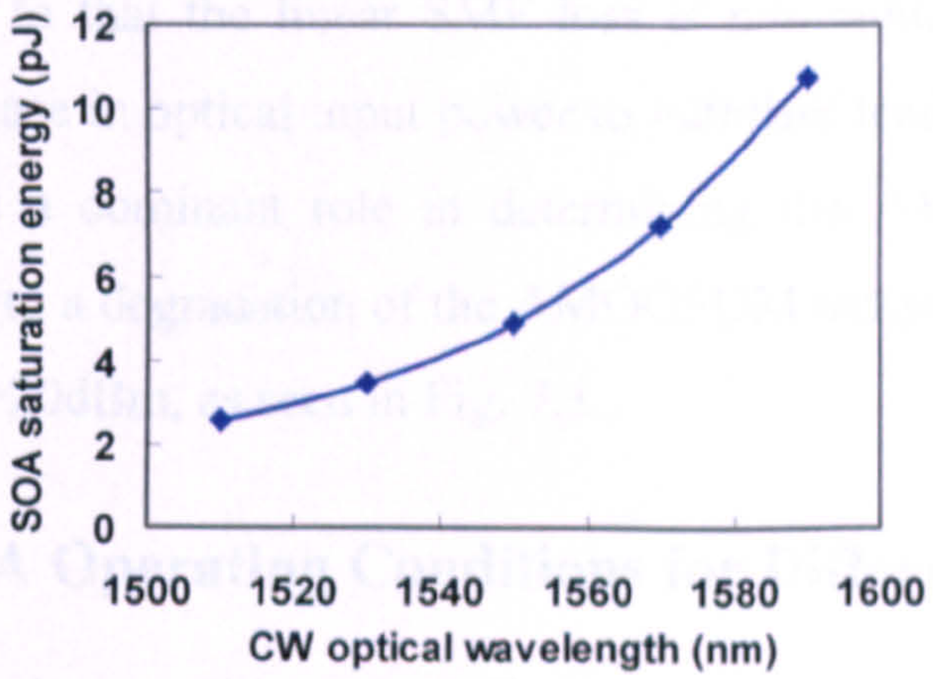

Fig. 7.5 SOA saturation energy as a function of CW wavelength.

Within the same optical input power range of ≤10dBm, for wavelengths of ≥ 1570nm the SOA effective carrier lifetime grows slowly with increasing CW wavelength, as shown in Fig. 7.4. Over this region, the signal ER curve becomes flat. Therefore, a slight degradation of the AMOOFDM transmission performance is observed in Fig. 7.3 for CW wavelengths of >1570nm. For optical input powers of ≤10dBm, the occurrence of a minimum SOA effective carrier lifetime at 1570nm can be explained by considering Eq. (3.1): a maximum SOA output optical power occurs in the vicinity of the CW wavelength of 1570nm. This can be understood by considering Fig. 7.1(a) and Fig. 7.1(b); On the other hand, the SOA saturation energy increases with increasing CW wavelength, as shown in Fig. 7.5, resulting

from a long wavelength-induced reduction in differential gain. The co-existence of the above two physical processes underpins the occurrence of the minimum SOA effective carrier lifetime observed in Fig. 7.4.

It can also be seen from Fig. 7.4 that, for optical input powers of ≤10dBm, for a given CW wavelength, both the SOA effective carrier lifetime and the signal ER decrease with increasing optical input power. It is clear from the above discussions that, this gives rise to an increase in signal line rate with increasing optical input power, as shown in Fig. 7.3, which agrees very well with the results presented in Chapter 6.

For optical input powers of >10dBm, the SOA operates in a strongly saturated optical gain region, the variations in both the SOA effective carrier lifetime and the signal ER reduce significantly across the entire wavelength window of 1510-1590nm. As a direct result, the transmission performance of the AMOOFDM signals is insensitive to CW wavelength, as shown in Fig. 7.3. The existence of a maximum transmission performance for 1550nm in Fig. 7.3, is mainly due to that the linear SMF loss is minimum at such a wavelength. However, a further increase in optical input power to >20dBm leads to an extremely small signal ER, which plays a dominant role in determining the AMOOFDM transmission performance. This leads to a degradation of the AMOOFDM transmission performance for optical input powers of >20dBm, as seen in Fig. 7.3.

7.4.2 Optimum SOA Operating Conditions for Different Wavelengths

The optimum SOA operating conditions for different CW wavelengths are explored in Fig. 7.6, where contour plots of signal line rate as a function of both optical input power and bias current are presented for different wavelengths varying in a wide range of 1510-1590nm. In computing Fig. 7.6, the transmission distance is fixed at 60km and a driving current with a constant PTP value of 80mA is considered.

Fig. 7.6 shows that, for a specific wavelength, there exists an optimum bias current and an optimum optical input power, corresponding to which a maximum signal line rate is obtained. Such bias current and optical input power dependence of the transmission performance agrees very well with that reported in Chapter 6, from which detailed explanations can also be found. From discussions in Chapter 6 and Section 7.4.1, it is clear

that the SOA effective carrier lifetime effect and the signal ER effect are the major contributors to the evolution trends illustrated in Fig. 7.6.

It is very important to note in Fig. 7.6 that, the optimum SOA operating conditions are wavelength dependent, i.e., with increasing CW wavelength, the optimum SOA bias current decreases with the optimum optical input power remaining almost unchanged. For example, for 1510nm, the optimum bias current and the optimum optical input power are approximately 200mA and 20dBm, respectively; whilst for 1590nm the values of these two parameters are approximately 50mA and 20dBm. The impact of CW wavelength on the optimum SOA bias current can be explained by considering the fact that, a long CW wavelength shifts the linear region of the current-gain curve towards a low bias current, as shown in Fig. 7.2. On the other hand, the insensitivity of optimum optical input power to CW wavelength is a direct result of deeply saturated optical gain of the SOA. For such a case, several key factors are insensitive to CW wavelength, which include SOA optical gain, effective carrier lifetime and signal ER.

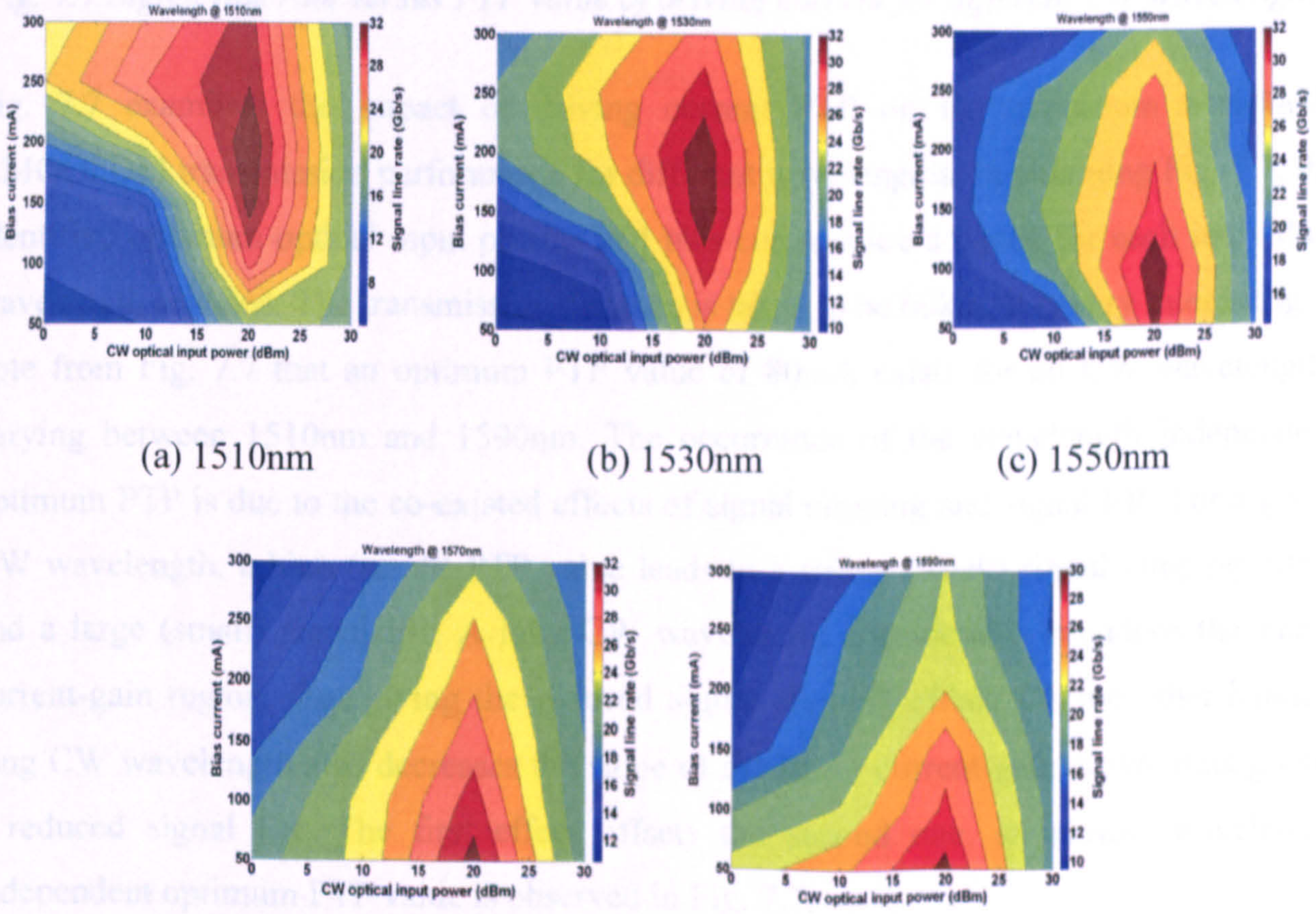

(a) 1510nm (b) 1530nm (c) 1550nm

(d) 1570nm (e) 1590nm

Fig. 7.6 Contour plots of signal line rate as a function of CW optical input power and bias current for different CW wavelengths.

It is worth addressing, in particular, that by operating the SOA at optimum operating conditions corresponding to different wavelengths, a <3Gb/s variation in maximum achievable signal line rate is obtained across an entire wavelength range of 80nm, as shown in Fig. 7.6. This indicates that colourless AMOOFDM transmitters are achievable when different optimum SOA operating conditions are chosen corresponding to different CW wavelengths.

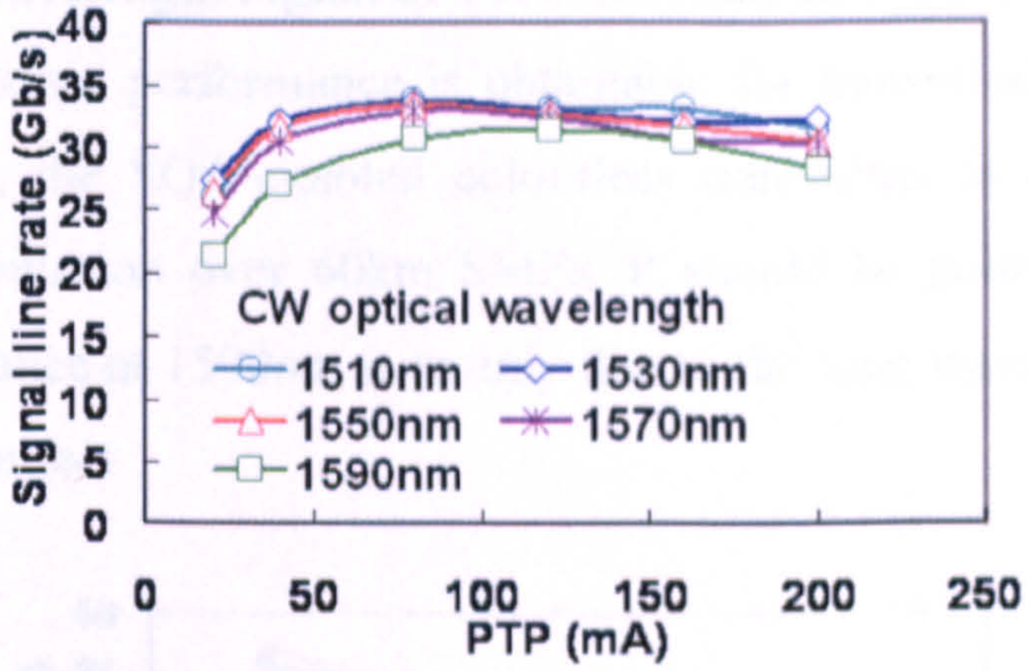

Fig. 7.7 Signal line rate versus PTP value of driving current for different CW wavelengths

Fig. 7.7 examines the impact of driving current PTP on the maximum achievable AMOOFDM transmission performance for different wavelengths. In obtaining Fig. 7.7, the identified optimum optical input powers and bias currents are adopted for each individual wavelength selected. The transmission distance is taken to be 60km. It is very interesting to note from Fig. 7.7 that an optimum PTP value of 80mA exists for all CW wavelengths varying between 1510nm and 1590nm. The occurrence of the wavelength independent optimum PTP is due to the co-existed effects of signal clipping and signal ER. For a given CW wavelength, a high (small) PTP value leads to a strong (weak) signal clipping effect and a large (small) signal ER. A long CW wavelength considerably broadens the linear current-gain region, thus giving the reduced signal clipping effect. On the other hand, a long CW wavelength also decreases the slope of the linear current-gain curve, thus giving a reduced signal ER. The first effect offsets the second one, an almost wavelength independent optimum PTP value is observed in Fig. 7.7.

7.4.3 Capacity versus Reach Performance under Optimum SOA Operating Conditions

It is clear from the discussions in Section 7.4.2 that the optimization of SOA operating conditions enables the realization of colourless AMOOFDM transmitters. Based on the identified optimum operating conditions for different CW wavelengths, the maximum achievable AMOOFDM transmission capacity versus reach performance is plotted in Fig. 7.8. Within a broad wavelength region of 1510-1590nm, an almost wavelength insensitive AMOOFDM transmission performance is obtainable for transmission distances of up to 150km. In particular, the SOA-enabled colourless transmitter is capable of supporting >30Gb/s signal transmission over 60km SMFs. It should be pointed out that the worst transmission performance at 1590nm is mainly due to the long wavelength-induced strong chromatic dispersion effect.

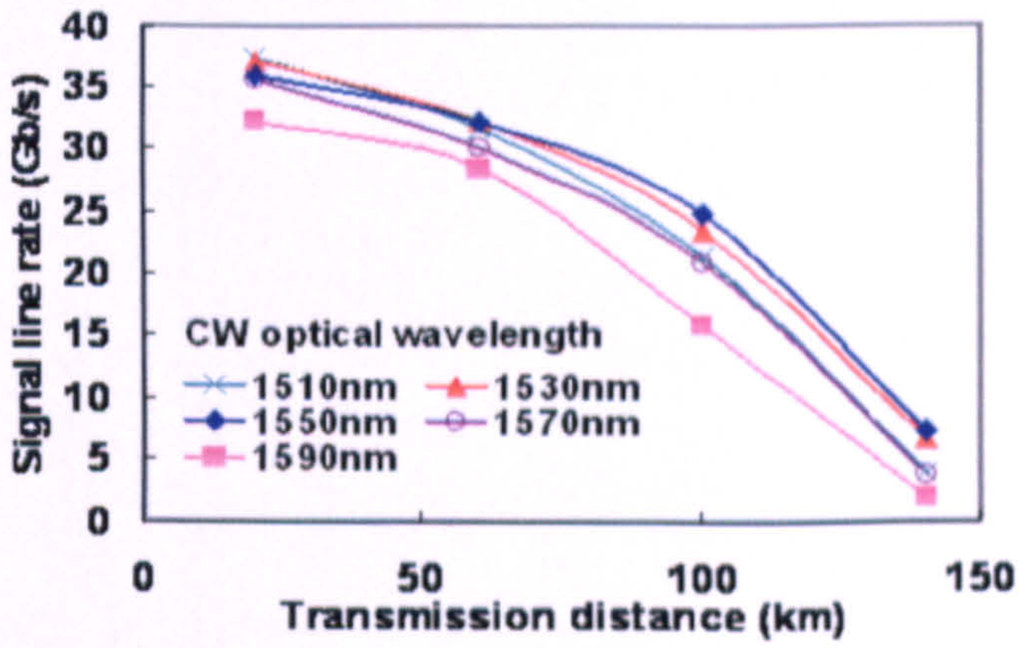

Fig. 7.8 Signal capacity versus reach performance for different CW wavelengths

It is also worth addressing that the transmission performance of the colourless transmitters is very robust to variations in SOA parameters such as saturation energy and SOA length. This strengthens further the technical basement of employing optimized SOA intensity modulators to achieve colourless AMOOFDM transmitters for WDM-PONs.

7.5 Conclusions

This chapter is a significant extension of Chapter 6. In this chapter, the wavelength dependent transmission performance of SOA modulated AMOOFDM signals has been investigated, for the first time, over IMDD SMF links without optical amplification and

chromatic dispersion compensation. A theoretical SOA model describing optical gain saturation and gain spectral characteristics has been developed, based on which optimum SOA operating conditions have been identified for different wavelengths varying in a broad range of 1510nm-1590nm. Numerical simulation results have shown that, within the entire wavelength window, the SOA intensity modulators operating at the identified optimum conditions enable the realization of colourless AMOOFDM transmitters. In addition, it is also shown that the colourless AMOOFDM transmitters are capable of supporting >30Gb/s transmission over 60km SMFs.

References

[7.1] K. Grobe and J.-P. Elbers, "PON in adolescence: from TDMA to WDM-PON," IEEE Commun. Mag. vol. 46, no. 1, pp. 26-34 Jan. 2008.

[7.2] P. Healey, P. Townsend, C. Ford, L. Johnston, P. Townley, I. Lealman, L. Rivers, S. Perrin, and R. Moore, "Spectral slicing WDM-PON using wavelength-seeded reflective SOAs," Electron. Lett. 37, no. 19, pp. 1181-1182 Sep. 2001.

[7.3] T. Duong, N. Genay, P. Chanclou, B. Charbonnier, A. Pizzinat, and R. Brenot, "Experimental demonstration of 10 Gbit/s for upstream transmission by remote modulation of 1 GHz RSOA using Adaptively Modulated Optical OFDM for WDM-PON single fiber architecture," in European Conference on Optical Communication (ECOC), (Brussels, Belgium, 2008), PD paper Th.3.F.1.

[7.4] E. K. MacHale, G. Talli, P. D. Townsend, A. Borghesani, I. Lealman, D. G. Moodie, and D. W. Smith, "Extended-reach PON employing 10Gb/s integrated reflective EAM-SOA," in European Conference on Optical Communication (ECOC), (Brussels, Belgium, 2008), paper Th.2.F.1.

[7.5] J. M. Tang and K. A. Shore, "Strong picosecond optical pulse propagation in semiconductor optical amplifiers at transparency," IEEE J. Quantum Electron., vol. 34, no. 7, pp. 1263-1269, July 1998.

[7.6] K. Obermann, S. Kindt, D. Breuer, and K. Petermann, "Performance analysis of wavelength converters based on cross-gain modulation in semiconductor-optical amplifiers," J. Lightwave Technol., vol. 16, no.1, pp. 78-85 Jan. 1998.

[7.7] N.A. Olsson, "Lightwave systems with optical amplifiers," J. Lightwave Technol., vol. 7, no. 7, pp. 1071-1082, July 1989.

[7.8] S.-L. Lee, "Analytical formula of wavelength-dependent transparent current and its implications for designing wavelength sensors and WDM lasers," IEEE J. Quantum Electron., vol. 7, no. 2, pp. 201-209 Mar./Apr. 2001.

8 AMOOFDM Modems Incorporating RSOAs as Intensity Modulators for WDM-PONs

Contents

8.1 Introduction 163

8.2 Transmission System Models 165

8.2.1 Transmission System and AMOOFDM Modems 165

8.2.2 RSOA Intensity Modulator Models 166

8.2.3 SMF and PIN Models 169

8.2.4 Simulation Parameters 169

8.3 Optical Gain Characteristics of RSOAs 170

8.4 Optimization of RSOA Operating Conditions 172

8.4.1 Optical Input Power and Bias Current Optimization 172

8.4.2 Optimization of Driving Current PTP 174

8.4.3 Capacity versus Reach Performance 175

8.5 Transmission Performance under Low-cost Optical Component-Enabled Practical Operating Conditions 176

8.5.1 Verification of the RSOA Intensity Modulator Model 177

8.5.2 Optical Input Power and Rear-facet Reflectivity Dependent Transmission Performance 179

8.5.3 Capacity versus Reach Performance 181

8.5.4 Impact of Negative Frequency Chirp 182

8.6 Conclusions 183

8.1 Introduction

In Chapters 6-7, the feasibility of utilizing SOAs as intensity modulators for IMDD AMOOFDM WDM-PONs has been thoroughly explored. It has been shown that SOA intensity modulators enable colourless AMOOFDM transmitters, this leads to significant enhancement on the wavelength control functionality and system flexibility for WDM-PONs.

As a special type of SOA, RSOA has also been implemented to facilitate colourless reflective ONUs for WDM-PONs, due to their salient advantages such as low component cost, compactness, low power dissipation, full coverage of the entire fibre transmission window and large-scale monolithic integration capability. Recently, use has already been made of RSOAs to achieve a wide range of key WDM-PON functionalities including, for example, intensity signal modulation [8.1], colourless network operation [8.2] and bidirectional transmission network architectures [8.3,8.4].

Therefore, it is greatly beneficial if use can be made of the advanced AMOOFDM modems incorporating RSOAs as intensity modulators in IMDD SMF transmission systems for WDM-PONs. Based on off-line DSP, experimental results have been reported of the transmission performance of RSOA intensity-modulated AMOOFDM signals over IMDD SMFs [8.5]. More recently, colourless real-time end-to-end OOFDM transmission at 7.5Gb/s over 25km SMFs has also been demonstrated experimentally using variable power loading and live-optimised RSOA intensity modulators with modulation bandwidths as narrow as 1GHz [8.6]. However, a number of crucial issues still remain unsolved, which are listed as followings:

- Identification of RSOA intensity modulator-associated physical mechanisms affecting significantly the system transmission performance.
- Investigation of the maximum achievable transmission performance of RSOA intensity-modulated AMOOFDM signals for various application scenarios.

- Optimization of the operating conditions of the RSOA intensity modulators for enhancing not only the transmission performance but also the system flexibility and performance robustness.
- Exploration of the feasibility of effectively utilizing the RSOA intensity modulation-induced frequency chirp to improve the transmission performance of WDM-PONs.

Compared to SOAs, the wide adoption of RSOAs as intensity modulators is mainly due to the fact that RSOAs have lower component cost, higher optical gain, smaller noise figure and larger optical signal ER [8.7,8.8]. However, SOAs exhibit better optical linearity as they have relatively higher input saturation powers. Therefore, extensive performance comparisons between RSOA and SOA intensity modulators are also of great importance for practical network designs.

Addressing all the aforementioned challenges forms the main topic of this chapter. In this chapter, detailed numerical simulations are undertaken to explore the transmission performance of RSOA intensity-modulated AMOOFDM signals in IMDD SMF systems for WDM-PONs without optical amplification and chromatic dispersion compensation. A comprehensive theoretical model describing the dynamic characteristics of RSOA intensity modulators is, for the first time, developed and experimentally verified rigorously using very recently developed real-time OOFDM transceivers at 7.5Gb/s [8.6]. Special attention is also given to performance comparisons between RSOA and SOA intensity modulators. Optimum RSOA operating conditions are identified, which are independent of RSOA rear-facet reflectivity and very similar to those corresponding to SOAs.

Whilst under low-cost optical component-enabled practical operating conditions, RSOA intensity modulators outperform considerably SOA intensity modulators in transmission performance, which decreases significantly with reducing RSOA rear-facet reflectivity and optical input power. In addition, simulation results also show that, for low optical input powers, use can be made of the RSOA/SOA intensity modulation-induced negative frequency chirp to improve the AMOOFDM transmission performance in WDM-PONs.

8.2 Transmission System Models

8.2.1 Transmission System and AMOOFDM Modems

In Fig. 8.1, the transmission system considered here is illustrated, which consists of an AMOOFDM transmitter, an in-line optical amplification-free IMDD SMF link without incorporating chromatic dispersion compensation, and an AMOOFDM receiver.

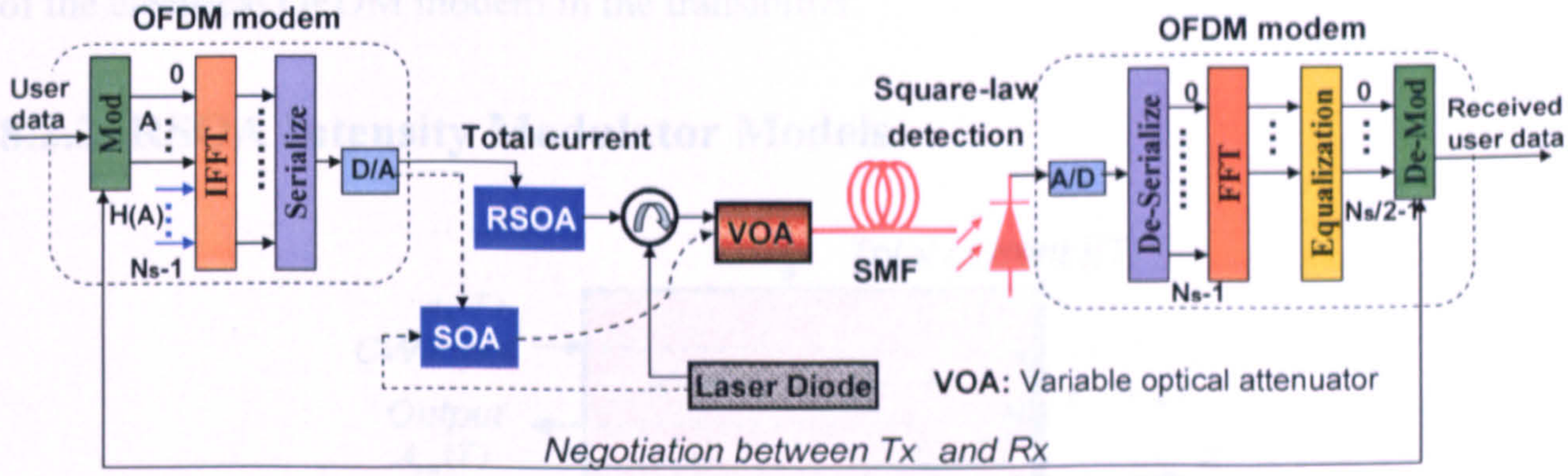

Fig. 8.1 Transmission system diagram together with block diagrams of the AMOOFDM transmitter and receiver.

The AMOOFDM transmitter is composed of an electrical OFDM modem, a RSOA/SOA intensity modulator subject to an injected CW optical wave at a desired optical wavelength and a specific optical power, an optical circulator and a variable optical attenuator. The use of the optical circulator is to separate the modulated AMOOFDM signal from the injected CW optical wave, and to prevent any backward propagating signals from re-entering the intensity modulator. The backward propagating signals may be produced by discrete optical reflection and Rayleigh backscattering in SMFs.

The generation, transmission and detection of the AMOOFDM signals are modelled following procedures similar to those reported in Chapters 6-7. The real-valued electrical signal emerging from the output of the electrical OFDM modem is up-shifted to ensure that each sample has a positive value. The up-shifted electrical signal is then attenuated as necessary and subsequently, together with a DC bias current, employed to directly drive the RSOA/SOA. The optical gain of the RSOA/SOA alters with the electrical current applied, the CW optical waveform injected into the RSOA/SOA is, therefore, modulated accordingly.

It should be noted that, the adjustment of the DC bias current and driving current is to enable the RSOA/SOA operating at optimum conditions. Such adjustment alters the output power of the modulated optical signal. An optical attenuator is therefore utilized to fix the optical power coupled into the SMF at a desired level.

At the AMOOFDM receiver end, the transmitted optical signal is detected using a square-law photo-detector. The received data is finally recovered following an inverse procedure of the electrical OFDM modem in the transmitter.

8.2.2 RSOA Intensity Modulator Models

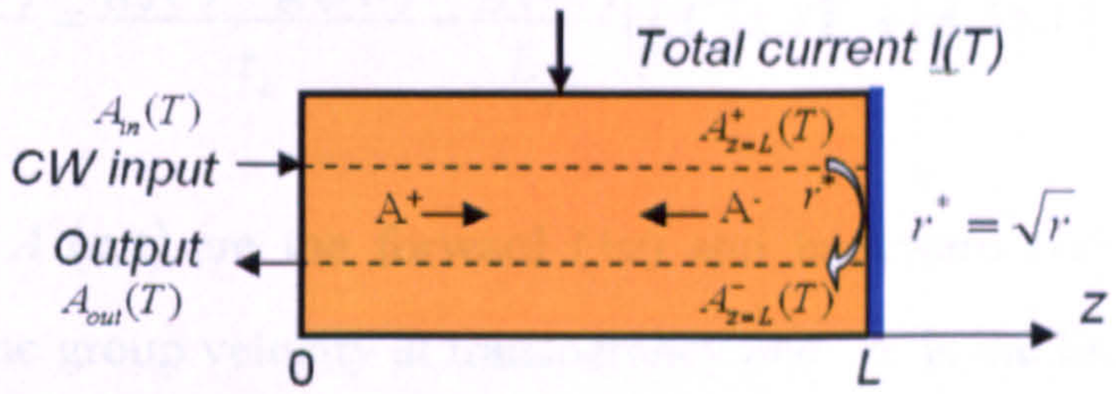

Fig. 8.2 Schematic diagram of RSOA intensity modulator.

The schematic diagram of the RSOA intensity modulator of a cavity length of L is shown in Fig. 8.2. A high reflective coating is applied at its rear-facet and a coating similar to that associated with a conventional SOA is applied at its front facet. The RSOA reflectivity, r, is denoted to as the RSOA rear-facet power reflectivity seen from the interior of the semiconductor waveguide. An optical signal is injected into the RSOA at z=0, and reflected at the rear facet at z = L. $A_{in}(T)$ is the injected optical field propagating forward along the cavity. $A_{out}(T)$ is the modulated backward propagating optical field at z=0.

The theoretical RSOA intensity modulator model developed here is a significant extension of the theoretical SOA intensity modulator models presented in Chapters 6-7, due to the inclusion of rear-facet reflectivity and dynamic optical gain saturation induced by counter-propagating optical signals. In developing the RSOA intensity modulator model, an assumption made in Chapters 6-7 is adopted, i.e., the impact of various ultrafast intraband dynamic processes including carrier heating, spectral hole-burning, two-photon absorption and ultrafast nonlinear refraction [8.9] are negligible, as the system configurations of OFDM modems adopted here are identical to those in Chapters 6-7. The validity of the developed RSOA intensity modulator model is verified by excellent agreement between

theoretical results obtained here and various experimental measurements at both device level [8.7,8.8] and system level [8.5,8.6].

Based on the comprehensive SOA theoretical model presented in [8.9,8.10], by taking into account Fig. 8.2 and after removing all the intraband dynamic processes, a set of coupled wave propagation equations for RSOAs are obtained

$$\pm\frac{\partial A^{\pm}(z,t)}{\partial z}+\frac{1}{v_g}\frac{\partial A^{\pm}(z,t)}{\partial t}=\frac{1}{2}g(z,t)(1-i\alpha)A^{\pm}(z,t) \tag{8.1}$$

$$\frac{\partial g(z,t)}{\partial t}=\frac{g_0(t)-g(z,t)}{\tau_c}-\frac{g(z,t)}{E_{sat}}\left(\left|A^{+}(z,t)\right|^2+\left|A^{-}(z,t)\right|^2\right) \tag{8.2}$$

where $A^{+}(z,t)$ and $A^{-}(z,t)$ are the forward (+z) and backward (-z) propagating optical signal fields. v_g is the group velocity at transparency and α is the linewidth enhancement factor. $g(z,t)$ is the optical gain defined as $g(z,t)=\Gamma a[N(t)-N_0]$ with $N(t)$ and N_0 being the carrier density and the carrier density at transparency, respectively. Here Γ is the confinement factor and a is the differential gain. $g_0(t)$ is the small signal gain, which can be expressed as $g_0(t)=\Gamma a N_0[I(t)/I_0-1]$, here $I(t)$ is the total injected current including the DC bias current and the driving current, and I_0 is the current required at transparency. τ_c is the carrier lifetime. $E_{sat}=\hbar\omega_0 wd/\Gamma a$ is the saturation energy with ω_0, w and d being the frequency of the optical signal, the width and depth of the RSOA active region, respectively. In Eq. (8.2), $\left|A^{+}(z,t)\right|^2+\left|A^{-}(z,t)\right|^2$ represents the total optical power carried by both the forward and backward propagating optical signals.

Following standard procedures presented in [8.10,8.11], when a transformation, $T=t-z/v_g$ with T being the time in a reference frame moving with the signal, is made to Eqs. (8.1) and (8.2), and when the optical field is defined as

$$A^{\pm}(z,T)=\sqrt{P^{\pm}(z,T)}\exp\left[j\phi^{\pm}(z,T)\right] \tag{8.3}$$

with $P^{\pm}(z,T)$ and $\phi^{\pm}(z,T)$ being the optical powers and optical phases of the forward and backward propagating signals, respectively, three equations governing $g(z,T)$, $P^{\pm}(z,T)$

and $\phi^{\pm}(z,T)$ can be derived. By integrating those equations over the entire RSOA cavity length L, a final set of equations describing the dynamic characteristics of the RSOA intensity modulator can be obtained:

$$\frac{dh(T)}{dT} = \frac{g_0(T)L - h(T)}{\tau_c} - \frac{P_{in}(T)}{E_{sat}}\{(\exp[\,h(T)] - 1)(1 + r\exp[\,h(T)])\} \tag{8.4}$$

$$P^{+}_{z=L}(T) = P_{in}(T)\exp[\,h(T)] \tag{8.5}$$

$$\phi^{+}_{z=L}(T) = \phi_{in}(T) - \frac{1}{2}\alpha h(T) \tag{8.6}$$

$$P_{out}(T) = P^{-}_{z=L}(T)\exp[h(T)] = rP_{in}(T)\exp[2h(T)] \tag{8.7}$$

$$\phi_{out}(T) = \phi^{-}_{z=L}(T) - \frac{1}{2}\alpha h(T) = \phi_{in}(T) - \alpha h(T) \tag{8.8}$$

In deriving Eqs. (8.4)-(8.8), $h(T)$ is defined as $h(T) = \int_0^L g(z,T)dz$, and the power and phase of the backward propagating optical signal at $z=L$ are written as

$$P^{-}_{z=L}(T) = rP^{+}_{z=L}(T) \tag{8.9}$$

$$\phi^{-}_{z=L}(T) = \phi^{+}_{z=L}(T) \tag{8.10}$$

$P_{in}(T)$ and $\phi_{in}(T)$ are the power and phase of the injected optical signal at z=0. $P_{out}(T)$ and $\phi_{out}(T)$ are the power and phase of the modulated output optical signal at z=0. The constant phase variation induced by the rear-facet reflection is not considered in Eq. (8.10). When the forward propagating optical signal is considered only, i.e, r = 0, Eqs. (8.4)-(8.8) are reduced to the forms identical to Eqs. (6.5)-(6.7) or Eqs. (7.2)-(7.4), which are used to simulate the dynamic characteristics of the SOA intensity modulator.

Apart from intensity modulation, the RSOA also imposes ASE noise onto the modulated optical signal. The total ASE power, P_{ASE}, can be calculated by [8.12]

$$P_{ASE} = (N_f G - 1) B_0 \hbar\omega_0 \tag{8.11}$$

where N_f is the RSOA noise figure, $G = r\exp[2h(T)]$ according to Eq. (8.7), is the optical gain. B_0 is the optical bandwidth and $\hbar\omega_0$ is the photon energy. After adding the ASE noises into $P_{out}(T)$ and $\phi_{out}(T)$, by using Eq. (8.3), the RSOA intensity modulated optical signal can be obtained. In the receiver, the transmitted optical signal is detected using a photon detector when a CW optical wave is chosen in the transmitter.

8.2.3 SMF and PIN Models

A standard theoretical SMF model which has been used in Chapters 4-7 is adopted here. In the receiver, a square-law photon detector utilized in Chapters 6-7 is considered here.

8.2.4 Simulation Parameters

In simulating the AMOOFDM modems, the parameters identical to those presented in Chapters 6-7 are adopted here. In addition, 1500 AMOOFDM symbols are employed here, which, prior to transmission over a SMF link, is oversampled to give a total number of sample points of 512488.

The parameters used in simulating the RSOA intensity modulator are representative for InGaAsP semiconductor materials at 1550nm, which are listed in Table 8.1. For fair performance comparisons between RSOAs and SOAs, in simulating the performance of the SOA intensity modulators, the same set of parameters are also employed, except that r is set to zero for the SOA intensity modulators. It should be pointed out, in particular, that, to obtain the RSOA/SOA parameters and examine the validity of the developed RSOA/SOA intensity modulator model, as discussed in Section 8.5, fitting the experimental measurements [8.6] with the numerical results are undertaken prior to performing numerical simulations at both device and system levels. During the fitting procedures, all the RSOA/SOA parameter values obtained in the experiments are treated as constants, and all the parameter values which are not exactly known are initially taken from Table 6.1 and Table 7.1 and subsequently adjusted within reasonable limits to obtain the best fit with all the experimental results [8.6].

The values of parameters of SMF and PIN detector are identical to those listed in Table 6.1 and Table 7.1. The optical power coupled into the transmission link is fixed at 6.3dBm. As in typical WDM-PONs nonlinear WDM impairments are negligible and the RSOA/SOA colourless operation capability has also been confirmed in [8.5,8.6] and Chapter 7, a single wavelength of 1550nm is, therefore, considered throughout this chapter.

Table 8.1 RSOA and SOA Parameters

RSOA & SOA	
Symbol	**Value**
L	300μm
w	1.5μm
d	0.27μm
τ_c	0.3ns
Γ	0.45
a	$3\times10^{-20}m^2$
α	5
N_0	$1.2\times10^{24}m^{-3}$
v_g	$8.43\times10^{7}m/s$
ω_0	1550nm
N_f	8dB

8.3 Optical Gain Characteristics of RSOAs

To gain an in-depth understanding of the simulated results presented in all the following sections, here brief discussions are first made of the RSOA optical gain characteristics with special emphases being given to optical gain differences between RSOAs and SOAs. Throughout this chapter, the optical gains for the RSOA and the SOA are defined as

$$G_{RSOA}(T)=P_{out}(T)/P_{in}(T)=r\exp[2h(T)] \tag{8.12}$$

$$G_{SOA}(T)=P^{+}_{z=L}(T)/P_{in}(T)=\exp[h(T)] \tag{8.13}$$

The simulated RSOA/SOA optical gain versus CW optical input power and bias current are plotted in Fig. 8.3 for different RSOA rear-facet reflectivity values. In obtaining Fig. 8.3, a 10 GHz sinusoidal electrical driving current having a fixed PTP value of 40mA is applied to ensure that the RSOA/SOA operating conditions discussed here are similar to those adopted in other figures of the chapter.

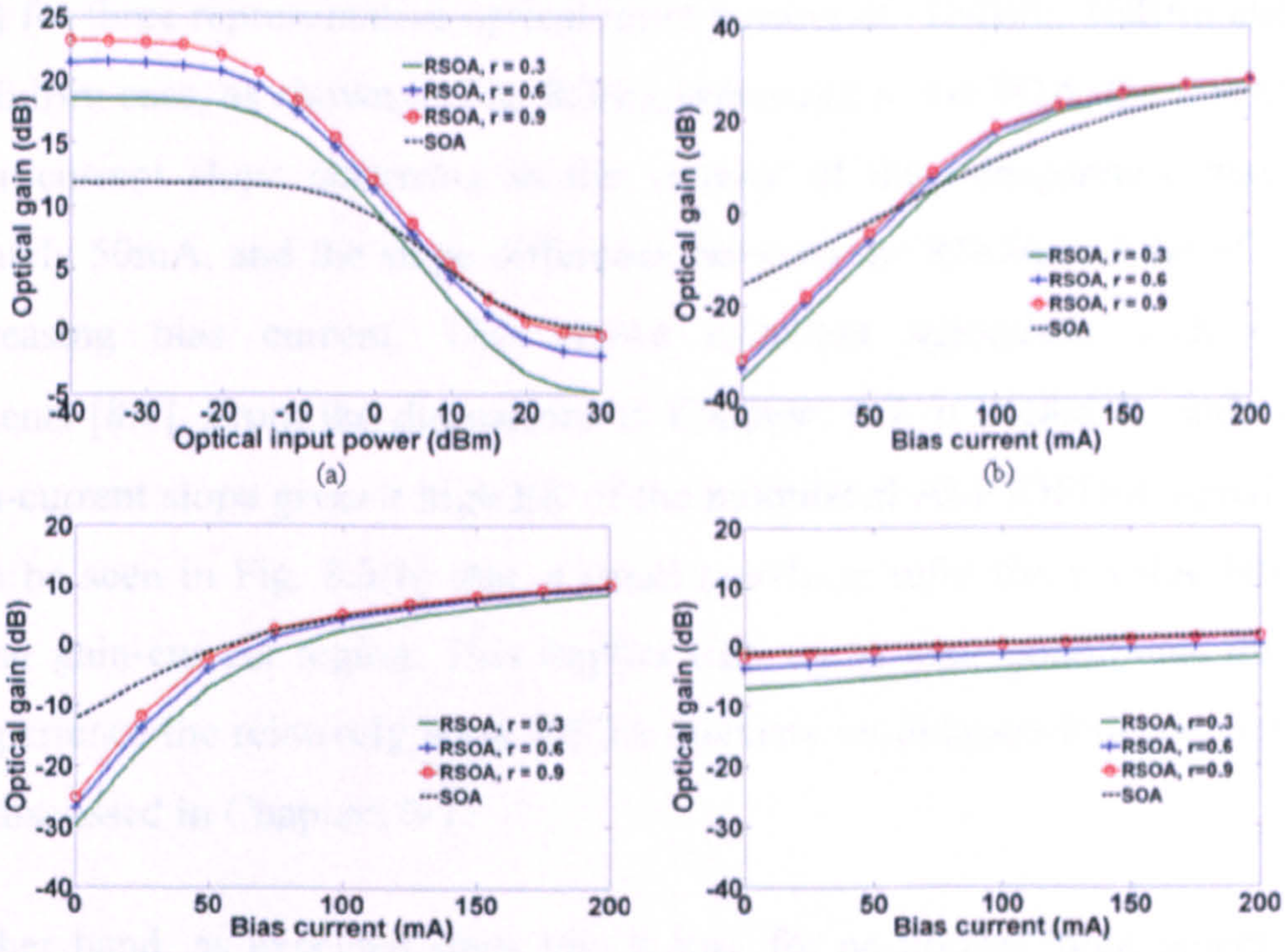

Fig. 8.3 RSOA/SOA optical gain characteristics under different operating conditions. (a) Optical gain versus optical input power with the bias current being fixed at 100mA. (b)-(d) Optical gain versus bias current for different optical input powers: -10dBm for (b); 10dBm for (c) and 22.5dBm for (d).

It can be seen from Fig. 8.3 that the RSOA and the SOA have similar optical gain evolution trends, except that considerable optical gain differences occur under specific operating conditions. As shown in Fig. 8.3(a), for optical input powers of <-10dBm, in comparison with the SOA, the RSOA has a much larger optical gain (smaller input saturation power), which increases (decreases) with increasing rear-facet reflectivity value. Such behaviors agree very well with experimental results reported in [8.7]. Whilst over the strongly saturated optical gain region corresponding to optical input powers of >10dBm, the optical gain differences between the RSOA and the SOA become very small and the RSOA exhibits a lower optical gain. This is because, under such cases, both devices have similar material optical gains of approximately 0dB, corresponding to which the RSOA rear-facet reflection-induced loss becomes pronounced.

Given the central role of the characteristics of optical gain versus electrical current in determining the quality of RSOA/SOA modulated AMOOFDM signals, the gain-current curves for various rear-facet reflectivity values are plotted in Fig. 8.3(b), Fig. 8.3(c) and

Fig. 8.3(d) for three representative optical input powers of -10dBm, 10dBm and 22.5dBm. For the -10dBm case, as shown in Fig. 8.3(b), compared to the SOA, the RSOA exhibits a stiffer gain-current slope occurring in the vicinity of the transparency bias current of approximately 50mA, and the slope difference between the RSOA and the SOA decreases with increasing bias current. This shows excellent agreement with experimental measurements [8.8]. From the discussions in Chapters 6-7, it is easy to understand that a sharp gain-current slope gives a high ER of the modulated AMOOFDM signal. Moreover, it can also be seen in Fig. 8.3(b) that, a small rear-facet reflectivity value brings about a broad linear gain-current region. This implies that, under such conditions, the modulated signals experience the relatively weak RSOA intensity modulation-induced signal clipping effect, as discussed in Chapters 6-7.

On the other hand, as expected from Fig. 8.3(a), for an optical input power of 10dBm, almost identical gain-current curves are observed in Fig. 8.3(c) over the positive optical gain region for both the RSOA and the SOA. In particular, very similar gain-current curves between the RSOA and the SOA are observed over both the positive and negative optical gain regions when the optical input power is increased to 22.5dBm, as shown in Fig. 8.3(d). This suggests that, under the strongly saturated optical gain region, the quality of RSOA modulated AMOOFDM signals is similar to that modulated by SOAs.

8.4 Optimization of RSOA Operating Conditions

The aim of this section is two-fold: a) understanding various physical mechanisms underpinning the transmission performance of the RSOA-based AMOOFDM modems in IMDD SMF systems; b) exploring the maximum transmission performance of the modems without considering practical limitations set by cheap components that have been made commercially available.

8.4.1 Optical Input Power and Bias Current Optimization

As the RSOA optical gain characteristics depend strongly upon its operation conditions, therefore, it is necessary to identify optimum RSOA operating conditions to maximize the transmission performance of the RSOA-modulated AMOOFDM signals. For a 60km IMDD SMF transmission system, Fig. 8.4 shows contour plots of signal line rate as a

function of CW optical input power and bias current for different RSOA rear-facet reflectivity values. For comparisons, the corresponding performance for the SOA-modulated AMOOFDM signals is also plotted in Fig. 8.4 (d). The driving current with a fixed PTP of 80mA is considered for both the RSOA and SOA cases. In numerical simulations, the signal line rate is calculated using the expression given by Eq. (2.52). The signal line rate is considered to be valid only when the total channel BER, BER_T, equals 1.0×10^{-3} is satisfied for a specific transmission system. BER_T is defined in Eq. (2.51).

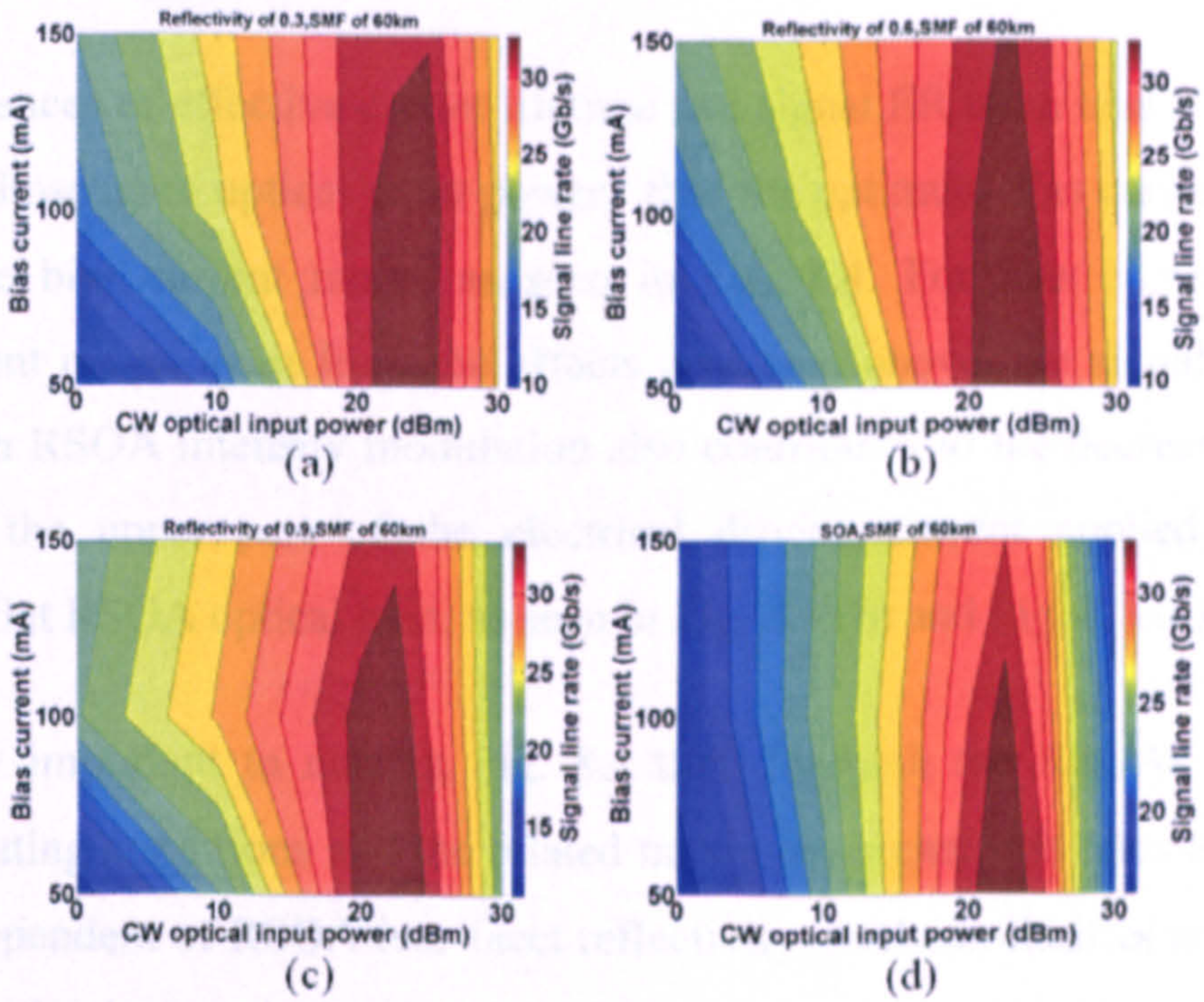

Fig. 8.4 Contour plots of signal line rate as a function of CW optical input power and bias current for RSOAs with different rear-facet reflectivity values of 0.3 in (a), 0.6 in (b) and 0.9 in (c) and SOAs in (d). An IMDD 60km SMF transmission system is considered.

Fig. 8.4 shows that, for a RSOA with any rear-facet reflectivity value, there exist an optimum bias current and an optimum optical input power, corresponding to which a maximum signal line rate is obtained. From discussions in Section 8.3, it is clear that, over the identified optimum conditions, the RSOA operates at a highly saturated optical gain region. The physical mechanisms behind the occurrence of the optimum operating conditions are the co-existed effects of effective carrier lifetime, which is defined in Eq. (3.1), and ER of modulated AMOOFDM signals: a large optical input power and/or a high bias current give rise to a short effective carrier lifetime, which corresponds to a large RSOA modulation bandwidth, thus leading to reduced spectral distortions imposed on the

modulated AMOOFDM signals. On the other hand, an increase in optical input power and/or bias current also brings about a reduction in ER of modulated AMOOFDM signals, thus resulting in an increase in minimum OSNR required for achieving a specific BER. For optical input powers (bias currents) less than the identified optimum value, the improvement in transmission capacity for high optical input powers (bias currents) is mainly due to the reduction in effective carrier lifetime; whilst when optical powers (bias currents) exceed the optimum value, the reduction in signal ER becomes a major contributor to the AMOOFDM performance degradation observed in Fig. 8.4.

As the dependences of effective carrier lifetime and signal ER upon bias current are not as significant as those upon optical input power, thus the optimum bias current occurs over a relatively wide bias current range, as seen in Fig. 8.4. For bias currents beyond the optimum current range, apart from the effects discussed above, the signal clipping effect associated with RSOA intensity modulation also contributes to the decrease in signal line rate, because the upper part of the electrical driving current applied to the RSOA experiences a flat RSOA optical gain, as seen in Fig. 8.3 (b) and Fig. 8.3 (c).

It is also very important to note in Fig. 8.4 that, for both the RSOAs and SOAs, the optimum operating conditions and the related maximum signal line rates are very similar, which are independent of RSOA rear-facet reflectivity. Such similarities are a direct result of the almost identical optical gains and gain-current slopes for these two components operating at highly saturated optical gain regions, as shown in Fig. 8.3(d).

8.4.2 Optimization of Driving Current PTP

The impact of driving current PTP on the maximum AMOOFDM transmission performance is explored in Fig. 8.5 for different rear-facet reflectivity RSOAs subject to various optical input powers including 22.5dBm (optimum), 10dBm and -10dBm. In obtaining Fig. 8.5, use is made of the identified optimum bias current of 100mA, and the transmission distance is fixed at 60km.

Fig. 8.5 shows that, under the identified optimum optical input power and bias current, there exists an optimum driving current PTP value of 80mA, regardless of the variation in RSOA rear-facet reflectivity. The occurrence of the optimum driving current PTP is due to the co-existence of the PTP-dependent effects of signal ER and signal clipping: a high

(small) PTP value produces a modulated AMOOFDM signal with a large (small) ER, which, however, suffers the strong (weak) signal clipping effect, as seen in Fig. 8.3. The observed rear-facet reflectivity independence of the optimum driving current PTP can be explained by considering Fig. 8.3(c) and Fig. 8.3(d), where almost identical gain-current curves under heavily saturated optical gain regions are shown for different rear-facet reflectivity values.

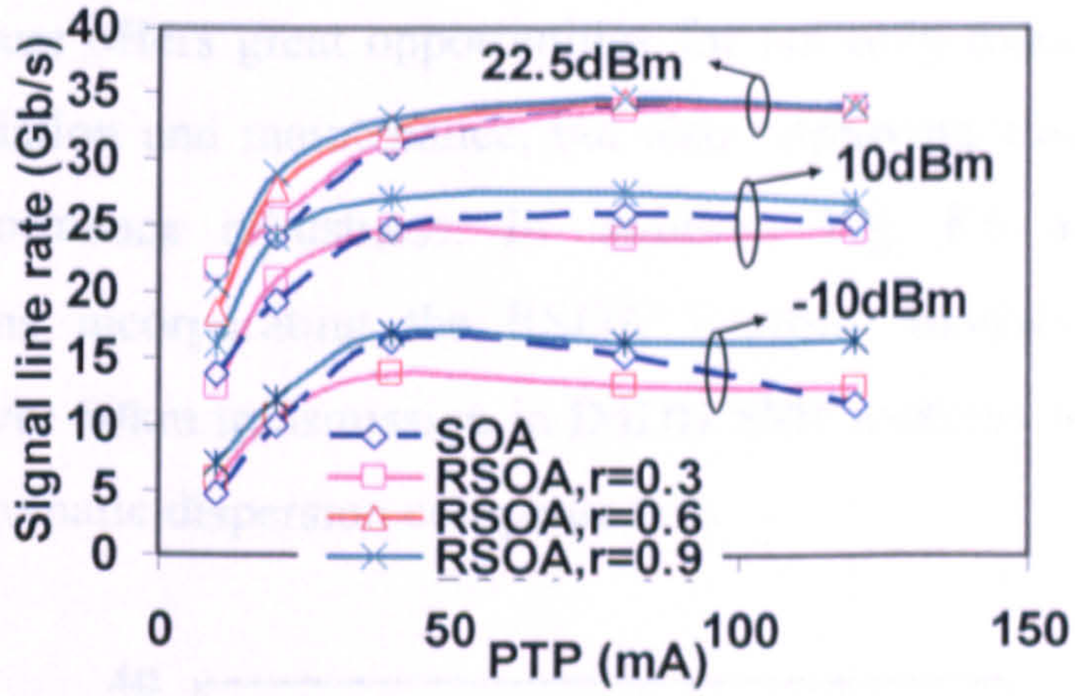

Fig. 8.5 Signal line rate versus PTP value of driving current for different RSOA rear-facet reflectivity and optical input powers.

It can also be seen in Fig. 8.5 that the optimum driving current PTP value decreases with decreasing optical input power. As an example, when the optical input power drops from 22.5dBm to -10dBm, the optimum driving current PTP value reduces from 80mA to 40mA. Comparisons among Fig. 8.3(b), Fig. 8.3(c) and Fig. 8.3(d) indicate that, for a small optical input power, the gain-current curve in the vicinity of the adopted bias current has a stiff slope and corresponds to a relative short linear region. To maximize the transmission performance, a small driving current PTP is, therefore, essential to balance appropriately the effects of signal ER and signal clipping.

8.4.3 Capacity versus Reach Performance

First of all, it is worth mentioning that the previously identified optimum RSOA operating conditions are independent of transmission distance. Based on these optimum operating parameters including a CW optical input power of 22.5dBm, a bias current of 100mA and a driving current PTP of 80mA, the maximum transmission capacity versus reach performance of the RSOA modulated AMOOFDM signals is plotted in Fig. 8.6 for

different rear-facet reflectivity values. It is very interesting to note in Fig. 8.6 that, under the above-mentioned optimum conditions, the transmission performance of RSOA-modulated AMOOFDM signals is, as expected from above discussions, almost identical to that corresponding to SOA-modulated AMOOFDM signals, and also independent of rear-facet reflectivity over the entire transmission distance range of interest of the present chapter. This means that, without sacrificing the system performance, use can be made of a great diversity of RSOAs and/or SOAs as intensity modulators in IMDD AMOOFDM systems. Such a feature offers great opportunities for not only reducing significantly the cost in system installation and maintenance, but also improving considerably the system flexibility and performance robustness. In addition, Fig. 8.6 also shows that the AMOOFDM modems incorporating the RSOA intensity modulators are capable of supporting 30Gb/s over 60km transmission in IMDD SMF systems without in-line optical amplification and chromatic dispersion compensation.

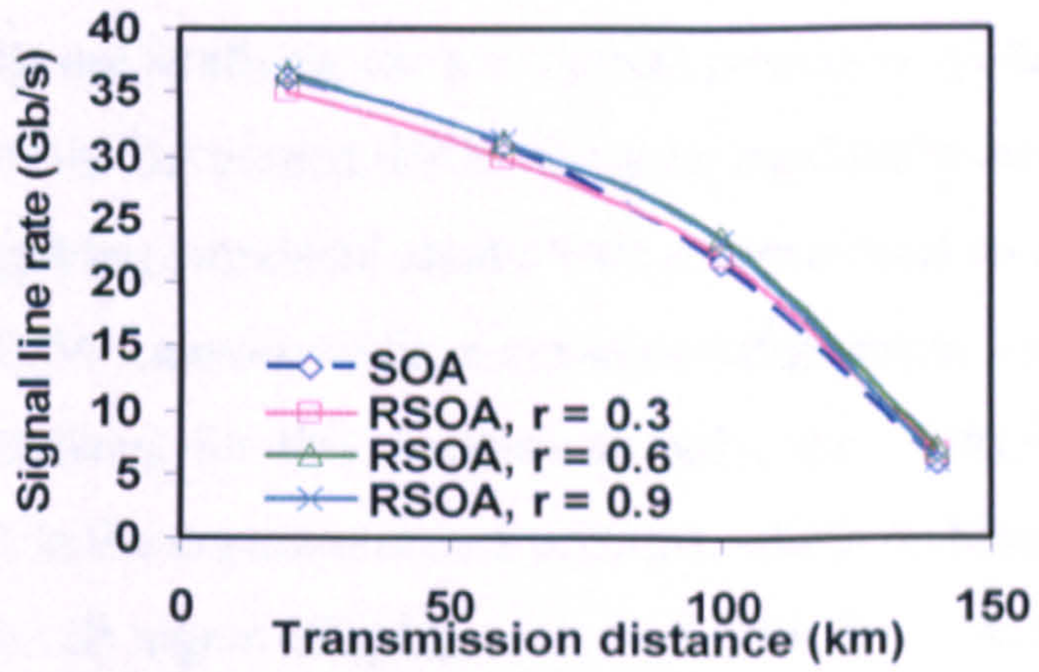

Fig. 8.6 Signal line rate versus transmission distance for RSOA and SOA intensity modulators operating under identified optimum conditions.

8.5 Transmission Performance under Low-cost Optical Component-Enabled Practical Operating Conditions

The RSOA optimum operating conditions identified in Section 8.4 require a CW optical input power as large as 22.5dBm. To satisfy such a requirement, a typical semiconductor laser followed by an optical amplifier needs to be incorporated into the RSOA intensity modulator. Clearly, this approach may result in costly RSOA-based AMOOFDM modems.

To enable the cost-effective practical implementation of the RSOA-based AMOOFDM modems in ONUs, use can be made of two promising strategies: a) a single tunable semiconductor laser in each RSOA intensity modulator, and b) a central light source supplied by the central office. The first technical solution makes economic sense because of the availability of commercial tunable semiconductor lasers at a price of a few hundred U.S. dollars. The second technical strategy can enhance the wavelength control functionality of WDM-PONs. Given the fact that, without utilizing optical amplifiers to boost the CW light power in ONUs, these two low-cost solutions are just capable of providing the RSOAs with optical input powers of typically <10dBm, therefore, it is of great importance if detailed explorations of the practically achievable transmission performance of the RSOA-based AMOOFDM modems subject to the aforementioned optical powers provided by low-cost optical components.

8.5.1 Verification of the RSOA Intensity Modulator Model

As experimental results are available for low optical powers only, here effort is first made to verify the validity of the developed RSOA intensity modulator model at both device and system levels, by comparing simulated results with experimental measurements using real-time end-to-end OOFDM transceivers in a system configuration similar to Fig. 8.1 [8.6]. To ensure fair comparisons, for this comparison only, the OOFDM modem parameters identical to those used in the experiments are adopted, which include 32 subcarriers in total, 25% cyclic prefix, 14.5dB signal clipping ratio, and 8-bit DAC/ADC operating at 4GS/s, as well as 16-QAM taken on all the 15 information-bearing subcarriers (whose powers are adjusted to compensate for the system frequency response roll-off effect [8.6]). The above parameters give a signal line rate of 6Gb/s (a raw signal line rate of 7.5Gb/s). In addition, the system parameters used in the numerical simulations are also identical to those adopted in the experiments [8.6]. These system parameters are listed as followings: an electrical OFDM signal with a PTP of 42mA, a DC bias current of 84mA, a CW optical input power of 5dBm, a 25km SMF, a received optical signal power of -5.5dBm and a receiver sensitivity of -17dBm. All other parameters that are not explicitly mentioned above are listed in Section 8.2.4.

RSOA frequency response comparisons between the numerical results and experimental measurements are made in Fig. 8.7(a), where excellent agreements between these two cases are observed over the entire signal spectral region of 0-2GHz. It can also be found in

Fig. 8.7(a) that, the RSOA intensity modulator has a 3dB modulation bandwidth of approximately 1.25GHz, which is mainly determined by the low CW optical input power-induced long effective carrier lifetime.

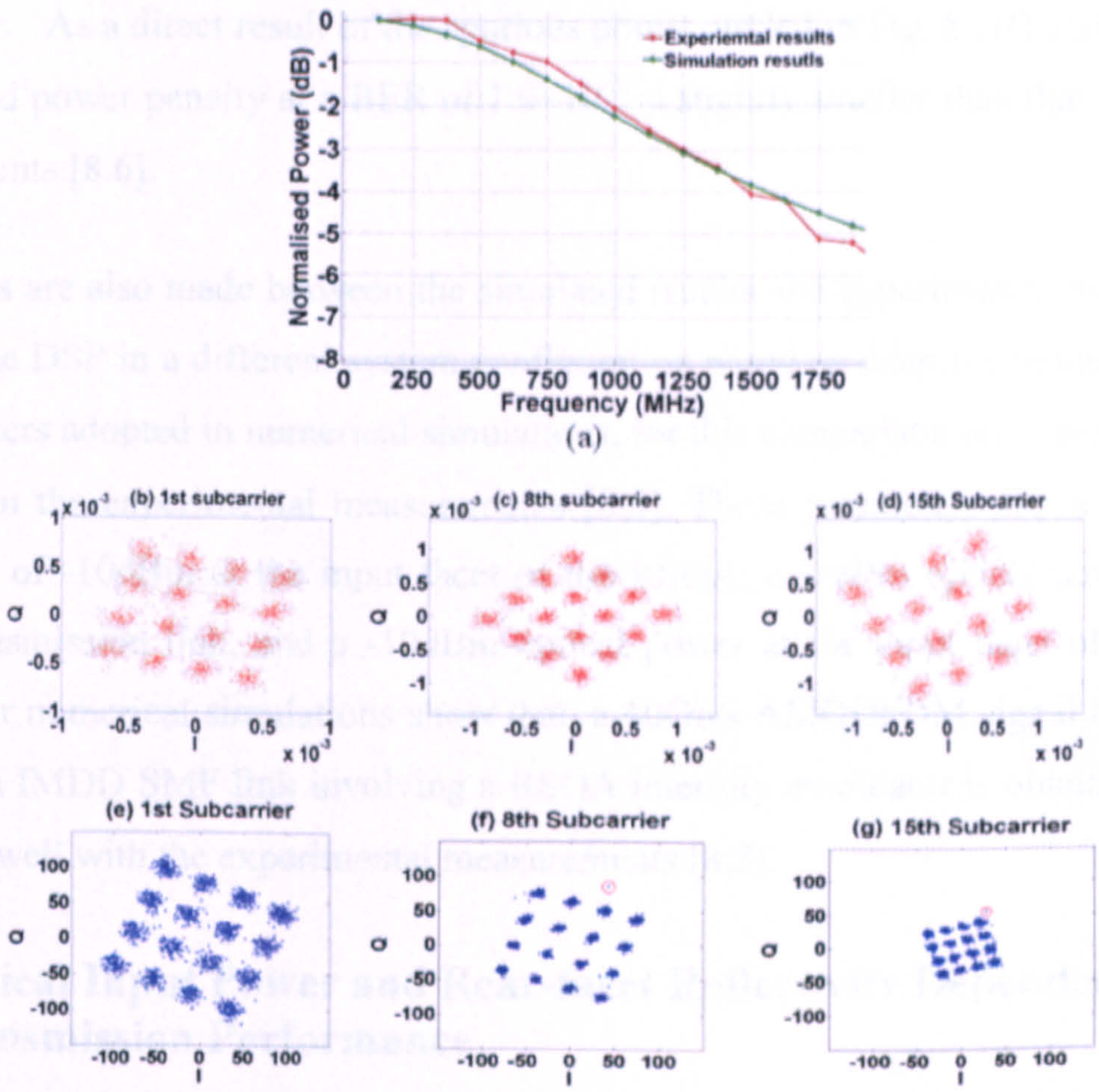

Fig. 8.7 Comparisons between simulations and real-time experimental measurements. (a) RSOA intensity modulator frequency response, and (b)-(g) constellations of representative subcarriers. (b)-(d) are simulated results and (e)-(g) are experimental results.

By adopting variable subcarrier powers similar to those reported in [8.6], and after transmission through 25km SMF, the representative subcarrier constellations recorded prior to channel equalization in the receiver, are also presented in Fig. 8.7, where the simulated constellations are shown in Fig. 8.7(b)-(d) and the corresponding experimentally measured constellations are shown in Fig. 8.7(e)-(g). Once again, the simulated results agree very well with the experimental measurements. In addition, in comparison with the experimental measurements, for the same subcarrier the numerical simulations also give very similar constellation rotation, which increases with increasing subcarrier frequency. The constellation rotation occurs due to the phase shift induced by fibre chromatic

dispersion. For high frequency subcarriers, the simulated constellation sizes are, however, larger than those measured in the experiments. This is due to the fact that the numerical simulations exclude the DAC/ADC-induced frequency response roll-off effect [8.6], which introduces extra losses to high frequency subcarriers, for example, a loss of 8dB for the15-th subcarrier. As a direct result of the spurious points circled in Fig. 8.7(f) and Fig. 8.7(g), the simulated power penalty at a BER of 1.0×10^{-3} is slightly smaller than that measured in the experiments [8.6].

Comparisons are also made between the simulated results and experimental measurements using off-line DSP in a different system configuration based on adaptive modulation [8.5]. The parameters adopted in numerical simulations, for this comparison only, are identical to those used in the experimental measurements [8.5]. These parameters are: a CW optical input power of -10dBm at the input facet of the RSOA, a -1dBm optical power coupled into the transmission link, and a -19dBm optical power at the input facet of the photon detector. Our numerical simulations show that, a 10Gb/s AMOOFDM signal transmission over a 20km IMDD SMF link involving a RSOA intensity modulator is obtainable, which agrees very well with the experimental measurements [8.5].

8.5.2 Optical Input Power and Rear-facet Reflectivity Dependent Transmission Performance

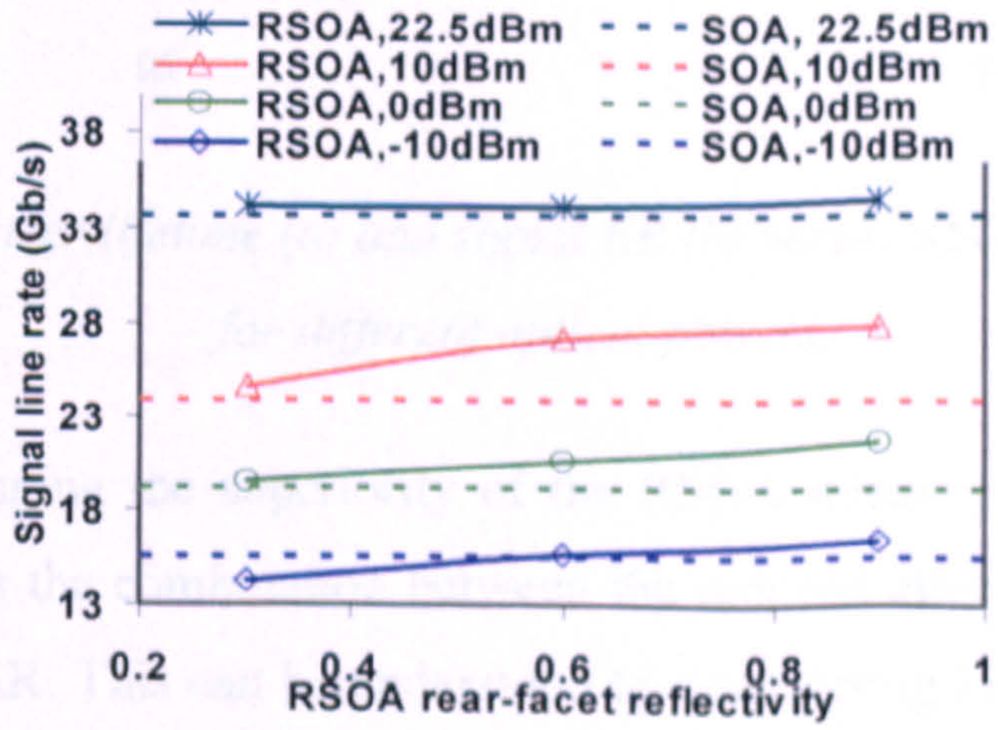

Fig. 8.8 Signal line rate versus rear-facet reflectivity value of RSOA subject to different optical input powers.

The dependence of the achievable signal line rate upon rear-facet reflectivity of a RSOA subject to three representative optical input powers of 10dBm, 0dBm and -10dBm is shown

in Fig. 8.8, where the bias current, the driving current PTP and the transmission distance are fixed at 100mA, 40mA (according to Fig. 8.5) and 60km, respectively. For performance comparisons between the optimum and practical operating conditions, the transmission performance achieved under the optimum operating conditions (22.5dBm optical input power), are also presented in Fig. 8.8, in which, once again, the corresponding transmission performance of the SOA-based intensity modulator is plotted for all the cases considered.

It is shown in Fig. 8.8 that, as expected from Fig. 8.4, the transmission performance drops quickly with decreasing optical input power. More importantly, in comparison with the SOA intensity modulator, the RSOA intensity modulator improves the AMOOFDM transmission performance, and such performance enhancement is more pronounced for high RSOA rear-facet reflectivity values.

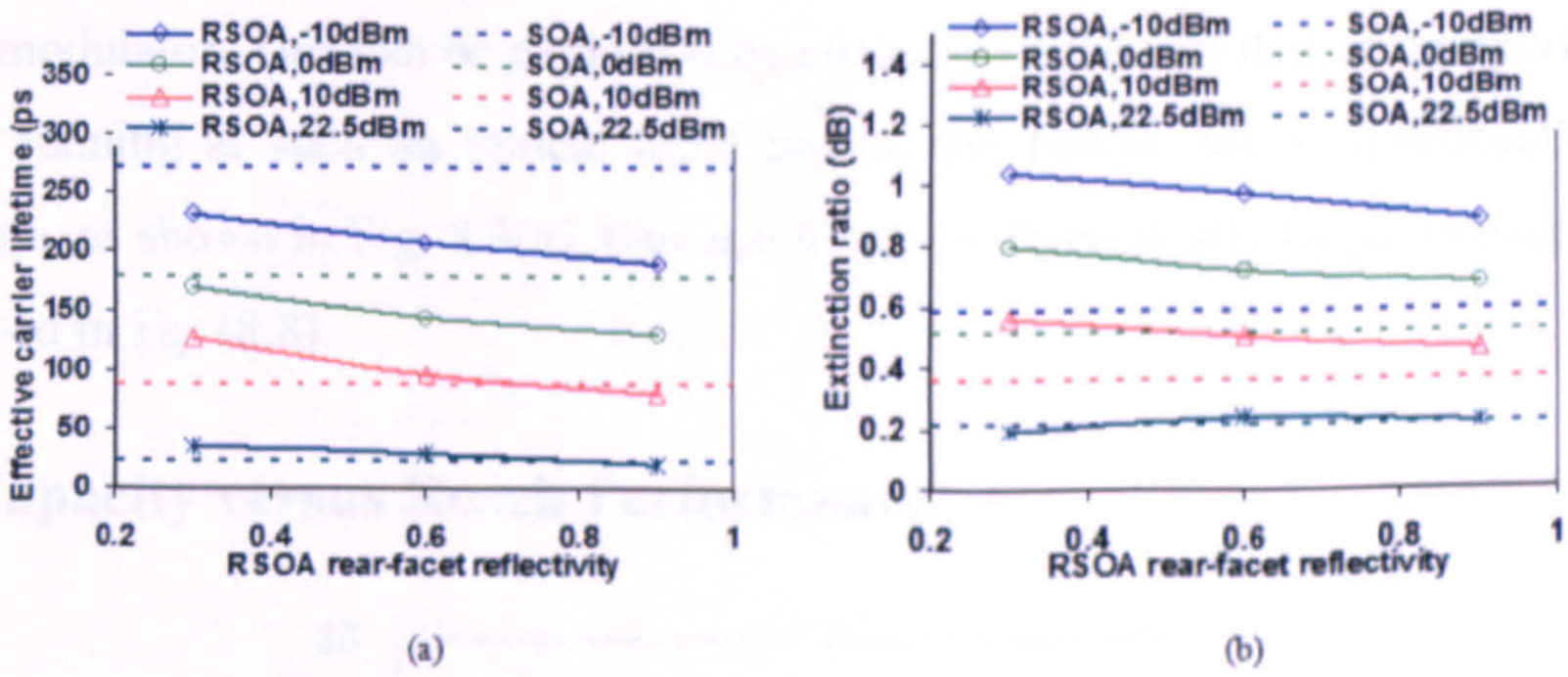

Fig. 8.9 Effective carrier lifetime (a) and signal ER (b) versus RSOA rear-facet reflectivity for different optical powers.

The physics underpinning the superiority of the RSOA intensity modulator to the SOA intensity modulator is the combination between the reduced effective carrier lifetime and the enhanced signal ER. This can be understood by considering Fig. 8.9. In obtaining Fig. 8.9, the simulation parameters identical to those adopted in Fig. 8.8 are considered. Fig. 8.9(a) shows that, compared to the SOA, the effective carrier lifetime of the RSOA is much shorter, thus giving rise to a wider modulation bandwidth. This is because, for an optical input power of <10dBm, the RSOA has a higher optical gain [as seen from Fig. 8.3(a)], thus leads to a larger optical output power, which is inversely proportional to the effective carrier lifetime [Eq. (3.1)].

The RSOA-induced enhancement in signal ER shown in Fig. 8.9(b) is in good agreement with experimental measurements [8.7]. Such enhancement is due to a small optical input power-induced stiff slope of the gain-current curve, as shown in Fig. 8.3(b). Furthermore, for a specific optical input power, a high RSOA rear-facet reflectivity leads to a large optical gain [Fig. 8.3(a)] and a slightly reduced slope of the gain-current curve [Fig. 8.3(b)]. As a direct result, both the RSOA effective carrier lifetime and the signal ER decrease with increasing rear-facet reflectivity, as seen in Fig. 8.9. For the practical optical input power range, it can be worked out easily from Fig. 8.9(a) that the RSOA modulation bandwidth is smaller than (or comparable to) the transmitted signal bandwidth.

It can also be seen in Fig. 8.9 that, for an optical input power of -10dBm and a RSOA rear-facet reflectivity value of 0.3, the RSOA outperforms the SOA in terms of both effective carrier lifetime and signal ER, but Fig. 8.8 shows that the RSOA intensity modulator supports the transmission performance slightly worse than that corresponding to the SOA intensity modulator. This can be explained by considering the fact that, in comparison with the SOA running at such an optical input power, the RSOA has a significantly higher optical gain, as shown in Fig. 8.3(a), thus resulting in a dramatically larger frequency chirp, as described in Eq. (8.8).

8.5.3 Capacity versus Reach Performance

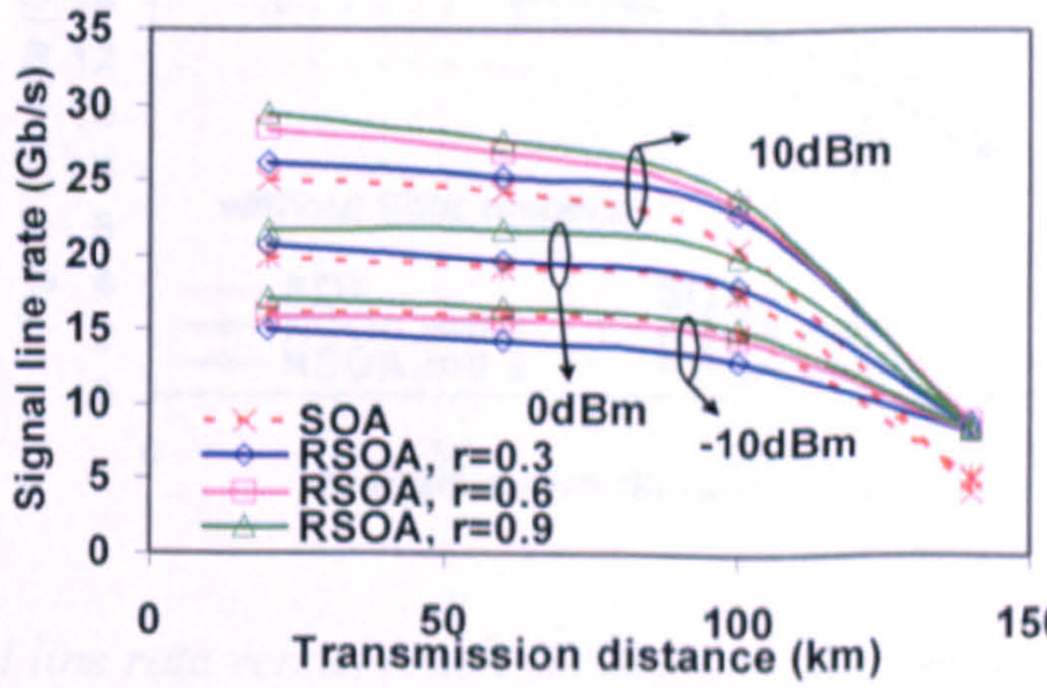

Fig. 8.10 Signal line rate versus reach performance for different optical input powers and rear-facet reflectivity values.

Fig. 8.10 shows the signal line rate versus reach performance of the RSOA/SOA intensity-modulated AMOOFDM signals for different practical optical input powers and rear-facet reflectivity values. In simulating Fig. 8.10, the parameters identical to those used in Fig.

8.9 are adopted. It is very interesting to note in Fig. 8.10 that, in comparison with the SOA intensity modulators, the RSOA intensity modulators subject to injected optical powers of >-10dBm are capable of improving the signal line rate over the entire transmission distance range including both the chromatic dispersion-dominant performance region (<100km) and the loss-dominant performance region (>100km) [8.13]. In addition, it can also be seen in Fig. 8.10 that, the use of RSOA intensity modulators is more effective in the loss-dominant performance region, as the RSOA enhanced signal ER can offset, to some extent, the transmission link loss.

Moreover, Fig. 8.10 also indicates that a RSOA having a large rear-facet reflectivity is always preferred, especially in the dispersion-dominant performance region. As an example, for an optical input power of 0dBm, an increase in RSOA rear-facet reflectivity from 0.3 to 0.9 can extend 20Gb/s AMOOFDM signal transmission distance from 60km to 100km. This confirms strongly the importance of the RSOA rear-facet reflectivity in determining the quality of the RSOA intensity modulated AMOOFDM signals under the practical operating conditions.

8.5.4 Impact of Negative Frequency Chirp

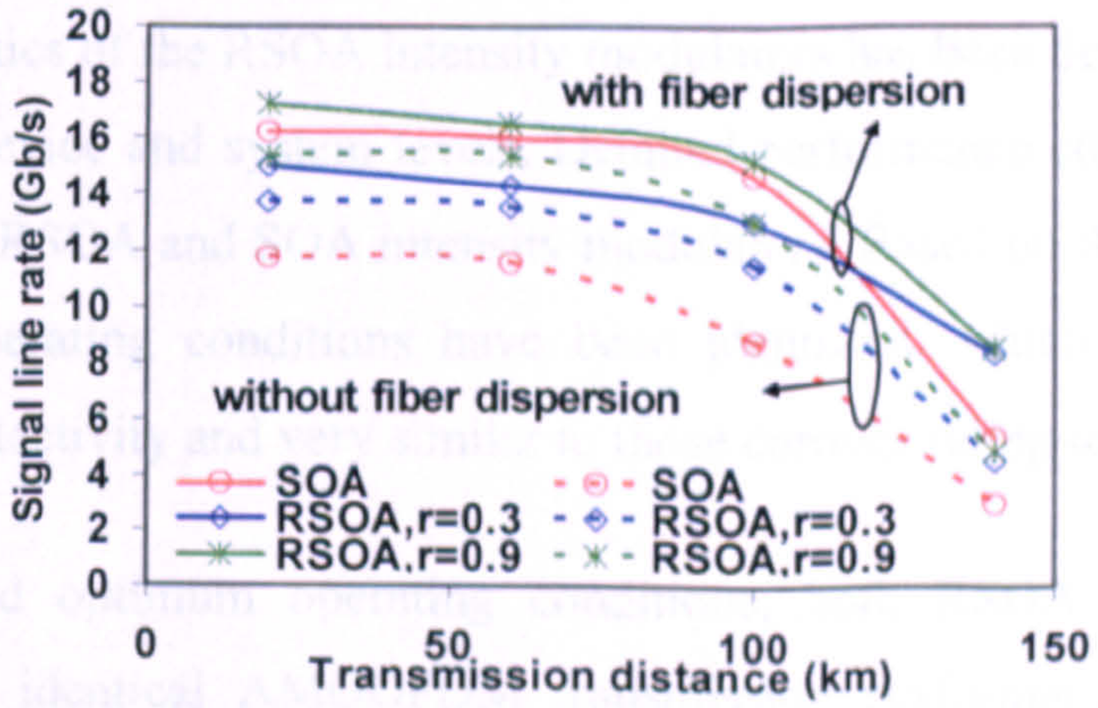

Fig. 8.11 Signal line rate versus reach performance for the cases of including and excluding chromatic dispersion. Optical input power is fixed at -10dBm.

Apart from cost-effectiveness, another benefit of employing a RSOA operating at low optical input powers is that it can produce a fair amount of controllable negative frequency chirp, which has an opposite sign compared to the dispersion parameter of a standard SMF.

Therefore, use can be made of such property to improve either the transmission capacity for a fixed link power budget, or the link power budget for a fixed transmission capacity.

To demonstrate the effectiveness of the aforementioned dispersion compensation approach for RSOA/SOA intensity modulated AMOOFDM signals in IMDD standard SMF transmission systems, in Fig. 8.11 performance comparisons are made for the cases of including and excluding chromatic dispersion. In Fig. 8.11 the optical input power is taken to be -10dBm. It can be seen in Fig. 8.11 that the "dispersion compensation" approach is capable of enhancing the transmission capacity over standard SMFs of up to 100km. It should be pointed out that, the RSOA negative frequency chirp is a function of operating conditions, suggesting that such dispersion compensation is dynamically controllable.

8.6 Conclusions

Extensive numerical simulations have been undertaken of exploring, for the first time, the transmission performance of RSOA modulated AMOOFDM signals over IMDD SMF transmission systems without in-line optical amplification and chromatic dispersion compensation for WDM-PONs. A comprehensive theoretical model describing the dynamic characteristics of the RSOA intensity modulators has been developed and verified rigorously at both device and system levels. Detailed performance comparisons have also been made between RSOA and SOA intensity modulators. Based on the theoretical model, optimum RSOA operating conditions have been identified, which are independent of RSOA rear-facet reflectivity and very similar to those corresponding to SOAs.

Under the identified optimum operating conditions, both RSOA and SOA intensity modulators support identical AMOOFDM transmission performances of 30Gb/s over 60km SMFs. Under low-cost optical component-enabled practical operating conditions, the RSOA intensity modulators with rear-facet reflectivity values of >0.3 outperform considerably the SOA intensity modulators in transmission performance, which increases significantly with increasing RSOA rear-facet reflectivity and optical input power. In addition, simulations also show that, for low optical input powers, RSOA/SOA intensity modulation-induced negative frequency chirp can be used to improve the AMOOFDM transmission performance in WDM-PONs.

References

[8.1] K. Y. Cho, Y. Takushima, and Y. C. Chung, "10-Gb/s operation of RSOA for WDM PON," IEEE Photon. Technol. Lett., vol. 20, no. 18, pp. 1533-1535 Sep. 2008.

[8.2] C. H. Yeh, C. W. Chow, C. H. Wang, F. Y. Shih, H. C. Chien, and S. Chi, "A self-protected colorless WDM-PON with 2.5 Gb/s upstream signal based on RSOA," Opt. Express., vol. 16, no. 16, pp. 12296-12301 Aug. 2008.

[8.3] W. Lee, M. H. Park, S. H. Chao, J. Lee, C. Kim, G. Jeong, and B. W. Kim, "Bidirectional WDM-PON based on gain saturated reflective semiconductor optical amplifiers," IEEE Photon. Technol. Lett., vo. 17, no.11, pp. 2460-2462 Nov. 2005.

[8.4] M. Omella, I. Papagiannakis, B. Schrenk, D. Klonidis, J. A. Lazaro, A. N. Birbas, J. Kikidis, J. Prat, and I. Tomkos, "10 Gb/s full-duplex bidirectional transmission with RSOA-based ONU using detuned optical filtering and decision feedback equalization," Opt. Express., vol. 17, no. 7, pp. 5008-5013 Mar. 2009.

[8.5] T. Duong, N. Genay, P. Chanclou, B. Charbonnier, A. Pizzinat, and R. Brenot, "Experimental demonstration of 10 Gbit/s for upstream transmission by remote modulation of 1 GHz RSOA using Adaptively Modulated Optical OFDM for WDM-PON single fiber architecture," presented at the European Conference on Optical Communication (ECOC), (Brussels, Belgium, 2008), PD paper Th.3.F.1.

[8.6] R.P. Giddings, E. Hugues-Salas, X.Q. Jin, J. L. Wei and J.M. Tang, "Colourless Real-Time Optical OFDM End-to-End Transmission at 7.5Gb/s over 25km SSMF Using 1GHz RSOAs for WDM-PONs," presented at the OFC/OFNEC, (OSA, 2010), Paper OMS4.

[8.7] L. Q. Guo, and M. J. Connelly, "A novel approach to all-optical wavelength conversion by utilizing a reflective semiconductor optical amplifier in a co-propagation scheme," Optics Communications., vol. 281, no. 17, pp. 4470-4473 Sep 2008.

[8.8] C. Arellano, and J. Prat, "Semiconductor optical amplifiers in access networks," presented at the International Conference on Transparent Optical Network (ICTON), (Barcelona, Catalonia, Spain, 2005), Paper We.A1.4.

[8.9] J. M. Tang and K. A. Shore, "Strong picosecond optical pulse propagation in semiconductor optical amplifiers at transparency," IEEE J. Quantum Electron., vol. 34, no. 7, pp. 1263-1269, July 1998.

[8.10] G. P. Agrawal, and N. A. Olsson, "Self-phase modulation and spectral broadening of optical pulses in semiconductor laser amplifiers," IEEE J. Quantum Electron., vol. 25, no.11, pp. 2297-2306 Nov. 1989.

[8.11] M. J. Connelly, *Semiconductor Optical Amplifiers*, (London: Kluwer, 2002).

[8.12] N. A. Olsson, "Lightwave systems with optical amplifiers," J. Lightwave Technol., vol. 7, no. 7, pp. 1071-1082, July 1989.

[8.13] J. M. Tang and K. A. Shore, "30Gb/s signal transmission over 40-km directly modulated DFB-based single mode fibre links without optical amplification and dispersion compensation," J. Lightw. Technol., vol. 24, no.6, pp. 2318-2327 Jun. 2006.

9 Wavelength Reused Bidirectional Transmission of AMOOFDM Signals in Colourless WDM-PONs Incorporating SOA and RSOA Intensity Modulators

Contents

9.1 Introduction 187

9.2 Theoretical Models 188

9.2.1 Wavelength-reused Bidirectional Transmission WDM-PON Architecture and AMOOFDM Modems Incorporating SOA and RSOA Intensity Modulators 188

9.2.2 SOA/RSOA Intensity Modulators 190

9.2.3 RB Noise 190

9.2.4 SMF and PIN Detector Models 193

9.2.5 Simulation Parameters 193

9.3 Transmission Performance 194

9.3.1 Verification of the RB Models 194

9.3.2 Downstream AMOOFDM Transmission Performance 195

9.3.3 Upstream AMOOFDM Transmission Performance and Optimization of RSOA Intensity Modulator Operating Conditions 196

9.4 SSB-SCM for Improving the Downstream and Upstream Transmission Performance 200

9.5 Conclusions 203

9.1 Introduction

In Chapters 6-8, we have investigated the use of RSOA/SOA intensity modulators to facilitate cost-effective colourless AMOOFDM transmitters for WDM-PON, with particular attention being focused on the AMOOFDM signal transmission in one direction only. From the system design point of view, it is highly beneficial if use is made of AMOOFDM in wavelength reused bidirectional transmission over a single SMF for WDM-PONs. In such wavelength reused WDM-PONs, a fraction of the downstream optical signal is fed into a RSOA intensity modulator for upstream data re-modulation in the ONU. Clearly, wavelength reuse improves both the cost-effectiveness and wavelength control functionalities of WDM-PONs. On the other hand, the bidirectional transmission of AMOOFDM signals over a single SMF significantly reduces the fibre installation and maintenance cost.

For the wavelength reused bidirectional WDM-PONs, a key issue is the impact of the effects of RB noise on the transmission performance of downstream and upstream AMOOFDM signals. Apart from the RB effect, another challenge of wavelength reused bidirectional WDM-PONs is how to suppress effectively crosstalk due to residual downstream optical signal-induced upstream signal fluctuations. To reduce the crosstalk effect, use can be made of a number of approaches listed as followings: a) an optical gain saturated SOA-based data eraser [9.1] to suppress the downstream optical signal prior to being re-modulated for transmitting upstream data; b) feed-forward current injection [9.2] in a RSOA intensity modulator to smooth the residual downstream optical signal waveform. Alternatively, use can also be made of different signal modulations for downstream and upstream signals. For example, downstream/upstream signal modulations can be Frequency Shift Keying (FSK)/On-Off Keying (OOK) [9.3], DPSK/OOK [9.4], Inverse Return-to-Zero (IRZ)/OOK [9.5], respectively. In all the above-mentioned signal modulation techniques, the constant downstream FSK and DPSK waveforms can reduce the crosstalk effect imposed on the RSOA intensity modulated upstream signals. However, OFDM modulation schemes in downstream/upstream as well as its crosstalk effects have not been investigated.

Moreover, given the fact that SOAs have many merits as stated in previous chapters, in addition to the RSOA intensity modulator in the ONU, the use of SOA intensity modulators in the OLT is also preferred to expensive external modulators. Such a SOA-based OLT and RSOA-based ONU configuration is capable of providing colourless WDM-PON operation (rather than just colourless ONUs), thus leading to a significant reduction in the installation and maintenance cost.

In this chapter, detailed numerical investigations are undertaken of wavelength reused bidirectional transmission of AMOOFDM signals in WDM-PONs incorporating a SOA and RSOA intensity modulator in the OLT and ONU, respectively. Based on the SOA and RSOA intensity modulator models developed in Chapter 6 and Chapter 8, respectively, a comprehensive theoretical model describing the performance of such network architecture is developed, taking into account the dynamic characteristics of the SOA and RSOA intensity modulators as well as the effects of RB noise and crosstalk. It is shown that the RB noise effect and the residual downstream optical signal-induced crosstalk are the dominant factors limiting the maximum achievable downstream and upstream transmission performances. Under optimum SOA and RSOA operating conditions as well as practical downstream and upstream optical launch powers, 10Gb/s downstream and 6Gb/s upstream over 40km SMF transmission of conventional DSB AMOOFDM signals are feasible. In particular, the aforementioned transmission performances can be improved to 23Gb/s downstream and 8Gb/s upstream over 40 km SMF when SSB-SCM is introduced in downstream systems.

9.2 Theoretical Models

9.2.1 Wavelength-reused Bidirectional Transmission WDM-PON Architecture and AMOOFDM Modems Incorporating SOA and RSOA Intensity Modulators

Fig. 9.1 illustrates the wavelength-reused bidirectional transmission WDM-PON architecture considered here, which consists of a SOA intensity modulator-based AMOOFDM downstream link and a RSOA intensity modulator-based AMOOFDM upstream link, both of which share the same optical wavelength and a single optical amplification- and dispersion compensation-free IMDD SMF system. The downstream link

is composed of an AMOOFDM transmitter, a SMF, a square-law photon detector and an AMOOFDM receiver. The downstream AMOOFDM transmitter includes an OFDM downstream transmitter, a laser diode, an SOA intensity modulator and a VOA. In the downstream OFDM transmitter, the generation of a real-valued electrical OFDM signal is modelled following a procedure similar to that described in Chapters 6-8. The real-valued electrical OFDM signal from the downstream OFDM transmitter is up-shifted, and then drives directly the SOA to modulate an injected optical CW wave by varying the SOA optical gain, as described in Chapters 6-7. Finally, the SOA intensity modulated AMOOFDM downstream signal is coupled and multiplexed, via a VOA, an optical circulator and a multiplexer, into a standard SMF.

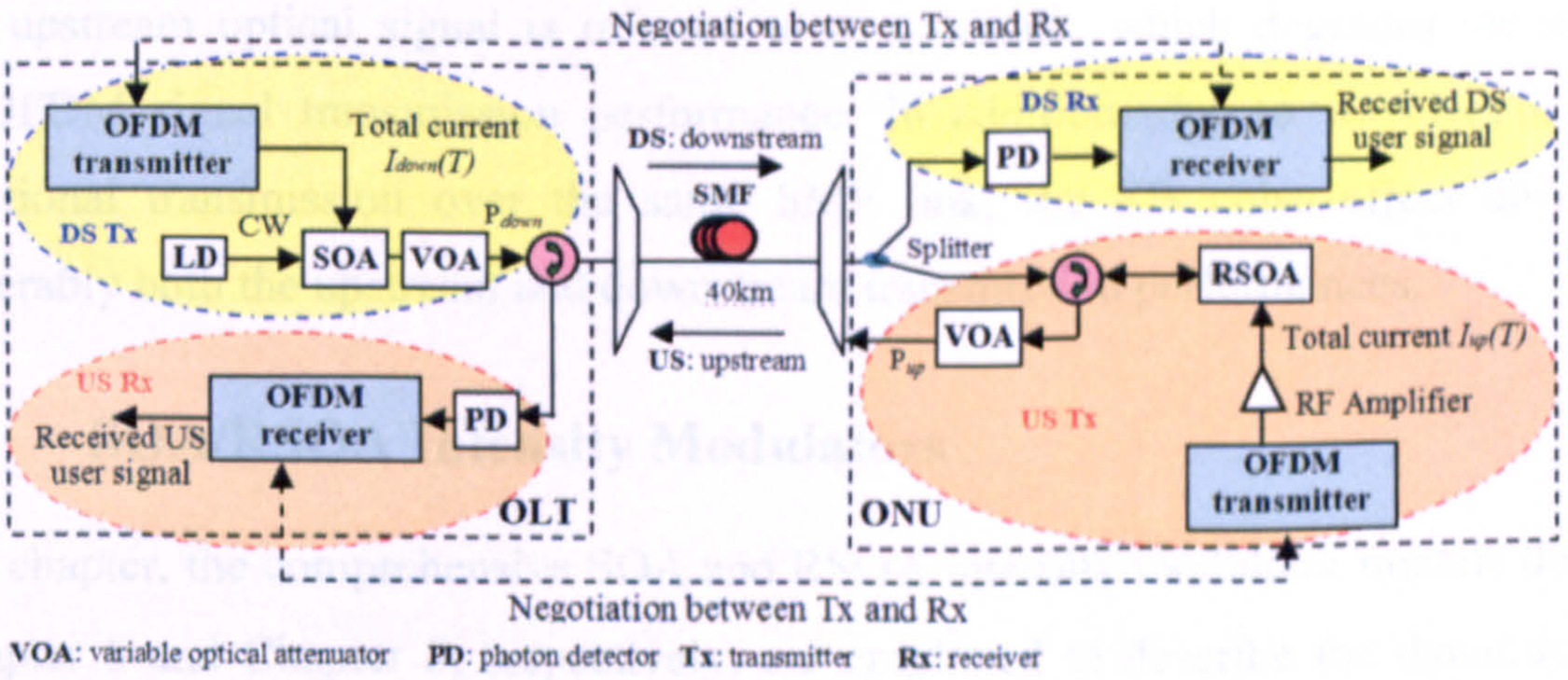

Fig. 9.1 Wavelength-reused bidirectional transmission WDM-PON architecture with SOA intensity modulated downstream AMOOFDM signals and RSOA intensity modulated upstream AMOOFDM signals.

After transmitting through the SMF, the received downstream AMOOFDM signal is de-multiplexed and subsequently split into two optical beams: the first one is detected using a square-law photon detector, and then recovered in the downstream OFDM receiver having an inverse procedure of the downstream OFDM transmitter.

On the other hand, the second optical beam split is utilized directly as an optical carrier of the upstream AMOOFDM signal. Via an optical circulator, the second optical beam is injected into a RSOA intensity modulator, which is driven by a real-valued up-shifted and electrically amplified OFDM signal generated by the upstream OFDM transmitter. In the RSOA intensity modulator, re-modulation of the injected downstream optical signal takes

place via the variation of the RSOA optical gain by the upstream electrical OFDM signal, as presented in Chapter 8 and [9.6]. The produced upstream AMOOFDM signal is coupled into the same SMF link compared to the downstream AMOOFDM signal. Here, an optical attenuator is employed to fix the coupled upstream optical power at a specific level. After upstream transmission through the SMF, the received AMOOFDM signal is detected by a square-law photon detector and recovered by an upstream OFDM receiver having an inverse procedure of the upstream OFDM transmitter.

From the above description, it is clear that, the residual downstream optical signal introduces waveform fluctuations into the RSOA modulated upstream AMOOFDM signal. Throughout this chapter, such a residual downstream signal-induced waveform distortion to the upstream optical signal is referred to as crosstalk, which degrades the upstream AMOOFDM signal transmission performance. In addition, due to wavelength re-used bidirectional transmission over the same SMF link, the RB noise effect also affects considerably both the upstream and downstream transmission performances.

9.2.2 SOA/RSOA Intensity Modulators

In this chapter, the comprehensive SOA and RSOA intensity modulator models developed in Chapter 6 and Chapter 8, respectively, are employed to describe the dynamic optical characteristics of the SOA/RSOA intensity modulated AMOOFDM signals. The validity of the SOA intensity modulator model has already been verified in Chapter 6. Also, the RSOA intensity modulator model was verified by comparisons between simulated results and experimental measurements using real-time end-to-end OOFDM transceivers, as detailed in Chapter 8.

9.2.3 RB Noise

It is well known [9.7-9.9] that, both RB noise and discrete reflection induced by passive components such as optical connectors may affect the system performance in bidirectional transmission systems. However, discrete reflection can be reduced to a level of 55 dB lower than that corresponding to the signal power, provided that the optical connectors with oblique end faces are applied [9.9]. For simplicity, in this chapter, the discrete reflection effect is not considered. In the WDM-PON architecture of interest of the present

chapter, the RB noise effect is, however, unavoidable, which mainly stems from two major sources:

- Downstream AMOOFDM signals. The associated RB noise affects upstream AMOOFDM signals.
- Upstream AMOOFDM signals. A fraction of the associated RB noise joins the downstream AMOOFDM signals, and the remaining part can be amplified and reflected by the RSOA intensity modulator, and finally joins the upstream signals.

Moreover, attenuation of downstream and upstream signals due to Rayleigh scattering is also included into the SMF attenuation coefficient.

First, we derive analytically the total RB noise power imposed on the upstream signal. For a downstream optical signal power launched into the SMF, P_{down}, which generates an upstream RB noise power at the output facet of the SMF, $P_{DD_{RB}}$, is given by [9.7]

$$P_{DD_{RB}} = P_{down} B(1 - e^{-2\mu L}) \tag{9.1}$$

where $B = S\alpha_s / 2\mu$ with α_s [km^{-1}] being the fiber scattering coefficient, S being the fiber recapture coefficient, and μ [km^{-1}] being the SMF attenuation coefficient. L is the fiber length. Depending upon the type of fibre and the selected wavelengths, for fiber links longer than 20km, $\zeta = B(1 - e^{-2\mu L})$ converges towards an almost constant value [9.8,9.9].

The value of ζ at 1550nm is measured in experiment with a system setup illustrated in Fig. 2.10(a). The measured results in Fig. 2.10(b) show that, for optical launch powers of approximately <7dBm, regardless of fibre length, ζ can be taken to be -34dB, which is, therefore, adopted in numerical simulations presented in this chapter. Whilst when CW launch powers exceed 7dBm, the SBS effect plays a dominant role in determining the backscattered optical power measured. Therefore, throughout this chapter, both downstream and upstream launch powers are limited to values of <7dBm.

The RB noise power contributed by the upstream optical signal and imposed on the upstream signal can be expressed as

$$P_{UD_{RB}} = \zeta P_{up} g_{ONU} e^{-\mu L} \tag{9.2}$$

where P_{up} is the upstream optical signal power launched into the SMF. g_{ONU} is the total optical gain of the upstream AMOOFDM transmitter , and is defined as

$$g_{ONU} = \frac{P_{up}}{P_{down} e^{-\mu L}} \tag{9.3}$$

Considering Fig. 9.1 and Eq. (9.3), it is clear that, g_{ONU} includes RSOA optical gain, splitter loss (-3dB), optical circulator insertion loss and optical attenuator loss. Based on Eqs. (9.1)-(9.3), the Optical Signal to RB Noise Ratio (OSRNR) of the upstream signal at the output facet of the upstream link can be expressed as

$$OSRNR_{up} = \frac{P_{up} e^{-\mu L}}{P_{DD_{RB}} + P_{UD_{RB}}} = \frac{g_{ONU} e^{-2\mu L}}{(1 + g_{ONU}^2 e^{-2\mu L})\zeta} \tag{9.4}$$

It can be derived easily from Eq. (9.4) that, a maximum OSRNR value occurs when $g_{ONU} e^{-\mu L} = 1$, corresponding to which, according to Eq. (9.3), the downstream and upstream launch powers are identical.

Similarly, the RB noise power imposed on the downstream signal is given by

$$P'_{DD_{RB}} = \zeta P_{up} \tag{9.5}$$

Thus the OSRNR of the downstream signal at the output facet of the downstream link can be written as

$$OSRNR_{down} = \frac{P_{down} e^{-\mu L}}{P'_{DD_{RB}}} = \frac{1}{g_{ONU} \zeta} \tag{9.6}$$

It is worth mentioning that RB noise has a coloured Power Spectral Density (PSD), which is proportional to the PSD of the generating optical signal, as shown in Fig. 9.2. In numerical simulations, the RB noise spectrum is discretised at a frequency resolution Δf , and the RB noise power in each frequency interval is calculated using Eqs. (9.1), (9.2) and

(9.5) in the frequency domain (shown by the red triangle arrows), then a white Gaussian noise within each frequency interval is generated, as shown in Fig. 9.2(blue graph). Finally, the generated RB noise is added into the received optical signals in the frequency domain.

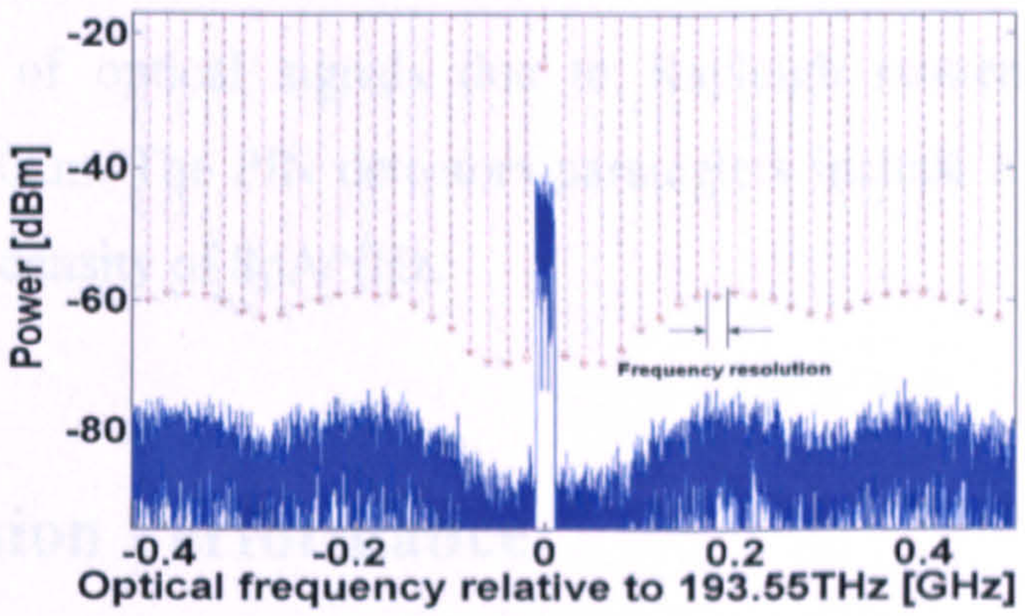

Fig. 9.2 RB noise power (red triangle arrow) and corresponding RB noise spectrum (blue graph).

9.2.4 SMF and PIN Detector Models

The theoretical SMF model used in previous chapters is used here, and the PIN detector model successfully used in Chapters 6-8 is considered in both downstream and upstream receivers.

9.2.5 Simulation Parameters

In simulating all the AMOOFDM transceivers involved in Fig. 9.1, parameters identical to those presented in Chapters 6-8 are adopted here.

The parameters used in simulating the SOA and RSOA intensity modulators here are representative for InGaAsP semiconductor materials operating at a wavelength of 1550nm, which are listed in Table 8.1. It should be noted that, here, the SOA (RSOA) cavity length of 500μm (300μm) and rear-facet reflectivity of 0.99 (0.0) are adopted. As the SOA intensity modulator is used in the relatively cost-insensitive OLT only, for all the simulations, optimum operating conditions identified in Chapter 6 are adopted, which are a CW optical input power of 20dBm, a bias current of 100mA and a driving current with a PTP value of 80mA.

The parameters adopted to simulate RB noise include a backscattering coefficient ζ equals -34dB based on the experiment measurement presented in Fig. 2.10 and a frequency resolution of 20MHz. The simulation parameters for SMFs are from Table 8.1 with the difference that a fibre attenuation coefficient of 0.22dB/km at 1550nm is adopted, which includes attenuation of optical signals due to Rayleigh scattering. The transmission distance is fixed at 40km. The PIN detectors parameters include a quantum efficiency of 0.8 and noise current density of 8pA/√Hz.

9.3 Transmission Performance

9.3.1 Verification of the RB Models

Apparently, the RSOA intensity modulator and the RB noise play central role in determining the network performance. Since the validity of the RSOA intensity modulator model had been verified in Section 8.5.1, by well agreements between simulation results and the experimental measurements of RSOA intensity modulated real-time end-to-end OOFDM transmission in a unidirectional system with a CW optical carrier wave being supplied locally [9.6], here effort is made to verify the validity of the RB noise model.

To confirm the validity of the RB model, comparisons of the transmission performance of RSOA intensity modulated AMOOFDM signals between numerical simulations and experimental measurements using off-line DSP are made in a more complicated transmission link, into which a CW optical wave is injected from the OLT and propagates in an opposite direction with respect to the modulated AMOOFDM signal over the same SMF [9.10]. In such a system, the RB noise effect is present. For this comparison only, the parameters adopted in numerical simulations are identical to those used in the experimental measurements [9.10]. These parameters are: a -1dBm CW optical power coupled into the SMF link in the OLT, an optical input power of -10dBm at the input facet of the RSOA, and a -14dBm optical power at the input facet of the photon detector. Our numerical simulations show that a 10Gb/s AMOOFDM signal transmission over a 20km IMDD SMF link is feasible at a BER of 1×10^{-4}, which agrees very well with the experimental measurements [9.10].

9.3.2 Downstream AMOOFDM Transmission Performance

Compared to the upstream signal, the downstream AMOOFDM signal suffers the RB noise effect only. To demonstrate explicitly the impact of such an effect on the transmission performance of the downstream AMOOFDM signal, the downstream AMOOFDM signal line rate versus upstream launch power is plotted in Fig. 9.3. In obtaining Fig. 9.3, the RSOA bias current and driving current PTP are fixed at 100mA and 280mA, respectively, and the downstream launch power is set to 6.3dBm, which gives rise to an optical power of -5.5dBm coupled into the RSOA. The alteration of the upstream launch power is realized by adjusting the VOA at the output of the RSOA intensity modulator, as shown in Fig. 9.1. It should be noted that the SOA operating conditions are given in Section 9.2.5.

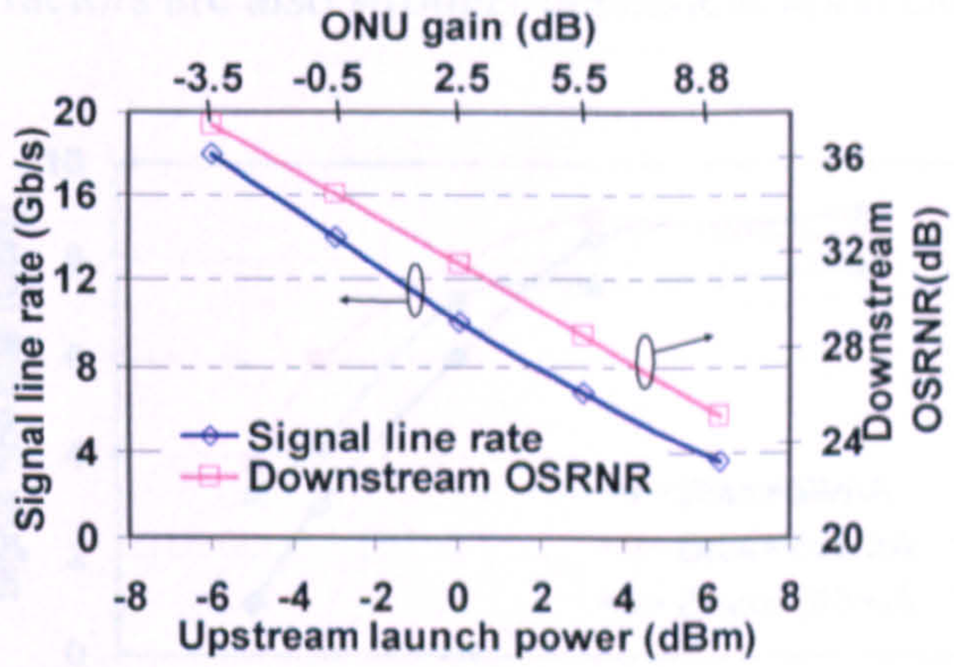

Fig. 9.3 Signal line rate and OSRNR of downstream AMOOFDM signals as a function of upstream launch power. The downstream launch power is fixed at 6.3dBm.

It can be seen from Fig. 9.3 that, 17Gb/s over 40km downstream transmission is feasible for upstream launch powers of <-6dBm. More importantly, the downstream signal line rate decreases almost linearly with increasing upstream launch power expressed in dBm. When the upstream launch power is increased to 6dBm, the downstream signal line rate is reduced to a value as small as 4Gb/s. Such a significant variation in downstream signal line rate is due to the RB noise effect induced by the upstream AMOOFDM signal. From Eqs. (9.5) and (9.6), it can be understood that a large upstream launch power corresponds a large RB noise power and high ONU gain, thus resulting in a reduction in downstream OSRNR, as seen in Fig. 9.3. The above discussions imply that the RB effect plays a dominant role in determining the maximum achievable downstream transmission

performance, and that a small upstream launch power is preferred for maximizing the downstream transmission performance.

9.3.3 Upstream AMOOFDM Transmission Performance and Optimization of RSOA Intensity Modulator Operating Conditions

In the previously discussed downstream transmission case, the upstream signal-induced RB noise is the only dominant factor limiting the achievable downstream signal bit rate, whilst the upstream transmission performance is mainly attributed to three factors listed as followings: 1) RB noise induced by both the downstream and upstream AMOOFDM signals, 2) crosstalk due to the residual downstream signal-induced fluctuation of the upstream signal, and 3) dynamic optical characteristics of the RSOA intensity modulator. In addition, these three factors are also strongly dependent upon each other.

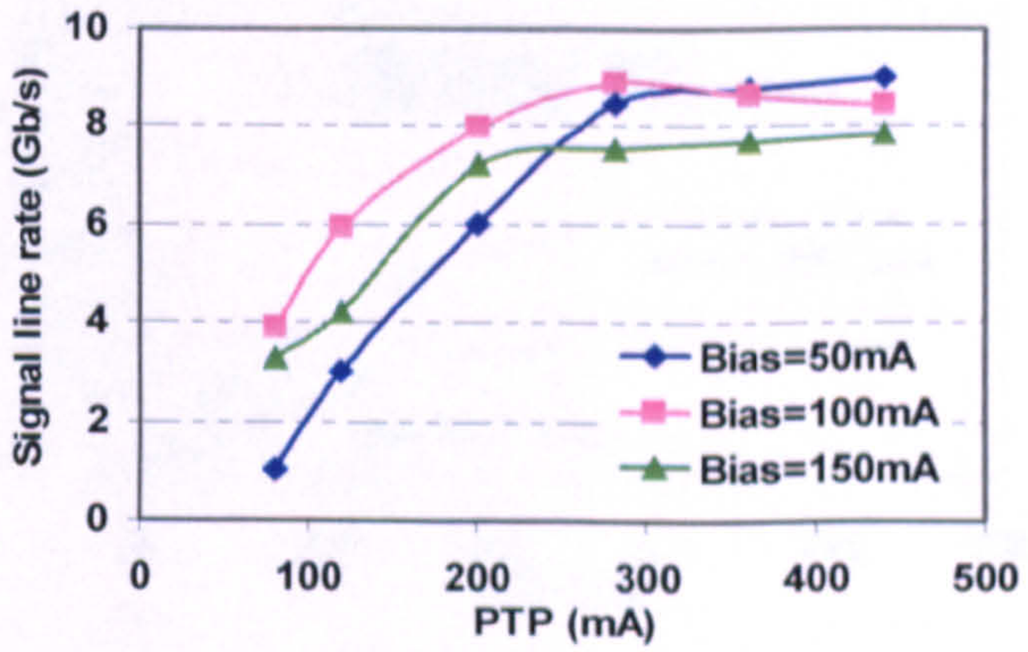

Fig. 9.4 Upstream AMOOFDM signal line rate versus driving current PTP for various RSOA bias currents.

To explore the dependence of the upstream AMOOFDM signal transmission performance on RSOA operating conditions, Fig. 9.4 is plotted to show the corresponding signal line rate versus electrical driving current PTP for different RSOA bias currents. In obtaining Fig. 9.4, both the downstream and upstream launch powers are fixed at 6.3dBm, which results in an optical power of -5.5dBm injected into the RSOA intensity modulator. As shown in Fig. 9.4, the driving current PTP affects significantly the achievable upstream AMOOFDM signal bit rate. It is also very interesting to note that, for various bias currents, there exists an almost identical optimum driving current PTP of 280mA, corresponding to which the maximum upstream signal line rate is obtained. Compared to the strong driving current PTP-dependent upstream transmission performance, the dependence of the

upstream transmission performance on RSOA bias current is not pronounced considerably, as shown in Fig. 9.4, and an optimum bias current of 100mA is identified.

To gain an in-depth understanding of the physical mechanisms underpinning the upstream signal line rate evaluation trends shown in Fig. 9.4, in Fig. 9.5 performance comparisons are made between two cases of modulating a centrally-supplied downstream CW optical wave (here referred to as CASE I) and re-modulating the downstream AMOOFDM optical signal (referred to as CASE II). For each of the above-mentioned cases, simulated results are also presented for conditions of including and excluding the RB noise effect. In obtaining Fig. 9.5, the bias current is set to 100mA and all other simulation parameters are identical to those adopted in simulating Fig. 9.4.

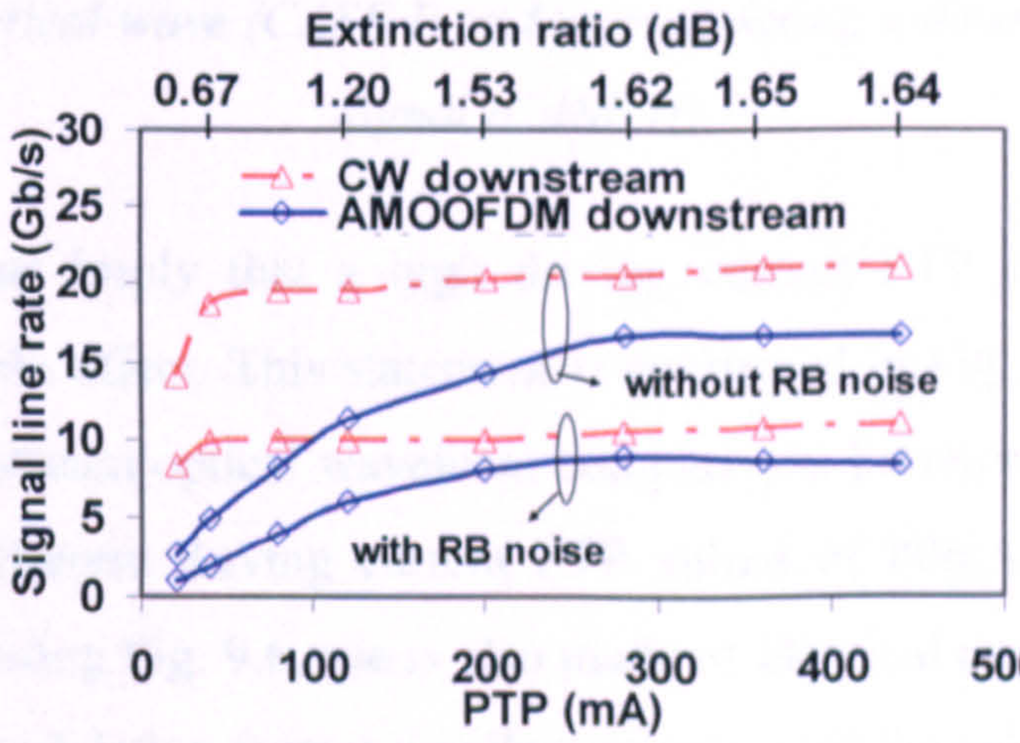

Fig. 9.5 Upstream signal line rate versus driving current PTP for cases of using a centrally-supplied downstream CW optical wave and re-modulating a downstream AMOOFDM signal. For each of these two cases, numerical results obtained under conditions of including and excluding the RB noise effect are also plotted.

In Fig. 9.5, the signal line rate difference between two red curves results from the RB noise effect, which, as expected from Eq. (9.4), is independent of the driving current PTP. In addition, Fig. 9.5 also indicates that the RB noise effect can halve the upstream signal line rate. On the other hand, for the case of excluding the RB noise effect, the upstream performance difference between the red (CASE I) and blue (CASE II) curves is due to the crosstalk effect, which, as seen in Fig. 9.5, plays a dominant role in determining the achievable upstream signal line rate for driving current PTPs of <200mA, beyond this value the effect becomes relatively weak.

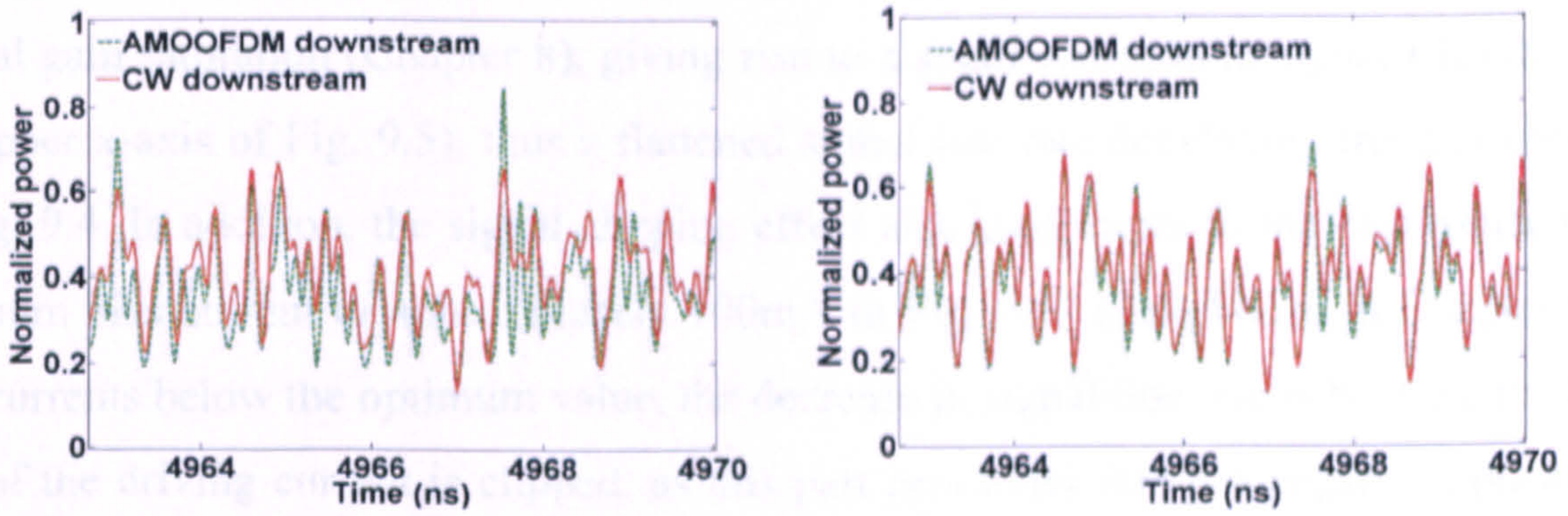

(a) (b)

Fig. 9.6 RSOA-modulated optical output waveforms for cases of using a centrally-supplied downstream CW optical wave (CASE I) and re-modulating a downstream AMOOFDM signal (CASE II).

The above discussions imply that a high driving current PTP is capable of reducing effectively the crosstalk effect. This statement is confirmed in Fig. 9.6, where normalized RSOA modulated upstream optical waveform comparisons between CASE I and CASE II are made between different driving current PTP values of 80mA and 280mA. For fair comparison, in calculating Fig. 9.6, use is also made of identical random bit sequences and the same subcarrier modulation format distribution across all the subcarriers. It can be seen from Fig. 9.6 (a) that, for the low PTP value of 80mA, there exist very strong unwanted waveform fluctuations for CASE II. However, such optical waveform fluctuations almost disappear when the PTP value is increased to 280mA, as seen in Fig. 9.6(b). The high driving current PTP-induced reduction in the crosstalk effect can be explained by considering the fact that, a high driving current PTP gives rise to a large ER of the RSOA modulated AMOOFDM signal (Chapter 8), as shown in the upper x-axis of Fig. 9.5. The large upstream signal ER can drown out the residual downstream signal waveform fluctuation in the RSOA intensity modulator.

From the above analysis, it is clear that both RB noise and crosstalk are dominant in determining the achievable upstream AMOOFDM transmission performance. Based on such an understanding, the driving current PTP dependent signal line rate behaviors shown in Fig. 9.4 can be explained easily: for driving current PTPs less than the optimum value of 280mA, the sharp increase in upstream signal line rate with increasing driving current PTP

is a direct result of the rapid reduction in the crosstalk effect. While a further increase in driving current PTP introduces the severe signal clipping effect owing to the strong RSOA optical gain saturation (Chapter 8), giving rise to a small variation in signal ER (shown in the upper x-axis of Fig. 9.5), thus a flattened signal line rate developing trend is observed in Fig. 9.4. In addition, the signal clipping effect also contributes to the occurrence of the optimum bias current of approximately 100mA in Fig. 9.4, as explained in Chapter 6: for bias currents below the optimum value, the decrease in signal line rate is because the lower part of the driving current is clipped, as this part penetrates into the negative optical gain region of the RSOA. Whilst for bias currents above the optimum bias current, the transmission performance degradation originates mainly from decreased signal ER and increased signal clipping, as the upper part of the driving current experiences an almost flat optical gain of the RSOA (Chapter 8).

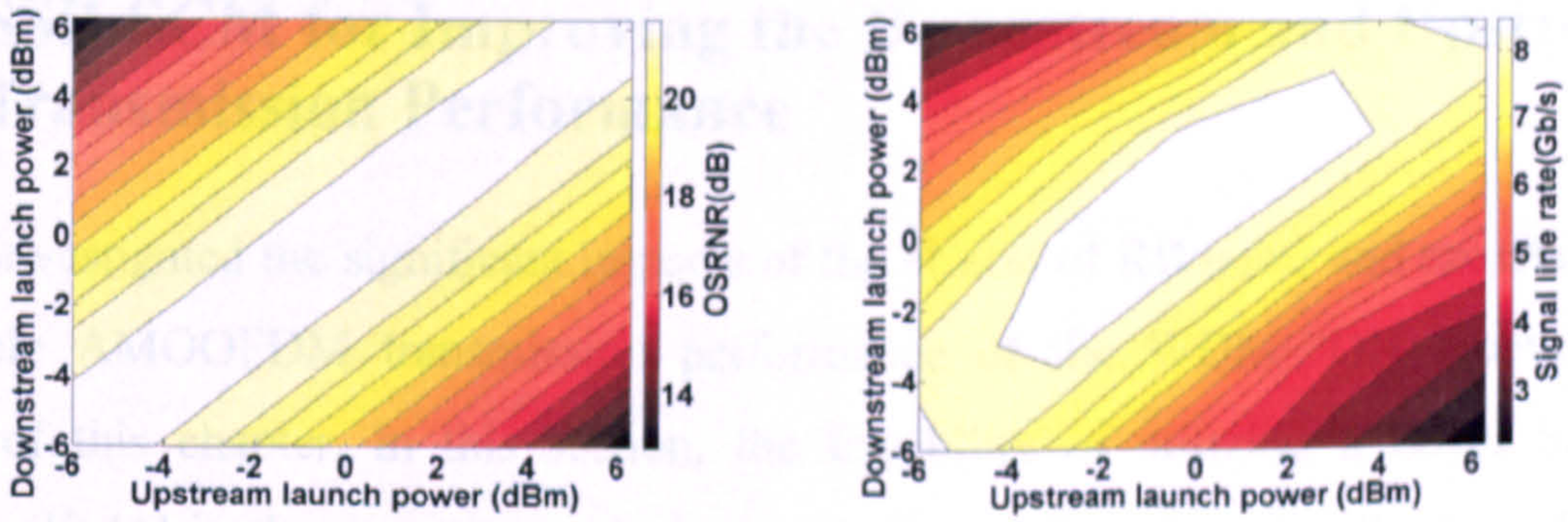

Fig. 9.7 Contour plot of upstream OSRNR (a) and upstream signal line rate (b) as a function of upstream and downstream launch powers.

The above-mentioned numerical simulations are performed based on an assumption that both the downstream and upstream launch powers are fixed at 6.3dBm. However, discussions in Section 9.2.3 indicate that the RB noise effect experienced by the upstream AMOOFDM signal depends upon both downstream and upstream launch powers. To explore such an interesting issue, contour plots of upstream OSRNR and corresponding signal line rate as a function of downstream and upstream launch powers are plotted in Fig. 9.7. In computing Fig. 9.7, the RSOA intensity modulator is assumed to operate at the optimum operating conditions identified in Fig. 9.4, and the variations in downstream and upstream launch powers are realized by adjusting the VOAs in the OLT and ONU. As predicted in Eq. (9.4), Fig. 9.7(a) shows that the maximum upstream OSRNR is obtainable

only when the downstream and upstream launch powers are very similar. As a direct result, the maximum upstream AMOOFDM signal line rate of 8Gb/s occurs when the difference between upstream and downstream launch powers is less than 3dB, as seen in Fig. 9.7(b).

Comparisons between Fig. 9.3 and Fig. 9.7 indicate that, there is a trade-off between the achievable upstream and downstream transmission performances. In practical system design, the specific downstream and upstream launch powers can be chosen according to specific requirements. For example, under optimum SOA and RSOA operating conditions as well as the downstream and upstream launch powers of 6.3dBm and 0dBm, respectively, the system performance of 10Gb/s in downstream and 6Gb/s in upstream over a single 40km SMF are feasible.

9.4 SSB-SCM for Improving the Downstream and Upstream Transmission Performance

Having investigated the significant impacts of the effects of RB noise and crosstalk on the achievable AMOOFDM transmission performance of the WDM-PON architecture of interest of this chapter, in this section, the feasibility of utilizing a novel SSB-SCM technique [9.11] in the downstream is explored, for the first time, to alleviate effectively these two critical effects to simultaneously improve considerably the downstream and upstream AMOOFDM transmission performance.

In the SSB-SCM technique, use is made of a RF modulator utilizing a Hilbert transform-based phase-shift approach to produce a real-valued SSB downstream electrical signal in the OLT. The generated SSB-SCM signal can be expressed as

$$S_{SSB}(t) = A_{DSB}(t)\cos(\omega_{RF}t) - H\{A_{DSB}(t)\}\sin(\omega_{RF}t) \tag{9.7}$$

where $A_{DSB}(t)$ is the real-valued double sideband (DSB) downstream electrical signal created by the conventional OFDM transmitter in Chapters 6-8. $H\{A_{DSB}(t)\}$ presents the Hilbert transform of $A_{DSB}(t)$. ω_{RF} is the intermediate RF carrier frequency, which is taken to be 15GHz [9.11]. $S_{SSB}(t)$ is utilized to drive directly the SOA intensity modulator in the OLT. The resulting downstream optical signal spectrum at the output of the SOA intensity modulator is shown in Fig. 9.8(a). In the corresponding downstream optical receiver, an

optical filter is inserted before square-law photon detection to remove the lower sideband of the received optical signal. RF down-conversion is performed to the converted electrical signal, prior to data recovery in the downstream OFDM receiver; whilst the upstream AMOOFDM transmitter has a configuration identical to that illustrated in Fig. 9.1, where a conventional real-valued DSB upstream electrical signal is used to drive the RSOA intensity modulator with the downstream optical signal being injected as an optical carrier wave. The RSOA-modulated upstream optical signal spectrum is shown in Fig. 9.8(b), from which it can be found that the upstream and downstream optical signal spectra are separated clearly. In the upstream optical receiver in the OLT, before performing square-law photon detection, an optical filter is employed to remove the residual downstream optical signal spectrum and a part of the RB noise power.

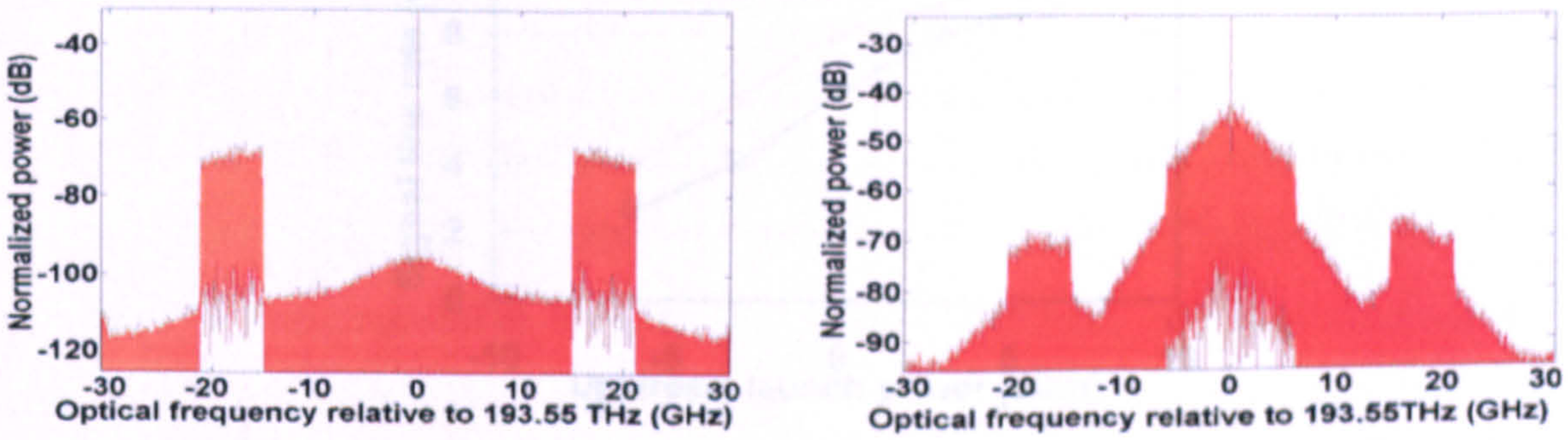

Fig. 9.8 Optical spectra of downstream and upstream AMOOFDM signals using the SSB-SCM technique.

From the above analysis, it is clear that the SSB-SCM technique is capable of preventing the downstream optical spectrum from overlapping with the upstream optical spectrum, thus resulting in a considerable reduction in the effects of RB noise and crosstalk, provided that appropriate optical filters are employed. The above-mentioned design also makes economic sense, as the simplicity of both the upstream optical transmitter and downstream optical receiver is still being preserved to satisfy the demands for low-cost transceivers in the ONU.

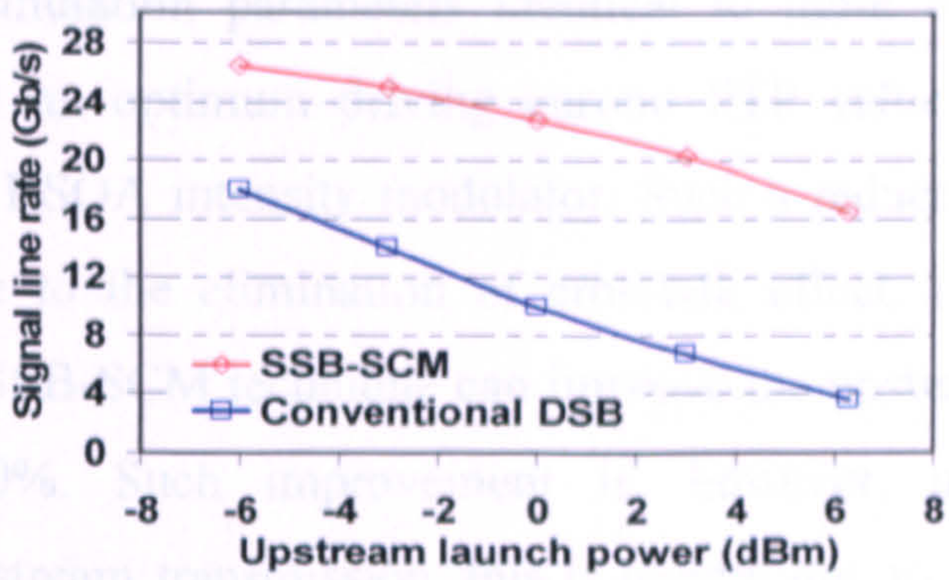

Fig. 9.9 Downstream signal line rate versus upstream launch power for SSB-SCM and conventional DSB AMOOFDM signals. The downstream launch power is fixed at 6.3dBm.

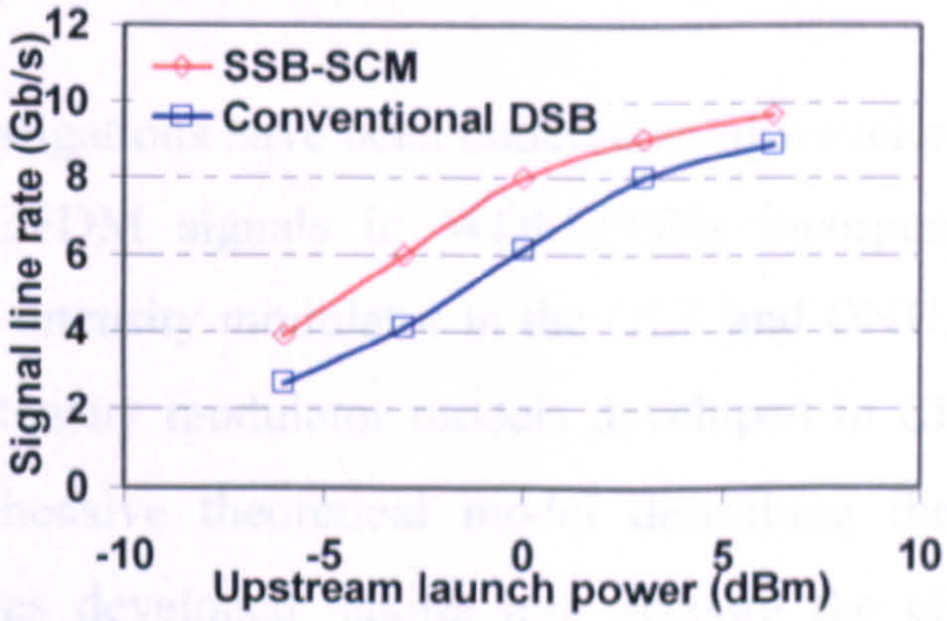

Fig. 9.10 Upstream signal line rate versus upstream launch power for both SSB-SCM and conventional DSB AMOOFDM signals. The downstream launch power is fixed at 6.3dBm.

The effectiveness of the SSB-SCM technique in improving the downstream AMOOFDM transmission capacity is shown in Fig. 9.9, where the transmission performance of a conventional DSB downstream AMOOFDM signal is also plotted for comparison. In obtaining Fig. 9.9, simulation parameters identical to those considered in Fig. 9.3 are adopted. It is shown in Fig. 9.9 that, in comparison with the conventional case and for upstream launch powers of <0dBm, the SSB-SCM technique can improve significantly the downstream transmission capacity by a factor of approximately 2, which can be further enhanced for upstream launch powers of >0dBm. The downstream signal capacity decay with increasing upstream launch power is because of a part of the RB noise induced by the residual upstream waveform still remains.

Compared to the conventional DSB baseband technique, the SSB-SCM technique can also enhance simultaneously the upstream transmission performance, as shown in Fig. 9.10. In

obtaining Fig. 9.10, simulation parameters identical to those adopted in Fig. 9.7 are considered, except that an optimum driving current PTP value of 80mA (rather than 280mA) is used in the RSOA intensity modulator. Such a reduction in optimum driving current PTP arises due to the elimination of crosstalk effect. In comparison with the conventional case, the SSB-SCM technique can improve the upstream AMOOFDM signal capacity by about 30%. Such improvement is, however, much lower than that corresponding to downstream transmission, this is mainly due to the fact that a reflected part of the RB noise associated with the upstream data signal still exists.

9.5 Conclusions

Detailed numerical investigations have been undertaken of wavelength reused bidirectional transmission of AMOOFDM signals in WDM-PONs incorporating a SOA intensity modulator and a RSOA intensity modulator in the OLT and ONU, respectively. Based on the SOA and RSOA intensity modulator models developed in Chapter 6 and Chapter 8, respectively, a comprehensive theoretical model describing the performance of such network architecture was developed, taking into account the effects of RB noise and crosstalk. It has been shown that the effects of RB noise and crosstalk due to residual downstream signal-induced waveform fluctuations are dominant factors limiting the achievable downstream and upstream performances. Under optimum SOA and RSOA operating conditions as well as practical downstream and upstream optical launch powers, 10Gb/s downstream and 6Gb/s upstream over 40km SMF transmissions of conventional double sideband AMOOFDM signals were feasible without in-line optical amplification and chromatic dispersion compensation. In particular, the aforementioned transmission performance can be improved to 23Gb/s downstream and 8Gb/s upstream over 40 km SMFs when SSB-SCM is utilized in the downstream systems.

References

[9.1] H. Takesue, and T. Sugie, "Wavelength channel data rewrite using saturated SOA modulator for WDM networks with centralized light sources," J. Lightwave Technol. vol. 21, no. 5, pp. 2546-2556 Mar. 2003.

[9.2] W. Lee, S. H. Cho, M. Y. Park, J. H. Lee, C. Kim, G. Jeong, and B. W. Kim, "Optical transceiver employing an RSOA with feed-forward current injection," presented at the OFC/NFOEC, (OSA, 2007), Paper OTuH1.

[9.3] K. Grobe and J.-P. Elbers, "PON in adolescence: from TDMA to WDM-PON," IEEE Commun. Mag., vol. 46, no. 1, pp. 26-34 Jan. 2008.

[9.4] W. Hung, C. K. Chan, L. K. Chen, and F. Tong, "An optical networking unit for WDM access networks with downstream DPSK and upstream re-modulated OOK data using injection-locked FP laser," presented at the OFC/NFOEC, (OSA, 2003), Paper TuR2.

[9.5] N. Deng, C.-K. Chan, and L.-K. Chen, "A centralized-light-source WDM access network utilizing inverse-RZ downstream signal with upstream data remodulation," Opt. Fiber Technol., vol. 13, no. 1, pp. 18-21 Jan. 2007.

[9.6] R. P. Giddings, E. Hugues-Salas, X. Q. Jin, J. L. Wei and J. M. Tang, " Colourless real-time optical OFDM end-to-end transmission at 7.5Gb/s over 25km SSMF using 1GHz RSOAs for WDM-PONs," presented at the OFC/NFOEC, (OSA,2010). Paper OMS4.

[9.7] P. Gysel and R. K. Staubli, "Statistical properties of Rayleigh backscattering in single-mode fibers," J. Lightwave Technol., vol. 8, no. 4, pp. 561-567 Apr. 1990.

[9.8] C. Arellano, K.-D. Langer, and J. Prat, "Reflection and multiple Rayleigh backscattering in WDM single-fiber loopback access networks," J. Lightwave Technol., vol. 27, no. 1, pp. 12-18 Jan. 2009.

[9.9] J. Ko, S. Kim, J. Lee, S. Won, Y. S. Kim, and J. Jeong, "Estimation of performance degradation of bidirectional WDM transmission systems due to Rayleigh backscattering and ASE noises using numerical and analytical models, " J. Lightwave Technol., vol. 21, no. 4, pp. 938-946 Apr. 2003.

[9.10] T. Duong, N. Genay, P. Chanclou, B. Charbonnier, A. Pizzinat, and R. Brenot, "Experimental demonstration of 10 Gbit/s for upstream transmission by remote modulation of 1 GHz RSOA using Adaptively Modulated Optical OFDM for WDM-PON single fiber architecture," presented at the European Conference on Optical Communication (ECOC), (Brussels, Belgium, 2008), PD paper Th.3.F.1.

[9.11] X. Zheng, J.L. Wei, and J.M. Tang, "Transmission performance of adaptively modulated optical OFDM modems using subcarrier modulation over SMF IMDD links for access and metropolitan area networks," Opt. Express., vol.16, no.25, pp.20427-20440, Dec. 2008.

10 Conclusions and Future Work

10.1 Conclusions

To accommodate the ever increase in bandwidth requirement from both individual and business users, PONs, the dominate technology of today's access networks, face tremendous challenges for upgrading into high-speed NG-PONs in a cost-effective manner. As discussed in Chapters 1-3, emergent candidate technologies such as OOFDM and WDM are widely considered as long-term solutions for NG-PONs. As electro-optic converters take the majority of the cost of PON system transceivers, from the operators' point of view, the use of low-cost electro-optic converters in NG-PONs is critical for CAPEX and OPEX savings.

To address the challenging issues, in this thesis, extensive numerical investigations have been undertaken to explore the feasibility of incorporating low-cost semiconductor laser devices including DMLs and RSOAs/SOAs as intensity modulators to facilitate cost-effective OOFDM transceivers for IMDD NG-PONs. DMLs are widely used in existing TDM-based GPONs and EPONs, while RSOAs/SOAs are promising for colourless OOFDM WDM-PONs.

In DML-based IMDD PON systems, real-time 11.25Gb/s OOFDM signal transmission over 25km SMF has been experimentally demonstrated successfully [10.1]. However, the optical power budgets of ~20dB measured in the real-time OOFDM systems may not satisfy the NG-PON requirements. On the other hand, for DSB OOFDM signals, strong subcarrier intermixing occurs upon square-law detection in IMDD PON systems, which further reduces the maximum achievable transmission capacity versus reach performance. As the achievable optical power budget, transmission capacity and reach are critical issues for considerations in practical NG-PON designs, it is very important to identify key physical factors that strongly affect the system performance, and to propose effective approaches for alleviating these effects. These targets have been thoroughly pursued in Chapters 4-5.

In Chapter 4, detailed explorations have been undertaken of the impacts of different physical mechanisms including OOFDM signal ER, DML-induced frequency chirp and subcarrier intermixing upon direct detection on optical power budget of DML-based OOFDM IMDD PON systems. It has been shown that the low ER of a DML-modulated OOFDM signal is the predominate factor limiting the achievable optical power budget, and the subcarrier intermixing effect upon square-law photon detection in the receiver reduces the optical power budget by at least 1dB. The use of a 0.02nm bandwidth optical Gaussian bandpass filter in the transmitter with a 0.01nm wavelength offset with respect to the optical carrier wavelength has been shown to be very effective in enhancing the OOFDM signal ER by approximately 1.24dB. This results in a 7dB optical power budget improvement at a total channel BER of 1×10^{-3}.

The reduction in the subcarrier intermixing effect upon square-law detection has been investigated in detail in Chapter 5, by using DML-modulated carrier suppressed SSB OOFDM signals over SMF IMDD systems. It has been shown that, for IMDD NG-PON systems excluding in-line optical amplification, 30Gb/s carrier suppressed SSB OOFDM signal transmission over 80km SMF is achievable, which doubles the performance corresponding to DSB OOFDM signals without carrier suppression; and for IMDD NG-PON systems incorporating in-line EDFAs, 10Gb/s carrier suppressed SSB OOFDM signal transmission over 1200km SMF is feasible. The obtained long-reach transmission performance is robust to variations in both DML operating conditions and optical launch powers.

For OOFDM IMDD WDM-PONs, the use of SOAs/RSOAs as intensity modulators is also highly preferred due to their salient features such as compactness, capability of monolithic integration with electronic components and wide wavelength coverage of typically >100nm. To explore such an interesting topic, the following works have been undertaken in Chapters 6-9: 1) Develop and verify accurate SOA and RSOA intensity modulator theoretical models describing the characteristics of intensity-modulated OOFDM signals; 2) Identify major physical mechanisms that affect the maximum achievable transmission performances of these modulators; 3) Explore the feasibility of achieving colourless SOA/RSOA-based OOFDM transmitters; and 4) Utilize SOA and RSOA intensity modulators to realize wavelength reused bidirectional transmission of OOFDM signals to simplify colourless WDM-PON system architectures. Firstly, the feasibility of SOA-

enabled intensity modulation of AMOOFDM signals has been presented in Chapter 6, over IMDD SMFs without in-line optical amplification- and dispersion compensation. A theoretical model describing the characteristics of SOA intensity modulators has been developed, based on which optimum SOA operating conditions have been identified at a fixed wavelength of 1550nm. Results have shown that the SOA intensity modulators under optimum operating conditions support a 30Gb/s AMOOFDM signal transmission over a 80km SMF, which doubles the transmission performance obtained using typical DMLs. In addition, key physical factors limiting the maximum achievable transmission performance of the AMOOFDM technique have also been identified. Moreover, excellent robustness of the optimum operating conditions and the transmission performance to variations in SOA parameters has also been shown.

As a significant extension of the work presented in Chapter 6, Chapter 7 has addressed the SOA-intensity modulated OOFDM signal transmission performances over a wide wavelength range from 1510nm to 1590nm. A theoretical SOA intensity modulator model describing both optical gain saturation and gain spectral characteristics has been developed, based on which optimum SOA operating conditions have been identified for various wavelengths within the aforementioned wavelength range. It has been shown that SOA intensity modulators operating at the identified optimum operating conditions are capable of achieving colourless AMOOFDM transmitters, supporting >30Gb/s AMOOFDM signal transmissions over 60km SMFs in the abovementioned wavelength range.

As a special type of an SOA, a RSOA is promising for facilitating colourless reflective ONUs for use in WDM-PONs. Therefore, AMOOFDM modems incorporating RSOAs as intensity modulators have been explored in Chapter 8. A comprehensive theoretical model describing the dynamic characteristics of RSOA intensity modulators has been developed, taking into account counter-propagation of the forward and backward optical signals and the rear-facet reflectivity in the waveguide. Special attention has also been given to performance comparisons between the RSOA and SOA intensity modulators. Results have shown that optimum RSOA operating conditions and corresponding optimum performances of 30Gb/s over 60km SMFs are independent of RSOA rear-facet reflectivity and they are very similar to those corresponding to SOAs. Whilst under low-cost optical component-enabled practical operating conditions, the RSOA intensity modulators

outperform considerably the SOA intensity modulators. For low optical input powers, the RSOA/SOA intensity modulation-induced negative frequency chirp helps to improve the AMOOFDM performance in IMDD SMF systems.

Having explored the performances of RSOA/SOA intensity modulated AMOOFDM signal transmissions in WDM-PONs in Chapters 6-8, another important aspect that has to be solved is the use of the RSOA/SOA intensity modulators to simplify colourless AMOOFDM WDM-PON system architectures. To address this issue, in Chapter 9, a wavelength reused bidirectional transmission of AMOOFDM WDM-PON has been proposed which consists of a SOA intensity modulator and a RSOA intensity modulator in the OLT and ONU, respectively. Results have shown that the RB noise effect and residual downstream optical signal-induced crosstalk are the dominant factors limiting the maximum achievable downstream and upstream transmission performances. Under optimum SOA and RSOA operating conditions as well as practical downstream and upstream optical launch powers, 10Gb/s downstream and 6Gb/s upstream over 40km SMF transmission of conventional DSB AMOOFDM signals are feasible. In particular, the aforementioned transmission performances can be further improved to 23Gb/s downstream and 8Gb/s upstream over 40 km SMF when SSB-SCM is introduced in downstream systems.

10.2 Future Work

Following the work presented in this thesis, a number of issues related to OOFDM PONs are important for future investigations. The short-term works are listed as follows:

1) Experimental demonstration of wavelength reused bidirectional OOFDM transmission in WDM-PONs using real-time OOFDM transceivers.

Real-time experimental demonstrations of wavelength reused bidirectional OOFDM transmission is critical for not only evaluating the true potential of the proposed wavelength reused bidirectional OOFDM transmission WDM-PONs, but also identifying the limitations set by hardware that theoretical simulations may not be able to cover. This work may also motivate further simulation work to seek advanced techniques.

2) Wavelength reused bidirectional transmission of OOFDM signals in WDM-PONs by injecting a reversed electrical OFDM current into the RSOA intensity modulator.

To further suppress the crosstalk effect arising from the residual downstream signals in wavelength reused bidirectional WDM-PONs, as discussed in Chapter 9, another efficient way is to inject an electrical OFDM current, which is the reverse of the residual downstream OOFDM signal waveform, into the RSOA intensity modulator. Such an electrical current with a reverse waveform with respect to the residual downstream OOFDM signal can be achieved by optical/electrical signal processing. This injected signal may efficiently smooth the residual downstream optical signal waveform. It is expected that a significant reduction of the crosstalk effect can be achieved by the technique.

3) Wavelength reused bidirectional transmission of OOFDM signals in WDM-PONs using phase modulation in the downstream transmission.

To reduce the above-mentioned crosstalk effect in a wavelength reused bidirectional OOFDM WDM-PON, another efficient approach is to implement phase modulation for downstream OOFDM signals. In this scheme, the electrical OFDM signal in the downstream transmitter changes only the phase of an optical CW signal and the downstream optical signal amplitude remains constant. Therefore, the generated downstream signal waveform is smoother than that corresponding to a conventional intensity-modulated OOFDM downstream signal. As a result, the crosstalk effect can be minimized. However, a coherent receiver is required in the ONU. This brings about advantages including: 1) a significant increase in OSNR sensitivity of the receiver thus improved downstream optical power budget, and 2) the downstream linear channel impairments can be completely compensated, leading to the improved downstream transmission performance. The disadvantage associated with the scheme is the relatively high cost of the optical modulators and coherent detectors.

The long-term work is to investigate high speed OOFDM signals for ≥40Gb/s transmission over SMF-based IMDD WDM-PONs with extended reach and high power split ratio. Such an advanced PON system aims to provide individual and business users with "future-proof" solutions to satisfy the requirements in bandwidth and allowable power budget. To

achieve this goal in a cost-effective way, SCM OOFDM with optical Raman amplification may be feasible solutions.

References

[10.1] G. P. Giddings, X. Q. Jin, E. Hugues-Salas, E. Giacoumidis, J. L. Wei, and J. M. Tang, "Experimental demonstration of a record high 11.25Gb/s real-time optical OFDM transceiver supporting 25km SMF end-to-end transmission in simple IMDD systems," Opt. Express, vol. 18, no.6, pp. 5541-5555, 2010.

APPENDIX

I. CONTRIBUTIONS TO PATENTS

[1] Jianming Tang, "Use of semiconductor optical amplifiers-based intensity modulator in signal Transmission," *UK Patent Application No*: 0919039.8, 30 Oct 2009.

[2] Jianming Tang, "Use of the same set of wavelengths for uplink and downlink signal Transmission," *UK Patent Application No*: 0919029.9, 30 Oct 2009.

II. LIST OF PUBLICATIONS

II-1. Journal Publications

[1] E. Giacoumidis, J. L. Wei, X.Q. Jin and J.M. Tang, "Improved transmission performance of adaptively modulated optical OFDM signals over directly modulated DFB-laser based IMDD links using adaptive cyclic prefix," Opt. Express., Vol. 16, no.13, pp.9480-9494, June 2008.

[2] X. Zheng, J. L. Wei and J.M. Tang, "Transmission performance of adaptively modulated optical OFDM modems using subcarrier modulation over SMF IMDD links for access and metropolitan area networks," Opt. Express, vol.16, no.25, pp.20427-20440, Dec. 2008.

[3] J. L. Wei, X. L. Yang, R.P. Giddings and J. M. Tang, "Colourless adaptively modulated optical OFDM transmitters using SOAs as intensity modulators," Opt. Express., vol. 17, no. 11, pp.9012-9027, May 2009.

[4] J. L. Wei, X.Q. Jin, and J.M. Tang, "The influence of directly modulated DFB lasers on the transmission performance of carrier suppressed single sideband optical OFDM signals over IMDD SMF systems," J. Lightwave Technol. vol. 27, no. 13, pp. 2412 – 2419, July 2009.

[5] J. L. Wei, A. Hamié, R. P. Giddings, and J. M. Tang, "Semiconductor optical amplifier-enabled intensity modulation of adaptively modulated optical OFDM signals in SMF-based IMDD systems," J. Lightwave Technol., vol.27, no.16, pp.3679-3689, Aug. 2009.

[6] M. A. Jarajreh, J. L. Wei, J. M. Tang, Z. Ghassemlooy, W. P. Ng, "Effect of number of sub-carriers, cyclic prefix and analogue to digital converter parameters on coherent optical orthogonal frequency division multiplexing modem's transmission performance, " IET Commun. vol. 4, no. 2, pp. 213-222, Jan. 2010.

[7] R. P. Giddings, X. Q. Jin, E. Hugues-Salas, E. Giacoumidis , J. L. Wei and J. M. Tang, "Experimental demonstration of a record high 11.25Gb/s real-time optical OFDM transceiver supporting 25km SMF end-to-end transmission in simple IMDD systems," Opt. Express, vol. 18, no. 6, pp. 5541-5555, March. 2010.

[8] E. Giacoumidis, J. L. Wei, X. L. Yang, A. Tsokanos and J. M. Tang, "Adaptive Modulation-Enabled WDM Impairment Reduction for Multi-Channel Optical OFDM Transmission in PONs," IEEE Photonics J., vol. 2, no. 2, pp. 130-140, Apr. 2010.

[9] J. L. Wei, A. Hamié, R.P. Giddings, E. Hugues-Salas, X. Zheng, S. Mansoor and J. M. Tang, "Adaptively modulated optical OFDM Modems utlizing RSOAs as intensity modulators in IMDD SMF transmission systems," Opt. Express., vol. 18, no. 8, pp. 8556-8573, Apr. 2010.

[10] J. L. Wei, E. Hugues-Salas, R.P. Giddings, X.Q. Jin, X. Zheng, S. Mansoor and J.M. Tang, "Wavelength reused bidirectional transmission of adaptively modulated optical OFDM signals in WDM-PONs incorporating SOA and RSOA intensity modulators", Opt. Express., vol. 18, no. 18 pp.9791-9808, May 2010.

[11] R. P. Giddings, E. Hugues-Salas, X. Q. Jin, J. L. Wei and J. M. Tang, "Experimental demonstration of colourless real-time optical OFDM transmission at 7.5Gb/s over 25km SSMF using a 1GHz RSOA," IEEE Photon. Technol. Lett. vol. 22, no. 11, pp. 745-747, Jun. 2010.

[12] X. Zheng, X. Q. Jin, R. P. Giddings, J. L. Wei, E. Hugues-Salas, Y. H. Hong and J. M. Tang, "Negative Power Penalties of Optical OFDM Signal Transmissions in

Directly Modulated DFB Laser-Based IMDD Systems Incorporating Negative Dispersion Fibres", IEEE Photonics J., vol.2, no. 4, pp. 532-542, Jun. 2010.

[13] J. L. Wei, C. Sánches, R.P. Giddings, E. Hugues-Salas, and J. M. Tang, "Significant improvements in optical power budgets of real-time optical OFDM PON systems," Opt. Express, vol. 18, no. 20, pp. 20732-20745, Sep. 2010.

II-2. Conference Contributions

[14] J. L. Wei, and J. M. Tang, "Improved dispersion tolerance of coherent optical OFDM signals by adaptive modulation," presented at the Semiconductor and Integrated Opto-Electronics Conf. (IEE/SIOE' 08), Cardiff, U.K., 31st, March-2nd, Apr, 2008.

[15] E. Giacoumidis, J.L. Wei, X.Q. Jin and J.M. Tang, "Influence of adaptive cyclic prefix on the transmission performance of adaptively modulated optical OFDM signals over directly modulated laser-based IMDD links," presented at the Semiconductor and Integrated Opto-Electronics Conf. (IEE/SIOE' 08), Cardiff, U.K., 31st, March-2nd, Apr, 2008.

[16] J. L. Wei, A. Hamié, and J. M. Tang, "SOA-Enabled Intensity Modulation of Adaptively Modulated Optical OFDM Signals for PONs," present at Asian-Pacific Microwave Photonics Conference (APMP 2009), Beijing, China, April. 22-24, 2009. (An invited talk)

[17] J. L. Wei, X. L. Yang, R. P. Giddings, J. M. Tang and K. A. Shore, "SOA Intensity Modulator-Enabled Colourless Transmission of Adaptively Modulated Optical OFDM Signals for WDM-PONs," presented at the 14th OptoElectronics and Communications Conference (OECC 2009), Hongkong, China, July 14-17, 2009.

[18] X. Zheng, J. L. Wei, X. L. Yang, R.P.Giddings, J. M.Tang and K.A. Shore, "Input/Output Reconfigurable Adaptively Modulated Optical OFDM Modems Using Subcarrier Modulation, " presented at the 14th OptoElectronics and Communications Conference (OECC 2009), Hongkong, China, July 14-17, 2009.

[19] R.P. Giddings, E. Hugues-Salas, X.Q. Jin, J. L. Wei and J.M. Tang, "Colourless Real-Time Optical OFDM End-to-End Transmission at 7.5Gb/s over 25km SSMF

Using 1GHz RSOAs for WDM-PONs," Proc. OFC 2010, San Diego, CA, USA, Paper OMS4.

[20] J. L. Wei, A. Hamié, and J. M. Tang, "Optimization and Comparison of the Transmission Performance of RSOA/SOA Intensity-Modulated Optical OFDM Signals for WDM-PONs," Proc. OFC 2010, Proc. OFC 2010, San Diego, CA, USA, Paper JThA53.

[21] J. L. Wei, E. Hugues-Salas, R.P. Giddings, X.Q. Jin, X. Zheng, and J.M. Tang, "Wavelength reused bidirectional transmission of adaptively modulated optical OFDM signals in SOA/RSOA intensity modulator-based WDM-PONs," in Future Network & Mobile Summit 2010 (Florence,Italy),Paper 260.

[22] X. Zheng, J. L. Wei, R.P. Giddings, J. M. Tang, "Simple Adaptively Modulated Optical OFDM Modems Using Subcarrier Modulation with Input/Output Reconfigurability," in Future Network & Mobile Summit 2010 (Florence, Italy), Paper 37.

[23] E. Giacoumidis, J.L. Wei, and J. M. Tang, "Adaptive Modulation Induced WDM Impairment Reduction in Optical OFDM PONs," in Future Network & Mobile Summit 2010 (Florence, Italy), Paper 36.

[24] R.P. Giddings, E. Hugues-Salas, X.Q. Jin, J. L. Wei and J.M. Tang, "Experimental Demonstration of Colourless Real-Time End-to-End Optical OFDM Transmission at 7.5Gb/s over 25km SSMF Using a 1GHz RSOA," in Future Network & Mobile Summit 2010(Florence,Italy),Paper 147.

[25] X. Zheng, X. Q. Jin, R. P. Giddings, J. L. Wei, E. Hugues-Salas, Y. H. Hong and J. M. Tang, "Negative Power Penalty of Optical OFDM Signal Transmission over Directly Modulated DFB Laser-Based IMDD Systems Incorporating Negative Dispersion Fibres," in Photonics in Switching (PS) Topical Meeting, (OSA, 2010), (Monterey, Florida, USA).

[26] J. L. Wei, E. Hugues-Salas, R.P. Giddings, X.Q. Jin, X. Zheng, and J.M. Tang, "Wavelength Reused Bidirectional Adaptively Modulated Optical OFDM

Transmission in Colourless WDM-PONs," Proc. ECOC 2010 (Torino, Italy), Paper P.6.04

[27] J. L. Wei, and J.M. Tang, "7dB optical power budget improvements of optical OFDM PON systems using narrow optical filters," *ACP* 2010 (Shanghai, China, 2010), Paper SuI 4.